Durham E-Theses

An Investigation of Hair and its Keratin Associated Proteins using Advanced Light Microscopy

THOMPSON, MATTHEW,JAMES

An Investigation of Hair and its Keratin Associated Proteins using Advanced Light Microscopy

Matthew James Thompson

2018

A thesis submitted for the degree of Doctor of Philosophy

Durham
University

Department of Biosciences

<u>Declaration</u>

I declare that the work described in this thesis was, unless otherwise stated, carried out by myself in the Department of Biosciences, Durham University, under the supervision of Dr Timothy Hawkins and Dr Arto Määttä. External contributions have been acknowledged accordingly. This thesis has been composed by myself and is a record of work that has not been submitted previously for a higher degree.

Matthew Thompson

Abstract

An Investigation of Hair and its Keratin Associated Proteins using Advanced Light Microscopy

Matthew Thompson

Supervisors: Dr Tim Hawkins and Dr Arto Määttä

Quantification and understanding of hair damage are often derived using semi-quantitative means which provide limited information regarding the whole hair. Furthermore, the roles of the varied keratin associated proteins (KAPs), which are the second most abundant proteins within hair, are poorly understood. Finally, the movement of compounds into the hair fibre has never previously been analysed dynamically or using the range of techniques currently available.

Fluorescence lifetime imaging microscopy (FLIM) and correlative techniques are utilised to quantify and understand the chemical changes taking place following damage. Super-resolution imaging techniques, including Airyscan and 3D structured illumination microscopy (3D-SIM) are used for the imaging of a selection of fluorescently-tagged KAPs within transiently transfected HaCaT cells in order to describe their cell biology. Fluorescence recovery after photobleaching (FRAP) is also applied to gather information regarding the dynamics of these proteins. Additionally, Airyscan and FRAP are utilised for the analysis of fluorescent dye movement within hair to characterise dye pathways and partitioning in hair dynamically.

FLIM provides a rapid and sensitive means to quantify oxidative damage to hair spatially, which is correlated to the conversion of tryptophan, through oxidation, to products including kynurenine. The uptake of dye into hair is dependent upon the size and lipophilicity of the molecule and may be limited due to a cuticle-cortex boundary observed. Knowledge of compound uptake into hair may be translated for the development of future cosmetics. The KAP subfamilies display distinct subcellular localisations to cytoskeletal components including epidermal keratins and actin structures. Functional characterisation of KAPs carried out in this study could allow a targeted approach to KAP-KAP and KAP-keratin interactions in future cosmetic treatments. This understanding may also be of relevance to the mechanism of certain diseases unrelated to the hair follicle, and indeed for the production of keratin-based biomaterials.

Table of Contents

List of Figures

List of Tables

<u>List of Abbreviations</u>

18-MEA: 18-methyleicosanoic acid

2D-SDS-PAGE: 2-dimensional sodium dodecyl sulphate polyacrylamide gel electrophoresis

3D-SIM: 3-dimensional structured illumination microscopy

AFM: atomic force microscopy

CMC: cell membrane complex

Co-IP: co-immunoprecipitation

DP: dermal papilla

EDTA: ethylenediaminetetraacetic acid

EM: electron microscopy

FLIM: fluorescence lifetime imaging microscopy

FRAP: fluorescence recovery after photobleaching

HGT: high glycine-tyrosine

HS: high sulphur

IRS: inner root sheath

JACoP: just another colocalisation analysis plugin

KAP: keratin associated protein

KIF: keratin intermediate filament

LC-MS: liquid chromatography – mass spectrometry

LSCM: laser scanning confocal microscopy

ORS: outer root sheath

PCR: polymerase chain reaction

RH: relative humidity

SDS-PAGE: polyacrylamide gel electrophoresis

SEM: scanning electron microscopy

SNR: signal to noise ratio

TCSPC: time correlated single photon counting

TEM: transmission electron microscopy

TET: transient electro-thermal technique

TIRF: total internal reflection fluorescence

UHS: ultra-high sulphur

UV: ultra-violet

VID: vertical imaging device

1. Introduction

The hair fibre is a skin appendage which is no longer living. Despite this, it continues to provide several functions such as thermoregulation, mechano-sensing, physical protection and camouflage (Robbins, 2012). Due to a large volume of prior research focusing on the use of wool for textiles, similarities are often drawn between human hair and wool (Plowman et al., 2007; Rogers et al., 1989). This literature review and the following study focus specifically on human scalp hair and protein components responsible for its structure.

Hair and wool have been studied extensively, particularly through the use of microscopy, both light and electron (Hadjur et al., 2002; Lagarde et al., 1994; Rogers, 1959), allowing new insights into hair formation and structure. In this literature review, the structure of hair will be discussed, exploring the morphological components such as the cuticle, cortex and medulla. Further, the chemical components of the hair are inspected, particularly proteins such as the keratins and keratin-associated proteins (KAPs). This information serves as a basis for the work in this thesis to build upon.

In this study the use of an alternative light microscopy method to quantify and better understand oxidative damage to hair will be examined, Fluorescence Lifetime Imaging Microscopy (FLIM) in particular, which will be detailed in chapter 3. Additionally, KAPs found within hair will be examined using a light microscopy approach to better understand their role in hair structure and cell biology. Hair will also be used for the investigation of compound uptake and partitioning within the fibre, a process of particular interest to the cosmetics industry. This work will be completed using a light microscopy approach. The results of these investigations have implications for both fundamental science and the cosmetics industry.

1.1. Human Hair Structure

The human hair fibre has three main components: the cuticle, the cortex, and the medulla. The cuticle forms the outermost barrier of the hair, providing a protective layer against damage of chemical, mechanical, or thermal nature for example (Robbins, 2012). The cortex accounts for the largest volume of these three components and consists of elongated cells packed with keratin intermediate filaments (KIFs), surrounded by a matrix of keratin associated proteins, to form the bulk of the fibre. The medulla, which is not always present, may occupy the central column of the hair. The cell membrane complex (CMC), which may be considered as the fourth component of hair, is a continuous network spanning the

entirety of the fibre (Jones, 2001; Robbins, 2009). Figure 1.1 provides an overview of hair structure.

1.1.1. Cuticle Morphology and Composition

The cuticle is the outermost layer of the hair. It is comprised of 3 – 9 layers of flattened cuticle cells which overlap circumferentially and longitudinally (Birbeck and Mercer, 1957). The multiple cuticle layers (figure 1.2) provide protection from insults such as ultra-violet (UV), torsional, and chemical damage. Following certain forms of damage, the exposed edges of cuticle cells may become physically altered, leading to a jagged, rather than smooth, appearance of these edges. These exposed edges of cuticle cells point towards the distal end of the fibre and so may have a role in anchoring of hair into the follicle (Jones, 2001).
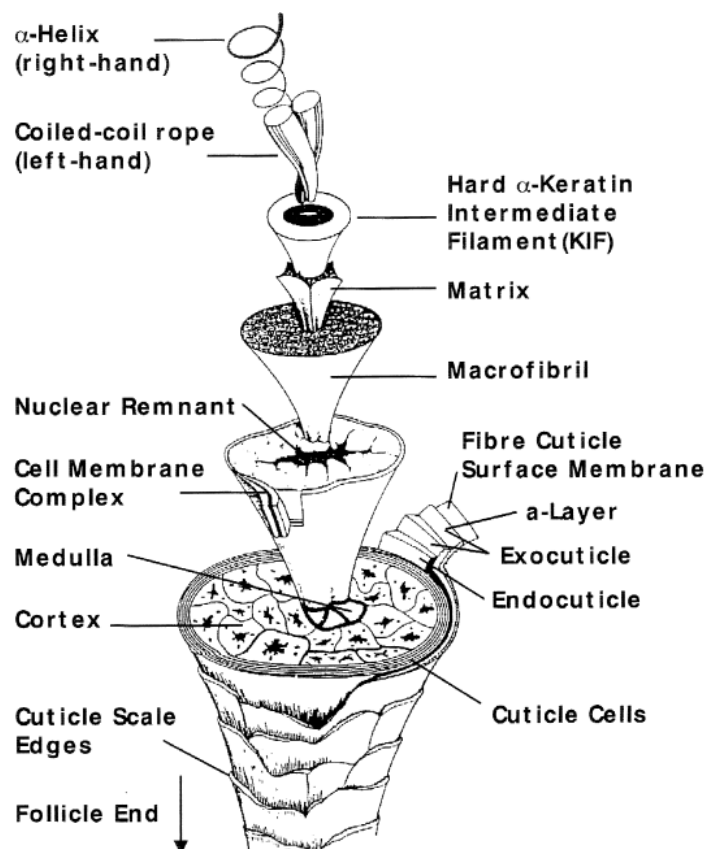
Figure 1.1: An exploded view of the human hair fibre. Diagram which shows an exploded view of the human hair fibre structure. Taken from Jones et al. 2001

During hair development the cuticle cells interlock and begin formation of layers within the cell. Organelles are degraded and replaced by laminae, occasionally leaving cellular remnants. In addition to these intracellular layers there is also the production of an extracellular resistant membrane known as the epicuticle (Jones and Rivett, 1997). The outer edge of each cuticle cell is coated with an epicuticle (Negri et al., 1993) which consists of a highly cross-linked protein matrix covalently bound by lipid; largely 18-methyleicosanoic acid (18-MEA). This lipid layer is termed the F-layer (Jones and Rivett, 1997; Wertz and Downing, 1989). This approximately 13 nm-thick layer provides a highly resistant hydrophobic barrier essential for the surface properties of hair (Jones, 2001; Leeder and Rippon, 1985).

The thickness of an individual cuticle cell is between 0.2 and 0.5 μm thick. Within each cuticle cell are 3 distinct layers which may be seen as laminations using transmission electron microscopy (Rogers, 1959). The outermost of these laminations is the α-layer, an approximately 110 nm-thick layer which is significantly cross-linked by both disulphide (cysteine – cysteine) and isopeptide (glutamine – lysine) bonds. This cross-linking results in a chemically resistant barrier (Rice et al., 1994).
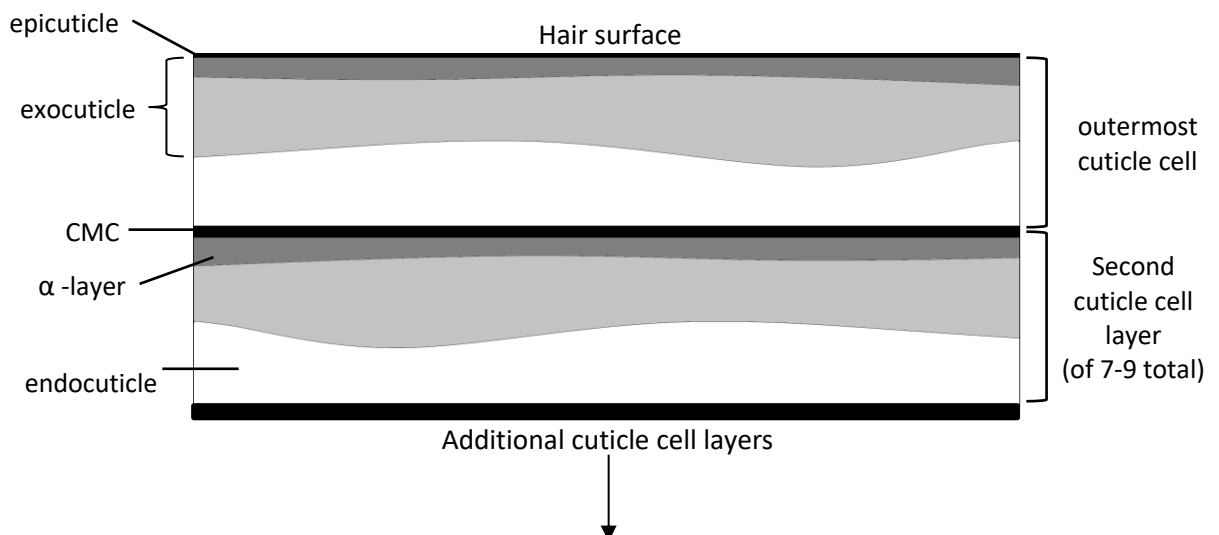
Figure 1.2: The organisation of the hair cuticle. *Diagram which illustrates a transverse section of the cuticle layers.*

The α-layer may be described as the upper part of the exocuticle, the layer immediately beneath the α-layer. This layer varies in thickness greatly, between 100 and 300 nm, within a single cell (Swift, 1999). The exocuticle is stabilised by significant disulphide cross-linking but lacks the isopeptide bonds of the α-layer (Swift, 1999). The endocuticle, varying between 50 and 300 nm thick, is beneath the exocuticle and is the innermost layer of an individual cuticle cell (Swift, 1999). This layer is the least cross-linked of the 3 layers, possessing no isopeptide bonding and a relatively low amount of disulphide cross-linking (Robbins, 2012).

In summary, around two thirds of the cell is exocuticle, including the alpha layer, the final third is made up by the endocuticle (Rogers, 1959). The high cysteine content, disulphide cross-linking, and isopeptide bonds of the cuticle, particularly in the exocuticle and α-layer, likely contribute significantly to stability. It is probable that the cuticle's barrier function and its ability to regulate water movement is dependent upon this extensive cross-linking (Rogers, 1959). However, the exact mechanism of the barrier function, and how compounds surpass it, is not fully understood (Jones, 2001).

1.1.2. Hair Cortex Structure and Composition

The vast majority of the hair fibre volume is provided by the cortex. This region contains longitudinally orientated spindle shaped cortical cells. These cells are approximately $1 - 6$ µm in diameter and 100 µm in length. During hair development, keratinization occurs where organelles are degraded and cells become tightly packed with keratin and associated proteins. During this process keratins are arranged as elongated filaments termed KIFs, which are in turn surrounded by an amorphous matrix of keratin associated proteins (KAPs). These KIFs are approximately 7.5 nm in diameter and can be seen in the cell's ultrastructure using TEM, appearing as lightly stained filaments surrounded by a densely stained proteinaceous matrix (Birbeck and Mercer, 1957; Rogers, 1959).

The combination of KIFs and KAPs results in the formation of macrofibrils throughout the hair cortex. These macrofibrils are semi-crystalline and can vary in diameter between $100 - 400$ nm (Bhushan, 2010). Previous studies in wool have identified different forms of cortical cell due to variation in the arrangement of macrofibrils (Birbeck and Mercer, 1957; Rogers, 1959). The orthocortex may be described as containing helically arranged KIFs, whereas the paracortex contains hexagonal parallel KIFs. The arrangement of paracortex and orthocortex regions within a fibre is thought to have a role in the macroscopic appearance of the hair, in particular the curl of the hair, where orthocortex occupies the convex fibre half and

paracortex is present in the concave fibre half (Matsunaga et al., 2013; Nagase et al., 2008; Orwin et al., 1973; Plowman et al., 2007).

1.1.3. <u>The Cell Membrane Complex</u>

The cell membrane complex (CMC) is a continuous network which spans the fibre and allows intercellular connections between individual cuticle and cortical cells in addition to connecting the cuticle and cortical layers. The CMC is composed of an approximately 15 nm – thick, low cross-link density proteinaceous layer, known as the δ-layer (Rogers, 1959). The δ-layer is then surrounded by lipids layers known as β-layers (Swift, 1999). There is also an intracellular membrane-associated layer, termed the i-layer which assists in the stabilisation of the CMC (Swift, 1999).

The proteins present in the δ-layer of the CMC are poorly characterised due to the difficulty of their extraction. They are thought to be non-keratinous globular proteins, with evidence suggesting the presence of glycoproteins (Leeder and Marshall, 1982; Robbins, 2009). In some cases the extraction of non-keratinous protein, thought to originate from the δ-layer, was achieved (Leeder and Rippon, 1985). Proteins which have been identified from the cuticle CMC include plakophilins, which are involved in the formation of the intracellular plaque in desmosomes, and desmogleins, desmosomal cadherins. This evidence suggests that the δ-layer could be a desmosomal remnant (Alibardi et al., 2013; Swift, 1999).

However, the composition of the CMC is known to vary depending on the location within the fibre. Differences in the cuticle and cortical CMC can be seen following histochemical staining, and due to varying effects of enzymes and reducing agents. The CMC of the cuticle has been shown to be more resistant to reducing agents, this suggests the presence of isopeptide cross-linking, as in the exocuticle (Orwin, 1979; Robbins, 2009).

The β-layers of the CMC vary depending on the location within the hair and also whether they are above or below the central δ-layer. The outer β-layer of the cuticular CMC contains a substantial quantity of covalently bonded 18-MEA, which becomes the new F-layer of the epicuticle at the hair's outermost surface when cuticle cells are lost (Wertz and Downing, 1989). On the other hand, the β-layers of the cortex are lipid bilayers containing no 18-MEA. Instead, the cortical CMC contains mostly fatty acids and cholesterol sulphate which are attached by only polar and ionic bonds to the cortical cell membranes and the δ-layer (Jones and Rivett, 1997; Robbins, 2009, 2012).

The CMC allows an alternative to the intracellular route for infiltration, providing access throughout the fibre. The β-layers provide a pathway for large hydrophobic reagents whereas the δ-layer may offer a route for the uptake of hydrophilic substances. Evidence shows that damage to this layer allows greater uptake of dyes and other reagents into the hair (Inoue et al., 2007; Naito et al., 1992). Therefore, the CMC plays an important but poorly understood role in the barrier function of the fibre.
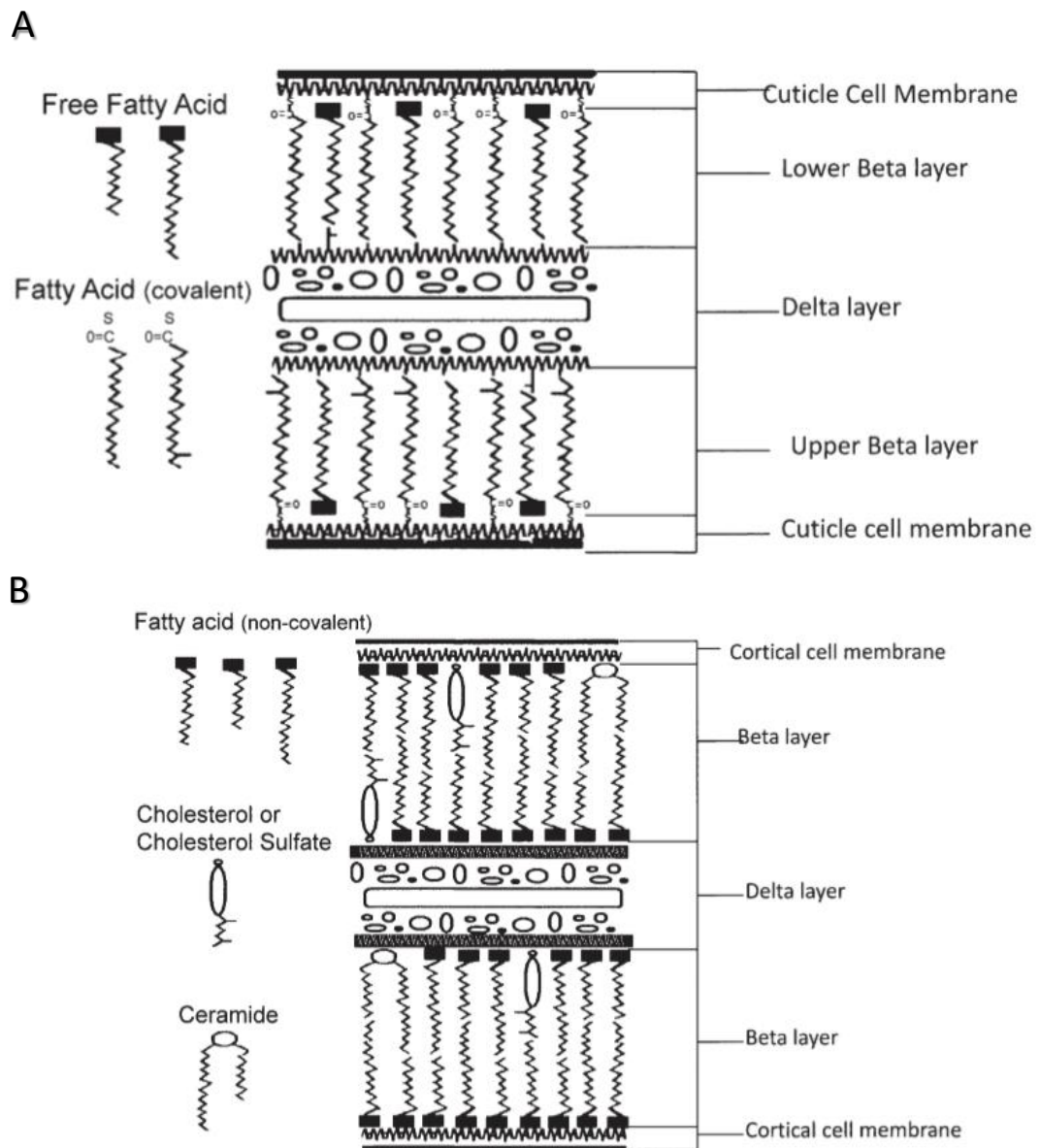
Figure 1.3: The composition of the cell membrane complex. *Schematic illustrating the composition of the cuticle (A) and cortical (B) cell membrane complexes. Taken from Robbins, 2009.*

1.1.4. The Medulla

The medulla in human hair is not always present. The presence of the medulla varies between individuals, and indeed between single hairs. When present, the medulla is a central column of loosely packed cells combined with vacuoles and may be either continuous or interrupted. Little work has been done with a focus on the human scalp hair medulla. However, it has been noted that occurrence generally increases in correlation with diameter of the hair fibre. The morphology of the medulla seen using scanning electron microscopy (SEM) includes cortical cells in an unorganised array, globular structures, and a smooth covering layer. TEM has previously been used to observe that the column contains KIFs much like cortical cells, therefore resembling a disorganised cortex, and is separated from the cortex by a CMC-like material (Clement et al., 1981; de Cássia Comis Wagner et al., 2007)

Isolation and extraction for further characterisation has proven difficult, in part due to its location at the centre of the fibre in addition to the non-obligatory nature. On the other hand, difficulties in solubilisation are thought to be due to the presence of isopeptide bonds. Again, due to its non-obligatory nature and central location, the medulla is not considered to hold a significant role in hair chemistry or physical properties (Bradbury and O'shea, 1969; Jones, 2001).

1.1.5. Organelle Remnants

Structures within the hair termed organelle or nuclear remnants are occasionally visible in cortical cells using fluorescence microscopy (Szabo et al., 2012). These are often regarded as nuclear remnants however there remains the possibility that these structures are in fact remnants from alternative organelles. There is little evidence for either of these arguments (Harland et al., 2014; Kelch et al., 2000). Nuclear remnants are thought to be the result of chromatin breakdown in the nucleus when hair keratinocytes begin terminal differentiation, leaving the nuclear envelope intact (Fischer et al., 2011; Szabo et al., 2012).

1.2. Protein components of hair

As discussed, lipids form several compartments in hair, most notably the F-layer of the epicuticle and the β-layers of the CMC throughout the fibre. Melanin is also an important component of hair, providing both the natural colouration of the fibre in addition to a photo-protective effect. However, the major component of hair is protein (Robbins, 2012). The cortex and cuticle layers are distinct in regard to protein composition but both of these

partitins are composed largely of keratins in the form of KIFs surrounded by a matrix of cysteine-rich proteins, namely KAPs (Rogers et al., 2006).

1.2.1. Keratins

Keratins are intermediate filament proteins which are responsible for a structural role in the cytoskeleton of many eukaryotic cells (Cooper, 2000). Certain keratins are also involved in keratinisation, occasionally termed cornification, where the cytoplasm of a cell is replaced largely by keratin intermediate filaments (KIFs). In some cases, such as in the epidermis of the skin, this may be referred to as soft keratinisation. Keratinisation in hair is referred to as hard keratinisation and the keratins involved are a subset of all human keratins, often termed hair-specific or hard keratins (Bragulla and Homberger, 2009; Langbein and Schweizer, 2005).

Keratins form KIFs through the combination of an equal number of type I and type II keratins (Crewther et al., 1983). Within hair, these KIFs are then surrounded by a matrix of relatively high-cysteine KAPs to produce macrofibrils which fill the cells of the hair fibre resulting in a rigid structure (Rogers, 1959).

Keratins, their structure, and their role in both the cytoskeleton and hair fibre are detailed in further depth within chapter 4.

1.2.2. KAPs

As described, KAPs are the second major protein component in hair and are relatively high in cysteine in comparison to keratins. These KAPs form a matrix of protein which surrounds KIFs and allows for the creation of macrofibrils (Bhushan and Chen, 2006; Rogers, 1959). The importance of KAPs for hair formation has been described, with KAP gene diversity correlating with hair evolution in mammals (Khan et al., 2014) and the association of these genes with shape variation in human hair (Liu et al., 2018).

A large number of KAP gene sequences have been described (Wu et al., 2008), and the expression of KAP mRNA during hair fibre production has been investigated (Rogers et al., 2006). However, their specific mechanism for interaction with keratin, and therefore stabilisation of the hair fibre, is poorly understood. It is likely that, due to KAP amino acid composition, interactions between KAPs and keratins occur through di-sulphide bonding (Powell et al., 1991).

However, KAPs vary dramatically in their cysteine content and in fact fall into three KAP families based upon amino acid composition: high sulphur (HS), ultra-high sulphur (UHS), and high glycine tyrosine (HGT) (Gong et al., 2012; Wu et al., 2008). Therefore, it is possible that certain KAPs may interact via alternate means with keratin or other binding partners, providing stability for the hair fibre through a variety of means (Rogers et al., 2007). Additionally, although the matrix of KAPs has previously been described as amorphous and perhaps considered to be unordered, recent work suggests there may be organisation of these KAP proteins, rather than complete homogeneity (Kadir et al., 2017). These findings further suggest that the large repertoire of KAPs expressed in hair may have discreet functions which are not yet understood.

KAPs, their expression within hair, and existing work aiming to characterise the function of these KAPs is described further during the introduction of chapter 4.

1.3. Melanin

Proteins found within hair, such as the main component keratin, are colourless. The primary source of natural colouration in hair is due instead to the presence of melanin granules. These granules are found primarily in the cortex and are most dense towards the outer surface of the cortex. Melanin determines hair colour due to its total amount, the size of granules, and the ratio between the two forms of melanin present, eumelanin and pheomelanin (Harrison and Sinclair, 2003).

In dark brown and black hair eumelanin is more prominent. In red and blonde hair there is less total melanin, and pheomelanin makes up a larger proportion (Ito and Wakamatsu, 2011). Both forms of melanin are derived from a common precursor dopaquinone which is formed from tyrosine (Riley, 1997).

Melanin forms in granules roughly 1 µm x 0.4 µm with the long axis parallel to the hair fibre, these granules are situated mainly between the closely packed keratin filaments of the cortex (Choi et al., 2012; Ulrich et al., 2004). Melanin has a broad absorption spectrum between the near-UV and near-infrared regions, eumelanin absorbs UV light unlike pheomelanin and so has a photo-protective effect on the hair proteins (Dimitrow et al., 2009).

1.4. Hair fibre production

The hair follicle is responsible for the production of hair fibre. At the base of the hair follicle is the bulb, which comprises the dermal papilla surrounded by the matrix and is where

proliferation takes place within the follicle (Schmidt-Ullrich and Paus, 2005; Schneider et al., 2009). The hair follicle is subject to the hair growth cycle, which consists of four stages, comprising: anagen (growth), catagen (regression), telogen (quiescence), and exogen (shedding) (Higgins et al., 2009).

Differentiation occurs during anagen. Here, stem cells which originate from the bulge, located in the outer root sheath (ORS), migrate to the bulb around the dermal papilla and continuously bud off daughter cells, these continue to divide until differentiating into cells of the ORS, inner root sheath (IRS), and, in the case of cells of the hair matrix, the hair shaft (Langbein and Schweizer, 2005; Oh et al., 2016; Panteleyev et al., 2001). Cells of the hair fibre undergo changes in shape, cell junctions, and position while within the bulb alongside the expression of hair-specific keratin. Beyond the bulb, as cells continue to migrate upwards, there is a period of controlled expression of keratin and KAP genes (KRTs and KRTAPs respectively) in a process termed keratinisation (Harland and Plowman, 2018).
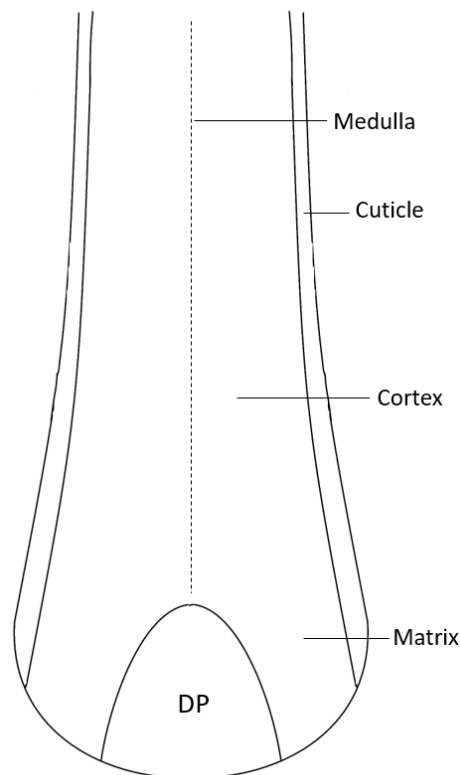
Figure 1.4: Schematic of hair synthesis within the hair follicle. *Diagram summarising the regions of the hair follicle during fibre production with the layers of hair and the dermal papilla (DP) labelled. Image adapted from Rogers, 2006.*

During keratinisation, KIFs are formed first (Langbein et al., 2001, 1999), followed by expression of a subset of KAPs, the HGT KAPs in particular (Rogers et al., 2006), resulting in stiffening of the fibre without the requirement of di-sulphide bonds (Bornschlögl et al., 2016). Finally, the remaining KAPs, which are high in cysteine, are expressed (Rogers et al., 2006a) and are likely oxidised in order to form di-sulphide bonds to stiffen the fibre. Additionally, desmosomes and other cell adhesions proteins are thought to become part of the CMC during this process (Alibardi et al., 2013). Keratinisation also involves the breakdown of the non-keratinous cell components such as the nuclei, which become elongated and degenerate. Finally, water is lost throughout keratinisation to eventually result in the fibre in its mature form (Alibardi, 2017; Harland and Plowman, 2018).

1.5. <u>Hair damage occurring from cosmetic or natural means</u>

Cosmetic hair products act upon the fibre in a variety of ways. The mechanism of action for these treatments is reasonably well understood. For example, changes are made to the organisation of the hair fibre during perming and straightening treatments which aim to alter the arrangement of proteins to modify hair's macroscopic properties (Dawber, 1996). Alternatively, bleaching and colouring products reach their desired outcome by either destroying or depositing natural and synthetic pigments respectively (Guerra-Tapia and Gonzalez-Guerra, 2014; Robbins, 1988).

Damage to the hair can arise through a variety of means, including through the process of using these cosmetic treatments which may produce unwanted, negative effects upon the hair. Alternatively, damage may be physical in nature, perhaps due to regular wear, or additionally due to natural photochemical insults such as exposure to UV radiation by sunlight (Longo et al., 2013).

Damage accumulation may result in undesired changes to the texture and appearance of hair due to alterations to the hair's surface morphology and chemical composition. In addition to being undesirable the damage may lead, in very extreme cases, to partial alopecia due to hair breakage (Ahn and Lee, 2002). A method for rapid detection and quantification of chemical change to the hair would be particularly useful to allow comparison of the efficacy of treatments and the accompanying damage.

However, methods to compare both the efficacy of treatments and additional unwelcome changes and damage to the hair are often qualitative. For example, a comparison may simply be accomplished through an individual's impression and opinion on the feel or appearance of treated hair. Other efforts may include the use of electron microscopy (EM) (Imai, 2011),

and atomic force microscopy (AFM) (Gurden et al., 2004) to detect and quantify damage. However, even these high-resolution techniques produce only semi-quantitative results, and are particularly affected by hair fibre variability between individuals. Also, these techniques provide information relating largely to just the hair cuticle and surface damage where sample preparation, particularly in the case of EM, can introduce artefacts. Another more quantitative means of examination is through chemical analysis, such as the quantification of cysteine or tryptophan (Dario et al., 2017; Fedorkova et al., 2014; Joo et al., 2016). This method is useful for accurately quantifying the degree of chemical change occurring. However, chemical analysis can be time-consuming and requires complete destruction of the sample, removing the possibility of investigating dynamic or spatial changes to the sample.

1.6. <u>The use of fluorescence for imaging of hair</u>

Much imaging of hair to date is completed using fluorescence, which may be through the use of fluorescent dyes which allow targeted or broad staining of structures within samples, and multiple dyes of different fluorescence characteristics may be used simultaneously. (Brady, 1992; Ehlers et al., 2007, 2006; Kelch et al., 2000).

However, hair alone is capable of fluorescence, also termed auto-fluorescence. This property is useful in allowing label-free imaging of the fibre using fluorescence microscopy. Techniques such as FLIM can derive chemical information from a sample by observation of this autofluorescence. However, due to hair autofluorescence, care must also be taken when attempting to visualise other fluorescent compounds within the hair to ensure that the fluorescence does not originate from endogenous fluorophores of the hair.

Within hair, the primary fluorescent component is the protein. In all proteins, there are fluorophores present in the form of the aromatic amino acid residues, tryptophan, tyrosine, and phenylalanine, in addition to cysteine. These largely absorb in wavelengths in the UV region (250 nm – 320 nm) (Millington, 2006). However, work completed using wool found fluorophores present which absorb within the visible spectrum, thought to be a mixture of protein oxidation products and forming part of the major protein structure of wool, rather than impurities or intercellular material (Melhuish and Smith, 1993; Simpson et al., 2002).

Human hair has also been the subject of similar studies, with findings suggesting that a series of emission peaks from 395 nm to 500 nm were attributed to products of oxidation or metabolic transformation of tryptophan. Namely, the fluorescent products were thought to be, N-formylkynurenine, kynurenine, and 3-hydroxykynurenine, with emission maxima of 420 nm, 460 nm, and 495 nm respectively. These compounds are thought to be responsible

for much of hair autofluorescence at visible wavelengths and are also expected to be the cause of photo-yellowing seen in hair and wool (Daly et al., 2009; Jachowicz and McMullen,
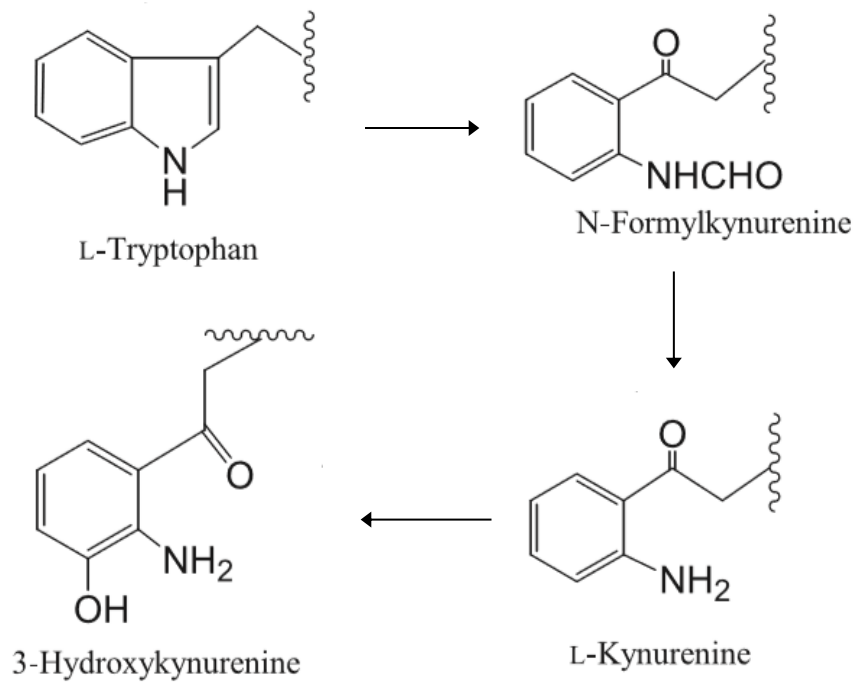
Figure 1.5: Metabolic and photo-oxidation products of tryptophan. *Schematic detailing the conversion of tryptophan to a number of fluorescent oxidation products. Image adapted from Daly et al. 2009.*

2011).

1.7. Advanced light microscopy techniques

Laser scanning confocal microscopy (LSCM) is a technique which uses the principle of fluorescence, whether this is autofluorescence, the localisation of a fluorescent stain, or a fluorophore conjugated to an antibody, in order to gather information on a sample. Samples are excited by a narrow beam of laser which is rapidly scanned across a sample. This property of the laser also allows for excitation and photobleaching of distinct regions of a sample which is utilised during fluorescence recovery after photobleaching (FRAP), allowing the visualisation of lateral fluorophore movement (Figure 1.6) (Axelrod et al. 1976).

A distinction between widefield fluorescence microscopy and LSCM exists due to the use of a pinhole, which prevents out of focus light from reaching the detector and therefore provides high resolution imaging (Figure 1.7). Additionally, this removal of out of focus light results in an optical section of a 3D sample. By gradually altering the focus and acquiring a series of these optical sections, a representation can be reconstructed of a 3-dimensional specimen such as hair (Lagarde et al., 1994; Pawley, 2006; Wilson, 2011).

However, removal of the out of focus light also reduces the amount of light reaching the detector, this can be an issue, particularly when the fluorescent signal is weak, and result in a low signal to noise ratio (SNR). While the pinhole can be increased in size to increase the image signal, this subsequently blocks less light, lowering the resolution and the ability to produce optical sections (Wilson, 2011).

Furthermore, there exists a limit to the resolution which can be gained through the use of conventional light microscopy. Simply, this is due to the fact that the resolution of a light microscope cannot be higher than half of the wavelength of the light (Huang et al., 2009). There exist techniques which aim to improve the resolution and SNR available through traditional LSCM while still being compatible with typical fluorophores.
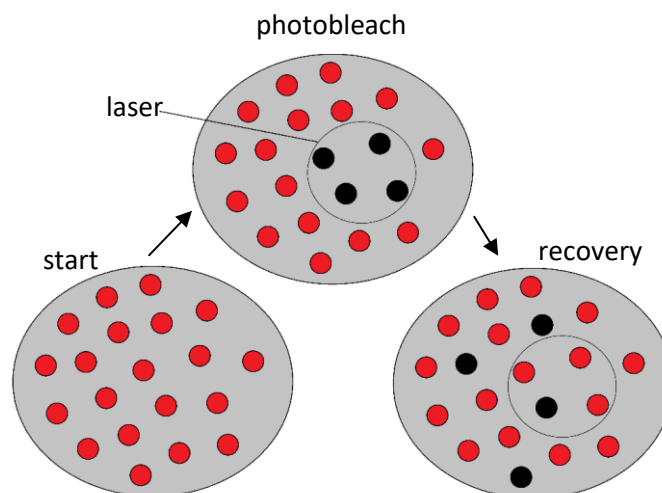
Figure 1.6: The principles of fluorescence recovery after photobleaching. Schematic detailing the process of FRAP. A sample contains fluorophores (red) before laser is selectively applied to a designated region to result in photobleaching (black). Recovery of fluorescence to this region, due to fluorophore movement, is then observed.
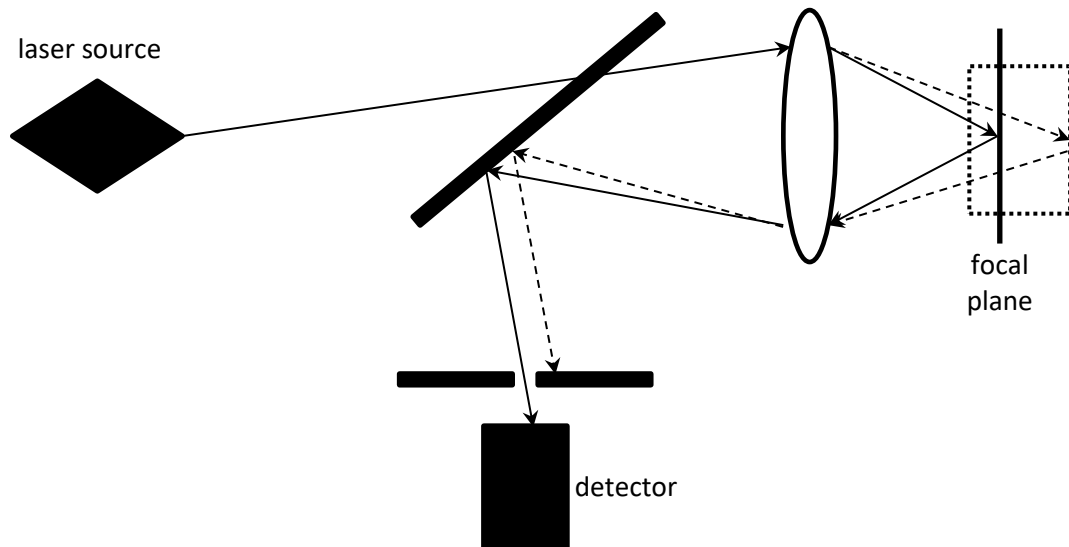
Figure 1.7: Schematic of an LSCM system. *Schematic detailing the action of a pinhole upon light returning from a sample. Only light which is emitted from the focal plane is able to pass through the pinhole. Image adapted from Wilson, 2011.*

The Zeiss Airyscan detector is a relatively new technology which provides improved resolution and SNR through the application of a hexagonally packed array of detectors, rather than the traditional pinhole design. This array of detectors combines the resolution benefits of a small pinhole (0.2 airy units) with the light collection, and therefore SNR, of a large pinhole. The Airyscan detector offers immediate benefits over traditional confocal microscopy systems by increasing both the spatial resolution and the SNR of all images while maintaining the optical-sectioning ability of a traditional confocal microscope. Additionally, the Airyscan uses linear deconvolution in order to achieve high resolution in all dimensions (140 nm in x and y, and 400 nm in z) (Huff, 2015).

Three-dimensional structured illumination microscopy (3D-SIM), performed using the Deltavision OMX during this work, also provides increased resolution over conventional LSCM. This involves the application of a pattered illumination field, the spatial frequencies of which mix with those of the sample features resulting in lower frequencies which are detectable by the microscope. Multiple images are acquired with illumination patterns of different phases and orientations to result in a resolution of approximately 100 nm in the lateral directions, and around 300 nm in the z direction (Huang et al., 2009).

FLIM is also used during this work and is distinct in observing the fluorescence decay, or lifetime, of a fluorophore, rather than its steady state fluorescence. FLIM is described further in chapter 3.

1.8. <u>Aims</u>

- To investigate hair and its keratin associated proteins using advanced light microscopy.

- To quantify and further understand hair damage using single-photon FLIM and correlative techniques such as 2D-SDS-PAGE and LC-MS.

- To functionally characterise the cell biology of a wide variety of KAPs within HaCaT keratinocytes, both alone and in the presence of hair-specific keratins, using advanced light microscopy techniques.

- To observe the movement of a range of fluorescent dyes into the hair fibre in order to determine uptake pathways.

2. Materials and Methods

2.1. Molecular Cloning

2.1.1. Bacterial Strains

The following *Escherichia coli* strains were used: DB3.1 for amplification of empty gateway vectors and DH5α for cloning of KAP coding sequences into gateway vectors.

2.1.2. Vectors used

The following vectors were used during this study:

Vector Name	Selection Antibiotic	Description
pDONR207	Gentamicin	Gateway donor vector
pEZYeGFP	Kanamycin	Gateway destination vector for mammalian expression under CMV promoter resulting in N-terminal eGFP-tagged fusion protein
pDESTmCherry-N1	Kanamycin	Gateway destination vector for mammalian expression under CMV promoter resulting in C-terminal mCherry-tagged fusion protein

Table 2.1: Vectors used during this study.

2.1.3. Chemically competent cells

Chemically competent bacterial cells were required for cloning. LB broth was prepared and autoclaved and an overnight culture of the desired *E. coli* strain was incubated at 37°C. This culture was then used to inoculate LB broth at a ratio of 1:100 and this was incubated at 37°C for 3.5 hours. This culture was then cooled on ice for 60 min and kept cold for the remainder of the protocol.

The culture was then centrifuged at 3000 x g for 10 min and cells resuspended in a volume of 80mM $MgCl_2$, 20mM $CaCl_2$ equal to 1/2 of the previous culture volume. Centrifugation was repeated, and cells resuspended in a volume of 100mM $CaCl_2$, 30 % glycerol equal to 1/100 of the original culture volume. Aliquots of cells were then frozen in LN_2 and stored at -80°C until use.

2.1.4. Transformation of *E. coli*

In order to transform *E. coli*, approximately 100 ng plasmid DNA was added to 100 μl chemically competent cells and incubated on ice for 30 min. Cells were then warmed to 42°C for 45 seconds using a heat block before chilling on ice for 2 min. 500 μl LB broth was then

added and recovery took place over 1 hr, shaking, at 37˚C. An appropriate volume of cells was then used for spreading on solidified LB-agar plates containing an appropriate selection antibiotic. Plates were incubated at 37˚C for 18 hours.

2.1.5. Plasmid DNA purification

The Promega Wizard Plus SV miniprep kit was used as per kit instructions for plasmid DNA purification. Single colonies of interest were picked for inoculation of 5 ml LB broth containing appropriate selection antibiotic. This culture was incubated, with shaking, at 37˚C for 18 hr before centrifugation at 3000 x g for 5 min. The cell pellet was resuspended and lysed per kit instructions before neutralisation. Spin columns were then used according to instructions to bind, wash, and elute the plasmid DNA in nuclease-free water.

2.1.6. Agarose gel electrophoresis

Agarose gels were used during cloning to confirm the length of inserted DNA fragments. Gels were prepared by dissolving 1.5% Agarose in 1x TAE buffer (40mM Tris-acetate, 1mM EDTA (Ethylenediaminetetraacetic acid)) with microwaving. Ethidium bromide was subsequently added to a final concentration of 0.5 μg/ml before the mixture was poured into gel trays incorporating a comb and allowed to set.

DNA loading buffer blue 5X (Bioline) was added to DNA samples prior to loading. GeneRuler 1kb Plus (ThermoFisher) DNA ladder was used as a molecular weight standard. Gels were run using an electrophoresis tank containing 1X TAE buffer for approximately 30 min at 100V.

2.1.7. Amplification of fragments using PCR

Polymerase chain reaction (PCR) was used to amplify desired fragments from gDNA. For cloning, high-fidelity polymerase Phusion (NEB) DNA polymerase was used as per instructions. PCR master mix was prepared to result in individual reactions as follows: 4 μl 5X HF buffer, 12.4 μl nuclease-free dH_2O, 0.4 μl 10mM dNTPs (dATP, dGTP, dCTP, dTTP), 1 μl/each forward and reverse primers (IDT), 1μl appropriate template DNA, 0.2μl Phusion DNA polymerase. PCR reaction was carried out as detailed in table 2.2.

PCR Step	Temperature (°C)	Duration (s)	Num. Cycles
Denaturation	98	30	1
Denaturation	98	10	
Annealing	60[1]	15	30
Extension	72	30[2]	
Extension	72	300	1

Table 2.2: PCR reaction parameters. *1: Annealing temperature was typically set to 5°C below primer T_m which was approximately 65°C. 2: Extension duration was set to 30s/kb, with a minimum of 30s which was sufficient for majority of desired fragments.*

2.1.8. Gateway cloning system

Gateway cloning was used in order to prepare constructs for expression in mammalian cells. The Gateway cloning system (Invitrogen) involves a BP reaction for insertion of desired fragments into a donor vector followed by an LR reaction to insert these fragments into destination vectors.

2.1.9. BP reaction

For insertion of amplified DNA, containing gateway ends, into pDONR207 a reaction was prepared containing 1 µl BP clonase II enzyme, 2 µl PCR product of interest, 100 ng pDONR207, and nuclease-free H_2O to create a reaction volume of 5 µl. The reaction was incubated at 25°C for 2 hrs and terminated through the addition of 1 µl Proteinase K and incubation at 37°C for 10 min.

Terminated reaction was then used for the transformation of chemically competent DH5α as described previously and plated onto LB-agar containing 25 µg/ml gentamicin. Success of the reaction was determined by DNA sequencing of the inserted fragment.

2.1.10. LR reaction

In order to transfer desired fragments from pDONR207 into the destination vector, the LR reaction was used. The reaction consisted of 1 µl LR Clonase II enzyme, 100 ng pDONR207 containing fragment of interest, 100 ng desired destination vector, and was made up to 5 µl using nuclease-free dH_2O. As with the BP reaction, incubation was necessary at 25°C for 2 hrs and terminated with addition of 1 µl Proteinase K and incubation at 37°C for 10 min. The reaction was used for transformation of DH5α *E. coli* and cells were plated onto LB-agar containing appropriate selection antibiotic. DNA sequencing was used to confirm that the fragment was inserted correctly.

2.1.11. DNA Sequencing

The internal genomics facility; Durham University Biological Sciences (DBS) Genomics, was used for all DNA sequencing reactions, using an Applied Biosystems 3730 DNA Analyser.

2.2. Cell culture

2.2.1. Mammalian Cells

Cells used were HaCat cells, which are a spontaneously immortalised keratinocyte cell line derived from adult human skin.

2.2.2. Passaging of cells

HaCaT cells were maintained in DMEM supplemented with 10% FBS, incubated at 37°C with 5% CO_2. Regular passaging of cells was carried out to maintain a confluence below 90%. Before trypsinisation, cells were first rinsed briefly in pre-warmed versene. Trypsin (0.05% trypsin in versene) was added for 15 min while incubating at 37°C before cells were dislodged through agitation of the cell culture flask. Trypsin was then diluted with an equal quantity of pre-warmed media and the cells were pelleted by centrifugation for 5 min at 200 x g. The pellet was then resuspended in media and used for re-seeding of cell culture flask or for seeding of glass-bottomed cell dishes or round coverslips for live cell imaging or indirect immunofluorescence respectively.

2.2.3. Transfection of HaCat cells

Transfection required the seeding of cells into either 35 mm glass-bottomed cell dishes (Ibidi) or onto round coverslips in a 12-well plate for live cell imaging or indirect immunofluorescence respectively. In either case, cells were seeded into 1.5 ml DMEM, containing 10% FBS, in order to reach 70% confluence following 24 hrs incubation. The number of cells required for this was approximately 150,000 per dish/well.

JetPEI (Polyplus Transfection) was used for transfection. A single transfection mixture for either a dish or a well consisted of 4 µl jetPEI reagent, 2 µg plasmid DNA, and a volume of 150 mm NaCl to result in a total of 100 µl. This mixture was vortexed and incubated at room temperature for 30 minutes. Media was aspirated from the HaCaTs and 1.4 ml fresh DMEM containing 10% FBS was added to the cells, seeded 24 hrs prior, and then the transfection mixture added dropwise. The vessel was then swirled gently before being returned to the cell culture incubator. Cells were incubated for 24 hrs before either live-cell imaging or fixation and indirect immunofluorescence.

2.3. Imaging of live cells

Imaging of live transfected HaCaTs required cells which were seeded and transfected on 35 mm glass bottomed dishes (Ibidi). Cell culture media was aspirated from the dish immediately prior to imaging and replaced with live cell buffer (75mM NaCl, 10mM HEPES, 0.5mM $CaCl_2$, 2.5mM KCl, 0.5mM $MgCl_2$) which does not contain phenol red and is therefore compatible with LSCM. In order to preserve the cells over the course of imaging, the Zeiss 880 heating chamber was heated to 37˚C and 5% CO_2 was supplied. Cells were imaged using the 1.4NA 63x oil immersion objective and excited with the appropriate laser. In the case of eGFP the 488 nm laser was used, mCherry was excited using the 594 nm laser. The Airyscan function of the Zeiss 880 was used to increase sensitivity and spatial resolution.

2.4. Cell fixation and indirect immunofluorescence

Fixation of HaCaT cells was required before indirect immunofluorescence in order to label cytoskeletal components. This process was performed on cells seeded and transfected on round coverslips as described previously. Media was aspirated from the well containing the coverslip and cells were simultaneously fixed and permeabilised for 30 min (3.7% PFA, 5mM EGTA, 50mM PIPES, 2mM MgSO4, 0.5% Triton X-100 and 0.02% glutaraldehyde). The coverslips were then briefly washed 3 times using 1X PBS. Blocking solution (1% BSA, 0.2% fish skin gelatin in 1X PBS) was then added and incubated at room temperature for 10 min. Coverslips were washed a further 3 times in 1X PBS before addition of primary antibody diluted in blocking solution at the dilutions stated in table 2.3. Following incubation at room temperature for 1 hr, the coverslips were washed 3X in PBS. Secondary antibody was then added, diluted in blocking solution with ratios detailed in table 2.3, and incubation carried out for 30 min. Coverslips were washed 3X in PBS and DAPI stain (0.1 µg/ml DAPI in PBS) was added for 10 min. Final 3X PBS washes were carried out and coverslips were then mounted on glass microscope slides using Vectashield before sealing with nail polish.

Type	Target	Other information	Dilution
Primary	Keratin 14	Rabbit monoclonal	1:100
Primary	α-tubulin	Rat monoclonal	1:250
Other	Phalloidin	594 nm	1:40
Other	DAPI	405 nm	0.1 µg/ml
Secondary	Donkey anti-rabbit	594 nm	1:500
Secondary	Goat anti-rat	594 nm	1:500
Secondary	Donkey anti-rabbit	488 nm	1:500

Table 2.3: Antibodies used during this study.

2.5. Imaging of fixed cells

Prepared slides were imaged using the Zeiss Laser Scanning Confocal 880 Microscope with Airyscan. The 1.4NA 63x oil immersion objective was used for imaging in addition to excitation using lasers at wavelengths of 405 nm, 488 nm, and 594 nm.

2.6. Image analysis

The Image J package FIJI was used for image analysis and export. In addition, Just Another Colocalisation Analysis Plugin (JACoP), was used with FIJI for Pearson's and Manders's colocalization analysis. For this analysis, images were cropped to include only the transfected cell of interest, and thresholds were set at 1200 for both the red and green channels for calculation of Manders's overlap.

2.7. Hair samples

Untreated hair samples were sourced by Procter & Gamble and were categorised by their ethnicity and colour. During this project, single-source untreated brown hair ponytails from 3 individuals of European ethnicity were used for the majority of bleaching and dye uptake experiments. In select experiments, grey hair from a person of European ethnicity was used where individual hairs were selected from a ponytail, only hairs which were deemed white, rather than grey, were used to represent white hair. Additional blended brown hair samples were also supplied by Procter & Gamble and were used for initial protein experiments before switching to single-source hair.

2.8. Hair treatments

2.8.1. Heat treatment

Heat treatment was carried out by Procter & Gamble. Briefly, a flat iron was heated to 400˚F and was applied to a portion of hair from the top down at a rate of 2 cm/sec. Three strokes were carried out in quick succession before the hair is allowed to cool for 30 seconds. The 3-stroke procedure is then repeated five times until reaching a total of 15 strokes to complete 1 heating cycle.

2.8.2. Bleaching

Hairs were bleached at room temperature for 30 minutes under the conditions specified by the experiment. Bleaching solutions contained varying concentrations of H_2O_2 ($0 - 9$ % v/v) and NH_3 ($0 - 6$ % v/v). Where pH was to be lowered to remain equal, such as in the case of varying H_2O_2 which was supplied in an acidic solution, acetic acid was used. All bleaching

solutions contained 0.1 % EDTA as a chelator. Following bleaching, hairs were washed 3 times in dH$_2$O and allowed to air dry before imaging.

2.8.3. UV exposure

UV treatments were carried out by Procter & Gamble. Briefly, sun exposure was simulated through irradiation with an Atlas Ci3000+ weather-o-meter. Internal and outer quartz filters were used to simulate broad-spectrum outdoor daylight, with a specific irradiance of 1.48 W/m^2 at 420 nm. During irradiation, both temperature and relative humidity (RH) were kept constant at 35°C and 80% respectively. Hair used was single source, previously untreated, light brown hair made into 2 g flat switches. Switches were irradiated for 20, 50, 100 and 200 hrs, with portions from each fibre covered in aluminium foil to maintain internal controls.

2.8.4. Relaxer

Relaxer treatments were carried out by Procter & Gamble. Motions Smooth & Straighten relaxer was applied to the hair using a colouring brush and treatment carried out as per product instructions. The product was left on hair for 20 minutes, and the hair stretched gently using the colouring brush after 5 minutes elapsed. Hair was rinsed thoroughly after 20 minutes with warm water before Motions Neutralising Shampoo was used. Finally, hair was rinsed thoroughly before air drying.

2.8.5. Perming

Perming treatments were carried out by Procter & Gamble. Naturelle Omni Perm was used as directed by product instructions. After shampooing and towel drying hair, the activator and waving lotion were mixed before application to hair. After 20 minutes the hair was rinsed thoroughly then the neutralizer was applied. Samples were then rinsed thoroughly before drying.

2.9. Screening of fluorescence using Synergy H4 plate reader

The fluorescence of a range of hair dye components, formed dyes, and of whole hair was assessed using the Synergy H4 plate reader. In the case of hair dye components and formed dyes, aqueous 1% (w/v) solutions were loaded into 96-well plates and excitation was provided at discreet wavelengths which correspond to laser wavelengths available on the Zeiss 880 comprising 405 nm, 458 nm, 488 nm, 514 nm, 543 nm. In the case of whole hair, short fragments of hair were immersed in water within a 96-well plate and excitation was provided in 20 nm increments from 260 nm to 540 nm. A well containing only water was also

subject to this excitation and fluorescence values from this control were subtracted from those of hair.

2.10. Testing of fluorescent dyes in hair

The utility within hair of a range of fluorescent compounds was tested. Hair sections, approximately 2 cm in length, were cut and incubated in 1 % (w/v) solutions of hair dye compounds including resorcinol and 2-methylresorcinol. This solution also contained 2% (v/v) monoethanol amine unless otherwise stated. Following incubation times of specified lengths at 50˚C, hair fragments were rapidly washed in acetone before air drying. Stained hairs were imaged using a Zeiss 880 Airyscan Laser Scanning Confocal Microscope with a 1.4NA 63x oil immersion objective. A range of excitation wavelengths were used to excite the hair dye compounds

For Nile red staining of whole hair, as opposed to staining of cryo-sections, fibres were incubated in a solution of Nile Red (2 mg/ml) for 24 hrs at 37°C before rapid acetone washing to remove external stain. During imaging, using a Zeiss 880 Airyscan Laser Scanning Confocal Microscope with a 1.4NA 63x oil immersion objective, the 514nm laser line was used to excite the Nile red stain.

2.11. Hair imaging methods

2.11.1. Longitudinal imaging of hair samples

To enable imaging of the longitudinal optical sections of hair. Approximately 1 cm lengths of fibre were cut using scissors and mounted in immersion oil (Immersol 518F oil (Zeiss)) onto a glass microscope slide under a glass coverslip of No. 1 thickness. These coverslips were then sealed using micropore tape before imaging with the Leica SP5 or Zeiss 880 for FLIM or LSCM respectively.

2.11.2. Transverse imaging of hair sections without physical sectioning

In order to directly image the transverse section of hair fibres, without the need for microtome sectioning, a novel method was employed. Hairs were cut with a sharp razor blade perpendicular to their longitudinal axis into approximately 3 cm sections. To allow cross sectional imaging, hairs were placed in a glass capillary needle inside a 3D-printed stand (figure 2.1) with a central hole to contain the capillary tube. This assembly was then placed in a 35 mm glass-bottomed dish. The 3D-printed stand serves to hold the glass capillary needle in a stable position while allowing light to enter from the sides. The glass capillary needle holds one or several hairs in a predictable location at the centre of the dish, in contact with the cover-glass. This assembly allows imaging of razor-cut ends of hair fibres with an inverted microscope. Hairs were imaged using a Zeiss 880 Airyscan Laser Scanning Confocal Microscope with a 1.4NA 63x oil immersion objective.
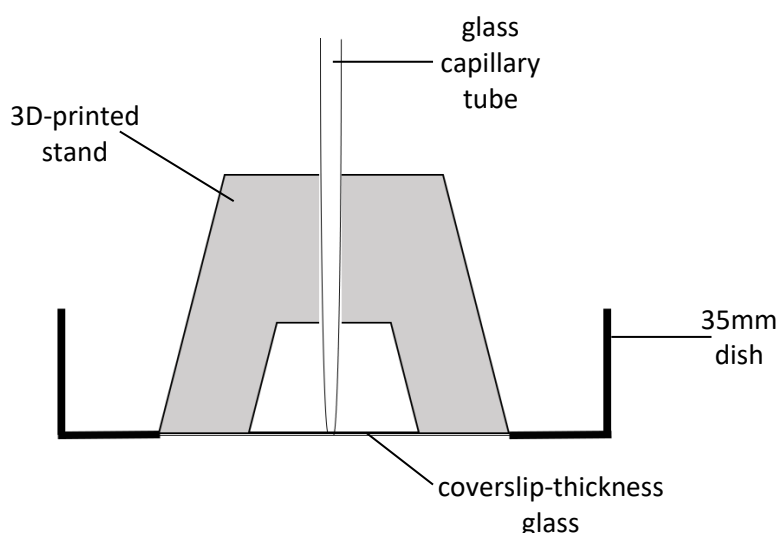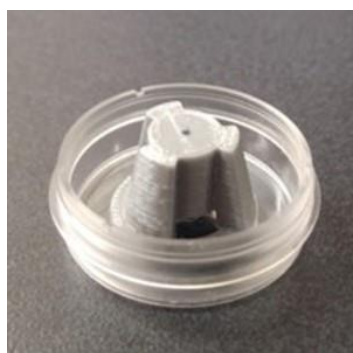
Figure 2.1: Assembly for imaging of hair transverse section. *The vertical imaging device (VID) comprises a 3D printed stand containing a glass capillary needle. This is placed securely into a 35 mm coverslip-thickness glass-bottomed dish.*

2.11.3. Cryo-sectioning of hairs for Nile Red labelling

In order to apply Nile red directly to hair sections without the use of resin, which was heavily stained with Nile red, cryo-sectioning was utilised. Several hairs of approximately 2 cm length were placed into thin plastic tubing approximately 4 mm in diameter. Fifteen % (w/v) gelatin solution was added and samples were frozen at -20°C for 18 hrs. The tubing, containing the hairs frozen within gelatin was then cut with a razor blade into lengths of approximately 4 mm. Gelatin blocks containing the hair were then removed from the plastic tubing. The gelatin block was then cut to size and frozen directly onto the cryostat chuck. Sections of 1 µm were cut from the block, with several sections being collected onto a single glass microscope slide. 10 µM Nile red was added directly to these sections before sealing under a No. 1 thickness glass coverslip using nail varnish.

2.11.4. FRAP of fluorescent compounds within hair

FRAP was employed on hairs containing fluorescent compounds in order to visualise dynamic movement of stain within the hair. Specifically, hairs which had been saturated with Rhodamine B were first removed from the stain and the surface dye removed through brief acetone washing. Transverse optical sections were directly imaged using the VID as described previously. The Zeiss 880 Airyscan LSCM was used with the 1.4NA 63x oil immersion objective. Following an initial image, 100% laser power was applied for 5 iterations to a selected region to result in photobleaching within that region. Time series acquisition was applied for varying periods of time to allow imaging of dye movement.

2.11.5. FLIM of hair samples

FLIM was used to observe the changing chemical composition of hair. Hairs were mounted for longitudinal imaging as described previously and optical sections were captured at a depth of 10 µm. FLIM was performed using the Leica SP5 confocal microscope and a 63x oil immersion lens in combination with Immersol 518F immersion oil. 470 nm and 640 nm pulsed lasers were available for use with FLIM using the TCSPC method (time-correlated single photon counting). However, the 470 nm pulsed laser was used for excitation of all samples, and emission was captured from 480 nm – 800 nm. Photons were collected until the maximum counts per-pixel reached 1000 which was sufficient to generate acceptable data upon performing pixel-by-pixel FLIM. In the case of spectral FLIM, emission was instead captured in 10 equal emission bands from 495 nm to 795 nm, with each window

encompassing 30 nm. Data was recorded and analysed with the Symphotime 32 software (Picoquant).

2.12. Hair Protein extraction

Protein extraction was carried out to solubilise hair protein for determination of protein composition. Approximately 1 g of hair was cut into small (c. 2 mm) segments and rinsed 3 times in ethanol. Samples were then air dried before chloroform/methanol added at 2:1 ratio and incubated 18hrs at room temperature. Chloroform/methanol was then removed, and the hair rinsed 3 times in ethanol. The hair was then air dried, portioned, and weighed. Extraction buffer (6M urea, 2.6M thiourea, 25mM Tris pH8.5, 50mM DTT) was added at ratio of 100ul per 2mg. The extraction is incubated at room temperature for 18hrs. Following incubation, the mixture is vortexed and filtered using a 40 μm mesh filter, removing the insoluble portion of the fibre. Chloroform/methanol precipitation was carried out and protein resuspended in freshly made lysis buffer (9M urea, 2M thiourea, 4% CHAPS, 1% DTT) at 5 times its original concentration. Protein content was then estimated using Bradford assay (Bradford, 1976) before use in SDS-PAGE and 2D SDS-PAGE.

2.13. SDS-PAGE

SDS-PAGE was used to separate proteins based on their size. The Bio-Rad Mini Protean II system was used to cast and run all gels. The running gel was first cast, which typically contained 12% (v/v) acrylamide, 0.1% (w/v) SDS, 375 mM Tris pH 8.8, 0.1% (w/v) ammonium persulphate (APS), and 0.04% TEMED (NNN'N'- Tetramethylethylenediamine). Stacking gel was then poured, containing 4% (v/v) acrylamide, 125 mM Tris pH 6.8, 0.1% (w/v) SDS, 0.1% (w/v) APS, 0.002% (v/v) TEMED.

Protein to be loaded was diluted 4:1 using 5x Laemmli sample buffer (312 mM Tris-HCl, pH 6.8, 10% (w/v) SDS, 50% (v/v) glycerol, 25% ß-mercaptoethanol, 0.05% bromophenol blue) and heated for 5 minutes at 95 °C. Electrophoresis was performed at 150V using the tris-tricine buffer system (cathode buffer (upper tank): 0.1M Tris, 0.1M Tricine, 0.1% (w/v) SDS and anode buffer (lower tank): 0.2M Tris, pH = 8.9) for the purposes of resolving low-MW proteins running buffer.

The gel was then stained with Coomassie stain containing 0.1% (w/v) coomassie R250 brilliant blue, 10% (v/v) acetic acid, 50% (v/v) methanol for at least 1 hr. Excess stain was then removed using 10% (v/v) acetic acid, 50% (v/v) methanol.

2.14. 2D-SDS-PAGE

Two-dimensional sodium dodecyl sulphate polyacrylamide gel electrophoresis (2D SDS-PAGE) was used to separate hair proteins based upon their size and isoelectric point. The desired mass of protein, ranging from 100 – 300 µg was diluted to 120 µl using lysis buffer. Ampholytes pH 4-7, 2.5 µl, was subsequently added in addition to a trace of bromophenol blue to make the sample visible in later stages. The sample was then added to the well of an Immobiline Drystrip re-swelling tray and the pH 4-7 IPG strip gently laid into the well. Paraffin oil was then used to cover the sample and rehydration took place for 18 hrs.

IPG strips were then washed using dH$_2$O and filter paper used to blot dry. Strips were placed into grooves of the plastic insert for electro focusing and wicks, soaked in water, were placed across the ends of strips and isoelectric focusing carried out for approximately 3 hrs.

Strips were then removed from the plastic insert and thoroughly washed using dH$_2$O. These were subsequently placed onto a set running gel containing 12% (v/v) acrylamide, 0.1% (w/v) SDS, 375 mM Tris pH 8.8, 0.1% (w/v) APS, and 0.04% TEMED. 1% (w/v) agarose was then added to cover the IPG strip and allowed to set.

Electrophoresis was carried out at 100V for 10 min, followed by 150V for approximately 1hr, using tris glycine running buffer (25mM Tris, 250 mM glycine, 0.1% (w/v) SDS).

The gel was then stained with Coomassie stain containing 0.1% (w/v) coomassie R250 brilliant blue, 10% (v/v) acetic acid, 50% (v/v) methanol for at least 1 hr. Excess stain was then removed using 10% (v/v) acetic acid, 50% (v/v) methanol.

2.15. Spot identification

LC-MS/MS was used to confirm the identity of protein spots following 2D-SDS-PAGE and in-gel digestion. Spots of interest were identified for excision from the gel using a scalpel. The gel piece was then washed by covering in a solution containing 200 mM ammonium bicarbonate, 40% acetonitrile and incubating at 37˚C for 30 min. The solution was then removed, and the washing step repeated. Gel pieces were then dried in a vacuum centrifuge for 30 min. 100 µl of trypsin digest solution (40nM ammonium bicarbonate, 9% acetonitrile, 0.1µg/ml TPCK-treated trypsin) was added and incubated for 4 hr at 37˚C. Following this, the liquid, containing the tryptic peptides, was removed and used for subsequent measurement performed on a QStar pulsar i mass spectrometer (Applied Biosystems/MDS Sciex) linked to an Ultimate 3000 UHPLC system (Dionex) with a Nanospray source (Protana) containing a 10 µm New Objective coated spray needle.

Measurement was performed by the Durham Bioscience Proteomics facility. Analysis was in trap and elute mode, using a Zorbax C18, 5 μm, 0.3 x 5 mm trap column (Agilent) and a PepMap 100® 3 μm, 100Å, 75 μm x 150 mm resolving column (Thermo scientific). Buffer A was 2% ACN, 0.1% (v/v) formic acid in water and Buffer B 80% ACN, 0.1% formic acid. Peptides were loaded onto the trap and washed in buffer A at 25 μL/min before switching of the trap in-line and peptide separation at 300 nL/min. Sequential linear gradients of 4 to 8% buffer B over 4 minutes, 8 to 40% B over 38 minutes and 40 to 90% B over 15 minutes were performed before 6 minutes of column washing at 90% B, return to 4% B and column equilibration for 9 minutes. MS acquisition was from 5 to 69 minutes and consisted of cycles of 1 precursor-ion (MS1) scan for 1 second (m/z 300 to 1600) followed by 3 x 3 second MS/MS acquisitions (m/z 100 to 1600). MS data was acquired using Analyst 1.1 software and rolling precursor ion exclusion windows prevented excessive multiple acquisition of the same precursor ion.

Precursor and product ion peak lists were generated from acquired .wiff files using an .mgf file output conversion script within Analyst and database searching performed with MASCOT MS/MS Ions search software on the publicly-available server at (matrixscience). Peptide mass tolerances in the search were 50 ppm for precursor ions and 0.6 Da for MS/MS ions, with fixed amino acid modification of carbamidomethyl [C] and variable modification of oxidation [M] specified.

2.16. Tryptophan and Kynurenine quantification

Hydrolysis and liquid chromatography – tandem mass spectrometry (LC-MS/MS) was used for determination of tryptophan and kynurenine concentration in hair. Approximately 1 g of hair was cut into small (c. 2 mm) segments and rinsed 3 times in ethanol. Hair was then air-dried before weighing and portioning of the hair.

For quantification of tryptophan, basic hydrolysis was employed. Conversely, acid hydrolysis was used for quantification of kynurenine. Either 4.2M NaOH, for basic hydrolysis, or 6M HCl, for acid hydrolysis, was added to hair samples to reach a ratio of 25 mg/ml. Hydrolysis was carried out at 110°C for 24 hrs. Samples were then diluted 1/1000 before separation by HILIC chromatography and amino acid detection and quantification with reference to external standards by monitoring their product ions upon fragmentation in a Hybrid Triple-Quadrupole mass spectrometer (Sciex QTRP 6500) which was performed by Durham Bioscience Bioanalytical facility. Amino acid concentrations were normalised to that of proline, which is not likely to be modified during treatment.

2.17. <u>Imaging</u>

2.17.1. <u>Zeiss 880 Airyscan</u>

The Zeiss 880 was the principle means used for the imaging of both hair and HaCat cells. The Airyscan function of the Zeiss 880 utilised an array of hexagonal detectors which allow for increased sensitivity and improved signal-to-noise. The superior sensitivity and resolution of the Zeiss 880 Airyscan was used to image both live and fixed cells in addition to hairs in both longitudinal and transverse orientation. In all cases imaging was completed using the 1.4NA 63x oil immersion objective.

2.17.2. <u>Super-resolution microscopy</u>

The system used for super-resolution was the OMX BLAZE, using 3D-SIM. The system is an Applied Precision OMX BLAZE Super-Resolution microscope supplied by GE Healthcare. 3D-SIM (structured illumination microscopy) provides an 8-fold improvement in volumetric resolution (xy 100nm by z 250nm) using a wide variety of common fluorophores at high frame rates (16 3D-SIM sections (0.125nm, 2µm) in 1s (240 images)).

The OMX BLAZE was also used to selectively image the basal surface of both live and fixed cells. TIRF uses the evanescent field generated by total internal reflection to excite fluorophores. Instead of illuminating an entire specimen with excitation light, as in widefield fluorescence microscopy, the evanescent field only penetrates the specimen to a depth of 70–200 nm.

3. Investigating the use of FLIM for quantification and understanding of hair damage

3.1. Introduction

Damage to the hair fibre can occur through various means, due to cosmetic treatments such as hydrogen peroxide bleaching, or through natural methods such as UV exposure. Although the mechanism of action for cosmetic treatments is largely understood, for example in the case of hydrogen peroxide bleaching (Guerra-Tapia and Gonzalez-Guerra, 2014; Robbins, 1988), comparing how these insults effect hair has depended largely on qualitative means. Further, this analysis often provides no spatio-temporal information. For example, hair feel or macroscopic appearance is often reported in order to determine the degree of change.

Attempts to measure damage in hair have been made using electron microscopy (EM), for structural analysis, and atomic force microscopy (AFM) for surface analysis (Gurden et al., 2004; Imai, 2011). However, these techniques still remain fairly qualitative due to their reliance on observing certain physical effects, such as cuticle peeling, which suffers from the inherent variability of hair, both from person-to-person but also hair-to-hair, and can be affected by artefacts induced during preparation and sectioning (Kaliyadan et al., 2016). Chemical analysis of hairs, by mass spectrometry for example, provides another means of quantifying changes to hair (Joo et al., 2016). Previously, quantification of tryptophan and cysteine has been used as a measure of damage, particularly following photooxidation, as these are the primary sites of keratin photodegradation (Fedorkova et al., 2014; Jachowicz and McMullen, 2011; Kerwin and Remmele, 2007). However, chemical analysis can be time consuming and additionally requires destruction of the sample which prevents the gathering of spatial information in regard to chemical changes and prevents dynamic analysis.

FLIM provides an opportunity to overcome the drawbacks of the techniques previously mentioned, as it allows for non-destructive and rapid imaging of a sample while also collecting quantitative fluorescence lifetime information to provide chemical insights. FLIM, in particular multi-photon FLIM, has been used previously to observe human tissues such as skin, and in a small number of cases hair (Dimitrow et al., 2009; Ehlers et al., 2007, 2006). However, very little work has been done to investigate how fluorescence lifetimes may change following chemical treatments to hair. FLIM may be useful to both quantify and detect spatially where chemical changes are occurring in hair, providing insights on where the greatest effect takes place. Additionally, FLIM performed in this chapter is implemented as LSCM and therefore benefits from optical sectioning and observation of fluorescence lifetimes at depth into the sample without the need for physical sectioning.

The use of FLIM to measure autofluorescence lifetime offers information not accessible by steady-state fluorescence techniques. Observation of the decay parameters of hair autofluorescence can provide insights into the composition of fluorescent components within the fibre, such as amino acids and lipids (Becker, 2012). Alternatively, varied interactions between identical fluorophores and their surrounding environment may result in altered lifetimes (Albani, 2014). The quantitative nature of FLIM may therefore be useful in determining the extent of chemical change following various degrees of treatment. The ability to quantify chemical change would be useful as a metric for hair damage following destructive and oxidative treatments such as hydrogen peroxide bleaching and UV irradiation.

Here we aimed to evaluate and develop TCSPC FLIM as a method for the quantification and investigation of hair damage, in particular oxidative damage following hydrogen peroxide bleaching. Fluorescence lifetimes would be measured following oxidative damage to quantify chemical change affected by hydrogen peroxide bleaching, and to further understand this effect. Further understanding would be accomplished through the combination of correlative methods such as the quantification of hair amino acids and examination of the soluble protein component of the hair fibre.

3.2. Results

3.2.1. Imaging of hair autofluorescence using single-photon FLIM

Initial imaging of hair fibres was carried out in order to characterise untreated hair using FLIM. FLIM images of hair optical sections were captured while 1 cm fibre fragments were in a longitudinal orientation. A single optical section was captured for each fibre section at a depth of 10 μm into the fibre which resulted in an image incorporating the cuticle and the inner and outer cortex. Excitation of fluorophores was provided by a 470 nm pulsed laser. Fluorescent lifetime data is collected pixel-by-pixel during FLIM acquisition at a diffraction-limited resolution of approximately 250 – 300 nm. However, for efficient comparison of bulk changes, all information collected from a single optical section can be summarised into an average lifetime for that optical section. Acquisition of images was carried out until 1000 photons had been counted within the brightest pixel, which often required around 3 minutes of continuous imaging. One thousand photons were found to provide sufficient data for performance of further analysis, beyond determination of an average lifetime, termed full-FLIM which is described later.
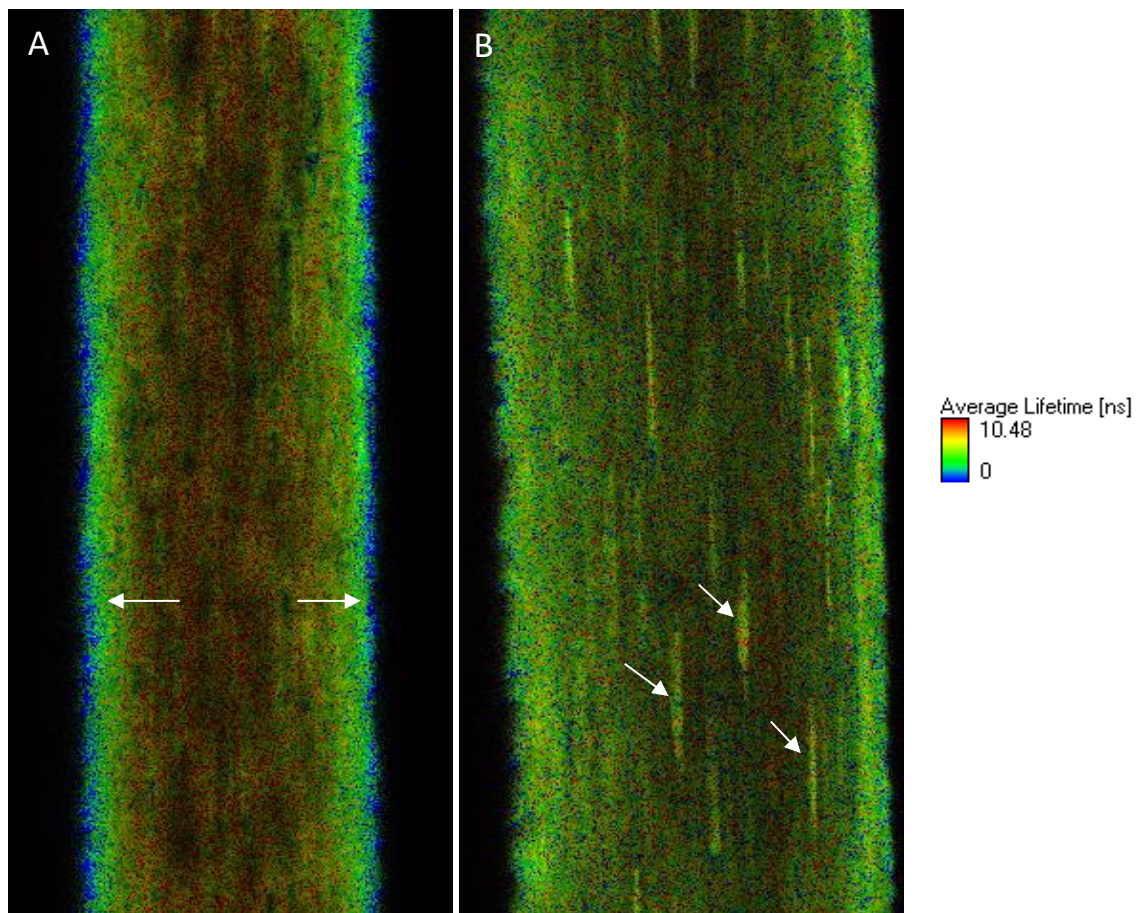
Figure 3.1: Features are visible within hair optical sections using FLIM. *FLIM acquisition of untreated hairs displayed distinct features in certain instances. A – Hair from certain individuals always displayed a distinct cuticle-cortex boundary, incorporating a low lifetime cuticle (labelled). B – Hair from another individual did not display the distinct cuticle-cortex boundary, image selected displays the organelle remnants often captured (labelled).*

Resulting images provide pixel-by-pixel information on the optical section, where the lifetimes of all photons received from a single pixel are averaged and then colour-coded according to a key. Images taken in this manner, of hairs from several individuals, resulted in an understanding of a typical untreated hair (Figure 3.1).

The average lifetime, i.e. the summary of an entire optical section, of untreated human hair remained fairly constant, at around 3.5 ns (Figure 3.2A). However, in all cases, fluorescence lifetime was shown to vary across the hair, rather than appearing homogenous in nature. Therefore, FLIM was able to highlight several structures within the fibre. The most noticeable was a distinct change in fluorescence lifetime between the regions of the outer cortex and the cuticle, where the cuticle is of markedly lower fluorescence lifetime in comparison to the

cortex (figure 3.1A). However, the presence of this distinction was not persistent in all samples. Instead, the individual of origin for the hair determined whether this was present, where all hairs imaged from certain individuals were seen to have a cuticle with a significantly lower fluorescence lifetime. Conversely, hair from alternate individuals would at all times display a much less distinct boundary between the cuticle and cortex (figure 3.1B). Hair from 3 individuals was used for the following work. Of these, 2 individuals had indistinct cuticle-cortex boundaries while the third displayed a cuticle of clearly lower fluorescence lifetime. This suggests that a fluorophore which possesses a low fluorescence lifetime is present in the hair cuticle of certain individuals, but not in others.

In many cases, there was also a gradient present throughout the cortex, where fluorescence lifetime was seen to be highest at the inner cortex while decreasing towards the cuticle, as can be seen in figure 3.1A, suggesting changing chemical composition throughout the fibre cortex. Distinct structures were often visualised within the cortex, particularly visible in figure 3.1B, appearing as streaks parallel to the hair's axis, which are consistent with the arrangement of organelle remnants previously described (Szabo et al., 2012). These structures were often seen to have a lower fluorescence lifetime than the remainder of the cortex. Due to the method by which images were collected, at a constant 10 μm depth, the medulla was not captured.

Figure 3.2A shows the variability in average lifetime between multiple hairs, both from a single individual, and between individuals. Results show that there is little variability in average lifetime between hairs from the same individual; there are small differences between individuals detectable. As the average lifetime reflects the lifetime of all fluorophores in the optical section, which contains a cross section of both the cuticle and cortex, it is extremely useful as a rapid measure for the whole hair. As there is little variability in average lifetime seen between hairs from the same individual, this method of analysis is used in future experiments in order to compare the change to hair sections following a range of treatment intensities.

However, the data can also be analysed further to attempt to identify, and determine the composition of, individual components responsible for the average lifetime. In addition to retrieval of the average lifetime, processing was also carried out to reveal individual lifetime components at each pixel, in a process which will be referred to as full-FLIM. Full-FLIM analysis was carried out on fluorescence lifetime data from untreated hair samples. This fluorescence decay was found to best fit to 3 exponentials, allowing fluorescence to be

grouped into 3 separate decay curves. This suggests that 3 components, or groups of similar components, are responsible for the majority of fluorescence detected.

A — bar chart with y-axis "Average lifetime (ns)" ranging 0 to 4, x-axis "Individual" showing bars 1, 2, 3.

B — line chart with y-axis "Counts" ranging 0 to 25000, x-axis "Fluorescence Lifetime (ns)" ranging 0 to 15, showing Component 2 and Component 3.
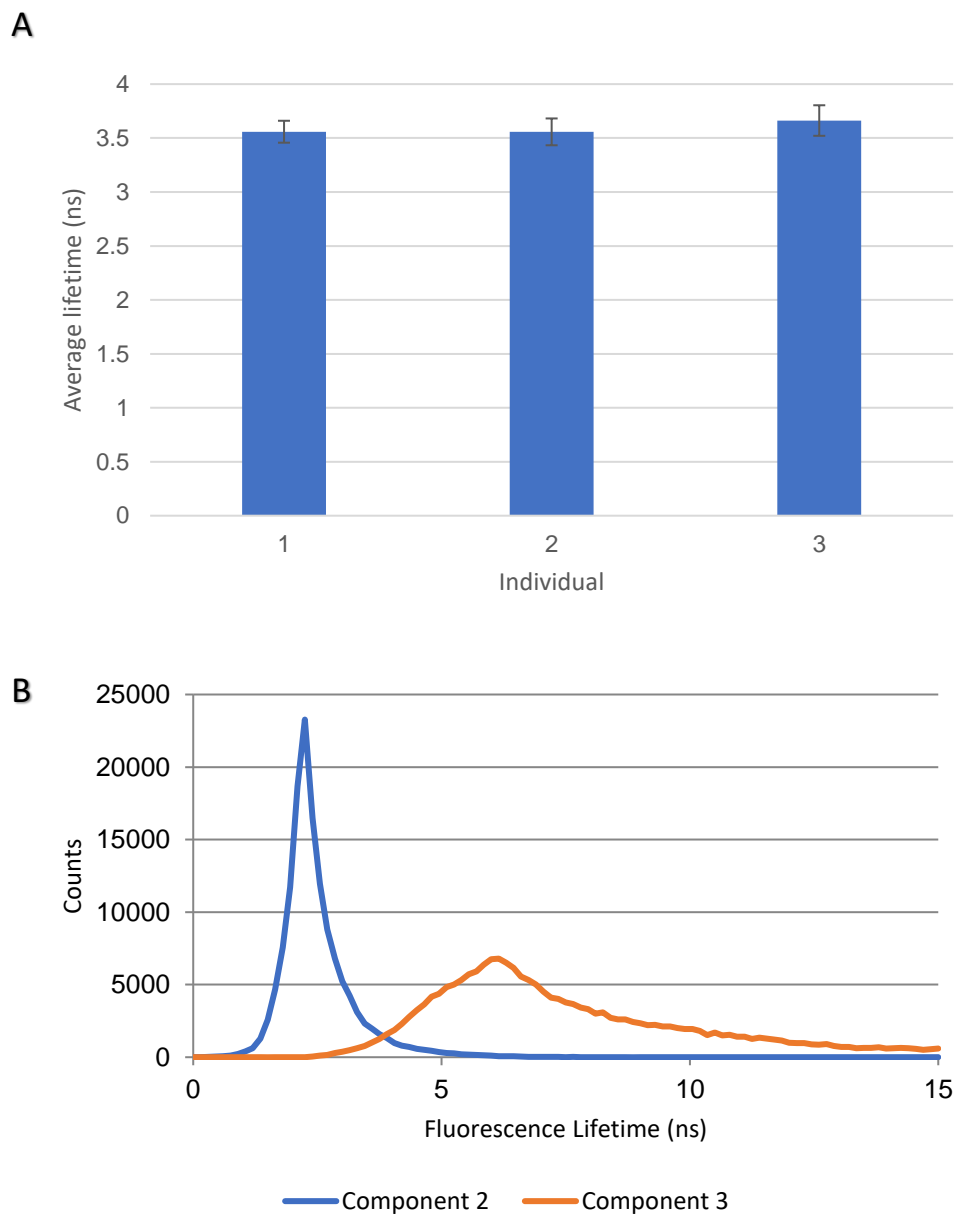
Figure 3.2: Average lifetime and individual fluorescent components of hair are characterised. *A – Average lifetimes from different hairs from the same individual show little variation, small variations are present between individuals. B – Full FLIM analysis reveals 3-exponential decay, where the majority of fluorescence is attributed to components 2 and 3.*

Analysis of this data revealed that of these 3 components, the majority of fluorescence, i.e. the majority of photons counted, was attributed to components 2 and 3. Component 1, the lowest lifetime component which consisted of a small amount of fluorescence of a very short lifetime, was seen to contribute a negligible amount of the total fluorescence. Therefore, the lifetime distribution of components 2 and 3 only are shown in figure 3.2B.

Component 2 distribution appears narrow and with a sharp peak at around 2.5 ns, a lifetime just below the average lifetime of hair, which has been shown here to be approximately 3.5 ns. Component 3, in contrast, occurs as a much broader peak at a higher fluorescence lifetime of approximately 6 ns. Therefore component 2 and component 3 are shown to be different fluorescent components, or groups of components which fluoresce, when excited at 470 nm, with different fluorescence lifetimes.

In summary, FLIM can be used to rapidly measure the lifetime of autofluorescence within a single fibre. The average lifetime of fibres from multiple individuals has been shown to remain fairly constant, at a value of approximately 3.5 ns. However, fibres from certain individuals have been shown to display unique characteristics, such as a cuticle-cortex boundary, which is not present in fibres from all individuals. Furthermore, full-FLIM has enabled the separation of hair autofluorescence, when excited at 470 nm into 3 separate components with distinct lifetimes, 2 of which are responsible for the majority of photons collected. The ability of FLIM to detect these components individually may be of use for observing changes to the composition of hair fluorophores.

Therefore, it was necessary to further investigate if the average lifetime of hair, shown to be constant in untreated hairs, is influenced by oxidative damage. Further, it was of interest to determine if oxidative damage resulted in a change to the composition of the distinct components detected, components 2 and 3 in particular. Finally, additional correlative techniques could be applied to attempt to identify the origin of fluorescence for the components of interest.

3.2.2. Imaging of hydrogen peroxide bleaching's melanin reduction within hair

Hair colouration is provided by melanin which is present in granules throughout the hair fibre cortex and is most prevalent in the upper cortex. Hydrogen peroxide bleaching of hair is a cosmetic treatment used to lighten hair's natural colour through the destruction of melanin and may be performed alone or alongside oxidative hair dyeing to reach a lighter hair colour. Bleaching is enabled by alkaline hydrogen peroxide, due to the combination of hydrogen peroxide and an alkaline environment, often created by the addition of ammonia. Ammonia

is also thought to further enable the process by facilitating hair swelling, and therefore penetration of the active substances into the fibre (Guerra-Tapia and Gonzalez-Guerra, 2014).

Before determining if FLIM was able to measure chemical change during this oxidative treatment, work was performed to examine the effect of bleaching treatment upon the melanin granules present within the fibre cortex.

LSCM images taken using the Zeiss 880 revealed that melanin may be visualised within hair using this means. An optical section of longitudinal hair, taken while exciting at 405 nm, is shown in figure 3.3A. Melanin was visible in this image as an absence of fluorescence, often in linear arrangements, that lack the autofluorescence present in the remainder of the optical section. It was determined that reflectance at 633 nm can also be used to image melanin within hair, as shown in figure 3C. Melanin was seen to reflect light at this wavelength resulting in punctae at the location where fluorescence was absent following excitation at 405 nm (figure 3.3E). Together, these techniques are a robust way of showing the distribution of melanin within the untreated fibre cortex. This is significant as the spatial distribution of melanin in an intact hair has not been published and allows observations to be made following, or during, changes to melanin such as during hydrogen peroxide bleaching. Optical sectioning can be employed with these methods in order to visualise this in 3D.

Following bleaching of a short section of hair from the same fibre, using 9 % H_2O_2 and 6% NH_3, for 30 minutes, melanin was found to be no longer visible as voids at 405 nm or reflectance at 633 nm (figure 3.3B, D, F). This loss of melanin was accompanied by a macroscopic change of colour in the hair fibre to that of a lighter colour. This is the desired effect of hydrogen peroxide bleaching, with other unwanted changes likely occurring to components of the hair cortex and cuticle due to the oxidative nature of hydrogen peroxide.

Work here accomplished the novel visualisation of melanin depletion within the intact hair fibre following hydrogen peroxide bleaching. This experiment also confirmed that parameters of hydrogen peroxide bleaching, used for further FLIM experiments, were sufficient to produce an adequate change to the macroscopic appearance of the hair and the microscopic arrangement of melanin.
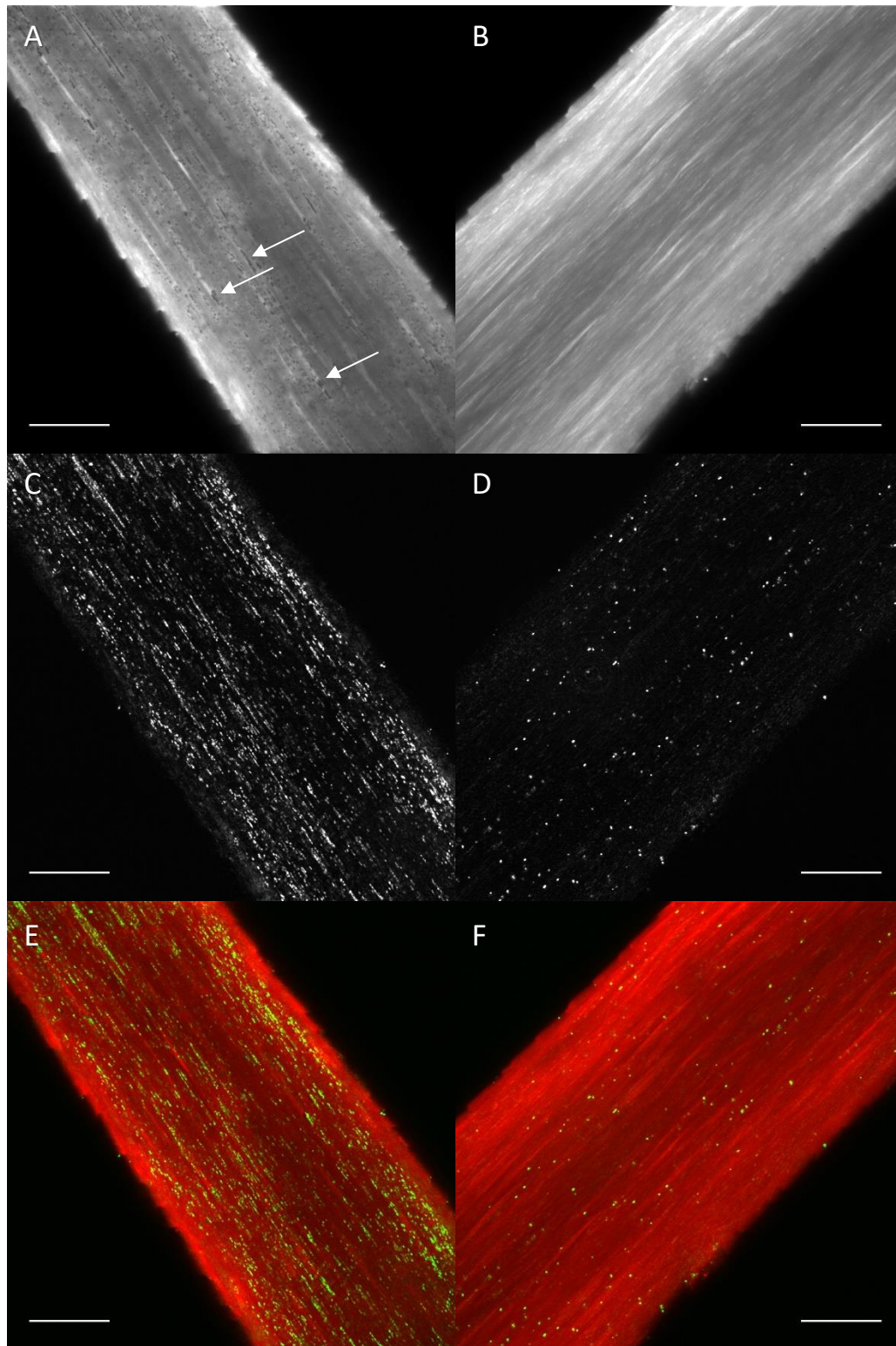
Figure 3.3: Melanin is destroyed during bleaching. *Untreated hair displays voids in linear arrangements when imaged at 405 nm, labelled in A. Corresponding punctae are present following reflectance at 633 nm (C) which colocalise to the voids when merged (E). Bleached hair does not possess dark voids or reflective punctae (B, D, F).*

3.2.3. Measurement of fluorescence lifetime of hair following hydrogen peroxide bleaching

In order to determine if hydrogen peroxide bleaching treatment would alter the fluorescence lifetime of hair, bleaching was carried out on short 1 cm hair fragments before subsequent FLIM capture while orientated longitudinally, as performed previously. Fragments of hair from the same fibre were retained untreated for measurement, to allow for comparison before and after treatment with minimal intrinsic variation between samples.

Following bleaching, FLIM images revealed an increase in fluorescence lifetimes of approximately 1 ns, from 3.5 ns to 4.5 ns, seen in figure 3.4A-D as a shift from blue-green colouration to yellow-red. This change in lifetime occurred throughout the fibre and did not appear to occur with any particular gradient within the cortex. Notably, when untreated hairs had previously displayed a distinct boundary between cuticle and cortex this was no longer present following bleaching (figure 3.4A, B). This may suggest that the low lifetime component present in the cuticle of hair from certain individuals is particularly affected, or destroyed, by hydrogen peroxide bleaching.

As described, average lifetimes are able to be extracted through the averaging of lifetimes for all photons collected from the optical section. Average lifetimes of bleached hairs were seen to be markedly increased in comparison to control hairs, as shown in figure 3.4E. Previously, untreated hairs had been seen to possess an average lifetime of around 3.5 ns. Following bleaching, a fairly consistent increase to approximately 4.5 ns was observed. This suggests a significant chemical change following oxidative damage is detectable using FLIM.

Experiments were carried out in order to investigate the degree to which varying severity of treatment would alter fluorescence lifetime and also to determine if an individual component of the treatment is responsible for lifetime increase. Hairs were bleached with increasing concentrations of H_2O_2, with NH_3 concentration (6 % v/v) and pH (10.3) remaining constant. In a simultaneous experiment, H_2O_2 was kept constant (6% v/v) while NH_3 concentration, and therefore pH, was increased. Finally, the effect of both H_2O_2 and NH_3 alone were investigated by increasing their concentration in the absence of the other. In all cases, untreated hair sections from the same fibre were retained from each sample and measured alongside treated samples to allow average lifetimes to be expressed in figure 3.5 as a percentage value of the untreated hair.
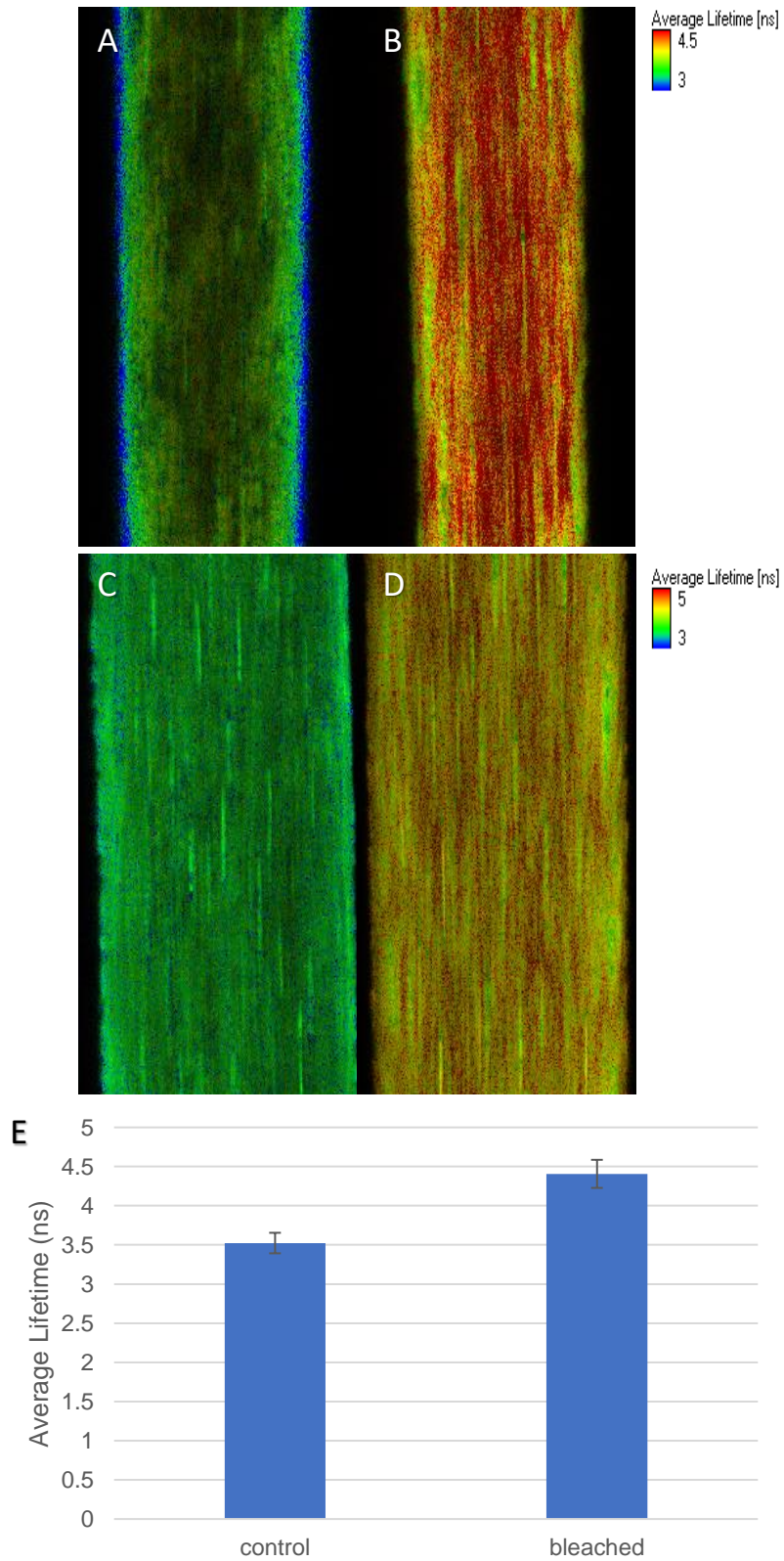
Figure 3.4: Peroxide bleaching results in average lifetime increase. *FLIM images from two individuals (A, B and C, D) both before (A, C) and after (B, D) peroxide bleaching. E – average lifetimes compared between control and bleached hair samples reveal an increase in average lifetimes following bleaching.*

Following treatment with increasing concentration of H_2O_2, it was observed that the resulting dose-response curve appears logarithmic in shape (figure 3.5A). Increasing hydrogen peroxide concentration during bleaching treatment initially resulted in large changes to average fluorescence lifetime. This effect was seen to trail off and eventually plateau with higher concentrations all reaching a fluorescence lifetime of approximately 4.5 ns, an increase of around 25% from untreated hair. Assuming that fluorescence lifetime increases due to oxidation of particular fluorophores by H_2O_2, it is possible that the plateau seen here is due to a lack of availability or depletion of the unmodified fluorophore, resulting in diminishing returns from greater H_2O_2 concentration.

A strikingly similar response is seen when increasing NH_3 concentration during bleaching. Initially, added ammonia resulted in a significant increase to fluorescence lifetime. However, as seen when increasing the concentration of hydrogen peroxide, added NH_3 had reduced effect at higher concentrations,

eventually resulting in a plateau (figure 3.5B) with average lifetimes increased approximately 25%. It is possible that the plateau seen in NH_3 and H_2O_2 dose-response curves is caused by a common limiting factor, such as availability of the unmodified fluorophore as discussed earlier.

To investigate this plateau effect further, pH measurements of treatment solutions were used to plot lifetime change, rather than NH_3 concentration (Figure 3.5C). This is not performed for the increasing H_2O_2 data as pH was kept constant for these measurements. An increase in pH, due to added NH_3, is seen to incur a linear increase upon average lifetime, with no plateau observed across the range of pH used. This linear increase with pH suggests that the primary function of NH_3 is to increase the pH and that any additional function, for example increasing hair swelling, does not have a large impact on bleaching in particular. It also indicates that the plateau seen from additional NH_3 is due to a lack of pH change at higher concentrations.

Unlike the results seen previously, both NH_3 and H_2O_2 resulted in little change to the average lifetime of hair's fluorescence when used alone, as seen in figure 3.6. Therefore, a significant change in fluorescence lifetime was only seen when both hydrogen peroxide and ammonia are combined. This suggests that, instead of fluorescence lifetime changes occurring due simply to an altered chemical environment, such as increased pH, they are instead due to hydrogen peroxide oxidation through the combination of hydrogen peroxide and ammonia.
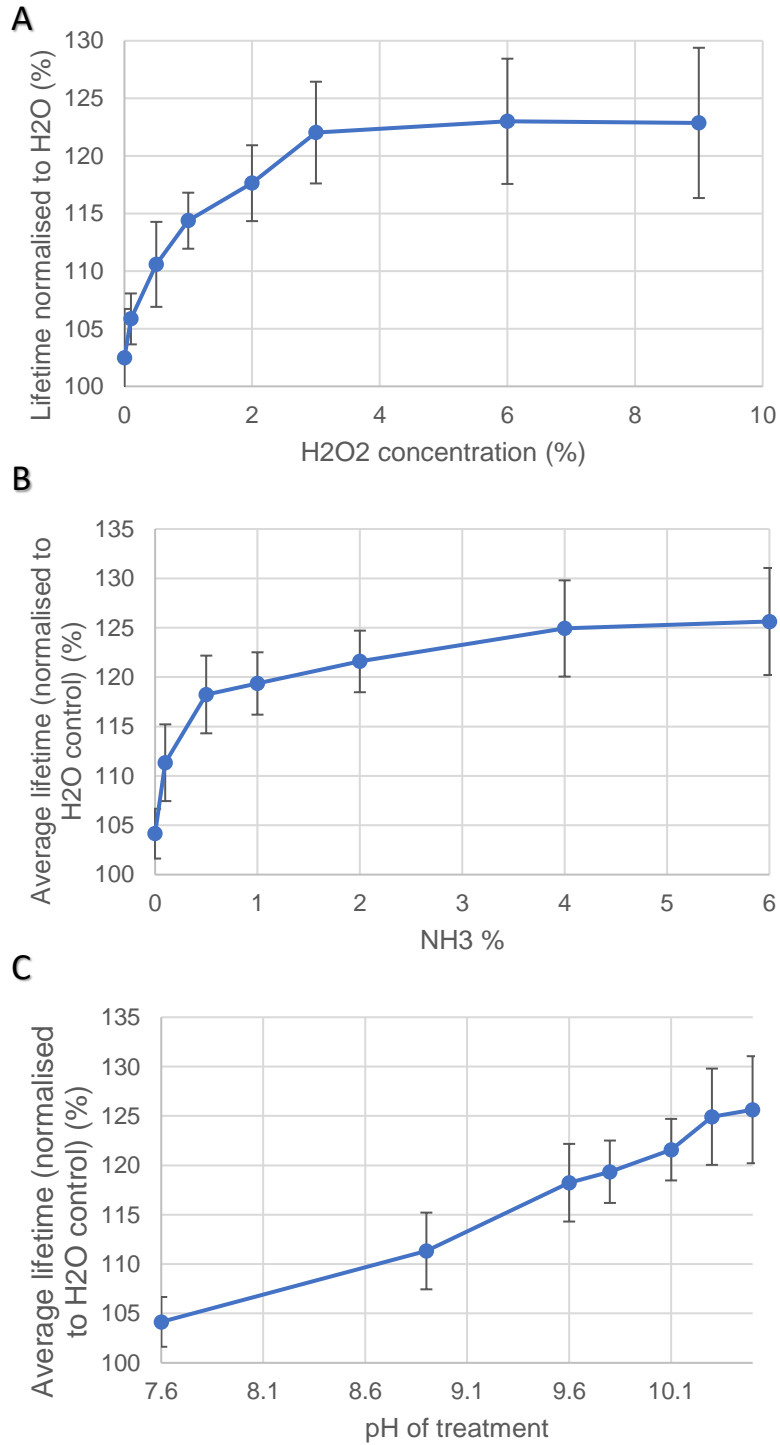
Figure 3.5: Increasing peroxide and ammonia concentration produces non-linear correlation with average lifetime. Average lifetimes compared when increasing H_2O_2 concentration in the presence of NH_3 (A), when increasing NH_3 concentration in the presence of H_2O_2 (B) and also when comparing pH increase to average lifetime (C).

In experiments discussed above, samples before and after bleaching were compared by average lifetime alone to allow for comparison between a large number of samples. Full-FLIM analysis of the individual fluorescent components in a number of samples was therefore carried out in order to further understand the reason for the increase in average lifetime.
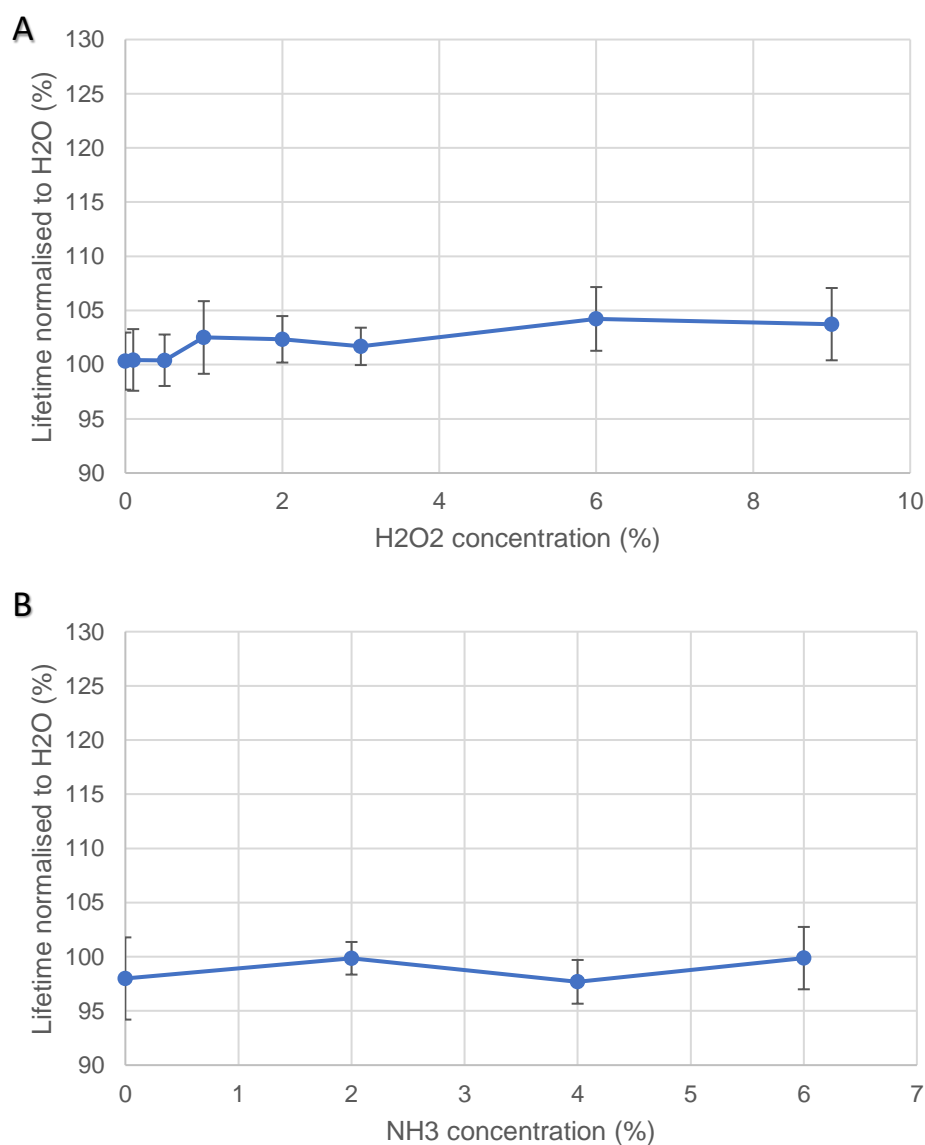
Figure 3.6: Peroxide or ammonia alone do not result in a change to average lifetime.
Average lifetimes compared to increasing concentration of H_2O_2 (A) or NH_3 (B) alone.

A
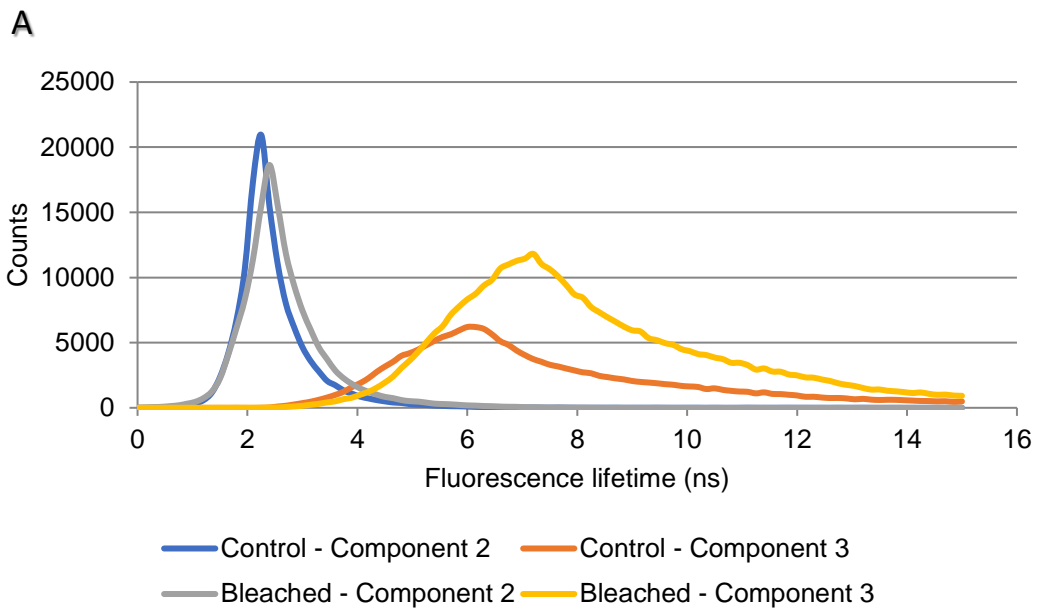
B

	Control	Bleached
Photons (Component 3)	179945	353004

Figure 3.7: Peroxide bleaching results in an increase to component 3 intensity and lifetime. *A - Component 2 and component 3 distributions for both control and bleached hair samples, including values (B) to illustrate the number of total photons attributed to component 3 before and after bleaching.*

Figure 3.7 displays the distribution of fluorescent components 2 and 3 both before and after bleaching following further analysis. Component 2 was seen to remain similar in distribution and amplitude following bleaching, with a sharp fluorescence lifetime peak of around 2.5 ns. In contrast, component 3 appeared markedly different following bleaching, in both its distribution and the number of counts attributed to it, resulting in greater area under the curve. The distribution of component 3 is shifted to higher lifetimes, with its peak increasing from 6 ns to around 7 ns. The area under the curve of component 3 is also significantly increased following bleaching, meaning that much more fluorescence is attributed to this component. The total number of counts attributed to component 3 following bleaching increased from roughly 18,000 to around 35,000 counts, almost doubling the previous value. When combined with earlier results, it can be concluded that an increase in fluorescence originating from high-lifetime component 3 and a shift of this component's fluorescence to yet higher lifetimes results in a higher average lifetime of hair fluorescence following hydrogen peroxide bleaching.

Results here show that a particular fluorescent component of hair, component 3, is responsible for changes to the average lifetime following hydrogen peroxide bleaching. This fluorescent component may be a single chemical species. However, due to the complex nature of the hair fibre and the many potential fluorophores, in addition to the broad shape of the peak, it is likely that component 3 is the result of several fluorescent molecules which may be similar in nature and therefore fluorescence lifetime. Hydrogen peroxide bleaching increases fluorescence originating from this component; this may be due to the fluorescent species becoming more fluorescent, or the production of additional fluorescent molecules. Also, fluorescence lifetimes are seen to increase as a whole within component 3, possibly due to modifications made to these fluorescent species.

3.2.4. <u>Spectral fluorescence lifetime imaging of hair</u>

Unlike regular fluorescence microscopy, FLIM is able to separate components without using their spectral characteristics, by instead using their fluorescence decay as shown previously. Here, individual component analysis was combined with spectral analysis, known as spectral FLIM or Spectral Lifetime Imaging (SLIM), to determine if component 2 and component 3 are spectrally distinct, and what the emission maxima of these 2 components are when excited at 470 nm. This information is useful in allowing us to observe the range of wavelengths where the greatest change in lifetime occurs, and also may aid in identification of the fluorophores responsible.

First, FLIM images were taken of untreated and bleached hair sections, collecting fluorescence in 10 equal narrow emission bands between 495 nm and 795 nm, following excitation at 470 nm. Photons were collected until the brightest pixel had accumulated 1000 counts, as described previously. Fluorescence average lifetime was then determined for each of these emission bands. Average lifetime was seen to vary throughout the emission spectra, as shown in figure 3.8.
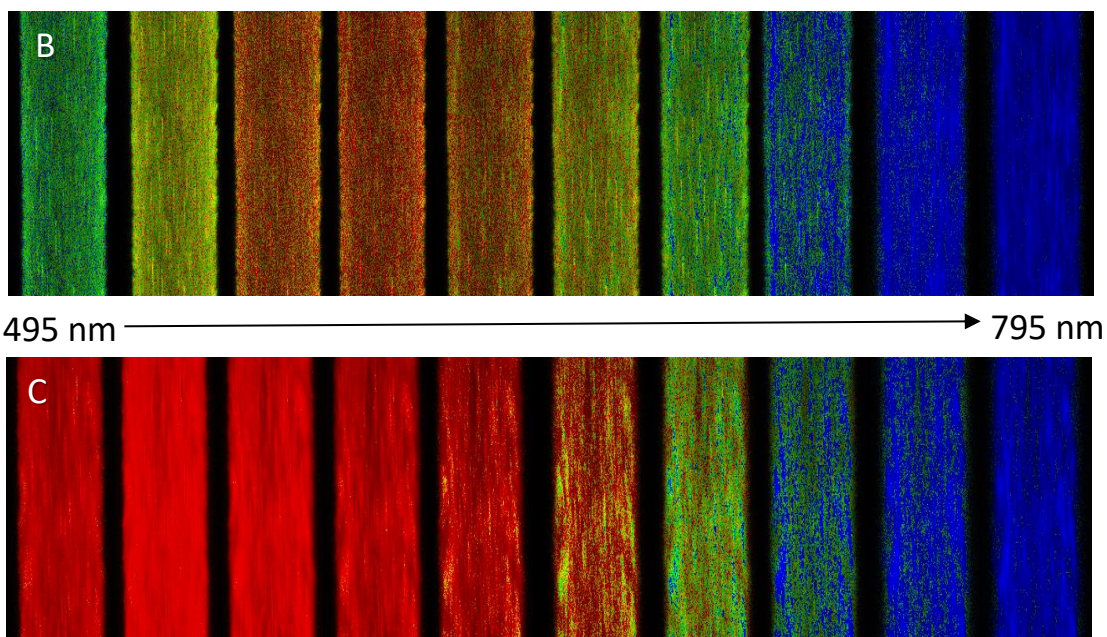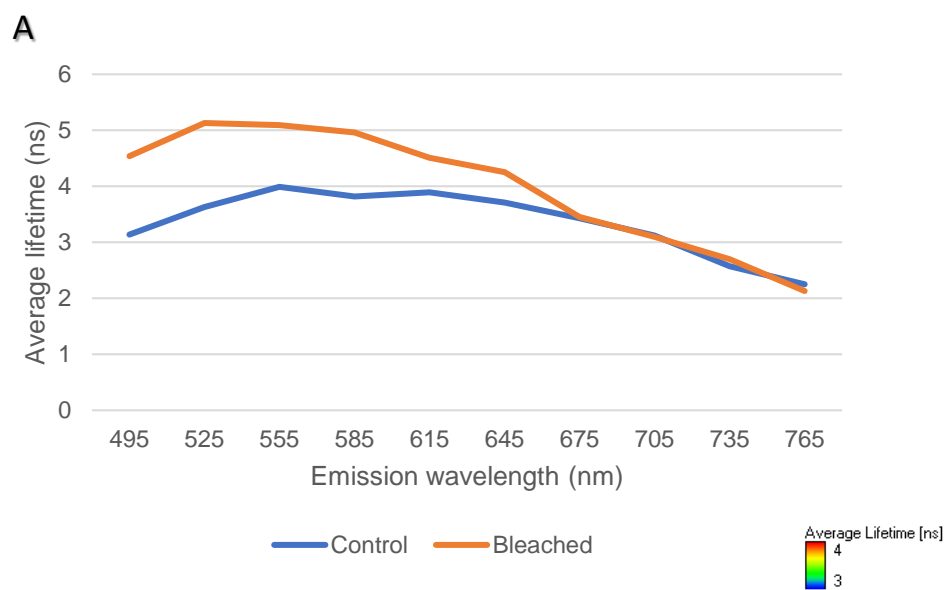
Figure 3.8: Lower emission wavelengths contain the largest difference in control and bleached hair fluorescence lifetimes. A – Graph displaying average lifetimes for control and bleached hair at a range of emission wavelengths. FLIM images of control (B) and bleached (C) hairs at 10 equal emission bands incorporating wavelengths from 495 – 795 nm.

When comparing average lifetimes of bleached and untreated samples at the range of emission wavelengths, the largest difference in average lifetime was seen at lower emission wavelengths. For example, a difference of approximately 1.5 ns was seen between bleached and control samples in emission measured at 495 nm. Average fluorescence lifetimes were seen to converge at higher emission wavelengths, and at wavelengths above 650 nm, no difference was observed. This reveals that the fluorophores responsible for the change in average lifetime, attributed to component 3, are most fluorescent at these lower wavelengths.

In order to create emission spectra of component 2 and component 3 separately it was necessary to alter the experimental method. Previously, FLIM acquisition is ended when 1000 photons have been captured within the brightest pixel. However, in this case acquisition was performed for a specified amount of time at each emission band. This allows direct comparison of photon counts between emission bands, rather than allowing the counts to be normalised as they would in a typical experiment. Full FLIM analysis was subsequently carried out at all emission windows, to separate emission spectra of the three components. Photon counts for components 2 and 3 could then be retrieved for each emission band, these identical time settings for each window allow production of an emission spectrum for each component.
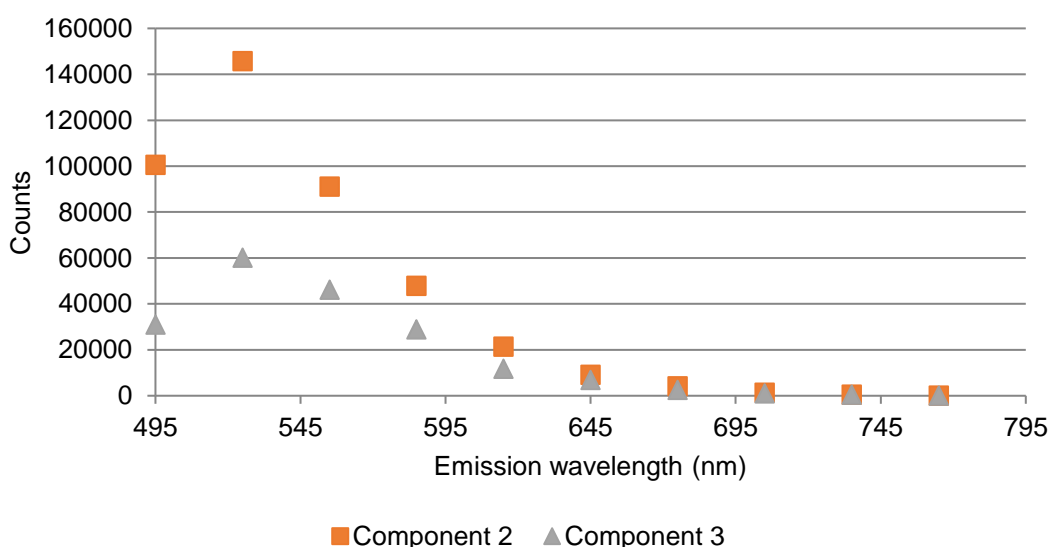
Figure 3.9: Components 2 and 3 are spectrally indistinct. Emission spectra are displayed for both component 2 and component 3, emission has the greatest intensity at 525 nm for both component 2 and 3.

Results obtained analysing component 2 and component 3 are shown in figure 3.9. This investigation revealed that component 2 and component 3 have similar emission maxima and distribution, with a greater proportion of fluorescence attributed to component 2 in untreated hair. Both components exhibited an emission maximum within the second emission band, at 525 nm. The emission maxima are therefore close to the excitation wavelength of 470 nm, and this may result from exciting these fluorophores at a wavelength which is higher than their excitation maxima. The majority of fluorophores within hair are likely to be most fluorescent when excited at UV wavelengths, below the 470 nm used here. However, several components within hair which originate from amino acids, such as the kynurenines discussed earlier, are excitable at 470 nm (Jachowicz and McMullen, 2011).

These data show that the fluorophores excited using the 470 nm pulsed laser emit fluorescence of similar wavelength. FLIM is therefore shown to be useful in distinguishing between fluorophores of hair which are indistinct using spectral characteristics alone.

3.2.5. <u>Investigating prolonged dialysis of hair and effect on average lifetime</u>

Full analysis of FLIM data suggests that fluorescence of hair, when excited at 470 nm, is altered following oxidative treatment. This may be due to alteration of existing fluorophores, or the creation of new fluorophores. Alteration may be accomplished through the modification of fluorescent amino acid residues, such as tryptophan which is known to be a major source of fluorescence in the hair (Smith et al., 1980). Oxidation of tryptophan residues may result in the formation of one of a number of tryptophan oxidation products, broadly termed kynurenines, which are able to fluoresce when excited at 470 nm (Jachowicz and McMullen, 2011).

In order to make further insights into this altered fluorescence, and in particular the solubility and mobility of newly modified chemical species, treated hairs were subjected to periods of dialysis in dH_2O before subsequent FLIM acquisition. Changes in fluorescence lifetime following soaking may reveal information regarding the ability of these chemical species to diffuse out of the fibre.

Hairs were soaked in distilled water for prolonged periods of time before FLIM imaging to determine if average fluorescence lifetimes may revert back to existing levels, therefore suggesting that new species are mobile and able to leave the hair. Conversely, if fluorescence lifetime was shown to remain the same, this may indicate that these fluorophores, attributed to component 3, are immobile or insoluble.

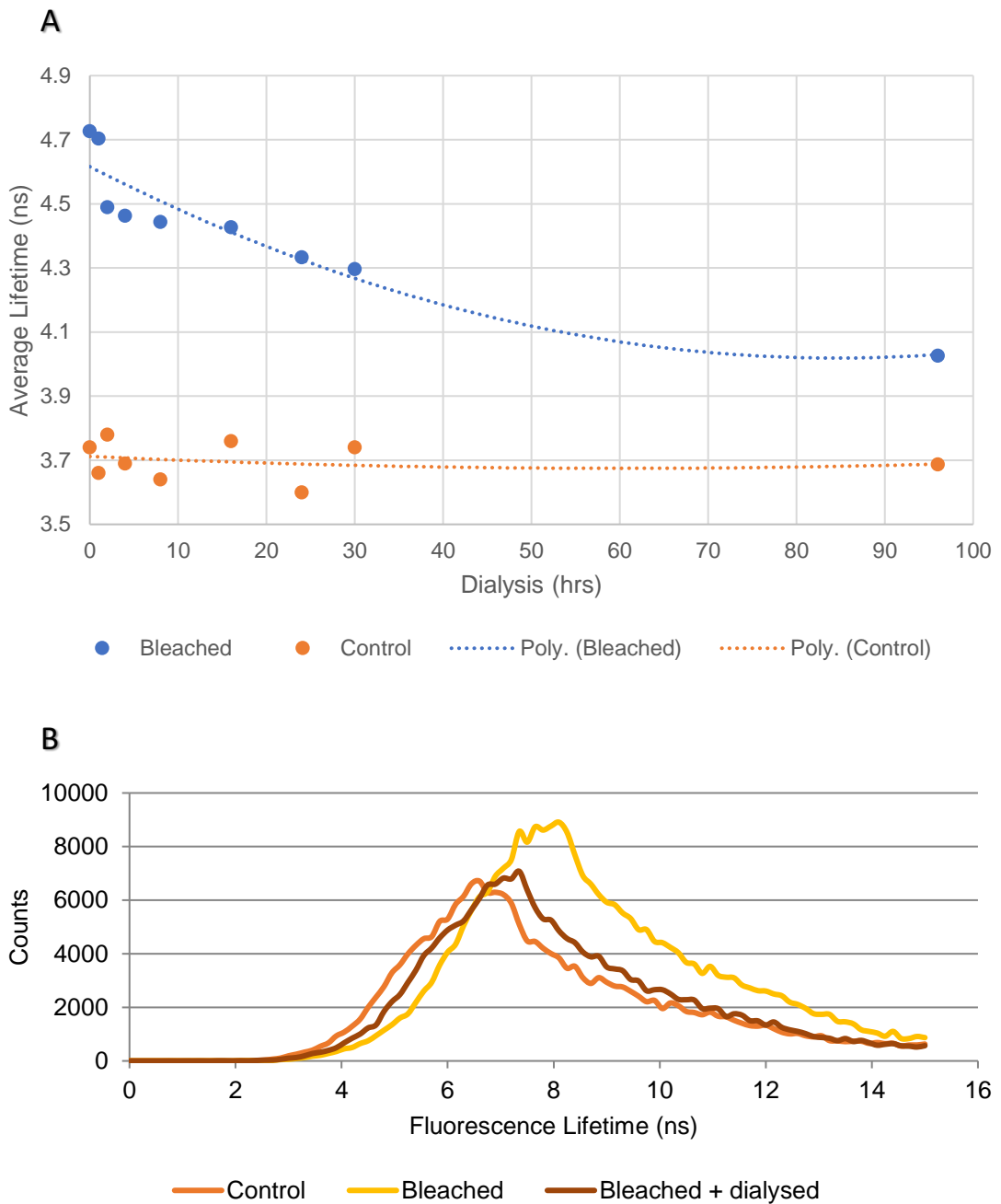
Figure 3.10: Prolonged soaking of bleached hairs results in average lifetime decrease.
A - Average lifetime values displayed for both control and bleached hairs following dialysis. B - Component 3 distributions for both control and bleached hair samples alongside bleached hair following 24 hr dialysis.

As observed previously, bleaching during this experiment was seen to cause an increase to the average lifetime of treated hairs. Following oxidative damage, the average fluorescence lifetime of treated hairs was approximately 4.7 ns. This was in contrast to untreated hairs which resulted in an average lifetime, before dialysis, of around 3.7 ns. However, following prolonged soaking, this difference of approximately 1 ns was seen to diminish. A trendline for the average lifetime of bleached hair following soaking shows that fluorescence lifetime drops to approximately 4.3 ns after 24 hours of soaking, as shown in figure 3.10A. During this experiment, the majority of the decrease in average lifetime appeared to take place within the first 4 hrs of dialysis. In contrast, untreated hair showed virtually no change at any timepoint following soaking.

The initial rate at which bleached hair's average lifetime was reduced was not seen to be maintained throughout the prolonged soaking period. Instead, following 96 hours of soaking, the fluorescence lifetime of bleached hair appeared to have stabilised, and was no longer dropping with further soaking. Over the time period of 96 hours, the difference in average fluorescence lifetime between untreated and bleached hairs decreased from approximately 1 ns to around 0.3 ns.

Full-FLIM analysis of component 3 lifetime distribution in samples of hair that were untreated, bleached, or bleached and subsequently dialysed is shown in figure 3.10B. As previously shown, component 3 increased in terms of total number of photons collected and the location of the fluorescence lifetime peak following bleaching, from approximately 6 ns to 8 ns. However, following dialysis, component 3 in bleached hair was seen to decrease in area and return to a lower lifetime at its peak, approximately 7 ns. This resulted in a distribution of component 3 which was similar to that seen from untreated hair.

Results here suggest that the majority of component 3 molecules responsible for increased average lifetime following bleaching are able to diffuse from the hair fibre during dialysis. These molecules may be fluorescent molecules such as kynurenines which are free or attached to short peptides originating from hair proteins. A proportion of the change however is irreversible by prolonged soaking. This may be due to alterations occurring to amino acid side-chains which are still incorporated into larger immobile proteins.

3.2.6. LC-MS quantification of tryptophan and kynurenine in hair

Previous results during this study have revealed that fluorescence of a particular component of hair increases following oxidative damage, resulting in an increase in average fluorescence lifetime. This component has been shown to fluoresce primarily at the lower wavelengths

observed, with an emission maximum of approximately 495 nm when excited at 470 nm. The component of interest has also seen to be largely soluble and mobile within hair, where dialysis is able to reverse the majority of fluorescence lifetime change.

Photooxidation is suspected to cause conversion of tryptophan residues to kynurenines, hydrogen peroxide bleaching may also cause similar modifications to tryptophan residues through oxidation (Fedorkova et al., 2014; Jachowicz and McMullen, 2011). This oxidation has the potential to create a wide range of oxidation products which can be broadly referred to as kynurenines. As these would fluoresce at the correct wavelength to be detected by FLIM, when excited at 470 nm, it was important to investigate if the increase seen in the area under the curve of component 3 correlates to an increase in kynurenines.

LC-MS was used to determine the amount of both L-tryptophan and L-kynurenine in completely hydrolysed samples of untreated and bleached hair. As basic hydrolysis was incompatible with kynurenine quantification, and acid hydrolysis incompatible with tryptophan, it was necessary to quantify these separately. Acid hydrolysis was employed for quantification of kynurenine, while basic hydrolysis was used simultaneously for quantification of tryptophan.
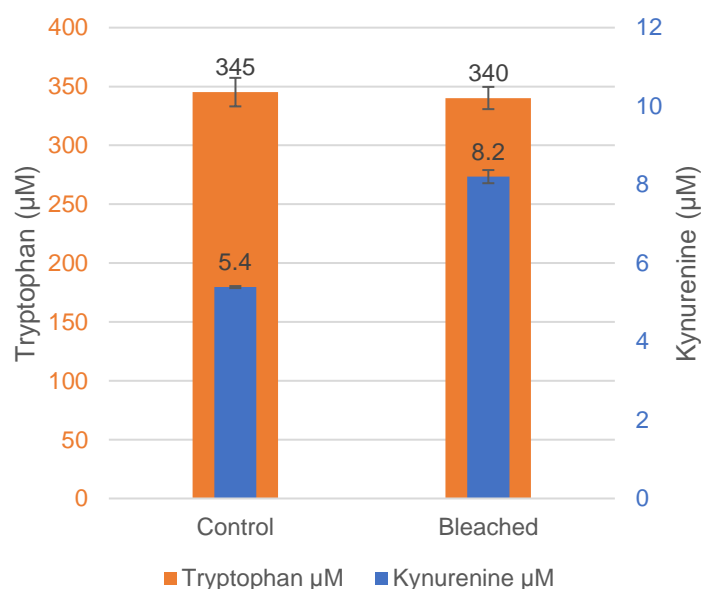
Figure 3.11: Kynurenine concentration is increased following peroxide bleaching. *LC-MS quantification of tryptophan and kynurenine in untreated and peroxide bleached hair. Each component is plotted against its own axis.*

It is important to note that L-kynurenine is not assumed to be the only tryptophan oxidation product that may be produced through oxidative damage. It is used here as a marker for all fluorescent tryptophan oxidation products, also known as kynurenines, although it is unknown if these would all be produced in equal quantities.

In hydrolysed untreated hair samples, L-tryptophan concentration was shown to be around 345 µM, in contrast to the much lower concentration of L-kynurenine, which was measured at around 5 µM. This is shown in figure 3.11. Following oxidative damage, a small but significant increase was seen in the concentration of L-kynurenine reaching approximately 8 µM. There also appeared to be a corresponding but insignificant decrease in the concentration of L-tryptophan, from 345 µM to 340 µM.

None the less, the increase seen in L-kynurenine concentration, which was used here as a representation of many fluorescent tryptophan oxidation products, correlates broadly to the increase in fluorescence attributed to component 3 following bleaching. Previous data within this study revealed that the counts attributed to component 3 approximately doubled following oxidative damage. Here L-kynurenine, which is not necessarily solely responsible for component 3, shows an approximately 50% increase in concentration within hair which has undergone oxidative damage. These data suggest that kynurenines may be produced during hydrogen peroxide bleaching through the oxidation of tryptophan. These fluorescent products are likely to contribute to hair's fluorescence and may be the cause of the additional fluorescence attributed to component 3. The broad nature of the component 3 peak may be explained due to the variety of tryptophan oxidation products possible.

3.2.7. Analysis of changes to hair protein composition following oxidative damage

Oxidative damage has been shown here to affect individual amino acids, in particular causing the oxidation of tryptophan to kynurenine. In order to investigate if bleaching affects whole proteins, possibly resulting in the loss of hair proteins from the soluble component, the composition of hair protein was investigated using SDS-PAGE following solubilisation of protein in strong denaturing conditions.

	Buffer:	Reason for testing:
1	25mM Tris pH 8.5, 5M urea, 2.6M thiourea, 50mM DTT	Most commonly used in recent literature
2	25mM Tris pH 8.5, 5M urea, 2.6M thiourea, 50mM DTT, 0.1% triton X-100	Investigating role of detergent
3	25mM Tris pH 8.5, 5M urea, 2.6M thiourea, 50mM DTT, 2% CHAPS	Investigating role of detergent
4	25mM Tris pH 8.5, 5M urea, 2.6M thiourea, 50mM DTT (3 volumes diluted with 1 volume of ethanol)	Preferential extraction of KAPs
5	25mM Tris pH 8.5, 6M guanidine hydrochloride, 50mM DTT	Use of alternative chaotropic agent
6	25mM Tris pH 8.5, 6M guanidine hydrochloride, 1.5M thiourea, 50mM DTT	Alternative chaotrope with thiourea
7	25mM Tris pH 8.5, 8M urea, 2.6M thiourea, 50mM DTT	Additional urea

Table 3.1: Extraction buffers used for protein solubilisation.

A number of protein extraction buffers, intended to solubilise a portion of hair protein using denaturing and reducing conditions, were trialled during this study. These buffers are described in table 4.1. Of the seven that were investigated, 6 resulted in very similar results. Proteins extracted by these buffers, when separated by SDS-PAGE (figure 3.12B), were seen to localise to a number of bands. High molecular weight bands are attributed to type I and type II hair keratins. Bands at lower molecular weights are instead attributed to KAPs. Buffers 1 – 3 and 5 – 7 each resulted in extraction of similar quantities of protein, as shown in figure 3.12A. When separated by SDS-PAGE, proteins extracted were seen to be of similar composition, Buffer 4, on the other hand, which was identical to buffer 1 with the modification that it was subsequently diluted with 1 volume of ethanol to 3 volumes of buffer, using a similar protocol to that described in Fujii et al., resulted in a significantly lower quantity of protein extracted. However, it resulted in extraction of KAPs alone, with little extraction of hair keratins. This is a phenomenon previously described, although the method by which ethanol results in a KAP-specific extraction is unknown (Fujii et al., 2013).

During investigation it was also discovered that single-source hair, hair from one individual, was more suitable than blended-source hair, pooled hair from many individuals, for study. Blended-source hair resulted in poorly resolved protein bands, seen much more clearly following separation of single-source solubilised proteins (figure 3.12C). This is likely due to individuals possessing subtle variations in protein repertoires within hair owing to the large number of hair keratins and KAPs (Langbein et al., 2001, 1999; Rogers et al., 2006).
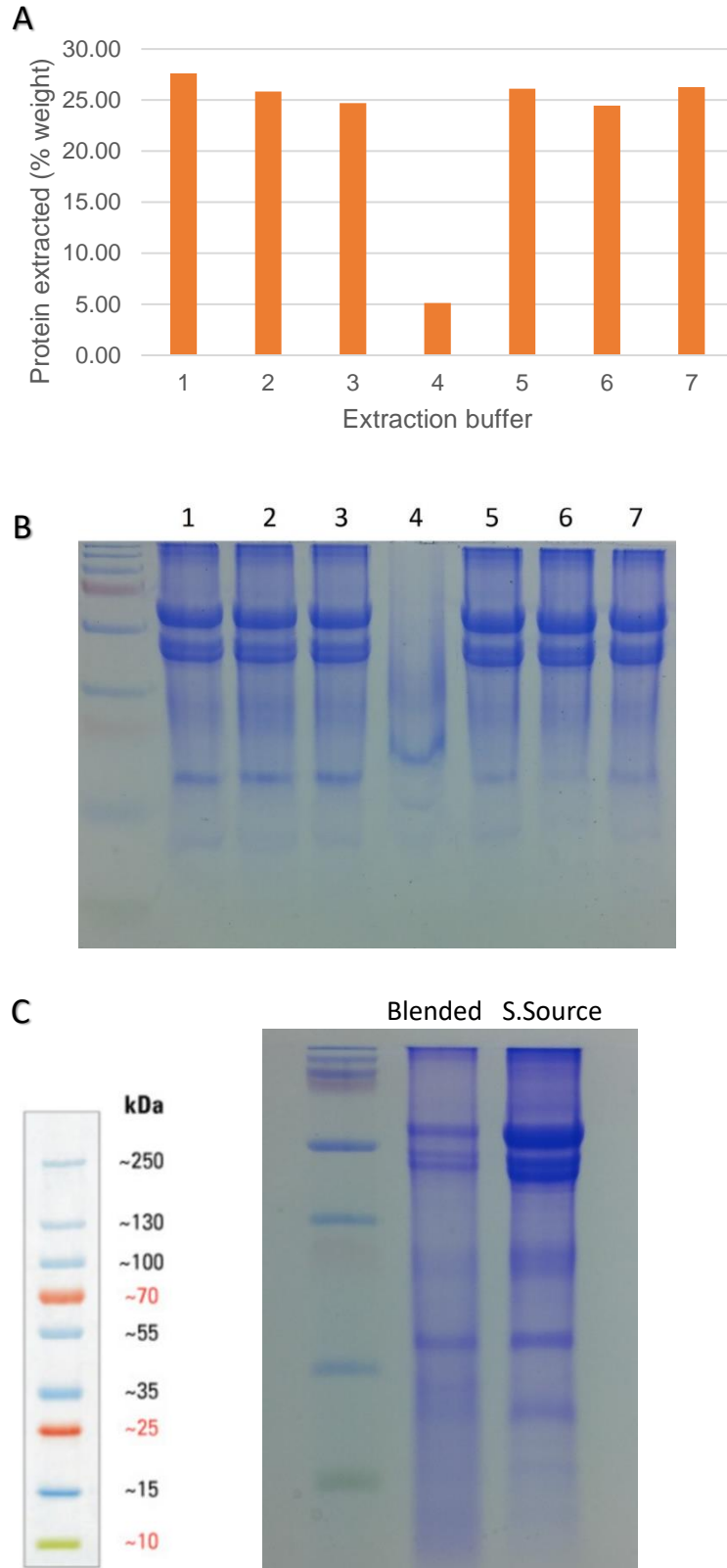
Figure 3.12: Buffers produce similar extraction with exception of KAP-specific extraction. *A – Graph to depict the degree of protein extraction when comparing several extraction buffers. B – SDS-PAGE of protein extractions with each extraction buffer. C - SDS PAGE performed with protein extraction from blended-source and single-source samples.*
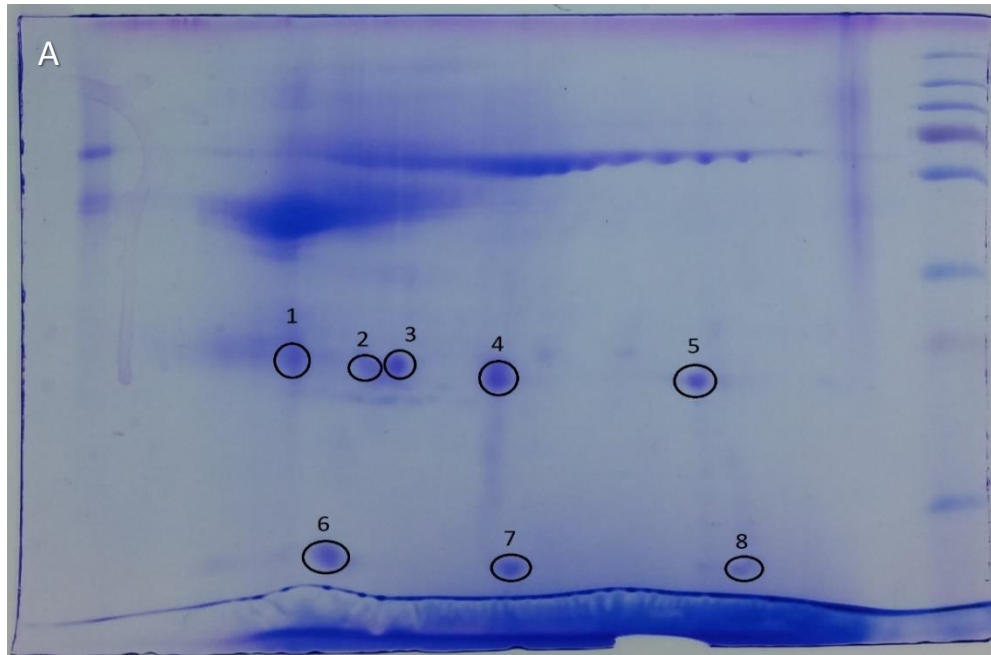
Spot	Identification
1	3.1
2	3.1
3	1.1/3.1
4	1.1/3.1
5	No ID
6	3.1/3.1/3.3
7	3.1/3.2
8	3.1

Figure 3.13: Spots at lower molecular weights are identified as KAPs. 2D-SDS-PAGE of solubilised hair protein with labelled spots used for in-gel digestion and identification (A) and resulting KAP identifications (B).

Buffer 1 was used for protein extraction and subsequent separation by 2D-SDS-PAGE, where separation by isoelectric point was performed between pH 4 and pH 7. Following subsequent separation of equal quantities of protein by molecular weight, untreated hair appeared as two partially separated lines of proteins at molecular weights of approximately 45 - 60 kDa which can be attributed to hair keratins. Additionally, several fully separated spots are visible at lower molecular weights. These spots are attributed to KAPs. In order to verify this, LC-MS/MS identification of protein spots was carried out following digestion with trypsin. Proteins were identified as KAPs; KAP1.1, KAP3.1, KAP3.2, and KAP3.3 in particular, as shown in figure 3.13B. The presence of these KAPs and the lack of others may be due to incomplete solubilisation of the hair protein repertoire and also the varying concentration of hair KAPs. Results may also suggest that the KAPs detected are among the most easily liberated from

the fibre, possibly due to their keratin-binding properties or location. However, little is known with regard to the specific binding of KAPs and hair-specific keratins.
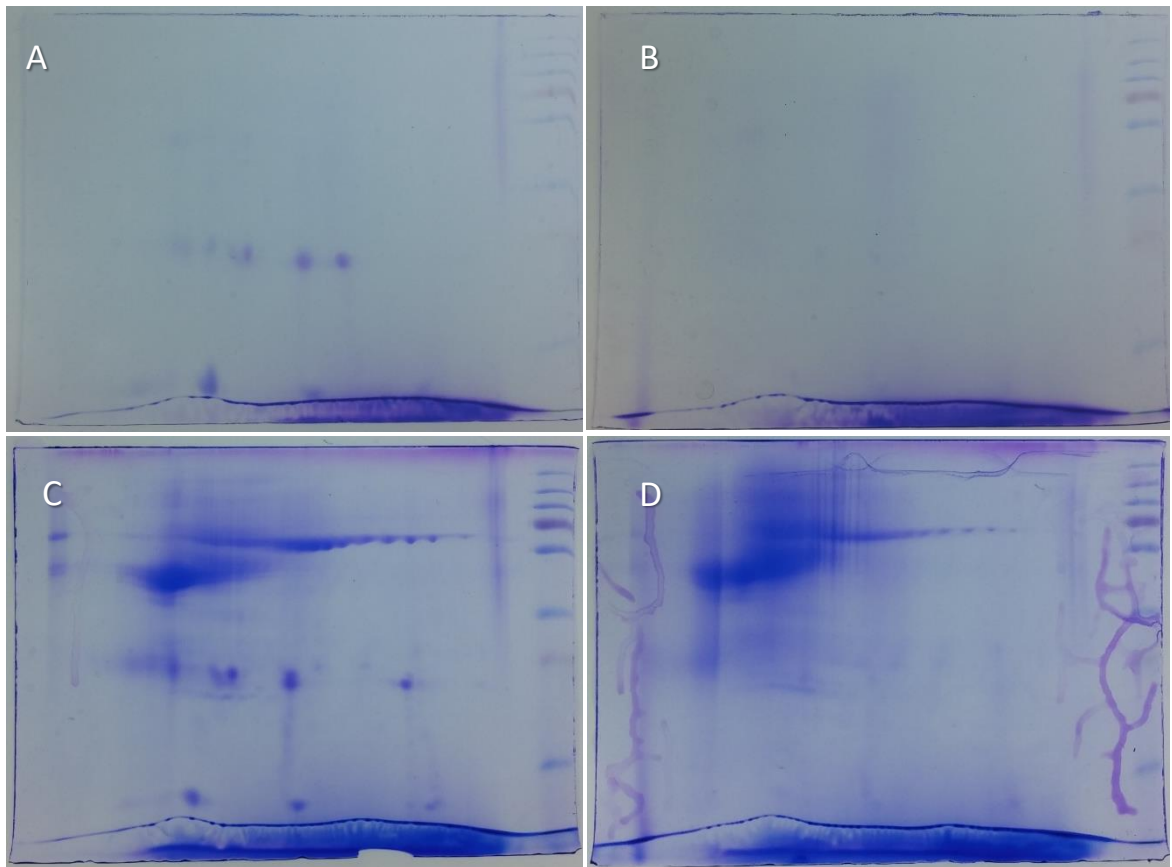
Figure 3.14: Peroxide bleaching results in KAP-loss from soluble protein component.
2D SDS PAGE following separation of control (A, C) and hydrogen peroxide bleached (B, D) samples. Extractions carried out with KAP-specific buffer 4 (A, B) and non-specific extraction buffer 1 (C, D).

Extracted protein composition, using both buffer 1 and KAP-specific buffer 4, from both untreated and bleached hair was compared (figure 3.14). Results showed that following bleaching, there is little change to the abundance and separation of hair keratins, seen only following extraction with buffer 1 (figure 3.14C, D). Conversely, KAPs are shown to decrease significantly in abundance to the point that they are no longer visible following separation. This is the case for both KAP-specific and non-specific extraction methods. This result suggests that while keratin filaments do not appear to be adversely affected by bleaching, KAPs are affected significantly by the oxidative damage.

Adverse effects upon KAPs, with minimal effect on hair keratin, could likely be due to the localisation of these proteins. Keratins form tightly packed KIFs within hair, surrounded by matrix which may serve to protect them to some degree from hydrogen peroxide oxidation. Conversely, KAPs are localised within this matrix throughout hair, although the exact organisation is undetermined, which could allow for greater access and effect of hydrogen

peroxide. The oxidative effect upon KAPs, which are hypothesised to aid in crosslinking within the fibre and create a stable matrix surrounding KIFs, is likely to result in the macroscopic changes to the hair associated with damage such as brittleness.

3.2.8. <u>Application of FLIM for detecting changes in hair following exposure to additional chemical and photochemical treatments</u>

Here we have shown that FLIM is a sensitive and rapid methodology for detection of chemical changes in hair, beyond that possible with steady-state fluorescence microscopy, while also providing the spatial information available for chemical change. FLIM has been shown here to detect chemical change in hair following oxidative damage due to hydrogen peroxide bleaching. In order to investigate if changes following other chemical treatments, or following UV exposure which is of particular interest due to the similarities of photooxidation with hydrogen peroxide oxidation, were detectable using FLIM, the technique was applied to appropriate samples.

Short 1 cm fragments of hair were exposed to UV radiation for increasing amounts of time. These hair sections were then used for FLIM acquisition, along with untreated sections of the same fibre, to determine if chemical changes were detectable using FLIM.

Untreated hair from the individual used for this experiment had an average fluorescence lifetime of approximately 3.2 ns. Following UV exposure this average lifetime was seen to increase up to around 4.2 ns, in the case of hair exposed for 200hrs (figure 3.15A). Several similarities were seen here in comparison to earlier results observing the response of average lifetime to hydrogen peroxide bleaching. The dose-response curve to UV appeared logarithmic in shape as did the dose-response to increasing hydrogen peroxide bleaching severity. This shows that initial UV exposure brings about the largest change, detectable by FLIM, with eventual plateauing. An additional similarity is the degree of change. Both hydrogen peroxide bleaching and UV exposure appear to plateau following an increase of approximately 1 ns to the average lifetime. These similarities may be due to that fact that both forms of damage are oxidative in nature and so chemical change, hypothesised here and in previous literature to be conversion of tryptophan to kynurenines (Fedorkova et al., 2014; Jachowicz and McMullen, 2011), in addition to the limiting factor, may be similar in both cases. The similarity in results for both photooxidation and hydrogen peroxide oxidation lend weight to the hypothesis that, while the mechanisms may vary, kynurenines are produced following each of these forms of damage.
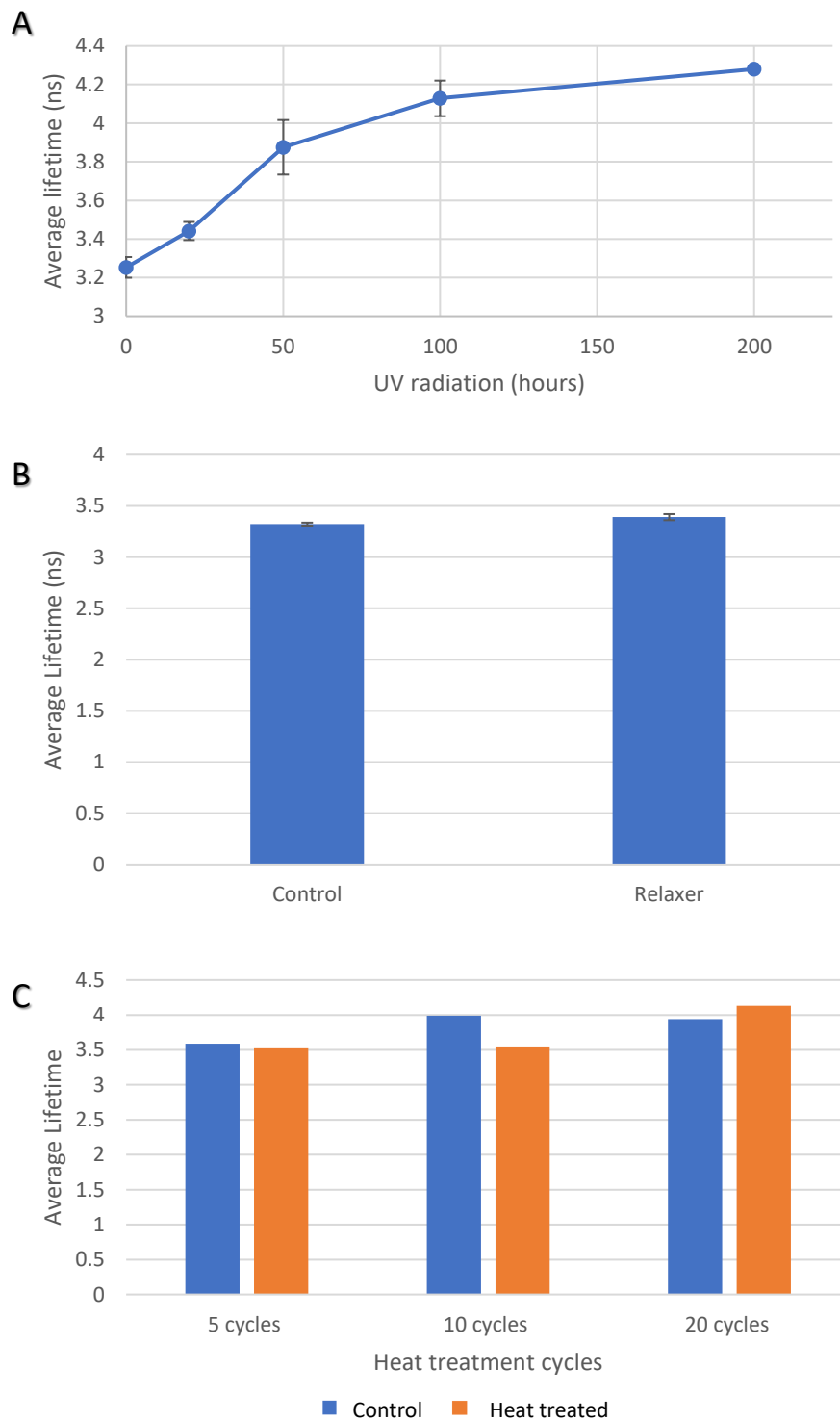
Figure 3.15: Oxidative treatments result in average lifetimes change not seen from non-oxidative treatments. *Average lifetimes compared for (A) increasing amounts of UV exposure, (B) relaxer treatment, and (C) heat treatment.*

Following measurement of samples subjected to treatments of a non-oxidative nature, including heat-treatment used for hair straightening, and relaxer treatment, which weakens internal hair bonds, di-sulphide bonds in particular, to chemically straighten fibres, no observable trend was shown (figure 3.15B, C). Therefore, FLIM measurement appears to be most useful in detecting chemical change brought about through oxidative means. Significantly, these data suggest that the chemical changes which appear to result in increases to fluorescence lifetimes, namely the production of kynurenines, are unique to oxidative damage.

3.3. Discussion

The aim of this study was to investigate the potential and develop the use of FLIM as an imaging modality for the assessment of hair damage, originating from hydrogen peroxide bleaching in particular, in order to quantify and localise the chemical changes taking place and to further understand these changes.

3.3.1. FLIM can discriminate between structures within hair

To begin, untreated hair was examined using FLIM. Importantly, there was seen to be little difference in the average lifetime of samples both between hairs from the same individual, but also between individuals. This is in contrast to the small amount of previous FLIM work undertaken on hair by Ehlers et al. which found differences between hairs from a number of individuals when using multiphoton FLIM at 740 nm (Ehlers et al., 2007, 2006). The use of 470 nm excitation with single-photon FLIM improves its utility as a method for detecting damage, as untreated hairs possess fairly constant average lifetime and therefore treated hairs would be more likely distinguishable from untreated hairs regardless of the individual of origin.

One difference of note which was particularly apparent between individuals was the presence of a distinct cuticle-cortex boundary. Within this study, hairs from an individual displayed commonality in either possessing this low-lifetime cuticle, or showing no distinct boundary between cuticle and cortex. Work during this study indicated that, rather than fluorescence lifetimes being influenced by the environment within the fibre, pH for example, the chemical composition was largely responsible for fluorescence lifetime. These findings together suggest that hair from an individual which displays this distinct boundary may do so owing to the presence or abundance of a chemical species not found in the remainder of the fibre. The identification of this chemical species is not investigated during this work. However, previous literature highlights a difference between protein composition between

individuals based upon age, race, and sex, which could be among the possible causes of the phenomenon occurring only in certain individuals (Giesen et al., 2011; Laatsch et al., 2014). It is of note that any boundary present before oxidative damage, was no longer visible following the damage. This observation may suggest that the low-lifetime fluorescent species is particularly subject to destruction or modification by oxidation.

A gradient of fluorescence lifetime was also described within the cortex of hairs imaged, where lifetime was seen to decrease towards the outer surface of the fibre. This is of interest as it suggests that chemical composition may vary throughout the cortex rather than possessing complete homogeneity. Previous work investigating the expression of keratin and KAP mRNA, the two largest groups of proteins within hair, described no gradient of expression within the cortex. Rather, proteins are often expressed equally throughout the cuticle, the cortex, or both, with the timing of this varying between proteins during production of the hair fibre within the follicle (Langbein et al., 2001, 1999; Rogers et al., 2006) although this does not rule out innate gradients in protein composition. Little work has been completed using antibodies to describe the location of proteins within formed hair. An alternate possibility is that this gradient is introduced through wear-and-tear of the fibre, possibly due to natural conditions it is subjected to. Interestingly, photooxidation through UV exposure would be a likely candidate for this if not for the fact that the increase in lifetime expected from UV would be more likely to produce a gradient in the opposite direction from that seen here. This is due to the rationale that the outer cortex is likely to be more susceptible to UV damage, while the inner cortex may be sheltered due to the presence of melanin in the outer cortex, in addition to the finding during this study that photooxidation causes an increase in fluorescence lifetime. If the gradient is caused by external stresses to the hair, it is possible that these stresses act by a mechanism not described within this study and serve to lower the lifetime of the outer cortex while the inner cortex is less affected.

3.3.2. Destruction of melanin following hydrogen peroxide bleaching is detectable using LSCM

Before the determination of FLIM's ability to detect oxidative damage, work was first completed to observe the desired effect of hydrogen peroxide bleaching – melanin destruction. Using techniques previously unpublished, melanin was visualised as both voids lacking fluorescence and as reflective punctae, depending on the imaging technique used. Imaging of both untreated and hydrogen peroxide bleached fibres revealed a significant reduction in melanin granules following treatment.

3.3.3. Oxidative damage results in altered fluorescence lifetimes of hair

Further experimentation, following confirmation that melanin destruction was achieved by the hydrogen peroxide bleaching treatment in use, aimed to determine if oxidative damage did indeed alter the fluorescence lifetime of hair. Using FLIM measurement, the average lifetime was seen to increase markedly following bleaching, an effect which increased more steadily to an eventual plateau with increasing hydrogen peroxide. Similar results were seen from increasing ammonia in the presence of hydrogen peroxide. Contrastingly, the effect of increasing either NH_3 or H_2O_2 alone is negligible in comparison. These data allow several conclusions to be made. Primarily, the increase in average lifetime is shown to occur only through the combination of hydrogen peroxide and ammonia. Altered chemical environment, high pH in particular, as an explanation for average lifetime increase is ruled out as all bleaching treatments were performed with equal amounts of NH_3 and so the increase occurs with added hydrogen peroxide. Additionally, experiments performed with increasing concentrations of NH_3 alone result in no change to average lifetime. This suggests that the cause of the fluorescence lifetime change is due to the combination of hydrogen peroxide in an alkaline environment, which is facilitated by NH_3, resulting in an oxidative effect. These data suggest that hydrogen peroxide bleaching is changing the composition of fluorophores in the hair responsible for lifetime.

Hydrogen peroxide (H_2O_2) is in equilibrium with hydrogen cations (H^+) and perhydroxyl anions (HO_2^-). Reaction of additional hydrogen peroxide with a perhydroxyl anion results in formation of hydroxyl (HO)• and perhydroxyl (HO2)• free radicals which are likely to interact with other molecules. Increased pH shifts the equilibrium towards the formation of perhydroxyl anions and therefore increases the rate at which the decomposition of peroxide takes place (Torres et al., 2014). Hydrogen peroxide alone may not cause a change in lifetime due to the lack of dissociation of perhydroxyl anion, reducing hydrogen peroxide's efficacy. Increased ammonia, and therefore pH, increases the chemical change detected, when peroxide is present, due to increased dissociation of the perhydroxyl anion. Ammonia alone, and therefore pH, have little effect on the lifetime of hair alone due to the lack of hydrogen peroxide's oxidising properties.

The plateau in fluorescence lifetime and apparent chemical change seen during this experiment is of interest. To investigate further, lifetime change was instead compared against pH, rather than ammonia concentration, when hydrogen peroxide is present. Results showed a linear correlation, with increased pH resulting in greater lifetime change. This

result suggests that the role of ammonia during hydrogen peroxide bleaching is largely to increase pH, rather than allowing greater uptake of active reagents through facilitation of hair swelling. This may be explained as the active ingredients of hydrogen peroxide bleaching are small. When bleaching is combined with oxidative dyeing, where larger dye molecules are used, ammonia may allow greater uptake of these compounds beyond the effect produced by high pH alone. The diminishing effect of increased hydrogen peroxide may be caused by a number of possibilities. Among these options are a lack of access to, or exhaustion of, what may be called a precursor. Assuming that fluorescence lifetime change is brought about by reaction of free radicals with a molecule in hair, hypothesised during this study to be tryptophan and its oxidation products, increased hydrogen peroxide may cease to have any effect once this molecule is fully reacted. Alternatively, it may be true that only a portion of this molecule is easily accessible during the course of the experiment. Further work during this study suggests the latter of these options is most likely, with only a small proportion of the tryptophan affected by oxidative damage.

3.3.4. A distinct fluorescent component is identified as the cause of increased average lifetime following oxidative damage

Further analysis of gathered data involved separation of fluorescence into 3 distinct components. Previous FLIM analysis of hair is extremely limited. Work by Ehlers et al. which utilised multiphoton FLIM involved excitation at 740 nm, causing functional excitation at 370 nm, resulted in 2 components termed fast and slow components (Ehlers et al., 2007, 2006). During this study, single-photon FLIM was used, with excitation taking place at 470 nm, which may explain differences in observations between these bodies of work. Components 2 and 3 were responsible for the vast majority of all hair fluorescence. Following bleaching, the distribution of component 2 remained unaltered, in contrast to component 3 which increased in fluorescence lifetime and in the number of photons attributed. It is possible therefore that component 3 originates from a chemical species, or group of similar chemical species, which are produced during bleaching. The composition of this group may also shift during bleaching to higher lifetime components. One possible explanation for this is that tryptophan residues within hair are oxidised by the bleaching treatment to one of a group of tryptophan-oxidation products known also as kynurenines. These kynurenines are excitable at the laser wavelength of 470 nm used here, and will produce emitted light within the wide spectral capture window used. Additionally, these kynurenines have previously been identified as the cause of hair yellowing and changes to emission in the 395 – 500 nm range, particularly 420 nm (N-formylkynurenine), 460 nm (kynurenine), and 495 nm (3-

hydroxykynurenine), following photo-oxidation (Daly et al., 2009; Jachowicz and McMullen, 2011; Longo et al., 2013; Millington, 2006; Schafer et al., 1997). Creation of kynurenines through oxidative damage caused by hydrogen peroxide bleaching may therefore contribute to the increase in intensity and fluorescence lifetime of component 3. Although the studies mentioned have highlighted kynurenine production during photooxidation, none have identified this following hydrogen peroxide bleaching despite similarities in the oxidative nature of damage caused. Further, the work undertaken by Ehlers et al found that, using multiphoton FLIM at 740 nm, the fluorescence lifetime of components was unchanged following oxidative colouring treatment, perhaps suggesting that the fluorophores excited by Ehlers et al. are distinct from those excited here at 470 nm (Ehlers et al., 2007).

3.3.5. Dialysis of hair results in partial reversal of fluorescence lifetime change following oxidative damage

Work within this study aimed to use prolonged soaking of the hair in dH_2O, or dialysis, to understand the mobility and solubility of the molecules responsible for altered fluorescence. Observation of the distinct lifetime components following dialysis showed a reversal of component 3 distribution and lifetime towards that seen in untreated hair. This suggests that a large proportion of the newly produced or altered molecules are highly mobile and readily able to diffuse from the fibre, despite a small portion remaining within the hair. Assuming that altered fluorescence lifetime is due to oxidation of tryptophan residues, these residues could belong to large intact proteins such as keratins, or smaller proteins such as the KAPs. Alternatively, alteration of tryptophan could occur to free amino acids or tryptophan belonging to short peptides. Results here suggest that the majority of tryptophan conversion occurs to residues which belong to mobile components such as free amino acids or peptides and possibly smaller proteins such as the KAPs. This could also be linked to the plateau seen earlier in average lifetime change despite increased hydrogen peroxide concentration. It is possible that, despite a large reservoir of tryptophan in the hair, only a small proportion of this is available for oxidation under the conditions of hydrogen peroxide bleaching, and this is preferentially occurring to tryptophan belonging to mobile components. This tryptophan is converted to one of a number of kynurenines which then diffuse from the hair under dialysis conditions.

Interestingly, there is little change in the lifetime of untreated hair following soaking. This could be due to the fact that the chemical species responsible for component 3 fluorescence are present in control hair only when attached to immobile components such as large

proteins, perhaps due to a lack of kynurenines produced through oxidative damage or due to regular washing removing any mobile components containing kynurenines.

In summary, dialysis is able to reduce the average lifetime of fibres towards those of untreated hair. However, this reversal is not complete, with distinction still possible between untreated hair and hair that is subjected to oxidative damage and subsequently dialysed. Importantly, this result does not indicate that the oxidative damage is being reversed by this dialysis, instead it is likely that the evidence of the damage is being, at least partially, removed.

3.3.6. Spectral FLIM highlights the range of emission wavelengths where average lifetime is affected

Spectral analysis in combination with FLIM, also known as SLIM, was utilised to determine the emission of individual components detected earlier using FLIM, particularly components 2 and 3. It was demonstrated that both component 2 and 3 are spectrally indistinct and have emission peaks in close proximity to the excitation wavelength of 470 nm. This result shows that, without the use of FLIM, changes to component 3 specifically would not be detectable. Data also suggests that component 3 excitation maxima is likely close to the excitation wavelength of 470 nm used here. This would also agree with the peak emission wavelengths of a number of kynurenines such as N-formylkynurenine (420 nm), kynurenine (460 nm), and 3-hydroxykynurenine (495 nm) (Daly et al., 2009). Furthermore, changes in average lifetime throughout the emission spectra, when untreated and damaged fibres were compared, revealed the largest change occurring below 600 nm. This also agrees with existing literature examining photodamaged fibres, where emission properties between 395 – 500 nm were shown to be altered (Daly et al., 2009; Jachowicz and McMullen, 2011).

In summary, results here agree with the hypothesis that changes in fluorescence may be due to changes in composition of tryptophan oxidation products, kynurenines. Additionally, FLIM was shown here to be essential in distinguishing between fluorescent components of hair which cannot be separated by emission characteristics alone at 470 nm excitation.

3.3.7. L-Kynurenine concentration is increased following oxidative damage

In order to strengthen the hypothesis that, as in photooxidation, hydrogen peroxide bleaching results in kynurenine formation and subsequently this affects average lifetime, measurement of tryptophan and its oxidation product kynurenine was carried out. Following quantification of tryptophan and kynurenine in hair samples, it was shown that, following

oxidative damage, there is a marked increase in the amount of L-kynurenine in hair. This can be compared to the increase seen in the number of photons attributed to component 3 following oxidative damage. When doing so it is important to remember that L-kynurenine is being used here as a marker for several tryptophan-oxidation products such as N-formylkynurenine and 3-hydroxykynurenine. The correlation between kynurenine and counts attributed to component 3, combined with knowledge of kynurenine excitation wavelengths, which are in close proximity to 470 nm (Daly et al., 2009), suggests that kynurenines are responsible either fully or partially for fluorescence lifetime component 3. The distribution of component 3 as a broad peak, rather than a narrow peak as in the case of unidentified component 2, may be due to the wide range of tryptophan-oxidation products possible and their varying fluorescence characteristics. As discussed earlier, the decrease in tryptophan is comparable to the increase in kynurenine, yet small in relation to the total reservoir within hair. This suggests that only a proportion of tryptophan is accessible for modification during the conditions used for hydrogen peroxide bleaching when the plateauing effect seen from additional hydrogen peroxide concentration is considered. This amount of tryptophan available for conversion could change with increased bleaching time. This small change in tryptophan may highlight the sensitivity of FLIM as a technique for measuring this oxidative damage. Additionally, it is possible that, rather than the increase in average lifetime being attributed entirely to conversion of previously unmodified tryptophan, a proportion may be due to reaction of existing tryptophan oxidation products to produce alternate products.

3.3.8. <u>Protein composition changes highlight adverse effects of oxidative damage on KAPs</u>

Oxidative damage has been shown within this study to alter individual amino acid residues. In order to determine if hydrogen peroxide bleaching also impacted whole proteins, in addition to amino acids such as tryptophan as previously investigated, 2D SDS-PAGE was used to observe hair protein composition. Following oxidative damage, KAPs in particular were observed to be particularly affected, with a near-complete lack of KAPs present following the 2D separation of hair's soluble protein fraction despite clearly visible spots, identified as KAPs following solubilisation of untreated hair. Due to the complex nature of radical reactivity with proteins there are several explanations for this result. Reaction of radicals with proteins is possible at a wide range of sites including amino acid side chains and the protein backbone. Reaction can result in the formation of additional radicals, further increasing complexity (Davies, 2016). The possibilities for proteins following radical reaction are many, including fragmentation, aggregation through hydrophobic or covalent

interactions, altered conformation, and altered interactions (Davies, 2016; Salvi et al., 2001). Therefore, one possibility is that the soluble KAPs, which may be those that are easily accessible to the oxidative effects, are fragmented during treatment resulting in insufficient whole protein remaining for separation by 2D-SDS-PAGE. Alternatively, modifications to side chains could result in additional interactions between KAPs and adjacent protein, causing KAP to no longer be solubilised during extraction. Finally, it is also a possibility that radical oxidation breaks interactions between KAPs and nearby proteins, either through change of conformation or through breakage of di-sulphide bonds, possibly through fracture of C-S linkages as described in previous literature examining hair proteins following photodamage (Hoting et al., 1995; Tatsuda et al., 1987). Loss of these interactions, possibly combined with backbone fragmentation, could lead to KAP loss in the bleaching solution or subsequent washes resulting in a lack of KAP in the soluble fraction following extraction. Earlier work examining the effect of dialysis would also support that molecules containing modified tryptophan, which may be these KAPs or KAP fragments, are lost following prolonged dH_2O soaking. Nevertheless, it is clear that KAPs are adversely affected following bleaching, and highlights a lack of literature regarding the interactions of KAPs with surrounding hair proteins.

3.3.9. Average lifetime changes following damage are specific to oxidative damage

Finally, FLIM was used to examine hairs following other potential forms of damage which may occur to hair. This included another form of oxidative damage, UV-exposure, which results in photooxidation. Non-oxidative forms of damage were also included such as that resulting from straightening with a flat-iron, termed heat-treated, and chemically straightened hair, where bonds within hair, particularly di-sulphide bonds, are relaxed, termed relaxer-treated.

Through the use of FLIM, hair following non-oxidative treatment, either heat-treatment or relaxer-treatment showed no correlation between average lifetime and treatment intensity. This supports the hypothesis that the oxidation of tryptophan is required for change to average lifetime. It is possible that FLIM, using other excitation wavelengths besides 470 nm used here, may detect alternate chemical changes within hair.

Unlike oxidation through hydrogen peroxide bleaching, photooxidation in hair has been studied by numerous groups previously. Hair, when exposed to UV radiation, is known to induce the formation of radicals through absorption of UVB light by amino acids such as tryptophan, tyrosine, and cysteine (Nogueira et al., 2006; Wardman, 1994). Work involving

a combination of both wool and human hair has revealed further that these radicals result in the production of a variety of tryptophan oxidation products such as N-formylkynurenine, kynurenine, and 3-Hydroxykynurenine which are detectable at wavelengths ranging from 395 – 500 nm and cause photo-yellowing of fibres (Daly et al., 2009; Jachowicz and McMullen, 2011; Longo et al., 2013; Millington, 2006; Schafer et al., 1997).

UV irradiation of hair samples and subsequent FLIM measurement produced strikingly similar changes to average lifetime when compared to oxidative damage following hydrogen peroxide bleaching. This similarity between oxidative treatments, further strengthens the hypothesis that oxidation of tryptophan is responsible for changes to fluorescence lifetime. Interestingly, a plateau was also created in the average lifetime following increased exposure to UV. This suggests that a similar mechanism is present in both photooxidation and hydrogen peroxide oxidation which appears to prevent modification of further tryptophan. As hypothesised for hydrogen peroxide oxidation, a lack of access to unmodified tryptophan could also be the explanation for this plateau following photooxidation as radicals are likely to be generated and therefore react at the periphery of the fibre, with the centre protected through the presence of melanin.

3.3.10. Summary

In summary, FLIM has been investigated as a method to both quantify and further understand hair damage. This investigation has determined that FLIM is useful for the quantification of oxidative damage, resulting from both hydrogen peroxide bleaching and UV exposure. Changes to average lifetime when excited at 470 nm have been shown to be specific to oxidative damage, FLIM does not detect changes in fluorescence lifetime following treatments which are not primarily oxidative. The combination of FLIM with correlative techniques, LC-MS in particular, has revealed that changes to fluorescence lifetime are correlated to the production tryptophan oxidation products also known as kynurenines. This finding is novel to hydrogen peroxide bleaching but is strengthened by previous findings following photooxidation. Other techniques such as 2D-SDS-PAGE have been useful in further visualising the effects of hydrogen peroxide bleaching upon hair proteins, where KAPs appear to be adversely affected by treatment.

4. Functional Characterisation of Keratin Associated Proteins (KAPs)

4.1. Introduction

KAPs have been shown, in previous work during this study, to be adversely affected by hydrogen peroxide bleaching. The exact mechanism by which they were modified, and the effects that this may have on the fibre, was not determined within this study. However, this highlighted a lack of information regarding KAPs and their interactions within hair. Little is known about both KAP-KAP and KAP-keratin interactions within the hair follicle which eventually lead to the formation of macrofibrils and a strong hair fibre.

The hair matrix, the area surrounding KIFs which contains KAPs, has previously been described as amorphous. Interactions between KIFs and KAPs could be assumed to be due to the formation of disulphide bonds, owing to KAPs as a whole possessing large amounts of cysteine. However, KAPs are not all high in cysteine and in fact fall into 3 groups when classified by amino acid composition; HS, UHS, and HGT. Also, the expression of an individual's repertoire of KAPs varies during production of the hair fibre (Rogers et al., 2006). This may indicate that KAPs do not act simply to produce an amorphous matrix held together by disulphide bonds, and instead may have distinct functions which contribute towards hair formation. Additionally, more recent work has begun to challenge the view that the matrix is simply amorphous. Transmission electron microscopy (TEM), solid-state ^{1}H NMR, and Transient Electro-Thermal Technique (TET) were used to show that the matrix had a well-defined nano-scale grainy structure. Additionally, the size of these granules was shown to be affected by chemical treatments (Kadir et al., 2017).

Following on from the evidence in the previous chapter suggesting that KAPs are adversely affected by bleaching, this study aimed to further investigate the poorly understood KAPs in order to begin to characterise the possible KAP-keratin interactions. To accomplish this, an approach was required which was distinct from the imaging of whole hair employed in the previous chapter. In order to separate out the many protein-protein interactions which are likely required for the formation of whole hair, it was necessary to investigate these proteins in an environment separate from that of hair. The observation of live cells transiently transfected with individual KAPs provides a means to begin to understand the role of KAPs. A subset of the large KAP family were to be selected, primarily through amino acid composition in addition to their location of expression during hair production. Following cloning, these KAPs would then be investigated through transient transfection into HaCaT

keratinocytes. Observation of these cells, using a light microscopy approach, would allow study of KAP behaviour and their interactions with cytoskeletal proteins.

4.1.1. KAPs

Keratin-associated proteins are the second major protein component of hair, behind keratin. KAPs were originally discovered while investigating the protein content that surrounds KIFs within the sheep wool fibre, this finding lead to the eventual discovery of KRTAP genes in other organisms, including humans. KAPs are comparatively high in sulphur compared to keratins and are considered to aggregate, in large part due to di-sulphide bonds, in order to form a matrix of ellipsoidal proteins in the cortex and cuticle (Bhushan and Chen, 2006b; Suzuta et al., 2012). KAPs then facilitate rigid hair formation through extensive di-sulphide bond crosslinking or hydrophobic interactions within keratin (Powell et al., 1991).

KAP genes, KRTAPs, are thought to have originated following the divergence of saurospids and mammals, leading to formation of either feathers, claws, and scales in saurospids, or hair in mammals. Within mammals there is significant structural and functional conservation of KAPs, suggesting their importance (Alibardi, 2009; Alibardi et al., 2009). Indeed Khan et al. conclude that the diversity of KRTAPs can be correlated with hair evolution in mammals and are necessary for the differences in mammalian hair phenotype (Khan et al., 2014).

Although KAPs are generally considered to contain cysteine in large quantities, there are distinct families of KAPs based upon their amino acid composition. KAPs are historically divided into three families, consisting of high sulphur (HS), ultra-high sulphur (UHS), and high glycine tyrosine (HGT) KAPs. Within these families, members are further divided into nearly 30 subfamilies, based upon phylogeny and amino acid composition, containing approximately 100 gene members in humans (Wu et al., 2008). KAP proteins possessing the same name in different species have low inter-species homology (Gong et al., 2012).

KAP genes are relatively small, usually around 1 kb. Discussion has taken place regarding the presence of introns within KAP genes. However, sequences appearing to resemble small introns are similar in sequence to repeat regions present within the remainder of the gene and are able to be translated in-frame. Therefore, it is likely that all KAPs are intron-less (Rogers and Schweizer, 2005; Wu et al., 2008).

Differences exist in the number of reported genes between various studies, for example between (Rogers et al., 2006) and (Gong et al., 2012). This is in part due to the fact that

KRTAPs may not have been fully characterised, leading to the addition of further genes over time. However, the reason for differing numbers of reported genes can also often be explained due to identification of pseudogenes as coding genes or vice versa. These pseudogenes are classified as a result of a gene interrupted by a frameshift or stop codon (Khan et al., 2014; Wu et al., 2008).

Anomalies may also be caused due to the identification of KAP alleles as separate genes. For example, analysis of the KAP4 subfamily by Kariya et al. identified size polymorphisms present (Kariya et al., 2005). There it was shown that the length of cysteine-containing repeats differed whilst the rest of the sequence remained homologous. The result of this is that pairs of what were originally thought to be separate genes, in this case KAP4.11 and KAP4.14, were in fact alleles of one another. This is not an isolated finding, as other examples of size polymorphisms were also identified in other studies (Fujikawa et al., 2012; Shimomura et al., 2002). These duplications and pseudogenes are thought to likely be involved in innovation and adaptation (Hughes, 1999; Wu et al., 2008).

The expression of KRTAPs has been studied between individuals to a certain extent, revealing that changes to KRTAP expression, and indeed presence, between individuals may occur due to genetics, age, or diet (Laatsch et al., 2014). For example, the expression of the KRTAP4 subfamily in particular was seen to decrease significantly in hair follicles of the elderly compared to younger individuals, changes such as these could be responsible for the macroscopic physical changes to hair that occur with age (Giesen et al., 2011). Additionally, it was recently described that KRTAP5.5 may be linked to the malignant switch in cancer cells, where KAP5.5 was shown to be a factor in the ability for cancer cells to invade the vasculature (Berens et al., 2017). Due to interactions assumed to take place between KAPs and keratins, this suggests a role for KAP5.5 in alteration of the cytoskeleton during metastasis.

The expression of KAPs varies throughout the production of the hair fibre, in addition to differential expression occurring between the cuticle and the cortex. In the cuticle the most prevalent KAPs or KAP subfamilies are KAP5, KAP10, KAP17.1, and KAP12 along with others in lower quantity. In the cortex, KAP subfamilies KAP1, KAP2, KAP3, KAP4, KAP9, KAP7 and KAPs KAP19.2, and KAP19.2 are thought to be present in the largest quantities. HGT KAPs are believed to be expressed at the earliest stages of fibre production whereas UHS KAPs, including those of the cuticle, are among the last KAPs expressed (Bringans et al., 2007; Rogers, 2004; Rogers and Koike, 2009). Figure 4.1 also displays this information.

Although KRTAP expression is now well characterised there is little functional understanding of the KAP proteins (Rogers et al., 2006a). The high cysteine content of certain KAPs suggests that they may have a role in binding to cysteine that is most prominent in the head and tail domains of keratins. However, some KAPs instead possess a high content of glycine and tyrosine, suggesting they may possess alternate binding partners, or function to stabilise KIFs via a different means (Rogers et al., 2007b). KAP-KAP interactions may also be important for the structure of hair, allowing the creation of a cross-linked and stable matrix (Rogers et al., 2008).

A number of studies have contributed knowledge towards understanding the function of KAPs. In a particular study, KAP2.1 was shown to self-interact via di-sulphide bonding. In addition, co-immunoprecipation (co-IP) was employed to show binding of KAP2.1 with K85, K86, and K34, whereas it did not interact with epithelial keratin K10, instead showing specificity for hair keratins. Using the same technique with truncated forms of K86, it was

cuticle KAPs:
KAP5, KAP17.1,
KAP10, KAP12,
KAP13.2, KAP15,
KAP23, KAP19.1,
KAP19.4,
KAP19.6, KAP21

cortex KAPs:
KAP1, KAP2, KAP3,
KAP4, KAP9, KAP7,
KAP19.1, KAP19.2, KAP6

Key:
HGT KAP
HS KAP
UHS KAP

matrix/cortex KAPs:
KAP8, KAP19.3,
KAP19.6, KAP19.7,
KAP20, KAP21,
KAP11, KAP13,
KAP15, KAP23
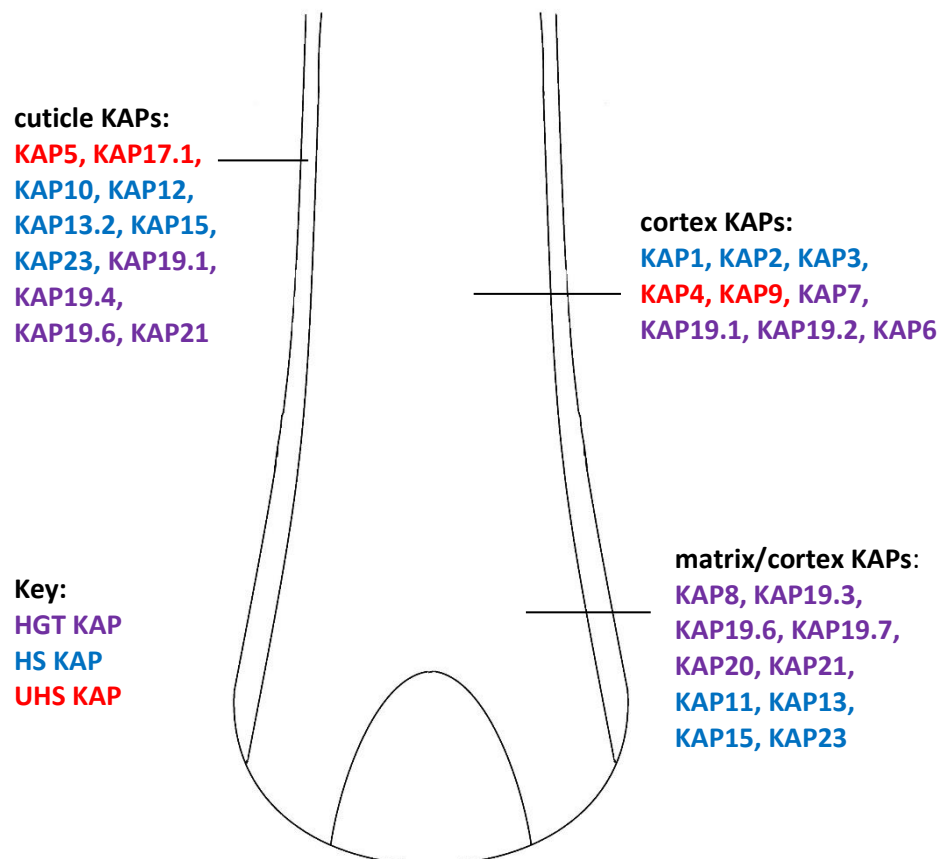
Figure 4.1: Schematic of KRTAP expression within the hair follicle. *Image adapted from Rogers, 2006 to describe mRNA expression of KAPs during keratinisation. Where KAP subfamily number is not included, this represents the whole subfamily.*

shown that interaction did not occur with the tail or rod domain of keratin, whereas interaction was possible with the head domain of K86 alone (Fujikawa et al., 2012).

In a later study KAP10.1 was the focus, normally expressed predominantly in the upper keratinising zone, similar to other cuticle-specific KAPs (Rogers et al., 2008a, 2007b). Experimentation was performed by means of co-transfection and revealed that, when co-expressed with K82, KAP10.1 exhibited granular localisation, appearing to colocalise to filaments of K82. This was seen in contrast to a diffuse cytoplasmic localisation when KAP10.1 was expressed alone, showing no interaction with the endogenous epithelial keratin present. Further investigation using co-IP succeeded in presenting that the head domain of K82 was necessary for its interaction with KAP10.1. In addition, colocalisation was shown between KAP10.1 and K85, and it was shown that KAP10.1 was also able to interact with K32, and with itself (Fujikawa et al., 2013).

Using an alternative method in a recent study, KAP1.1 localisation was detected in the cytoplasmic areas surrounding KIF bundles within cortical cells that were presently undergoing differentiation. Following further differentiation, this same cytoplasmic labelling was not visualised, and instead labelling suggested that KAP1.1 became localised to macrofibrils. Sulphydryl oxidase was also shown to be present in differentiating cortical cells. These results suggest that KAP1.1 requires di-sulphide cross-linking to associate with KIFs. Alternatively, another KAP expressed later in the differentiation process may assume a bridging role (Alibardi, 2017).

A bridging role for HGT KAPs was also hypothesised by Matsunaga et al. In this study it was suggested that KAP8.1 was able to not only bind the head domain of K85 but was also able to change its arrangement in relation to nearby keratins. It was speculated that KAP8.1 was able to bind head domains of multiple K85 proteins. This bridging role is suggested to cause a change to a helical arrangement, rather than parallel, between KIFs. In addition, it was suggested that this bridging and change in alignment results in production of orthocortex. Further evidence for this is provided as sheep lacking HGTs exhibit a lack of curl in their wool (Li et al., 2009). The interaction was speculated to occur due to cation-pi interactions, owing to the high tyrosine composition of KAP8.1 in addition to the high arginine composition of the keratin head domain. HGT KAPs are expressed shortly after the production of hair-specific keratins during differentiation. Therefore, although other KAPs have been shown to bind keratin head domains (Fujikawa et al., 2012), these are expressed later in the keratinising zone of hair and may be unable to regulate KIF arrangement. Matsunaga et al.

also present the hypothesis that HGT KAPs may provide a role in stabilising the interaction between the Desmoplakin C-terminus and KIFs (Choi et al., 2002; Matsunaga et al., 2013).

In some cases, KAPs from other mammalian species are studied. For example, Fujimoto et al., 2014 focused upon the investigation of KAP11.1 of mouse origin. As discussed earlier, there is often limited sequence homology between KAPs of the same name between species. However, this work can be useful with regard to the study of human KAPs providing that the sequence homology is considered. Mouse KAP11.1 was shown to interact with hair keratins K31, K33a and K33b, and K34. Notably, there was a lack of interaction between KAP11.1 and K39. The interaction was suggested to occur via the head domain of keratin, and further evidence was provided for this by facilitating interaction with KAP11.1 via the replacement of the K39 head domain with that of K31. These interactions were able to take place in the absence of di-sulphide bonding. However, di-sulphide cross-linking may function to further stabilise the interaction within the hair fibre. KAP11.1 dimer formation was also presented, a phenomenon which required di-sulphide cross-linking (Fujimoto et al., 2014).

In summary, despite some initial work investigating KAP interactions, the exact function of individual KAPs or KAP subfamilies remains speculation. It appears likely that HS and UHS KAPs in particular may interact with the head domains of KIFs. However, this interaction does not seem to require di-sulphide bonding in all cases. Additionally, HGT KAPs have also been shown to interact with KIFs, and may alter the macroscopic alignment of the cortex early in the production of the hair fibre. Throughout these studies, the first member of the subfamily is often used to represent that subfamily, due to the relative homology between subfamily members. Additionally, a recurring technique is the use of a cell line caused to express a given KAP in order to observe behaviour.

4.1.2. Keratins

Keratins are proteins known to form intermediate filaments (IFs). These IFs are so named due to their diameter, which is intermediate to that of actin filaments (c. 7 nm) and microtubules (c. 25 nm) (Cooper, 2000). Intermediate filaments provide a largely structural role in the cytoskeleton of eukaryotic cells and may be composed of a variety of proteins. There are six groups of intermediate filament proteins, two of which are keratins, named type I and type II keratins. Each of these groups contain both soft keratinising keratins which are abundant in the cytoplasm of epithelial cells, and hard keratinising keratins found in hair, nails, and horns of mammals.

As discussed, keratins form a major structural component of cells and can be characterised into two types: type I and type II keratins. Keratins K9 – K23, K25 – K28, and K31 – K38 are the acidic type I keratins, with K9 – K23 involved in soft keratinisation, K25 – K28 specific to the inner root sheath of the hair follicle, and K31 – K38 involved in hard keratinisation within the hair fibre. Keratins K1 – K8, K71 – K80, and K81 – K86 are the basic keratins referred to as type II. Of these proteins, K1 – K8 and K71 – K80 are involved in soft keratinisation, with K71 – K75 being specific to the soft-keratinising and cornifying cells forming the inner root sheath of hair follicles. K81 – K86 are produced specifically in the hard-keratinising cells of human hair (Bragulla and Homberger, 2009; Langbein and Schweizer, 2005). In summary, keratins found in hair may be one of 9 type I keratins: K31 – K38, including K33a and K33b, or one of 6 type II keratins: K81 – K86.

The cuticle and cortex show differential expression of hair-specific keratins (Moll et al., 2008). Keratins expressed to the greatest extent in the cuticle are K32, K35, K82, and K85. In the cortex the most prevalent keratins are K31, K33a, K33b, K34, K35, K36, K37, K38, K81, K83, K85, and K86 (Langbein et al., 2001, 1999).

The molecular weights of all keratin proteins range from 40 – 70 kDa, with type I keratins often around 45 kDa whereas type II typically range in weight from 50 – 60 kDa (Sun et al., 1983). Type I keratins typically possess isoelectric points (pI) of 4.9 – 5.4, whereas type II commonly have a pI of 6.5 – 8.5. However, keratins specific to hair have a pI range of 4.7 – 5.4 (Marshall, 1983). These pIs may be altered due to post-translational modifications of amino acids (Bowden et al., 1984).

A keratin monomer possesses three domains consisting of a central rod, which is comprised of helical domains interrupted three times by non-helical domains. The rod is then surrounded by non-helical termini (Haines and Lane, 2012; Robbins, 2012). Variations between individual keratin proteins is largely in amino acid composition. This composition varies between epithelial, epidermal, and hair-specific keratins in addition to the differences present between the three domains (Strnad et al., 2011). The rod domain is the most highly conserved, exhibiting the least variation in amino acid composition, therefore keratins possess a relatively common central helical rod while differing in their N- and C- terminal domain size and sequence (Jenkins and Powell, 1994; Langbein and Schweizer, 2005). For example, the proportion of cysteine in hair-specific keratin termini is higher than that of epidermal and epithelial keratin, indeed some epithelial keratins contain no cysteine. In hair-specific keratins, the C-terminal tail domain has the highest prevalence of cysteine, followed

by the N-terminal head, with the rod domain containing the lowest proportion of cysteine (Strnad et al., 2011). In comparison to the other major protein group found in hair, KAPs, keratins are relatively low in cysteine with an average of 6 % (Bhushan and Chen, 2006).

Keratin monomers combine to form keratin intermediate filaments (KIFs). In hair, KIFs are formed due to the combination of an equal number of type I and type II hair-specific keratins (Bhushan and Chen, 2006b). Keratin monomers initially form coiled-coil heterodimers of one type I keratin in addition to one type II keratin. Two heterodimers then coil together in a staggered anti-parallel array to form a tetramer. Following this, tetramers then assemble end-to-end in order to form protofilaments which subsequently coil in bundles of eight to eventually form KIFs. These formed KIFs typically have a diameter of 7-8 nm (Crewther et al., 1983; Er Rafik et al., 2004; Haines and Lane, 2012).

In the human hair fibre, KIFs are surrounded by a substance termed the matrix in order to form macrofibrils, this matrix is composed of a variety of comparatively high-sulphur matrix proteins, otherwise known as KAPs (Rogers, 1959a). These two main protein components, with very different chemical composition, form the major component of hair. The macrofibrils, consisting of KIFs in a protein matrix, fill the cells of the hair cortex and provide rigidity (Lee et al., 2006; Shimomura and Ito, 2005). This rigidity is reinforced by an intercellular layer comprising cell adhesive proteins found in desmosomes, gap junctions, and tight junctions (Bazzi and Christiano, 2007; Orwin et al., 1973).

Di-sulphide bonds are thought to be particularly important for hair structure and rigidity. During the late stage of differentiation in the follicle, oxidising conditions are present which cause di-sulphide bonds to form between cysteine residues. This process brings about a change in the molecular alignment of keratins, resulting in lateral compaction of the KIFs (Fraser and Parry, 2007; Wang et al., 2000). 'Strand sliding' has been shown to occur within keratin tetramers lacking stabilisation through di-sulphide bonds (Chou and Buehler, 2012). Cysteine residues in the termini of keratins are also considered to form disulphide bonds with the sulphur-rich proteins in the KAP matrix (Robbins, 2012).

To summarise, KIFs and therefore keratins are essential for hair structure and when embedded in matrix form structures which are highly anisotropic, providing hair with unique mechanical properties such as strength and elasticity.

4.1.3. The HaCaT Cytoskeleton

HaCaT cells are an immortalised keratinocyte cell line derived from adult human skin. Keratinocytes are the dominant cell type in the epidermis, the surface epithelium of skin. Epithelia throughout the body are responsible for the protection of tissues and organs from environmental stresses. To accomplish this, the epithelial cytoskeleton must be constantly remodelled. The following section describes components of the HaCaT cytoskeleton.

4.1.4. Keratin

The most diverse and abundant of the cytoskeletal components are keratins. These form IFs which are not polarised, and additionally are not involved in intracellular transport but instead are primarily a scaffold for the cytoskeleton. Keratins are found only in epithelial cells and there are over 50 isotypes expressed in epithelia (Bragulla and Homberger, 2009). The keratin network in epithelial cells has been revealed to be highly dynamic (Windoffer et al., 2004). Rigid IFs must adapt to changing structural requirements such as during division, migration, and wound healing. Nucleation of keratin filaments occurs at the periphery, often in close proximity to lamellipodial focal adhesions. Nucleation is followed by elongation during actin-dependent translocation toward the peripheral keratin network. Precursor particles are integrated into the network where filaments move towards the nucleus and bundle. Some then disassemble into soluble oligomers while others mature into a stable network surrounding the nucleus. This process allows cycling of keratin filament proteins and adjustment to the keratin network without the loss of structural integrity (Windoffer and Leube, 2001).

Keratin filaments are assembled as heterodimers of one type I and one type II keratin. The assembled network of filaments extends from a ring surrounding the nucleus out to the plasma membrane where they are anchored by desmosomes and hemidesmosomes (Haines and Lane, 2012). Desmosomes are composed of desmosomal cadherins (desmogleins and desmocollins) that link to apposing cells via extracellular domains. Cytoplasmic components include plakoglobin and plakophilins which bind IFs via desmoplakin in order to provide mechanical stability (Delva et al., 2009).

Other proteins such as plectin associate with the keratinocyte cytoskeleton. In the epidermis Plectin functions as a cyto-linker and binds IFs as well as actin and microtubules while linking them to desmosomes and hemi-desmosomes (Castañón et al., 2013). Plectin is also thought to have a role in the localisation of KIF nucleation to focal adhesions (Windoffer et al., 2011)

and to have a role in maintaining normal keratin bundling around the nucleus to maintain nuclear shape (Almeida et al., 2015). Certain proteins such as filaggrin, involved in formation of the cornified envelope in the epidermis, show functional similarity to KAPs in aggregating keratins (Cabanillas and Novak, 2016).

Keratins vary in production depending on the cell. In undifferentiated keratinocytes, such as in the basal keratinocytes of the stratified epidermis, K5 (type II) and K14 (type I) are produced as the primary keratins (Bragulla and Homberger, 2009). K14 is also expressed in the basal cells of the inter-follicular epidermis and in the upper part of the outer root sheath of hair follicles (Langbein and Schweizer, 2005).

4.1.5. Actin

Actin is the most abundant protein in many eukaryotic cells. It is highly conserved and participates in more protein-protein interactions than any known protein. This characteristic, along with the ability of actin to transition between G-actin (monomeric) and F-actin (filamentous) under the control of nucleotide hydrolysis and a large number of actin-binding proteins (ABPs), make actin important in many cellular functions. These functions include motility, maintenance of shape and polarity, and regulation of transcription. Additionally, interaction of actin with myosin allows muscle contraction (Dominguez and Holmes, 2011).

There are 3 isoforms of actin; alpha-, beta-, and gamma- with variation occurring in only a few amino acids towards the N-terminus. The structure of actin consists of a 375 amino acid polypeptide chain folded into two major alpha/beta-domains, which due to their location are known as the outer and inner domains. Two clefts form between these domains, where the upper cleft binds nucleotide and the lower cleft, lined by predominantly hydrophobic residues, constitutes the major binding site for most ABPs and also mediates the contact between subunits in the filament.

Nucleotide hydrolysis by F-actin is a factor in regulating transition between actin forms, as the ATP state is more stable than the ADP-state. Filaments are polarised, with monomers joining the fast-growing plus end of the filament in the ATP state. Hydrolysis subsequently takes place within the filament and ADP-actin monomers dissociate faster from the minus end. This process is known as treadmilling. Although this process can account for some of actin's dynamic nature, numerous ABPs are also heavily involved. These carry out a variety of functions such as monomer sequestration, end-capping, filament severing, and filament crosslinking (Pollard and Borisy, 2003).

Microfilaments are further organised into higher order structures including closely packed bundles and loose 3-D networks. The formation of filaments and subsequent further organisation is organised by a variety of ABPs. Proteins that cross-link filaments into bundles are usually small and rigid proteins. On the other hand, proteins responsible for the formation of networks tend to be large flexible proteins allowing cross-linking of perpendicular filaments. Regardless, actin binding domains of many of these proteins are similar in structure, separated by spacer sequences that vary in length and flexibility.

Within a cell, actin filaments are particularly abundant beneath the plasma membrane to provide mechanical support, shape, and to allow movement, migration, and division (Cooper, 2000). The combination of filaments concentrated at the cell periphery and ABPs results in the formation of a 3D network known as the cell cortex (Cooper, 2000; Salbreux et al., 2012).

Many cells have a specialised region of plasma membrane in order to form contacts with adjacent cells or other substrates. These regions also serve as attachment sites for bundles of actin filaments that anchor the cytoskeleton to areas of cell contact. Cells may bind via attachment of transmembrane proteins (integrins) to extracellular matrix (ECM) in discreet regions called focal adhesions. Focal adhesions also serve as attachment sites for large bundles of actin filaments known as stress fibres. Stress fibres are contractile bundles of actin filaments cross-linked by alpha-actinin which anchor the cell via attachment at focal adhesions through interactions with integrin (Carragher and Frame, 2004; Tojkander et al., 2012).

Actin is also anchored at cell-cell adherens junctions. In epithelial cells these junctions form a continuous structure called the adhesion belt, or *zonula adherens*, around each cell where a contractile bundle is linked to the plasma membrane. Contact at these locations is mediated by transmembrane proteins known as cadherins (Hartsock and Nelson, 2008; Niessen, 2007). Adherens junctions are highly dynamic complexes and play a crucial role in the mechanical stability of keratinocytes (Vasioukhin et al., 2001).

Most cell surface protrusions also rely on actin filaments. Many protrusions are transient responses to the environmental stimuli. Pseudopodia are extensions of moderate width based on 3D cross-linked actin responsible for phagocytosis. Lamellipodia are broad sheet-like extensions at the leading edge created by a network of actin filaments. On the other

hand, filopodia are thin projections of the plasma membrane supported by actin bundles (Cooper, 2000).

4.1.6. Summary

Previous work (Fujikawa et al., 2012, 2013; Fujimoto et al., 2014; Matsunaga et al., 2013) in the study of KAPs has generally aimed to characterise a single KAP, representing its sub-family. This has often been carried out by observing the protein's behaviour when expressed in a cell line. This method allows the interactions of individual proteins to be investigated, in contrast to observations of the hair fibre as a whole where many interactions are likely to be taking place – therefore proving difficult to analyse.

For this study we used HaCaT keratinocytes, due to their expression of epidermal keratin as discussed and also their ease of use in cell culture and for transfection. An advanced light microscopy approach was used to observe cells, transfected first with KAPs alone to understand interactions with endogenous cytoskeletal proteins in HaCaTs. Further work would then aim to characterise the interactions of these KAPs with co-transfected hair-specific keratins.

4.2. Results

4.2.1. Selection of KAPs for further characterisation

Investigation and characterisation of KAPs will increase the understanding of hair fibre formation and structure. However, before experimentation with KAPs begins, it is necessary to first select a subset of KAPs. Due to the large KAP repertoire of humans (Rogers et al., 2006), it is not reasonable within this study to characterise all of these individually. Instead a number of KAPs were to be chosen, primarily based upon amino acid composition, in addition to where they are expressed within hair during fibre production.

To begin, the coding sequences for the full repertoire of human KRTAPs were compiled as described in chapter 2. As discussed previously, there are often discrepancies between the number of KAPs reported. Therefore, table 4.1 is included to summarise the KAP subfamilies at the time of this study. Table 4.1 also details several parameters for each KAP subfamily such as amino acid composition and where the protein is expressed within the fibre, if such information is available.

KAP subfamily	Functional gene members [1]	Family	Avg. Cys (%)	Avg. Gly + Tyr (%)	Expression (Cuticle/ Cortex)[2]
1	4 (1, 3-5)	HS	25.0	12.8	Cortex
2	4	HS	27.2	6.3	Cortex
3	3	HS	19.0	5.8	Cortex
4	11 (1-9, 11, 12)	UHS	35.7	3.5	Cortex
5	11	UHS	33.4	24.9	Cuticle
6	3	HGT	13.9	57.2	Cortex
7	1	HGT	6.9	34.5	Cortex
8	1	HGT	6.3	42.9	Cortex
9	8 (1-4,6-9)	UHS	32.7	4.9	Cortex
10	12	HS	26.2	2.6	Cuticle
11	1	HS	14.1	9.8	Cortex
12	4	HS	22.3	5.2	Cuticle
13	4	HS	12.4	20.0	Cuticle
15	1	HS	10.9	18.2	Cuticle
16	1	HS	18.4	3.9	
17	1	UHS	36.2	29.5	Cuticle
19	8	HGT	9.7	56.3	Both
20	3	HGT	10.1	58.3	Cortex
21	3	HGT	18.7	44.4	Cuticle
22	2	HGT	10.7	35.4	
23	1	HS	7.7	23.1	Cuticle
24	1	HS	9.1	12.6	
25	1	HS	6.9	9.8	
26	1	HS	10.0	10.0	
27	1	HS	9.2	4.3	
29	1	HS	17.3	8.5	
TOTAL	92				

Table 4.1: Summary of human KRTAPs at time of study. *KAP coding sequences were retrieved from NCBI gene database. Amino acid compositions were subsequently determined using ProtParam tool (Expasy). Averages are determined through combination of all subfamily members. **1**: Gene numbers are specified only where these are not sequential and starting from KAPx.1. **2**: mRNA expression location (Rogers et al., 2006).*
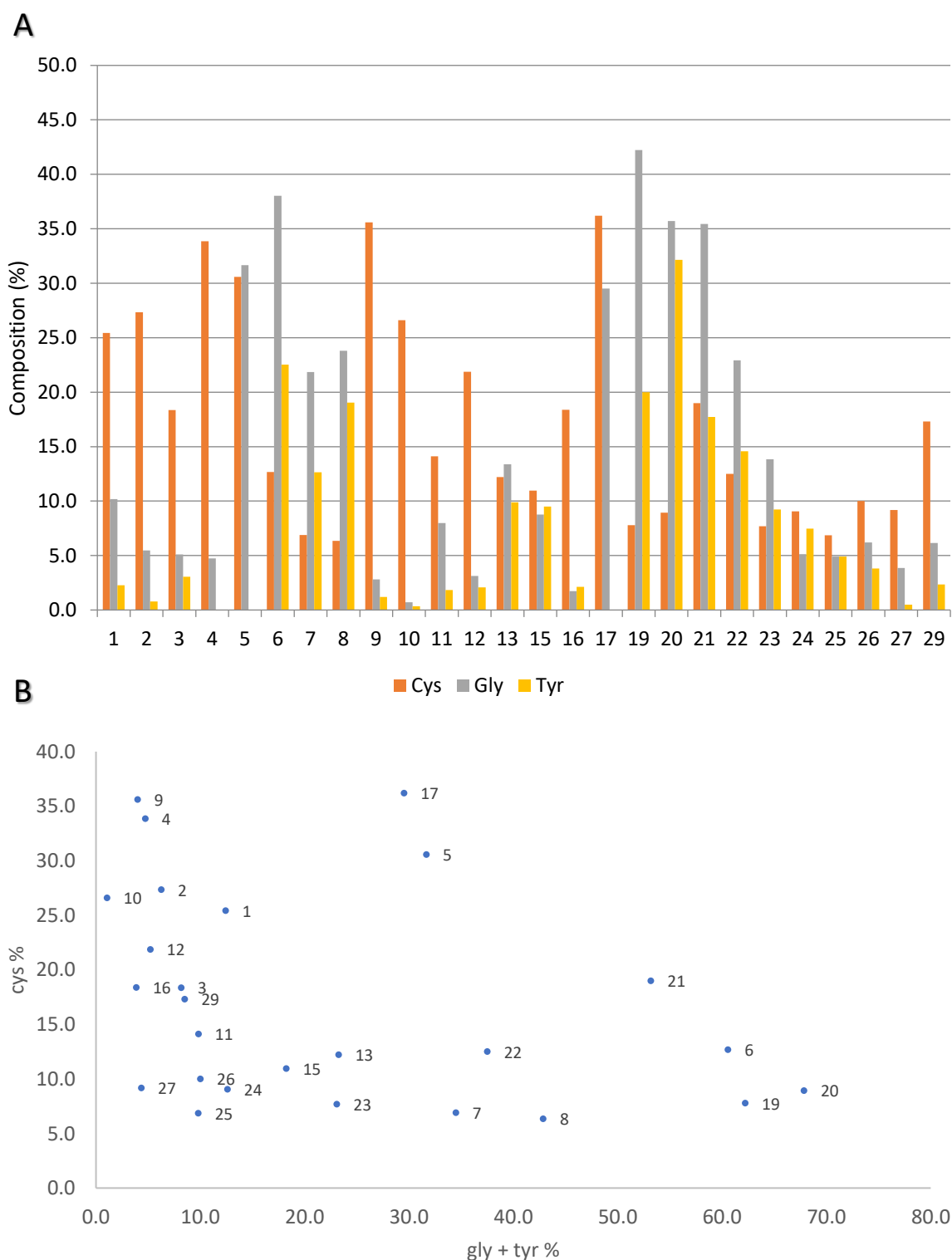
Figure 4.2: Amino acid compositions of the first subfamily member of each KAP subfamily. *Amino acid proportions of Cys (cysteine), Gly (glycine), and Tyr (tyrosine) for the first subfamily member of each KAP subfamily were retrieved using ProtParam tool (Expasy). These are represented as a bar chart (A) and as scatter plot (B) where Gly and Tyr composition are combined for plotting against Cys composition.*

Graphical representations of the amino acid compositions of the first member of each KAP subfamily are also displayed in figure 4.2, specifically the amino acids cysteine, glycine, and tyrosine. Using this information, a number of KAPs, each the first member of their subfamily (i.e. KAPx.1) were selected to provide a wide variety in terms of composition of these amino acids. In addition, one further KAP was selected which was not the first member of its subfamily. KAP19.2 has been shown to be expressed in the cortex alone, which is different to that of KAP19.1 which is expressed in the cuticle and cortex (Rogers et al., 2006). Both of these KAPs were therefore chosen to determine if they displayed different functional characteristics despite similarities in amino acid composition. The repertoire of 10 KAPs chosen for further study is detailed in table 5.2.

Chosen KAP	Classification	Fibre location
1.1	HS	Cortex
3.1	HS	Cortex
5.1	UHS	Cuticle
7.1	HGT	Cortex
8.1	HGT	Cortex
11.1	HS	Cortex
17.1	UHS	Cuticle
19.1	HGT	Both
19.2	HGT	Cortex
21.1	HGT	Cuticle

Table 4.2: KAPs selected for further study. *Selection was based upon amino acid composition and location of mRNA expression, for cloning into pEZYeGFP and subsequent study in HaCaT keratinocytes.*

4.2.2. Cloning of KAP coding sequences into pEZYeGFP

With this selection of 10 KAPs, including HS KAPs; 1.1, 3.1, 11.1, UHS KAPs; 5.1, 17.1, and HGT KAPs; 7.1, 8.1, 19.1, 19.2 and 21.1 we aimed to begin to characterise the possible differences between the KAP families and sub-families, potentially understanding further the need for such a large number of different proteins to complete the task of forming this matrix in the hair fibre. To accomplish this, KAP coding sequences were to be cloned into a mammalian eGFP-fusion expression vector for transfection into HaCaT cells.

The coding sequences of the 10 KAPs chosen for further study were amplified using specific PCR primers and genomic DNA from HaCaT cells, methodology for this amplification is detailed in table 2.2. Genomic DNA was a suitable template as all KAPs chosen for study are encoded by a single exon. KAP coding sequences were amplified with primers containing attB sites for subsequent BP cloning into entry vector pDONR207 before LR recombination into the destination vector pEZYeGFP, resulting in a construct as shown in figure 4.3, for expression as an N-terminal eGFP-tagged fusion protein in mammalian cells.

Empty vector control - pEZYeGFP

eGFP-KAP expression construct – pEZYeGFP
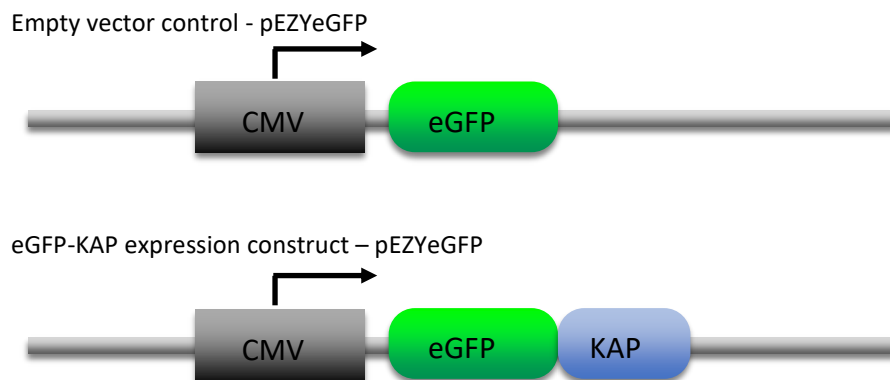
Figure 4.3: Schematic of pEZYeGFP-KAP constructs. *KAP coding sequences were amplified using PCR from genomic DNA of HaCaT cells. Gateway cloning was utilised to insert coding sequences into pEZYeGFP, a mammalian expression vector which results in expression of the desired gene under CMV promoter with an N-terminal eGFP tag.*

4.2.3. Observation of live HaCaTs transiently transfected with eGFP-KAPs

Initial experiments were carried out using live HaCaT cells, transiently transfected with pEZYeGFP-KAP to observe the localisation and any interactions of the KAPs with endogenous proteins in HaCaT cells. pEZYeGFP with no gene inserted was used as a negative control.

Transfected cells were observed live, 24 hours after transfection, using LSCM. A large number of transfected cells (typically >50) were observed before a smaller number of representative cells (approximately 5) were selected for imaging. Images of cells expressing each eGFP-KAP are shown in figure 4.4. Cells transfected with empty pEZYeGFP exhibited diffuse GFP throughout the cell, including the nucleus. Therefore, as expected, eGFP alone did not localise to any particular structure within HaCaT cells. In cells expressing eGFP-KAP a variety of localisations were observed, as detailed below.

4.2.3.1. High Glycine Tyrosine KAPs (KAP7.1, KAP8.1, KAP19.1, KAP19.2, and KAP21.1)

Strikingly, eGFP-KAP7.1 very clearly appeared to label keratin-like filamentous structures in all cases, with very little cytoplasmic background. This localisation is shown in figure 4.4. The localisation of HGT eGFP-KAP7.1 to a keratin-like filamentous network suggests an affinity of KAP7.1 for the endogenous epidermal keratin of HaCaT cells. In addition to the labelling of a keratin-like filamentous network, there was also occasionally the presence of punctae at distinct locations along the periphery of cells where filaments terminated at cell-cell boundaries. This phenomenon was observed in approximately 20% of transfected cells and may suggest affinity of KAP7.1 to another protein involved in cell-cell adhesion.

eGFP-KAP8.1 also often appeared as filaments in most cases, as displayed in figure 4.4, with around 90% of transfected cells containing labelled keratin-like filaments. However, in the case of KAP8.1 there was, at all times, lower contrast between filaments and cytoplasmic background in comparison with the filaments seen labelled by eGFP-KAP7.1. This could suggest that these KAPs display an affinity to the same filaments, but to differing degrees or with altered dynamics, such as transient binding in the case of eGFP-KAP8.1.
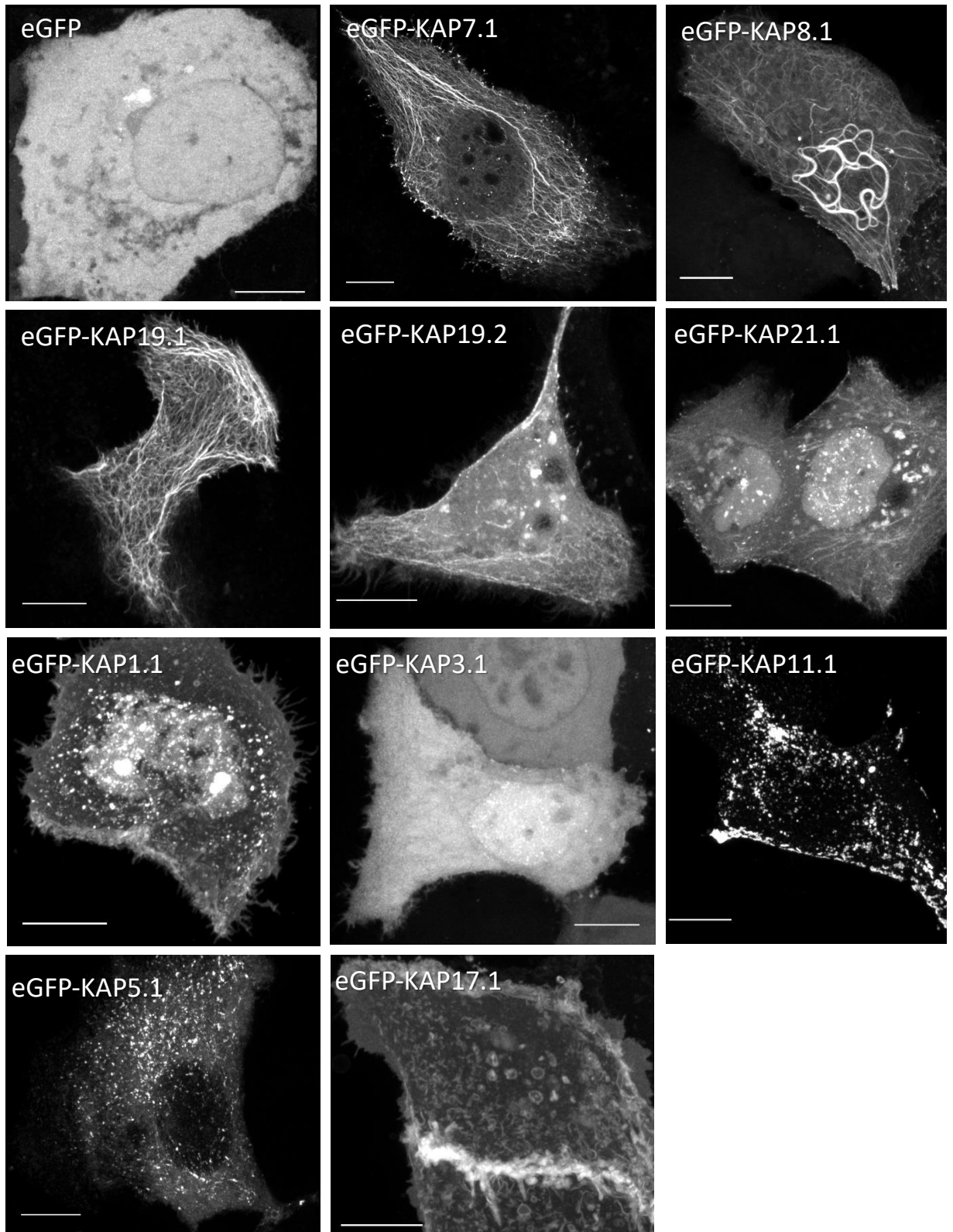
Figure 4.4: Keratin-associated proteins exhibit a variety of localisations in HaCaT cells. *HaCaT cells were transfected with pEZYeGFP-KAP constructs containing the 10 selected KAP coding sequences. LSCM using the Zeiss 880 Airyscan detector was used to capture images of live cells, 24 hrs after transfection. Representative images are shown comprising HaCaTs expressing: eGFP alone; HGT eGFP-KAPs: KAP7.1, KAP8.1, KAP19.1, KAP19.2, KAP21.1; HS eGFP-KAPs: KAP1.1, KAP 3.1, KAP11.1; and UHS eGFP-KAPs: KAP5.1, KAP17.1. Scale bars 10 um.*

eGFP-KAP19.1 exhibited localisation very similar to KAP 7.1 where labelled filaments, which are keratin-like in nature, appear with good contrast above cytoplasmic background. However, unlike cells transfected with eGFP-KAP7.1, no punctae were observed at the peripheral filament termini.

eGFP-KAP19.2 also occasionally decorated keratin-like filaments, in approximately 50% of transfected cells. However, this occurred to a lesser degree in both proportion of cells with filaments and the contrast of filaments vs the cytosolic background in comparison to previously discussed HGT KAPs.

eGFP-KAP21.1 decorated keratin-like filaments in approximately 50% of transfected cells, with significant cytosolic background. Peripheral punctae, as observed following transfection with eGFP-KAP7.1 were also observed here in around 10% of transfected cells.

In summary, all HGT eGFP-KAPs show localisation to an epidermal keratin-like network. Differences in the degree of this localisation may reflect different affinities for epithelial keratins or dynamics of interaction. In addition to this localisation, KAP7.1 in particular, and KAP21.1 to a lesser degree, also localised to discrete punctae at peripheral ends of the observed filaments. This may suggest that although the suspected affinity to keratin filaments is shared by all studied members of the HGT KAP subfamily, KAP7.1 and KAP21.1 are unique in their localisation to apparent cell-cell adhesion proteins.

4.2.3.2. High Sulphur KAPs (KAP1.1, KAP3.1, and KAP11.1)

Following transfection of eGFP-KAP1.1, this protein formed granules of irregular size, often around 1 μm, throughout the cytoplasm suggesting a degree of self-aggregation or aggregation with other cytoplasmic proteins. The granules did not appear to be organised in any way. In addition to granules, KAP1.1 also accumulated in a faint band around the periphery of the cell and highlighted thin filamentous protrusions. However, the degree to which this arose varied and was apparent in only a small proportion of cells expressing KAP1.1, roughly 5% of transfected cells. This variability may have been due to stress, cell signalling, or growth stage of the cell.

In the majority of cells, eGFP-KAP3.1 exhibited a phenotype very similar to that seen from eGFP alone. This was observed as diffuse fluorescent protein throughout the cell, including the nucleus, showing no particular localisation at structures or organelles. However, in very infrequent cases, around 5% of cells observed, KAP3.1 could be seen to localise to distinct

punctae at the cell periphery. This may be due to localisation to the same cell-cell adhesion proteins decorated by KAP7.1 in particular, however the lack of filamentous labelling by KAP3.1 means that this wasn't possible to determine.

KAP11.1 transfection resulted in the formation of irregular-sized granules, often in the range of 0.5-2 µm, throughout the cytoplasm. The organisation of the granules did not appear random, with structures often forming in linear arrangements through the cytoplasm and also clearly localising to the cell edges.

To summarise, HS KAPs do not display the same decoration of filamentous structures seen from HGT KAPs. Instead, a common behaviour is the formation of granules, which may be due to aggregation of HS KAP monomers due to their high cysteine content.

4.2.3.3. Ultra-High Sulphur KAPs (KAP5.1 and KAP17.1)

KAP5.1 was similar to KAP11.1 in localisation and showed the formation of granules throughout the cytoplasm while being excluded from the nucleus. As seen from KAP11.1, these granules could often be seen to form linear arrangements. However, unlike KAP11.1, granules formed were often smaller in size, approximately 1 µm or smaller, and there was no apparent localisation along the cell periphery.

Cells transfected with KAP17.1 always exhibited localisation to an approximately 2 µm-thick band at the cell periphery, where contact was made with another cell. This was a localisation which was also seen rarely in cells expressing KAP1.1. In all cells expressing KAP17.1 which were not completely surrounded by neighbouring cells, projections were observed at the cell's leading edge which appeared filopodia-like in nature. Additionally, there was the presence of fine filaments, particularly visible within the cell's leading edge and also at the apical surface, resembling actin. This apparent localisation to actin is unexpected for a KAP and therefore clearly warrants further investigation.
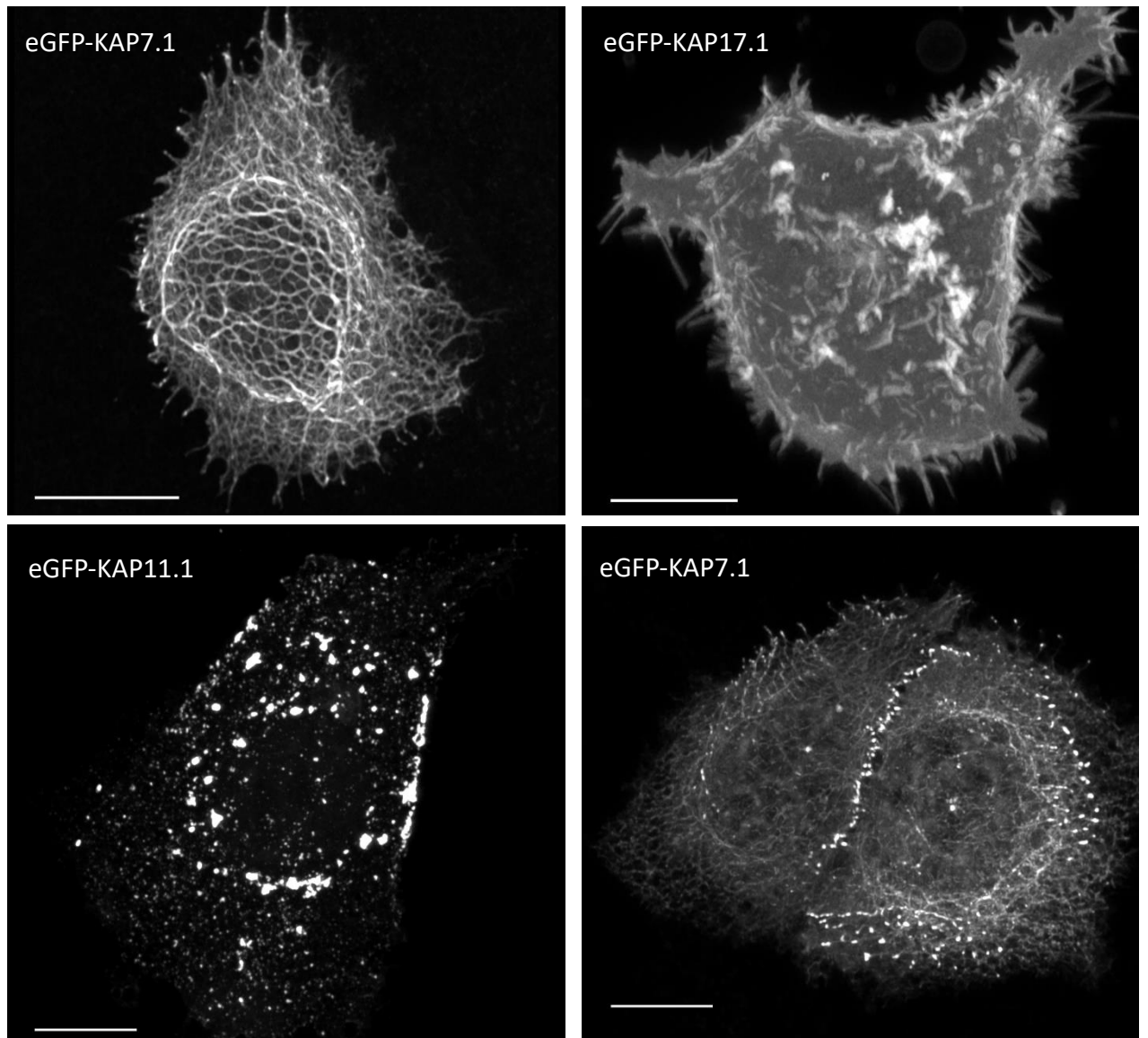
Figure 4.5: Four repeating localisations are observed in HaCaT cells expressing a variety of KAPs. Representative images were captured to demonstrate the four main localisations of interest which were observed. Live HaCaT cells expressing eGFP-KAP7.1 display decorated keratin-like filaments; KAP17.1 localises to actin-like structures; KAP11.1 forms granules, often appearing in linear arrays; and KAP7.1 occasionally forms punctae which are clearly visible at filament termini. Scale bars 10µm.

4.2.3.4. Summary

There were a number of recurring localisations, seen to differing degrees, throughout the various eGFP-KAPs. Examples of these four localisations are displayed in figure 4.5. The localisations observed are likely to be caused by interactions between eGFP-KAPs and the cytoskeletal components of HaCaT cells.

The striking decoration of keratin-like filaments by HGT KAPs in particular suggests an affinity of these KAPs for epidermal keratin not displayed by KAPs of other families and may be of

importance for the role of HGT KAPs. Also of great interest is the localisation of UHS KAP17.1 in particular to actin-like structures. The interaction of KAP with actin is unexpected and may uncover a previously unknown role for KAPs. The formation of fluorescent punctae, particularly by HGT KAP7.1, at the peripheral termini of filaments may also be of great interest, potentially highlighting a role for certain KAPs in cell-cell interactions.

Observations here, and qualitative interpretations as to the degree to which individual KAPs exhibited each of the localisations, are summarised in table 4.3.

KAP	HS/ UHS/ HGT	Keratin-like filaments	Actin-like arrangement	granules	punctae	Notes
1.1	HS	-	+	+	-	Cells exhibit varying localisation
3.1	HS	-	-	-	+	Diffuse cytosolic protein
5.1	UHS	-	-	+++	+	Granules often in linear arrangements
7.1	HGT	+++	-	-	+++	High ratio of filamentous to cytosolic protein
8.1	HGT	++	-	-	-	Low ratio of filamentous to cytosolic protein
11.1	HS	-	-	+++	+	Often in linear arrangements or at periphery
17.1	UHS	-	+++	-	-	Strong accumulation in a peripheral band
19.1	HGT	+++	-	-	-	High ratio of filamentous to cytosolic protein
19.2	HGT	+	-	-	-	Low ratio of filamentous to cytosolic protein
21.1	HGT	+	-	-	+	Low ratio of filamentous to cytosolic protein

Table 4.3: Summary of the degree to which KAPs localise to the observed structures. *The repertoire of cloned KAPs exhibit four localisations to varying degrees. Qualitative examination of a number of cells (minimum 50) for each KAP transfection was used to estimate the degree to which each KAP conforms to a given localisation.*

4.2.4. Investigating interactions between KAPs and cytoskeletal components using indirect immunofluorescence

The differing localisations of KAPs in HaCaT cells may be due to interactions of the KAPs with endogenous cytoskeletal components, specifically actin and epidermal keratin. As discussed earlier, the interaction with actin in particular is unexpected behaviour for a KAP. The following experiments aimed to investigate colocalisation between KAPs and specific components of the HaCaT cytoskeleton using immunofluorescence. HaCaT cells transfected with pEZYeGFP-KAP were fixed and cytoskeletal components were subsequently immuno-fluorescently labelled.
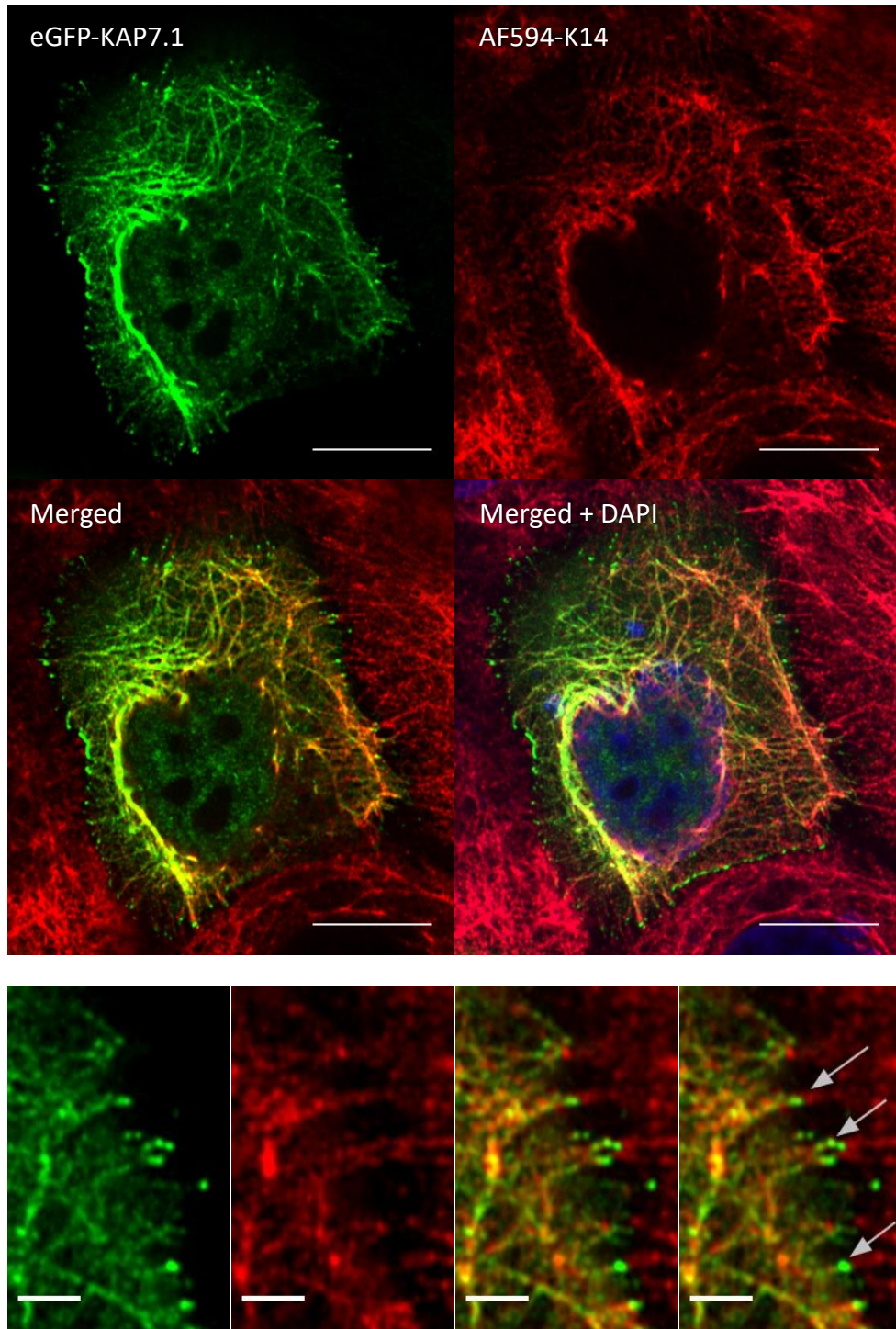
Figure 4.6: HGT KAPs colocalise to the epidermal keratin filament network. *HaCaT cells transfected with eGFP-KAP7.1 (green) were fixed and K14 (red) labelled using indirect-immunofluorescence. DAPI counterstaining was also employed (blue). Scale bars 10µm. Below is a cropped portion showing the upper right of the cell where KAP7.1 punctae, highlighted by arrows, can be seen at the termini of keratin filaments between two cells. Scale bars 2µm.*

4.2.4.1. <u>Investigating colocalisation of KAPs with epidermal keratin 14</u>

KAPs are hypothesised to bind and stabilise KIFs in hair, surrounding them in a matrix to produce macrofibrils (Bhushan and Chen, 2006; Suzuta et al., 2012). However, the keratin-like filamentous structures labelled in live HaCaT live cells transiently transfected with a variety of KAPs suggest interactions of HGT KAPs specifically with epidermal keratins, endogenous to HaCaT cells – primarily type I K14 and type II K5 in undifferentiated cells.

To investigate the localisation of KAPs in relation to the epidermal keratin network, cells were transfected, as described previously, with the full repertoire of pEZYeGFP-KAP constructs. Subsequently, fixation and labelling of endogenous K14 by indirect immunofluorescence was employed for colocalisation experiments. Confocal microscopy using the Airyscan detector was used to observe the localisation of each eGFP-KAP in relation to epidermal keratin staining.

4.2.4.1.1. <u>HGT KAPs</u>

Labelling of keratin-like filaments, seen to some degree in cells transfected with all HGT KAPs studied, and particularly in HGT KAPs KAP7.1 and KAP19.1, was shown to colocalise to K14 labelling following fixation and indirect immunofluorescence. This result suggests that indeed these eGFP-KAPs are capable of associating with epidermal keratins found in HaCaT cells. In cells transfected with KAP7.1 and KAP19.1 the KAP protein is present at all labelled K14 filaments. This colocalisation is shown in figure 4.6 with an example of a cell transfected with eGFP-KAP7.1 and colocalisation analysis by Pearson's and Mander's methods for KAP7.1 and K14 is shown in figure 4.8. This colocalisation analysis should be used in combination with images to determine the degree of interaction. In the case of eGFP-KAP7.1 in figure 4.6, colocalisation appears clearly and this also is confirmed by the colocalisation analysis in figure 4.8

In cells transfected with KAP8.1, KAP19.2, and KAP21.1, where contrast between filaments and cytoplasmic background was previously seen to be low, eGFP-KAP-labelled filaments, where visible, were seen to colocalise to the K14 network. Images of this are not shown. Together, these results confirm that a sub-section of KAPs, HGT KAPs specifically, colocalise with epidermal keratin K14 in HaCaT cells to varying degrees. The fluctuating degree to which the variety of HGT KAPs decorate K14 filaments suggests different affinities of these proteins for epidermal keratin.
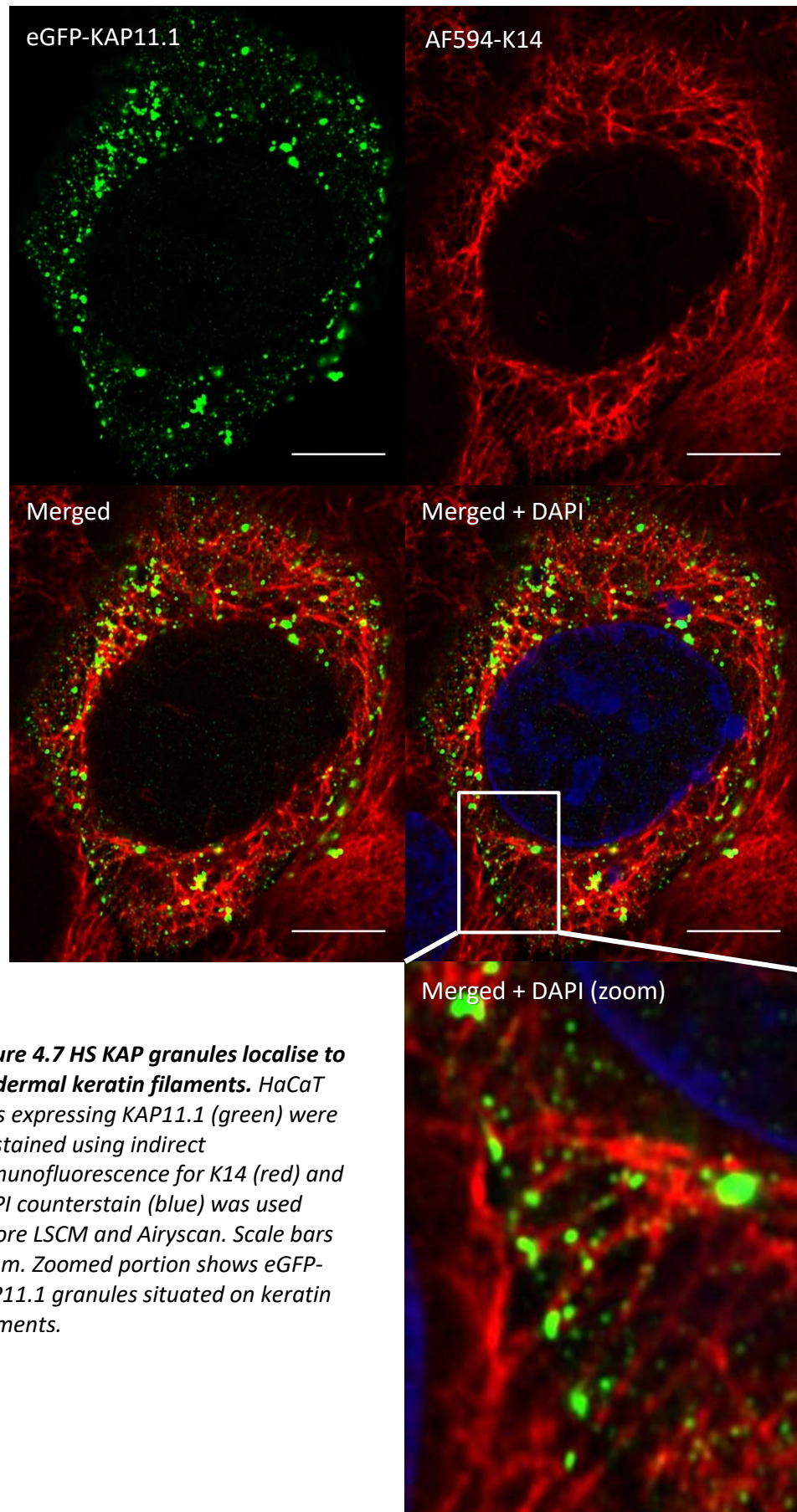
Figure 4.7 HS KAP granules localise to epidermal keratin filaments. *HaCaT cells expressing KAP11.1 (green) were co-stained using indirect immunofluorescence for K14 (red) and DAPI counterstain (blue) was used before LSCM and Airyscan. Scale bars 10μm. Zoomed portion shows eGFP-KAP11.1 granules situated on keratin filaments.*

KAP7.1 in particular also exhibited punctae at the cell edges where cell-cell borders were present, shown in figure 4.6. These punctae are also present in cells expressing HS eGFP-KAP11.1, and also KAP21.1 to a lesser extent. In the case of HGT KAPs the arrangement of protein appears differently at the periphery in comparison to the regular distribution of KAP along the keratin filaments. This may suggest that these KAPs have an affinity for proteins present at the cell membrane adjacent to peripheral ends of keratin filaments, in addition to K14 itself. Significantly, K14 staining highlighted that these punctae were localising to keratin filament termini, specifically termini where the filaments meet those from an adjacent cell as shown in figure 4.6. Taken together these results indicate that HS KAP11.1 and HGT KAP7.1 in particular may colocalise to proteins involved in cell adhesion, in addition to epidermal keratin, at these sites.

4.2.4.1.2. <u>HS and UHS KAPs</u>

In the case of KAP5.1 and KAP11.1 transfected cells, which previously showed granule formation, often in linear arrangements, many of these granules were seen to localise to, or along, K14 filaments. This is most clear when observing that there are no granules present where there are large gaps in the K14 network. Evidence of this is provided in figure 4.7 with an example of eGFP-KAP11.1 co-imaged with K14. Colocalisation analysis, shown in figure 4.8 of KAP11.1 and K14 resulted in low scores for Pearson's and also Mander's M1 – the proportion on K14 overlapping KAP. However, Mander's M2 – the proportion of KAP overlapping K14 is much higher. These results, when used in combination with images suggest that although KAP11.1 does not colocalise entirely throughout the K14 network, the KAP11.1 granules do colocalise to discreet points along keratin filaments. The reason for the M2 score not being closer to 1 may be explained, as although granules do localise to the K14 filaments, they are often larger in diameter than the keratin bundles they are associated with, resulting in KAP signal being determined as not colocalising despite being part of a granule that is clearly localised to K14.
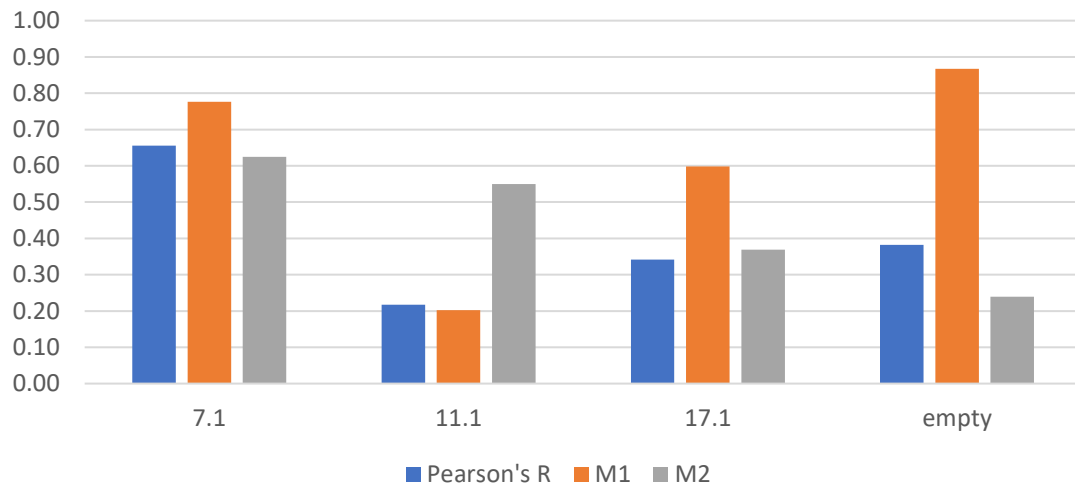
KAP	Pearson's R	M1	M2
7.1	0.66	0.78	0.62
11.1	0.22	0.20	0.55
17.1	0.34	0.60	0.37
empty	0.38	0.87	0.24

Figure 4.8: Colocalisation analysis suggests colocalisation of KAP7.1 and K14.
Colocalisation analysis was carried out using both Pearson's (Pearson's R) and Mander's (M1 + M2) methods. Both methods provide a score from 0 (no colocalisation) to 1 (complete colocalisation). Pearson's method considers signal intensity of the two colours to determine the degree of colocalisation. Mander's method requires setting of thresholds, which was performed manually, M1 represents the proportion of K14 overlapping eGFP. M2 represents the proportion of eGFP overlapping K14

The fine filaments, filopodia-like projections, and peripheral band labelled in cells expressing eGFP-KAPs which exhibited actin-like behaviour, KAP17.1 in particular, did not appear to display colocalisation with K14. Colocalisation analysis, particularly Mander's M1, suggests some degree of colocalisation however this is due to the cytosolic eGFP-KAP present. For example, a high M1 is also seen for colocalisation of eGFP alone with K14, due entirely to diffuse cytosolic protein.

The keratin network, in cells expressing the variety of eGFP-KAPs and eGFP alone, appears unaltered in all cases. Due to the variety of cells observed and imaged, varying in size, shape, growth stage, stress etc. there was inherent variability in the nature of the keratin network observed. However, the expression of each eGFP-KAP, including those KAPs which colocalise

with K14, did not appear to change the nature of the epidermal keratin nor the cell morphology, images not shown.

4.2.4.2. <u>Investigation of colocalisation of a selection of KAPs with actin</u>

Certain KAPs, UHS eGFP-KAP17.1 in particular, when imaged in live HaCaT cells appeared to localise to actin-like structures and areas at the cell periphery rich in actin. Significantly, in live cells, KAP17.1 and occasionally KAP1.1 exhibit a localisation consistent with that of actin. This included accumulation at the periphery where bordering another cell, and the presence of filopodia-like projections and fine filamentous structures, particularly at the leading edge of transfected cells. To investigate whether

KAPs colocalise with the cytoskeletal network of actin, a selection of eGFP-KAPs were transfected into HaCaTs before cells were co-imaged with actin labelling using Phalloidin. These cells were then observed using LSCM and Airyscan.

In cells expressing eGFP-KAP17.1, localisation to the periphery at cell-cell borders was consistent with actin staining, likely due to the presence of adherens junctions forming a band around the cell where neighbouring cells are present, also known as zonula adherens. The same could also be seen where filopodia at the cell's leading edge, and fine filaments visible towards the apical surface stained by phalloidin, were also decorated by eGFP-KAP17.1. This peripheral band and labelling of filopodia can be seen in figure 4.9. Colocalisation analysis of KAP17.1 and actin also suggests good colocalisation, seen in figure 4.10, where Pearson's R, M1, and M2 are all high suggesting a good degree of colocalisation.

However, stress fibres stained by phalloidin, seen spanning the cytoplasm of cells in figure 4.9, are not decorated by eGFP-KAPs above the substantial cytoplasmic eGFP-KAP signal. Therefore KAP17.1 was seen to localise to certain actin structures but not all. This suggests that the organisation of actin, and possibly the ABPs present, are important for interaction with eGFP-KAP17.1.
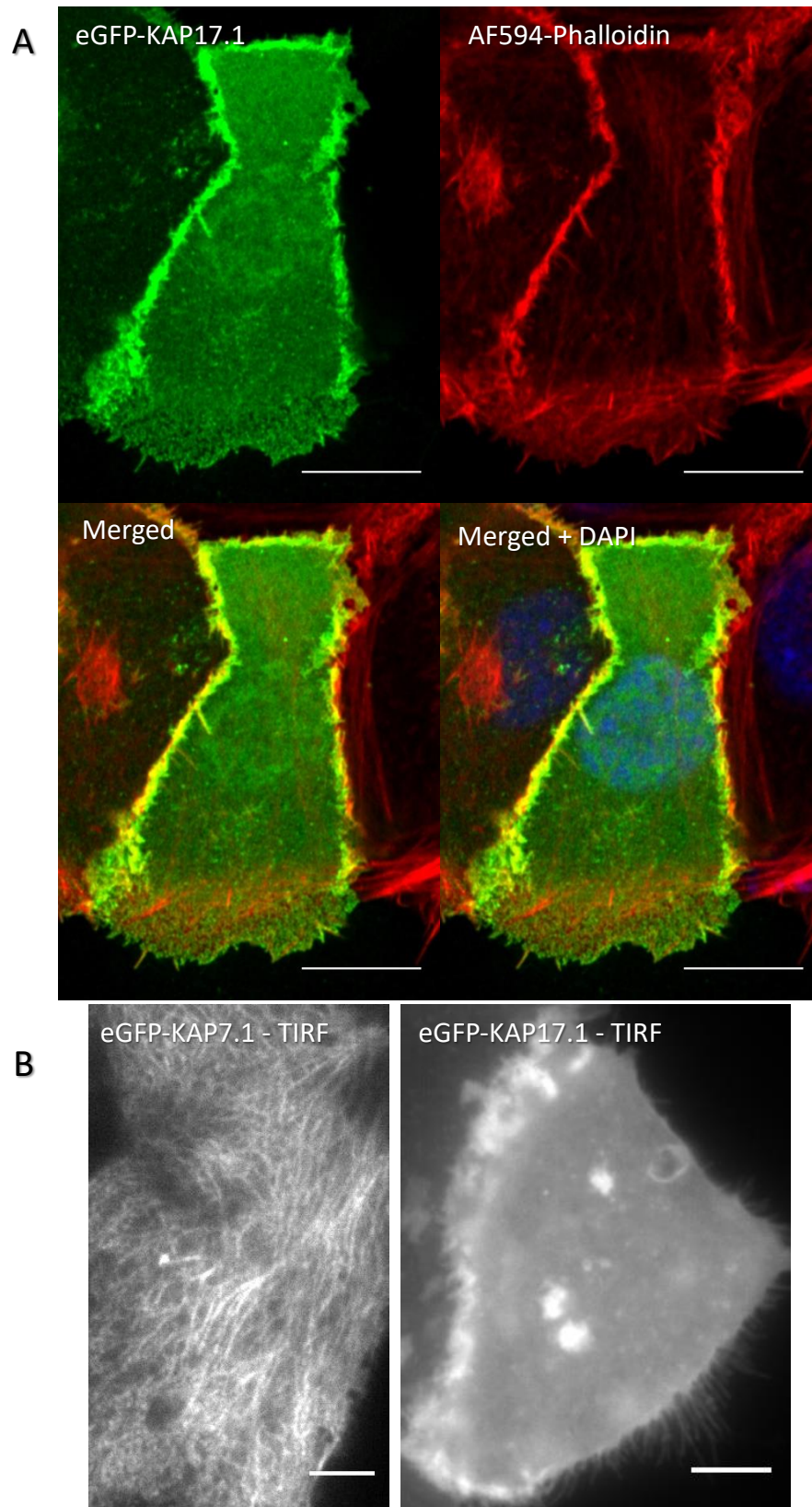
Figure 4.9: KAP17.1 localises to actin structures in HaCaTs. *A - HaCaT cells expressing KAP17.1 (green) were co-stained for actin (red) using Phalloidin before LSCM using the Airyscan detector. Scale bars 10μm. Below - TIRF of KAP7.1 and KAP17.1 confirms localisation of filaments to within 200 nm of the coverslip. B - Live cells, transfected with either KAP7.1, or KAP17.1 were imaged using the OMX and TIRF. Scale bars are 5 μm.*
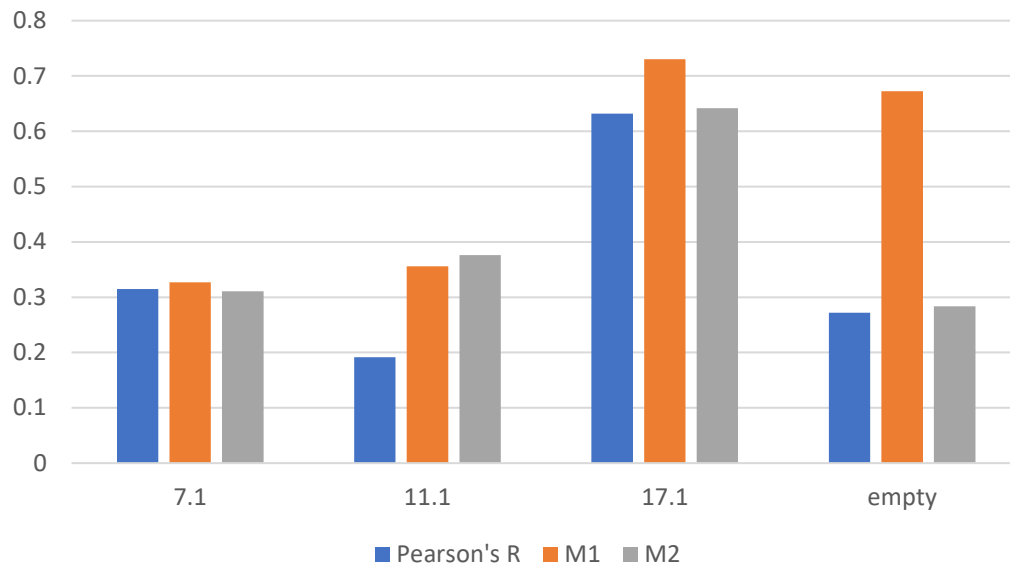
KAP	Pearson's R	M1	M2
7.1	0.31	0.33	0.31
11.1	0.19	0.36	0.38
17.1	0.63	0.73	0.64
empty	0.27	0.67	0.28

Figure 4.10: Colocalisation analysis suggests colocalisation of KAP17.1 with actin.
Colocalisation analysis was carried out using both Pearson's and Manders's methods.
M1 represents the proportion of actin (red) overlapping eGFP (green). M2 represents the
proportion of eGFP overlapping K14.

Phalloidin was also used to observe the localisation of KAPs to the actin network in cells
containing HGT KAP7.1 and HS KAP11.1. Here no colocalisation was observed. Figure 4.10
containing colocalisation analysis shows poor colocalisation of both KAP7.1 and KAP11.1 to
the actin network. As in the colocalisation analysis of K14 and KAPs, eGFP-alone results in a
high M1 score due to the cytosolic distribution.

Expression of KAPs 7.1, 11.1, and 17.1 did not have a significant observable effect on the
arrangement of the actin cytoskeleton, even in the case of KAP17.1 which shows
colocalisation, images not shown.

4.2.4.3. Investigating colocalisation of KAP17.1 with actin in live cells

In order to observe the dynamics of actin alongside eGFP-KAP17.1 in real time, a live cell actin stain; SiR-actin, was added during the imaging of live cells transfected with KAP17.1. SiR-actin binds to actin and is fluorescent when excited at 594 nm (Lukinavičius et al., 2014). Time series imaging of live cells was carried out using LSCM and the Airyscan detector.

Similar to when staining fixed cells with Phalloidin, KAP17.1 was seen to localise to various actin structures within cells that were stained with SiR actin, as shown in figure 4.11. Using time series imaging the dynamic movement of filopodia was seen where KAP17.1 also remains localised to these structures. Remodelling of filopodia can be seen in figure 4.11 where filopodia show colocalisation of both SiR-actin and eGFP-KAP17.1.
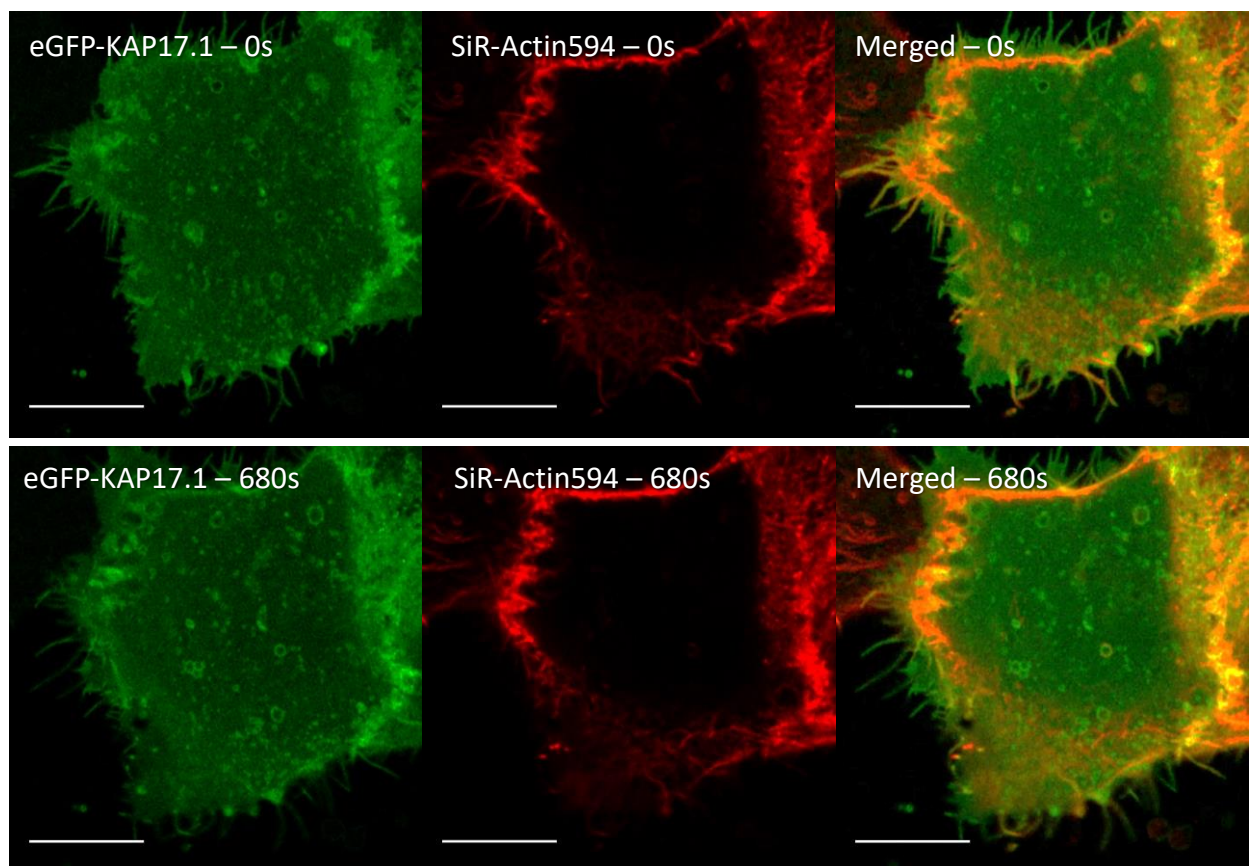
Figure 4.11 Remodeling of actin in HaCaT cells results in immediate change in KAP17.1 localisation. *Time series images taken of live HaCaT cells expressing KAP17.1 (green) and co-stained with SiR actin (red) at 0 s and 680 s. Scale bars 10µm.*

4.2.4.4. <u>Investigating colocalisation of select eGFP-KAPs and tubulin</u>

As a number of KAPs have exhibitied colocalisation to both epidermal keratin or actin in HaCaT cells we decided to also investigate if select KAPs would localise to the third and final cytoskeletal network component; microtubules. Cells, transfected with a selection of previously cloned eGFP-KAPs, were co-labelled using immunofluorescence for α-tubulin.

None of the eGFP-KAPs expressed, which included KAP7.1, KAP11.1, and KAP17.1, in addition to eGFP alone, show localisation to the microtubule network. In addition, the expression of these KAPs was also seen not to affect the microtubule network, data not shown

4.2.4.5. <u>Summary</u>

Taken together these data following investigation of eGFP-KAP localisation in HaCaT cells show that selected KAPs show different associations with cytoskeletal filaments in HaCaT cells. HGT KAPs show colocalisation with K14 epidermal keratin networks with potentially different affinities, in particular KAP7.1 and KAP 19.1 show a striking association. Selected KAPs of the HS & UHS families, particularly KAP11.1 and KAP5.1, show punctate features throughout transfected cells, potentially aggregates or higher order complexes, which are seen to associate along an epidermal keratin filament. Significantly, KAP17.1 shows colocalisation to actin-rich structures which co-label with both phalloidin or SiR-actin. No evidence is seen to suggest than any of the selected KAPs associate with microtubules in HaCaT cells.

4.2.5. <u>Observing dynamics of KAPs expressed in live HaCaTs</u>

Work within this study has demonstrated that certain KAPs colocalise with cytoskeletal components of HaCaTs. Observing this behaviour dynamically may allow us to further discover details about the nature of this association. To investigate the dynamics of these KAPs within live cells, time series imaging was carried out over a number of minutes. During these time series, FRAP was used to allow the observation of fluorescent protein movement into a photobleached region of the cell. FRAP employs the use of high laser power to photo-bleach fluorescent molecules within a designated region of a sample. In this case, eGFP-KAP is photobleached in a region of a cell and recovery is observed with time-series imaging to reveal the dynamics of eGFP-KAP.
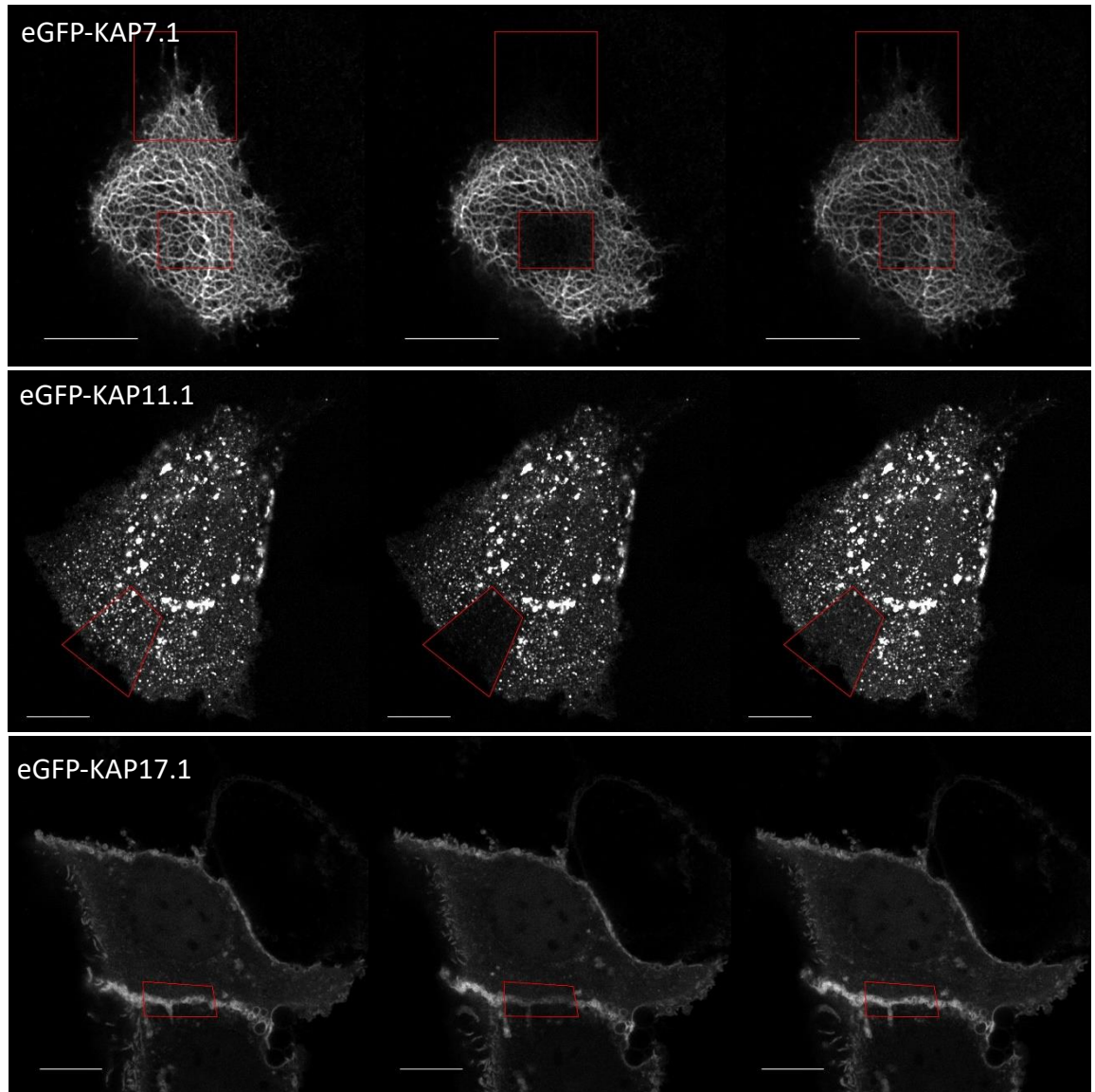
Figure 4.12 FRAP uncovers dynamics of KAP proteins in HaCaT cells. *Live cells expressing KAP7.1, KAP11.1, and KAP17.1 were imaged using LSCM and the Airyscan detector over a time series for 3 minutes following photobleaching of a designated region. Red boundary marks the photobleached region(s). Images shown are (left to right) before photobleaching, immediately after photobleaching, and following the end of recovery. Scale bars 10µm.*

Live cells representing each of the localisations were observed to determine if the labelled structures were dynamic. HS KAP11.1 was chosen to represent granule-forming KAPs, HGT KAP7.1 represented keratin filament labelling KAPs and UHS KAP17.1 was used to represent the KAPs with actin-like localisation.

4.2.5.1. <u>HGT eGFP-KAP7.1</u>

Following photobleaching of both peripheral and central areas of eGFP-KAP7.1-expressing cells there was near-complete recovery in around 3 minutes as shown in the images in figure 4.12 and also in the recovery curve in figure 4.13. The recovery of the central region occurs slightly more rapidly in comparison to the peripheral region, this is unsurprising due to the extra surface area that the central region has with unbleached portions of the cell, leading to increased diffusion back into this region. During this time the fluorescence of the whole cell decreased, as shown in figure 4.12, likely due to both the intended photobleaching and subsequent diffusion of fluorophore but additionally due to lesser photobleaching while imaging.

During the approximately 3-minute time series (supplementary movie 1), there is little movement of the filaments, this is as expected as keratin is less dynamic than other cytoskeletal components such as actin, with keratin dynamics mainly due to recruitment of subunits at the cell edge (Windoffer and Leube, 2001). The fast recovery of eGFP-KAP7.1 to the photobleached region is therefore unlike what would be expected for the recovery of keratin subunits within a filament and suggests a transient nature of association between eGFP-KAP7.1 and epidermal keratin. Flux of eGFP-KAP7.1 on and off established epidermal keratin filaments would explain the recovery of fluorescence over a short time period.

Cells expressing KAP7.1 also occasionally exhibited fluorescent punctae at the periphery of the cell where fluorescent filaments end. FRAP carried out on the peripheral region of a cell with this phenotype allowed visualisation of fluorescence recovering to not only the filaments but also these punctae, data not shown.
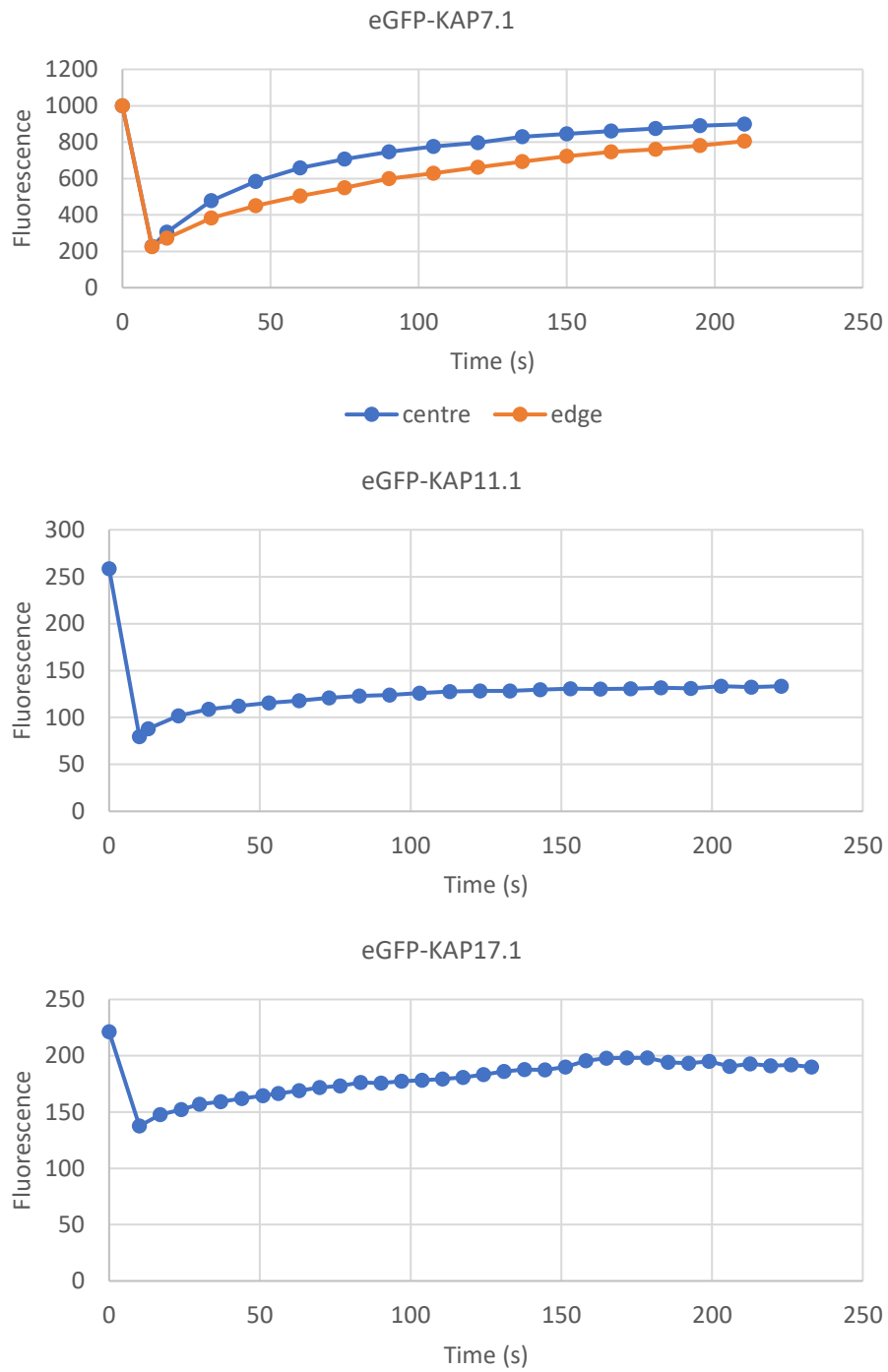
Figure 4.13 Recovery of fluorescence reveals differences between KAP dynamics.
Recovery curves plotted by measuring average brightness within the photobleached region, normalised to the average brightness in a non-photobleached region of the cell.

4.2.5.2. HS eGFP-KAP11.1

Before photobleaching, the cell expressing KAP11.1 had many fluorescent granules of varying size and shape, accompanied by weak cytosolic fluorescence. As can be seen in figure 4.12, following photobleaching there was observable of the cytosolic fluorescence within 3 minutes. However, although a small degree of recovery occurred, there was substantially less recovery of fluorescence in the larger granules, this led to very little recovery of total fluorescence over the 3 minutes, as seen in figure 4.13. Granules in unaffected portions of the cell were seen to be either fixed or free-moving, with the majority appearing stationary (supplementary movie 2). In summary, the granules observed are found to associate with keratin and are, in the main, immobile and do not recover within the experiment's time frame. This suggests that granules, once associated to the keratin network, display little flux on and off filaments. Association of new fluorescent KAP may occur much more slowly, or not at all.

4.2.5.3. UHS eGFP-KAP17.1

KAP17.1 exhibited largely peripheral localisation before photobleaching, with filopodia visible at the leading edge of the cell, as seen in figure 4.12. Photobleaching of the fluorescent area between cells lead to a rapid recovery of fluorescence, shown in figure 4.13, which occurred from either side of the photobleached area, towards the centre, which suggested that KAP17.1 protein can move easily within these peripheral bands. The time series also allows us to see the dynamic nature of the fine filaments at the cell's leading edge, which clearly move in a wave-like motion similar to what would be expected from actin (supplementary movie 3). Over the course of 3 minutes there is significant recovery of fluorescence, as seen in figure 4.13C.

4.2.6. Investigation of KAP7.1 and KAP17.1 at the base of the cell using TIRF

To study the localisation to filamentous structures of KAP7.1 and KAP17.1 in HaCaTs with increased temporal resolution and improved signal-to-noise, transfected live cells were imaged using TIRF microscopy.

Using TIRF, filaments were visible clearly at the base of a cell expressing eGFP-KAP7.1, shown in figure 4.9, confirming that some of these filaments decorated by KAP7.1 are within 200nm of the coverslip. Filaments appear similar to those expected from keratin, and time series measurements over 3 minutes show little movement of the filaments other than a small

amount of flexing, also consistent with expected keratin dynamics over the time period (Windoffer et al., 2011). However, during the time series, discrete fluctuations in brightness are visible along the filaments and appear to show movement of eGFP-KAP7.1 through the filament or dynamic association and dissociation to the filament. This observation, taken with earlier FRAP measurements of KAP7.1, further suggests a transient association between eGFP-KAP7.1 and epidermal keratin

TIRF was also used to image cells expressing KAP17.1, Filopodia, labelled with eGFP-KAP17.1 were observed within 200nm of the coverslip, as expected from filopodia, in addition to the presence of the peripheral protein band. This is shown in figure 4.9.

4.2.7. <u>Identification of the KAP7.1 keratin-binding domain</u>

The colocalisation of KAP7.1 to K14 may be due to a keratin-binding domain present within KAP7.1. To investigate this, and to elucidate the possible location of a domain, KAP7.1 was truncated to 4 equal sections using specific PCR primers and KAP7.1-pEZYeGFP as a template. Primers were designed to create attB ends for first cloning into pDONR207 then subsequent cloning into pEZYeGFP. Each was then expressed in HaCaT cells to examine the labelling of filament structures through LSCM and Airyscan of live cells.

eGFP-KAP7.1 truncated expression constructs pEZYGFP
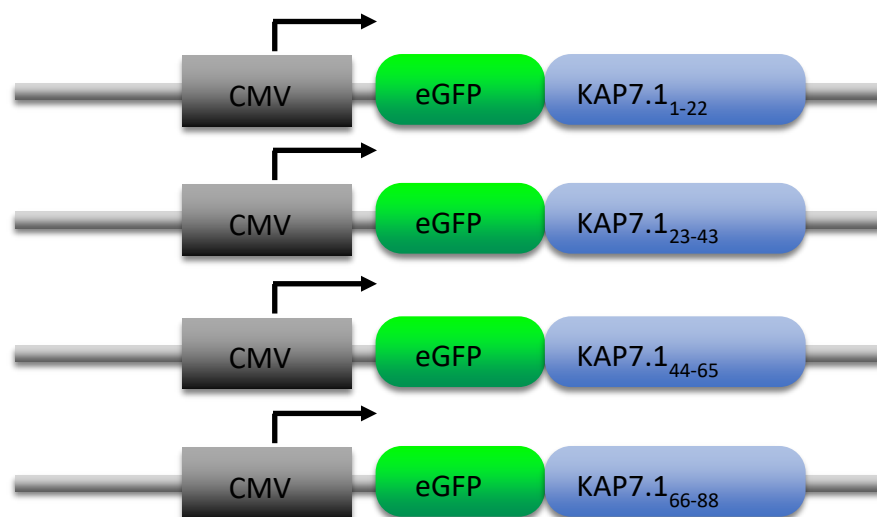
Figure 4.14 Schematic of pEZYegfp-truncated KAP7.1 constructs. Coding regions were amplified using PCR from previously cloned pEZYeGFP-KAP7.1. Subscript denotes the amino acid numbers included in each truncated form of KAP7.1, together comprising the whole protein. Gateway cloning was used to insert coding sequences into pEZYeGFP.

KAP7.1$_{1-22}$, when expressed in HaCaT cells, formed granules as displayed in figure 4.15 similar to those seen in KAP5.1- and KAP11.1-transfected cells. As previously, this may be due to self-aggregation, causing granules to form.

eGFP-KAP7.1$_{23-43}$ and eGFP-KAP7.1$_{44-65}$ both exhibited similar behaviour, appearing to be largely cytosolic with no specific localisation as shown in figure 4.15, this was similar to the organisation of free eGFP and eGFP-KAP3.1 seen previously in live HaCaT cells.

KAP7.1$_{66-88}$, consisting of the C-terminal end of the original KAP7.1 protein, showed the most similarity to full-length KAP7.1, localising to keratin-like filaments with the appearance of the K14 network previously visualised. This is shown in figure 4.15. Despite this localisation, there is substantial cytosolic protein with poor contrast of filaments, similar to that seen in HGT KAPs such as KAP8.1.

To verify that the filaments to which KAP7.1$_{66-88}$ were localising were in fact keratin, cells transfected with KAP7.1$_{66-88}$ were fixed and stained for K14 as previously described. Filaments seen on the eGFP-KAP7.1$_{66-88}$ channel, again with poor contrast against cytosolic KAP7.1$_{66-88}$, were indeed shown to colocalise to K14-stained filaments, as shown in figure 4.15.

Taken together these data show that the domain required for interaction with epithelial keratin is located at the carboxy terminal end of the KAP7.1 protein sequence from residues 66-88. Although this region is sufficient to give some filament association it is less that the full-length protein suggesting that additional regions of the protein or specific conformation is required to achieve the protein's full affinity to keratin.
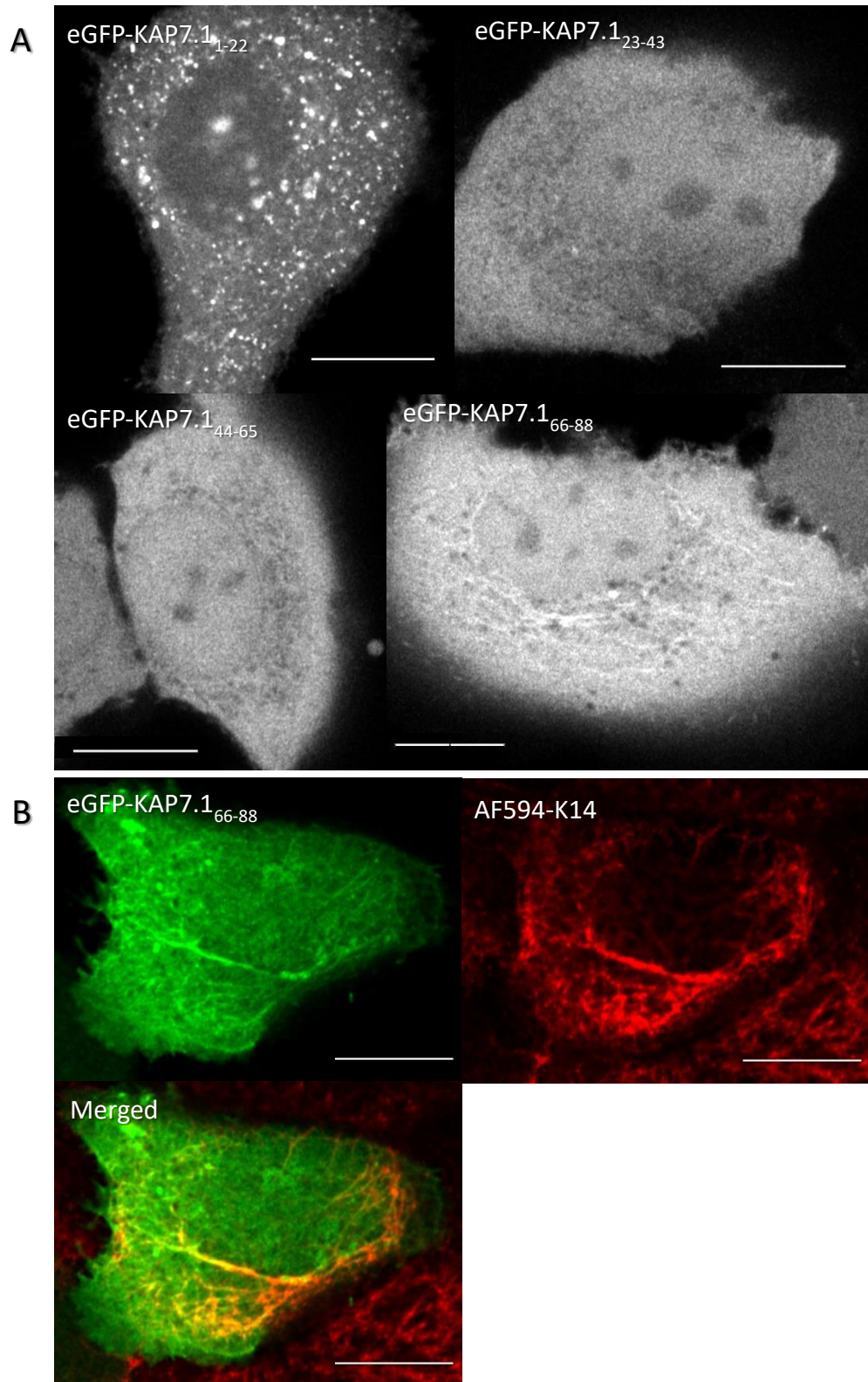
Figure 4.15 Truncated forms of KAP7.1 show distinct behavior when expressed in HaCaTs. *KAP7.1 was truncated into 4 parts of equal length and these were cloned into pEZYeGFP for transfection into HaCaTs. Images were captured of each truncated portion transfected into live HaCaTs using LSCM and the Airyscan detector (A). Scale bars 10μm. B - cells transfected with eGFP-KAP 7.1$_{68-88}$ (green) were fixed and co-stained for K14 (red) using indirect immunofluorescence. Scale bars 10μm.*

4.2.8. Characterisation of hair-specific keratins K82 and K85 in live HaCaT cells

In hair, KAPs form a matrix surrounding intermediate filaments made from hair-specific keratins. These keratins are distinct from the epidermal keratins endogenously expressed in HaCaT cells. To determine what interactions, if any, take place between KAPs producing the variety of localisations seen and hair-specific keratins, it was necessary to clone hair-specific keratins for expression in HaCaTs.

Keratin 82 and keratin 85 were chosen for this study. These are both type II keratins which are found in hair and are somewhat distinct in structure (Langbein et al., 2001b) and their location within hair. K82 is expressed within the keratinizing cuticle cells specifically, whereas K85 is particularly expressed in the hair cortex, with presence in the cuticle to a lesser degree (Langbein et al., 2001b). Additionally, previous work has showed associations between KAP10.1 and K82 and K85 (Fujikawa et al., 2013) and also between KAP8.1 and K85 (Matsunaga et al., 2013)

Keratin 82 and 85 coding sequences were synthesised by IDT with gateway ends compatible for immediate cloning into donor vector pDONR207 and then subsequent cloning into pDESTmCherry- N1, this results in keratin expressed in mammalian cells with a C-terminal mCherry tag. Using this alternate tag will allow us to differentiate between keratin-mCherry and eGFP-KAP in the same cell.

Before co-transfections were performed we first aimed to characterise the expression of hair-specific keratin in HaCaT cells during transient transfection. Cells were transfected with the K82 and K85 constructs separately, as described previously, and live cells were imaged using LSCM and the Airyscan detector.

KeratinmCherry expression construct. pDESTmCherry-N1

Figure 4.16 Schematic of pDESTmCherry constructs. *Pre-synthesised coding sequences for K82 and K85 (IDT), incorporating gateway ends, were inserted into pDESTmCherry using gateway cloning. pDESTmCherry facilitates expression of the inserted gene in mammalian cells with a C-terminal mCherry tag.*

Both K82 and K85, when expressed in HaCaT cells organised into an epidermal keratin-like network as shown in figure 4.17. This network was similar for both K82 and K85, and resembled the network previously stained using K14. These filamentous networks are present with very good contrast against the cytoplasmic background.

A

B
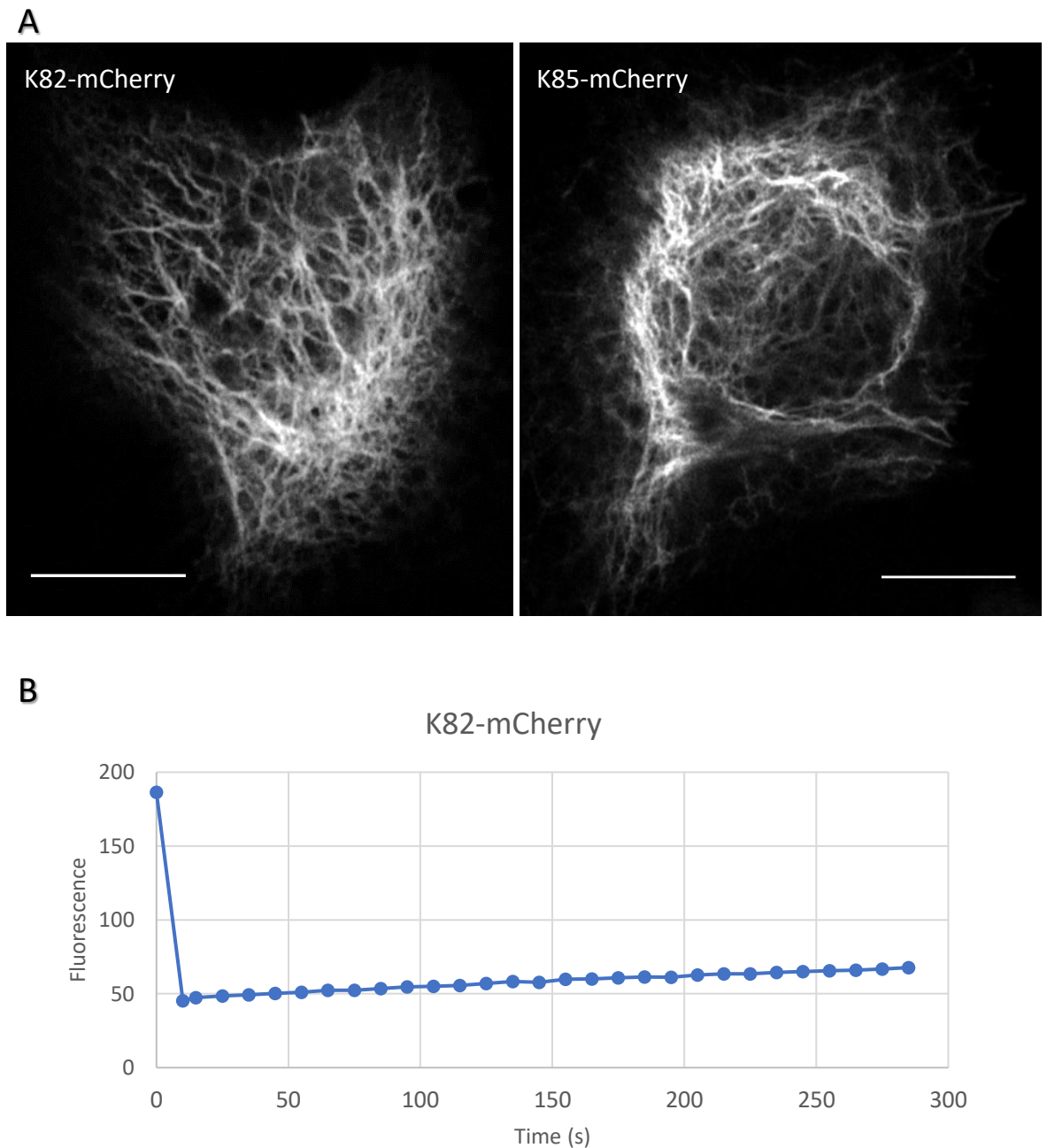
Figure 4.17 Hair-specific keratins appear as an epidermal keratin-like network in HaCaTs. A - Following cloning of K82 and K85 coding sequences into pDESTmCherry, live cells were imaged following transfection with K82 and K85. Scale bars 10µm. B - Time series imaging incorporating FRAP was carried out, recovery is shown here.

Time series measurements incorporating FRAP were carried out to assess the dynamics of K85. Following photobleaching, very little recovery of fluorescence was seen following over 5 minutes of time series measurement, as shown in figure 4.17. This recovery is much slower than that seen for the HGT KAP7.1 which displayed similar localisation to K85. The recovery of K85 is as what may be expected for the recovery of epidermal keratin (Windoffer et al., 2011) and so may suggest incorporation of K85-mCherry subunits into the epidermal keratin bundles. This is in contrast to eGFP-KAP7.1 whch is hypothesised to associate to the filaments with a transient nature.

4.2.9. Examining colocalisation of hair-specific keratins with epidermal K14

Keratin intermediate filaments are formed through the interactions of type I and type II keratins. As only a single, type II hair-specific, keratin is transfected, interaction with type I epidermal keratins may allow incorporation into the observed filaments. To investigate whether the transiently transfected hair-specific keratins were colocalising to the existing epidermal network, cells expressing both K82 and K85 separately were fixed and stained for K14 as a marker for epidermal keratins using immunofluorescence as described previously.

Strikingly, both K82 and K85 were shown to colocalise partially with the existing K14 network, which does not appear altered in comparison to that of neighbouring cells. However, the proportion of the two labelled forms of keratin, hair-specific and epidermal, appeared to form a gradient in the cell from base to apex. At the basal surface of the cell, fluorescence originates from the hair-specific keratin predominantly as shown in figure 4.18. In contrast, at the apical surface K14 is more prominent. An example of a maximum projection is shown in figure 4.18 where there are filaments present at the base of the cell which appear red, whereas filaments closer to the apical surface become yellow, due to equal proportion, and then green – due to the dominance of K14. A similar gradient is seen from the nucleus towards the leading edge, where K14 in particular appears to be most prominent at the leading edge. These phenomena are identical for both K82 and K85.
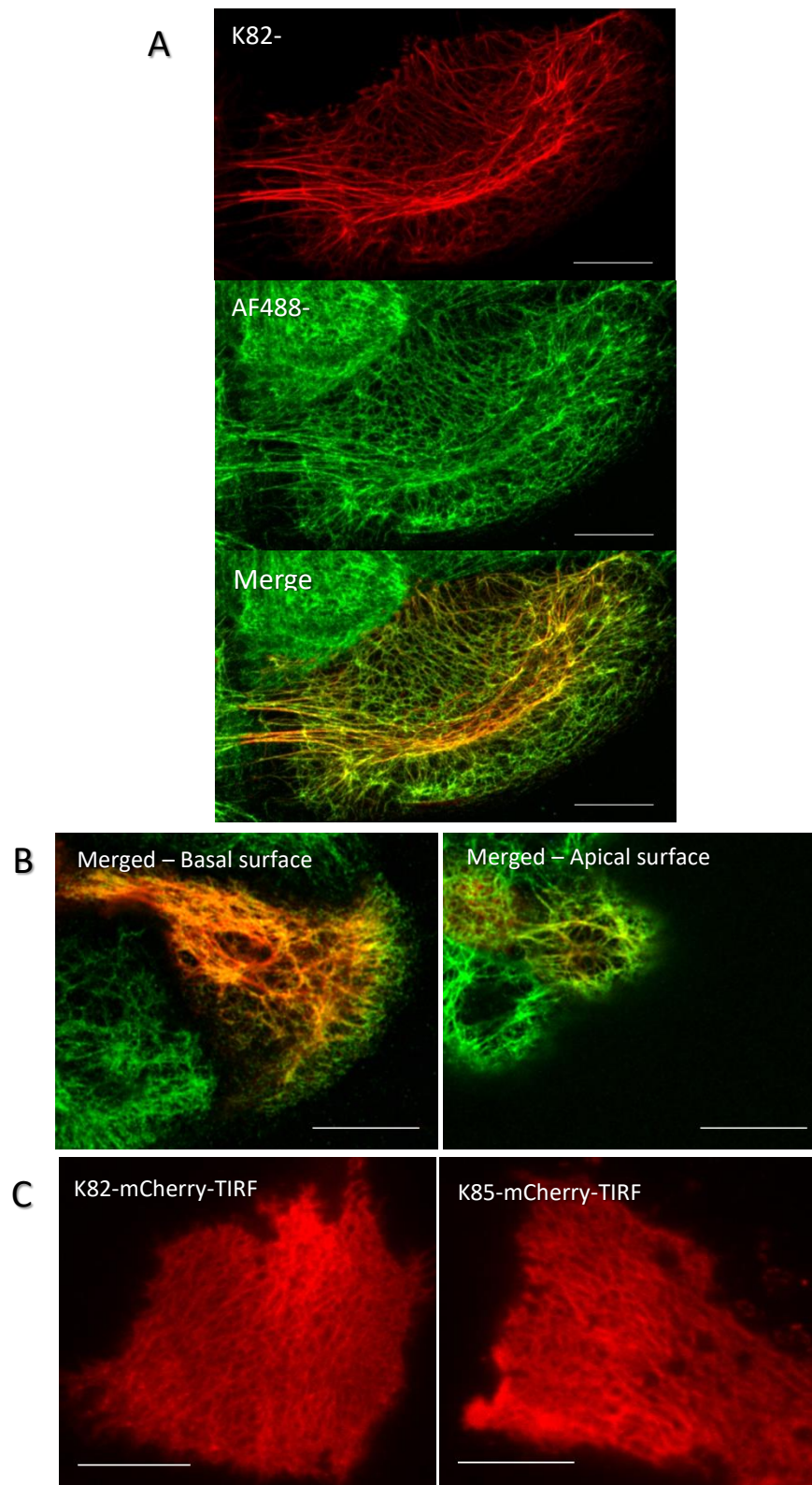
Figure 4.18 Hair-specific keratins localise to the epidermal keratin network with the greatest abundance toward the basal surface. *HaCaT cells transfected with hair specific keratins (red) were co-stained for K14 using immunofluorescence (green) and imaged using LSCM using the Airyscan detector. A - Maximum projection of a z-stack encompassing a cell transfected with K82 (red) and K14 (green) from apical to basal surface. B - Single z-slices from the same cell taken with identical imaging settings at the basal and apical surfaces imaging K85 (red) and K14 (green). Scale bars 10µm. C – TIRF used to show hair-keratin structures at the base of the cell.*

To observe this with greater spatial resolution, particularly in the z-axis, 3D-SIM was utilised to image cells transfected with hair-specific keratin and labelled for K14. This clearly showed that hair-specific keratins formed an extensive network at the base of the cell with fewer filaments extending upwards, shown in figure 4.19. Conversely, K14 was shown to be present at greater proportions at the apical region of the cell.

In summary, the colocalisation of hair specific keratins to the epidermal keratin network of HaCaTs is partial, due to the gradient seen. However, filaments seen at the base of the cell which are strongly labelled for hair-specific keratin cannot be comprised of K82 or K85 alone as these require a type I keratin binding partner. In the case of undifferentiated HaCaT cells this is K14. An explanation for the results shown is that K82 and K85 express a preference for association to filaments at the base of the HaCaT cell. K14 is likely present in equal amounts throughout the keratin network. The apparent gradient seen in K14 labelling could be due to interference upon antibody-binding or epitope masking by K82 and K85.

4.2.10. <u>The use of TIRF to image extensive hair-specific keratin network near the cell basal surface</u>

In order to capture the arrangement of the hair-specific keratin network at high spatio-temporal resolution, TIRF was employed to capture images of this network where it meets the coverslip.

TIRF of cells expressing K82 and K85 allowed the visualisation of filaments formed within 200nm of the coverslip, this includes the basal filaments where we believe hair-specific keratin incorporation is most prevalent. Here, an extensive network of filaments was visible, and the movement of these filaments could be observed at high temporal resolution, as seen in figure 4.18. However, as observed in earlier time series experiments, filaments were fairly static with only slight flexing of filaments visible over a number of minutes. To image keratin dynamics this experiment would be repeated over much longer time scales (Windoffer et al., 2011).
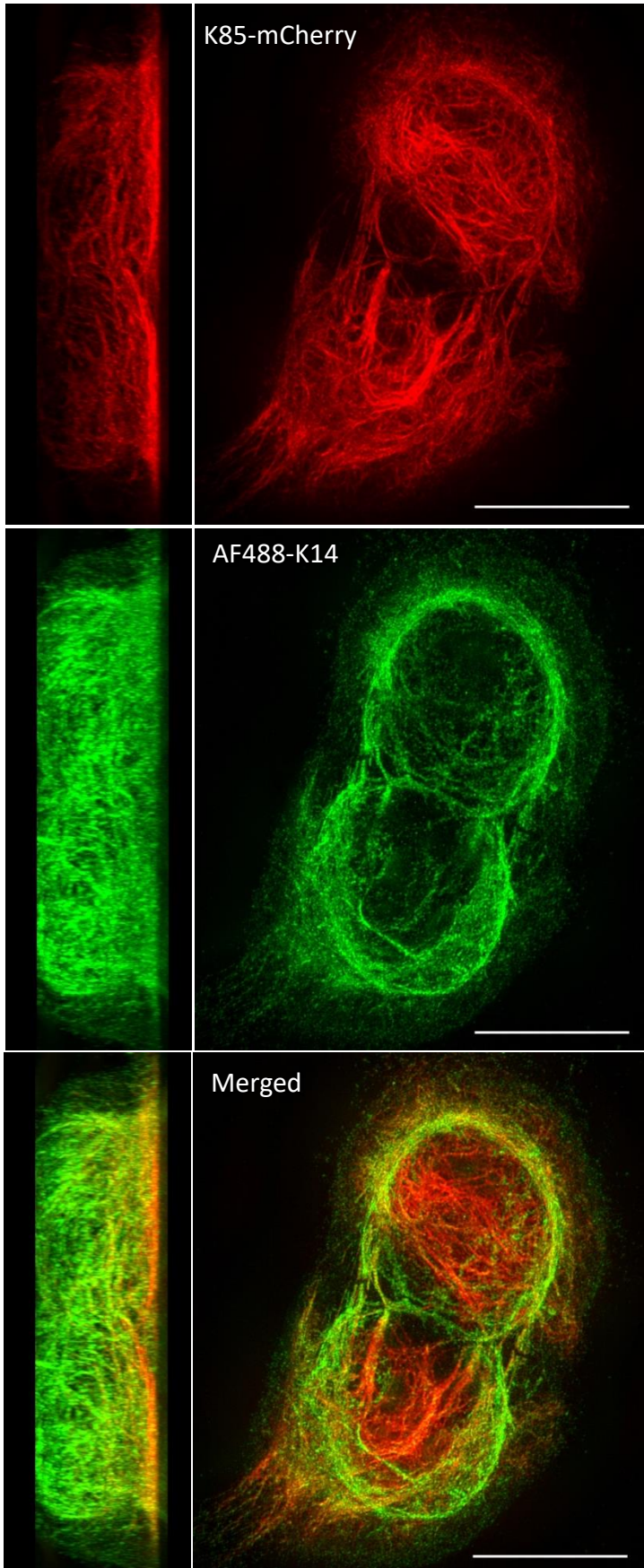
Figure 4.19 3D-SIM highlights the differences in abundance of hair-specific keratin K85 and K14 between the apical and basal surfaces of HaCaTs. *Cells transfected with K85 (red) and co-stained for K14 (green) were imaged using 3D-SIM. Orthogonal views were created from a 3D projection. Scale bars 10μm.*

4.2.11. <u>Examining co-expression of hair-specific keratins and selected HS and HGT KAPs</u>

To determine if the co-transfection of hair-specific keratins would alter the localisation of several KAPs when expressed in HaCaTs, both K85 and K82 were transfected alongside KAPs encompassing the 4 main localisations seen previously. KAP7.1, KAP11.1, and KAP17.1 were co transfected separately with both K82 and K85.

In cells expressing both KAP7.1 and K82, the expression of hair-specific keratin alongside KAP7.1 resulted in complete co-localisation of these two proteins, as seen in figure 4.20. The localisation of both KAP7.1 and K82 appeared identical to their localisation when expressed in HaCaTs alone. The gradient from base to apex of the cell between the eGFP and mCherry channels, seen in the varying abundance of K14 and hair-specific keratin during co-labelling, was not observed between KAP7.1 and K82. Therefore, both KAP7.1 and K82 appear equally distributed throughout the cell. When co-transfection was performed between KAP7.1 and K85, similar results were obtained.

Previous results have shown KAP7.1 to colocalise completely with K14. However, in this more recent experiment KAP7.1 is also seen to colocalise completely to K82. If KAP7.1 was still colocalising to K14 we may expect to see filaments at the apex of the cell which were labelled with eGFP alone, due to the preference of K82 for the base of the cell. This is not the case, and one possible explanation for this may be that the affinity of KAP7.1 for the hair-specific keratins is greater than the affinity for epidermal keratin, resulting in KAP7.1 being preferentially recruited to the keratin bundles towards the base of the cell incorporating hair-specific keratin. In this case there may be unlabelled keratin networks in this cell, towards the apex.

The co-transfection of KAP11.1 with K82 also provided interesting results. KAP11.1, while still forming granules, very clearly colocalised to K82 filaments, as shown in figure 4.21. However, in some cases KAP11.1 appeared as whole filaments in addition to granular expression. Therefore, the localisation of KAP11.1 was clearly altered by the co-transfection of K82. Interestingly, KAP11.1 was also seen to alter the behaviour of K82. While K82 was still seen to form filaments as previously, granules, forming along the filaments, were also observed. These granules are seen to colocalise to the KAP11.1 granules, as seen in figure 4.21. Therefore, results suggest that eGFP-KAP11.1 has a greater affinity for K82 than for epidermal keratin and further KAP11.1 has the ability to recruit K82-mCherry into formed granules.
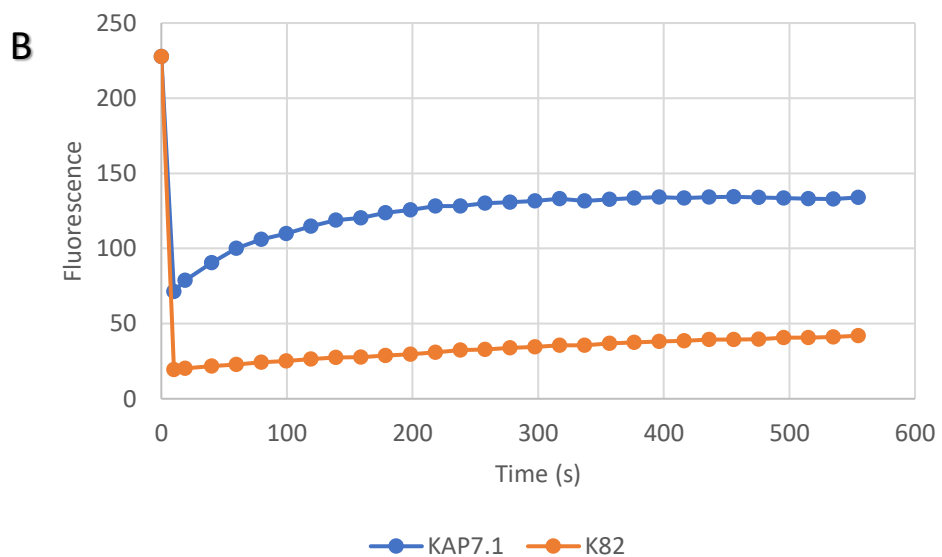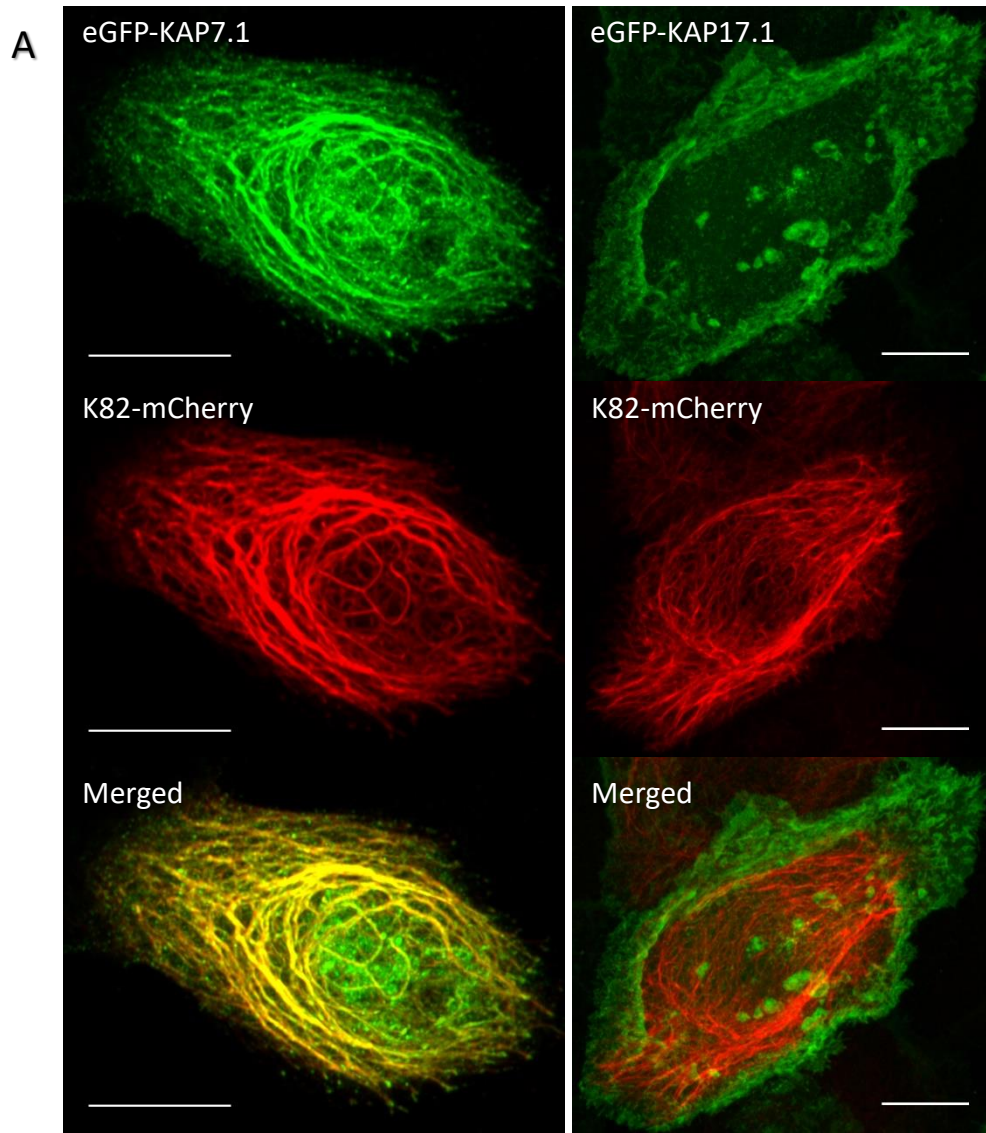
Figure 4.20: Co-transfections with hair-specific keratins reveals colocalisation with certain KAPs. *A - Live HaCaT cells transfected with hair-specific keratin and either KAP 7.1 or KAP17.1 were imaged using LSCM and the Airyscan detector. Scale bars 10μm. B – Recovery curve of live cell expressing eGFP-KAP7.1 and K82-mCherry following photobleaching.*
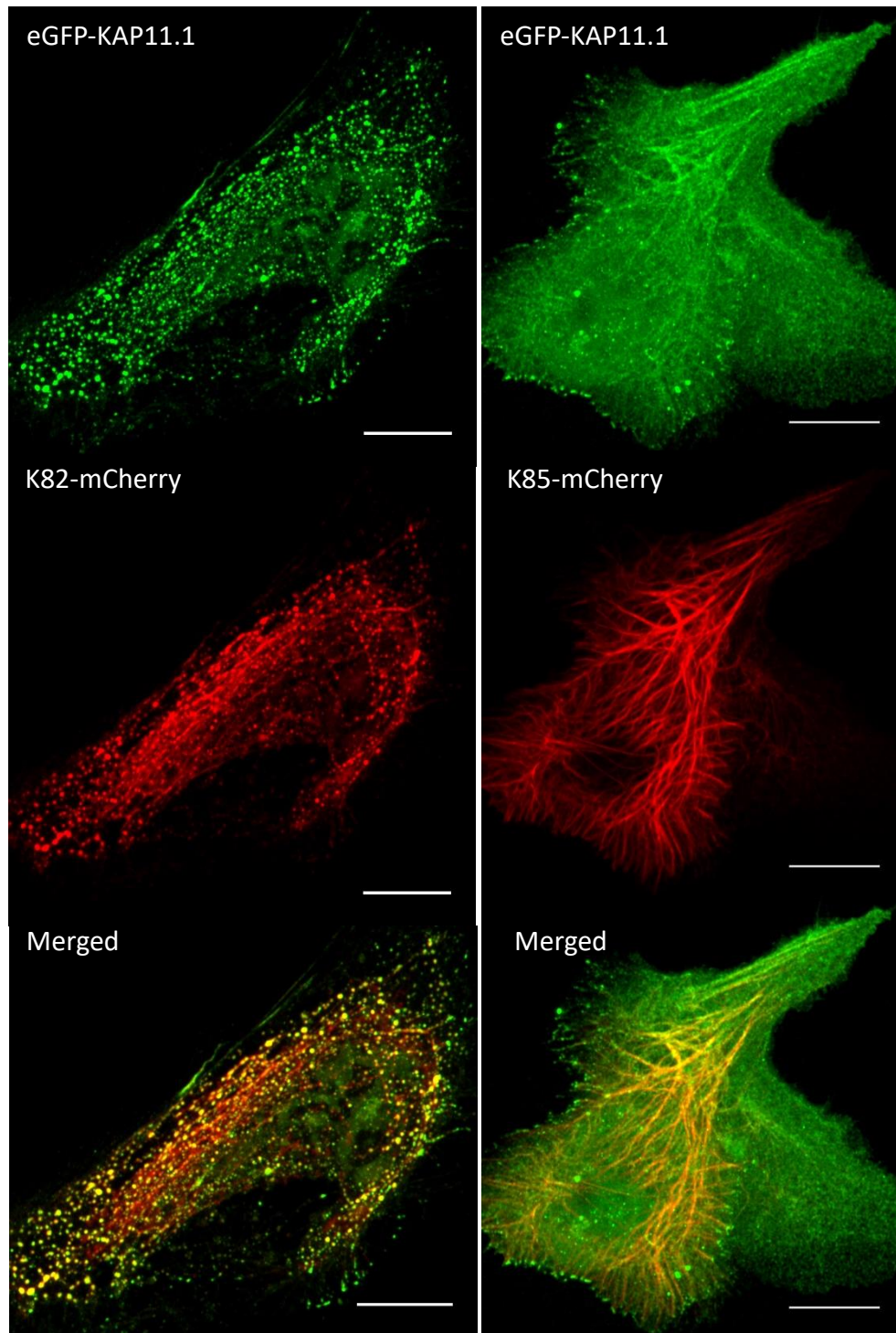
Figure 4.21 Co-expression of KAP11.1 and hair-specific keratins results in a change in protein behavior. Live HaCaT cells transfected with KAP11.1 and either K82 or K85 were imaged using LSCM and the Airyscan detector. Scale bars 10μm.

Following co-transfection of KAP11.1 and K85, it was observed that the phenotype was different to that seen during co-expression of KAP11.1 and K82. K85 behaviour appeared unaltered to when expressed alone in HaCaT cells, producing filaments typical of an epidermal keratin network. However, the expression of KAP11.1 was altered in comparison to its behaviour when expressed alone. This is shown in figure 4.21. Rather than the previous granular formation, KAP11.1 instead appeared largely cytosolic. In addition to the cytosolic distribution there was clear localisation to both punctae at keratin-filament termini, as seen previously from KAP11.1 alone, and also to K85 filaments as seen in figure 4.21. This localisation of HS KAP11.1 to filaments occurred with poor contrast to the cytosolic background, much like that seen in HGT KAP8.1 when expressed alone in HaCaTs. However, unlike the previously seen expression of KAP11.1, this localisation was observed as complete filament structures, rather than granules in linear arrangements. K85 therefore has altered the behaviour of KAP11.1 following co-transfection.

The variation in behaviour of KAP11.1 when expressed with each hair-specific keratin may indicate a biological function. Within hair, cortically expressed KAP11.1 is most likely to interact with K85, also preferentially expressed in the cortex, rather than K82 which is unique to the cuticle.

Co-transfection of each hair-specific keratin alongside KAP17.1 caused no change to the localisation of either KAP17.1 or hair-specific keratin. Both proteins behaved as seen previously when observed alone, as shown in figure 4.20. Therefore, results suggest that KAP17.1 does not bind to the selected hair keratins.

4.2.12. Dynamics of co-expressed hair-specific keratins and selected KAPs investigated in live HaCaTs

To better understand the dynamics of both KAP7.1 and K82 when expressed together, time series imaging of live cells which were co-transfected was carried out for a number of minutes, incorporating FRAP.

Following photobleaching, the recovery of KAP7.1 was seen to be rapid in comparison to K82, which agreed with earlier experiments. However, although direct comparisons are difficult due to the inherent variability of transfected cells, recovery of KAP7.1 is much less complete than when examined following transfection of eGFP-KAP7.1 alone, without the presence of K82. KAP7.1 alone recovered approximately 75% of fluorescence following a 3-minute recovery whereas the recovery of KAP7.1 in the presence of K82 plateaued at

approximately 33% over a similar time frame. This difference could suggest that the interaction between KAP7.1 and K82 is stronger than that between KAP7.1 and epidermal keratin, and that there is a greater immobile portion of KAP7.1 in the presence of hair-specific keratin.

K82, on the other hand, did not recover significantly over the circa 9-minute time series following photobleaching, results shown in figure 4.20. Again, this is consistent with results from previous experiments.

4.3. Discussion

The aim of the work detailed in this chapter was to characterise and further understand KAPs, their cell biology, and role in stabilisation of the hair fibre, alongside hair-specific keratins. This work was accomplished using a subset of KAPs to represent the large protein group, with representatives taken from the 3 large families; HS, UHS, and HGT, and from a variety of sub-families. Literature previously published on the behaviour of these proteins is very limited, and often focuses on a single KAP using a variety of approaches, occasionally including light microscopy among other biochemical methods, to provide characterisation. This study employed a broader approach using light microscopy techniques with a repertoire of KAPs, in order to further understand how they differ in their function.

4.3.1. KAPs exhibit distinct behaviours in live HaCaT cells

Following cloning of the KAP selection into a suitable expression vector, work began by examining the behaviour of eGFP-KAPs within HaCaT cells. The repertoire of KAPs exhibited a variety of localisations when transiently expressed within HaCaTs. Most notable among these was the decoration of keratin-like filaments by HGT KAPs in particular, and actin-like structures by UHS KAP17.1. Although the decoration of keratin filaments is of interest, as this could suggest KAPs may interact with epidermal keratin, the localisation to actin-like structures is particularly striking as there is no precedent for the interaction of KAPs with actin. Also of interest was the presence of fluorescent punctae at the cell edge, seen most frequently in cells expressing eGFP-KAP7.1 and eGFP-KAP11.1.

Previous work involving the transfection of KAP into mammalian cells is extremely limited, comprising only the work of Fujikawa et al. where HS KAP10.1 was shown to produce diffuse localisation when expressed alone in HaCaTs (Fujikawa et al., 2013). This is much like the

localisation seen during this study from eGFP alone, and from eGFP-KAP3.1. Therefore, the localisations seen during this study have not been described of KAPs previously.

Localisation of KAPs to granules was also observed during this study, particularly with certain HS and UHS KAPs, KAP11.1 and KAP5.1 respectively. This localisation is likely due to interaction of KAP monomers together resulting in the formation of aggregates. Self-interaction, being interactions between monomers of a KAP, has been identified in previous studies such as in Fujikawa et al. where HS KAP2.1 is seen to self-interact through the formation of disulphide bonds (Fujikawa et al., 2012), possibly due to the high amount of cysteine in these proteins. The formation of granules during this study could be an artefact of over-expression or alternatively could suggest a function of these particular KAPs for the creation of a dense network of crosslinks within the fibre. Interestingly, KAP5.1 is preferentially expressed in the cuticle whereas KAP11.1 is predominantly expressed in the cortex (Rogers et al., 2006a). If self-interaction is indeed an intended function of these KAPs, they could each fill a similar niche for increasing cross-linking in their respective layers of the fibre.

This diverse behaviour of eGFP-KAPs when expressed in HaCaTs, which particularly for the HGT sub-family seems to correlate to their KAP family, may suggest distinct roles for individual KAPs or KAP subfamilies in their production of the matrix surrounding KIFs of the hair fibre. The presence of these distinct roles could further challenge the view that this matrix is amorphous in nature, and lend evidence to the hypothesis that it relies on defined KAP-KAP and KAP-keratin interactions (Kadir et al., 2017).

The decoration of keratin-like filaments is a trait shared by all HGT eGFP-KAPs studied, and was exclusive to HGT KAPs. HGT KAPs are among the first expressed during production of the hair fibre. This may suggest a role which is specific to HGT KAPs and involves interaction with keratin filaments in a manner which is different to that of KAPs from other families, this could involve interaction with epidermal keratins of the inner or alternatively could be a unique means of interaction with hair-specific keratins.

Matsunaga et al. previously suggested a role for HGT KAPs, and demonstrated this with KAP8.1 specifically, in changing the alignment of KIFs through unique binding interactions to produce orthocortex and therefore curling of the fibre (Matsunaga et al., 2013). They hypothesise that the expression of KAPs early in the production of the fibre (Rogers et al., 2006a) may allow them to undertake this role while HS and UHS KAPs later would be unable

to alter the alignment of fixed KIFs. As previously stated, the colocalisation seen here between K14 and HGT eGFP-KAPs could be due to a role for KAPs in interacting with epidermal keratins of the hair follicle, this could be with keratins which possess similarity to K14 or K14 itself which is expressed in basal cells of the inter-follicular epidermis and in the upper part of the outer root sheath (Langbein and Schweizer, 2005). Alternatively, colocalisation could be due sequence homology between epidermal keratin and the specific region of hair-specific keratins which KAPs bind in order to alter alignment as described in other work (Matsunaga et al., 2013).

As discussed, the finding that eGFP-KAP17.1 localises to actin is of great interest as this is not an expected behaviour of a KAP. There is no existing literature regarding the interaction of KAP with actin and very little in fact discussing the role of actin within the hair fibre due to the dominance of keratin. However, actin has been shown to be present in hair follicles (Vermorken et al., 1981). Also, work has been published hypothesising the importance of actin bundles as a tensile scaffold in the hair follicle (Furumura and Ishikawa, 1996). KAP17.1 is found in the cuticle predominantly (Rogers et al., 2006a), if KAP17.1 possesses a function to interact with actin or an associated protein, this could be due to the need for the cuticle to be extremely rigid through means of crosslinking with other cytoskeletal components. However, it is also possible that an alternate KAP, not included in those studied here, possesses a similar role within the cortex. Interestingly, of all KAP subfamilies KAP5 has an amino acid composition most similar to KAP17.1, this can be seen in figure 4.2, KAP5.1 has been shown to localise granules when transfected within HaCaTs during this work, and did not colocalise to actin. No other KAP subfamilies have a similar amino acid composition to KAP17 (figure 4.2).

Due to the colocalisations observed being of great interest, it was necessary to confirm these through co-labelling of the cytoskeletal components which KAPs were suspected to colocalise to.

4.3.2. <u>KAPs localise to a variety of cytoskeletal components in HaCaT cells</u>

To confirm localisation targets of the KAPs, co-staining experiments were carried out. Co-labelling with K14 highlighted that HGT KAPs were indeed colocalising with epidermal keratin as previously suspected. As discussed, this colocalisation suggests HGT eGFP-KAPs are able to interact with epidermal keratin which is a novel finding.

Interestingly, granules formed by HS KAP11.1 and UHS KAP5.1 were also seen to colocalise to epidermal keratin filaments, suggesting that despite their aggregation, which may be due to monomers assembling, owing to their high cysteine content, interaction with epidermal keratin was still possible. This colocalisation of granules to epidermal keratin filaments suggests that they are able to interact with epidermal keratin with affinity different to that of HGT KAPs. It is important to note that in all cases of colocalisation reported, direct interaction with the cytoskeletal component cannot be confirmed from colocalisation alone. In the case of all KAPs which show a degree of colocalisation to epidermal keratin this is of interest as, although previous work examining KAPs has highlighted interactions between individual KAPs and hair-specific keratins (Fujikawa et al., 2013, 2012; Fujimoto et al., 2014; Matsunaga et al., 2013), no interaction has been shown between KAPs and epidermal keratins previously. In fact, in the case of Fujikawa et al. HS KAP10.1 was specifically shown not to colocalise to K14 in HaCaT cells (Fujikawa et al., 2013).

KAP17.1 was shown, through co-staining, to localise to several actin structures such as filopodia, and also to a peripheral band present at cell-cell boundaries likely to be the adherens band, formed due to the presence of adherens junctions at these locations. Notably, KAP17.1 did not localise to all actin structures, such as stress fibres. This may be due to the KAP typically interacting with the actin subunit in a location which is not accessible when actin is arranged as stress fibres. Alternatively, KAP17.1 could interact with an actin-binding protein which is present only in certain actin structures, but not in stress fibres. The interaction of KAP17.1 with actin or an actin-binding protein could be an important link between cytoskeletal networks to provide rigidity during formation of the hair fibre. Of particular interest here could be plakins such as desmoplakin, plectin, periplakin, and envoplakin, these proteins associate with IFs to create cross-links between cytoskeletal networks of keratin and actin (Fuchs and Yang, 1999; Ruhrberg and Watt, 1997). It is of note that Matsunaga et al. previously described interaction of HGT KAP8.1 with the desmoplakin C-terminus (Matsunaga et al., 2013). Novel work in this study provides further evidence that other KAPs may function to bind cytoskeletal proteins, besides keratin. A role for KAPs in binding actin-associated proteins would serve to strengthen cross-links between keratin and actin networks within the fibre.

Further work examining actin used SiR actin-594nm which binds actin within live cells in order to allow visualisation of eGFP-KAP17.1 alongside actin in live HaCaTs. Similarly, colocalisation was seen here between KAP17.1 and many actin structures. It is of note that

SiR actin is based upon jasplakinolide which is known to affect actin polymerisation, so the dynamics observed may not be representative of unlabelled actin (Holzinger, 2009).

A number of KAPs studied, including HS, UHS, and HGT KAPs, but HGT KAP7.1 in particular, could be seen to localise to discreet punctae at the periphery of the cell, particularly at cell-cell boundaries. The clear accumulation of what were typically filament-decorating KAPs at this location suggests an alternate interaction with a protein other than epidermal keratin. Co-staining for K14 of cells displaying this localisation revealed that these punctae are present where epidermal keratin filaments from two cells meet. The interaction of KAPs with cell-adhesion proteins is of interest as this could serve to strengthen the connection between individual cells and the continuous network joining these, the CMC. Of particular interest is work by Alibardi et al. which suggests that the CMC is a desmosomal remnant, due to the presence of desmoglein and plakophilin (Alibardi et al., 2013). KAPs interacting with cell adhesion proteins could serve as a key link in stabilising interactions between individual cells and their surroundings within the fibre. As discussed previously, Matsunaga et al. have previously shown, in a cell-free environment, the interaction of KAP8.1 with desmoplakin (Matsunaga et al., 2013). Work within this study extends these findings to alternate KAPs and to within epidermal cells. The localisation seen along with the literature suggested that the strong localisation visualised may be due to interaction of certain KAPs, particularly HGT eGFP-KAP7.1 with a desmosomal adhesion protein. Unfortunately, attempts to confirm this within the study by co-labelling for desmoplakin failed due to non-specific antibody labelling.

Throughout experimentation involving co-labelling of cytoskeletal components, KAPs were not seen to alter the organisation of the structures that they decorated. The inherent variability of keratin and actin networks within HaCaTs makes subtle changes hard to detect. However, the cytoskeleton of cells neighbouring those imaged, which often did not express eGFP-KAP due to the transient nature of the transfection, were seen to be indistinguishable from cells expressing eGFP-KAP. During this work, cells were fixed and therefore it is unknown whether dynamics of these cytoskeletal components may be affected despite no clear change in organisation.

4.3.3. Dynamics of KAPs following photobleaching reveals insights into protein interactions

To investigate the dynamics of eGFP-KAPs within live cells, and to uncover further insights into the nature of interactions between KAPs and cytoskeletal components, time-series imaging incorporating FRAP was utilised. Of particular interest was the behaviour seen

during the recovery of eGFP-KAP11.1 and eGFP-KAP7.1. KAP7.1 recovery appears fairly complete in a matter of minutes. Recovery into the centre region appeared faster than that to the periphery, which is likely due to the surface area to non-photobleached regions being larger. However, changes in the keratin dynamics at these regions also varies, with greater dynamics and nucleation occurring at the periphery (Kolsch et al., 2010) and could provide an alternate explanation for this difference. Nevertheless, both recover substantially despite this difference. The recovery occurs much faster than would be expected for epidermal keratin, which is less dynamic than other cytoskeletal components such as actin (Windoffer et al., 2011), although unfortunately testing the recovery of epidermal keratin was not accomplished within this study. Experimental data captured therefore suggests that, rather than KAP7.1 being incorporated fully into the epidermal keratin network, KAP7.1 interacts with an established filament and is in constant flux on and off the filament, allowing rapid recovery following photobleaching. This may suggest the interaction of KAP7.1 with its binding partner is transient in nature, or alternatively requires further stabilisation within hair, possibly by another KAP. Alternatively, it could point to the fact that K14 is not KAP7.1's primary binding partner, and homology of K14 to hair-specific keratins allows a lower degree of interaction.

Conversely, KAP11.1 following photobleaching was shown to recover poorly to the photobleached region. Observing images captured it is clear to see that this is owed to the fact that, although the low level of cytosolic fluorescence recovers rapidly, the formed granules recover very little over a number of minutes, this suggests that turnover of protein within these granules is low. As KAP11.1 is a HS KAP, this low turnover may be due to strong di-sulphide bonding occurring between monomers. Furthermore, the granules appear, for the most part, stationary within the cell, likely due to their interactions suggested previously with epidermal keratin. This results in largely the recovery of just the weak cytoplasmic background during this time.

4.3.4. Truncated forms of KAP7.1 express differential affinity for epidermal keratin

To determine if colocalisation to K14 by KAP7.1 was due to a specific sequence or binding domain. KAP7.1 was truncated into four sections of equal length. Co-staining of cells, transfected with each of these individually, for K14 found that they display distinct behaviour. KAP7.1$_{66-88}$ in particular showed the most affinity to epidermal keratin filaments, and therefore the greatest similarity to the behaviour of full-length KAP7.1. However, as the colocalisation seen here was to a lesser degree than in full-length KAP7.1, it can be assumed

that KAP7.1$_{66-88}$ does not possess the entire domain, or indeed the proper 3-dimensional structure that is present in KAP7.1. Therefore, it can be summarised that the domain of KAP7.1 necessary for colocalisation to epidermal keratin is likely present in KAP$_{66-88}$ but may require proper folding or interactions of another domain for proper function.

4.3.5. <u>Hair-specific keratins integrate with epidermal keratin filaments</u>

K82 and K85, after cloning into a suitable mammalian expression vector, were transfected into HaCaTs for initial characterisation. Both K82-mCherry and K85-mCherry appeared to present similarly, in the form of keratin-like filaments, much like the localisation seen from HGT KAP7.1, for example. However, time series measurements utilising FRAP suggested very little recovery of fluorescence to the photobleached region of hair-specific keratin, unlike eGFP-KAP7.1 which displayed good recovery over a short time period. These findings suggest that, while HGT KAPs may transiently associate with the epidermal keratin, K82 and K85 may associate through a more permanent interaction, possibly due to integration, as type II keratin monomers, into the epidermal keratin bundles. As discussed earlier, very little recovery of epidermal keratin would be expected over this time frame although measurement was not made during this study (Windoffer et al., 2011).

Further work aimed to confirm that the hair-specific keratins studied were indeed localised to epidermal keratin within HaCaT. Co-staining of K14 confirmed that K82-mCherry and K85-mCherry were in fact colocalising to the existing epidermal keratin network. By assessing these results together, we could conclude that, rather than a low-affinity, dynamic interaction with existing filaments, as in the case of HGT KAP7.1, among others, K82 and K85 are able to integrate into epidermal keratin filaments.

Interestingly, colocalisation was not seen to be complete between K14 and hair specific keratin. Both K82-mCherry and K85mCherry appeared to express a striking preference for colocalisation with filaments toward the basal surface of the cell. In contrast, K14 labelling was shown to be most prevalent at the apical surface of the cell. As K14 is the primary type I keratin expressed within undifferentiated HaCaTs, and K82 and K85 are type II keratins, K14 would be essential for formation of filaments with K82 and K85. Therefore, the abundance of K14 labelling at the apical surface, and apparent lack towards the basal surface is likely due to the presence of K82 and K85 interfering with or obscuring antibody binding. As the hair-specific keratins are most abundant at the base of the cell, this interference prevents labelling primarily in this location. However, although the K14 gradient may be due to an

antibody labelling artefact, the abundance of hair-specific keratin at the base of the cell could not be caused due to this. Therefore, hair specific keratin is shown to preferentially localise to the base of HaCaT cells. One previous study has examined the transfection of Flag-tagged K82 into HaCaTs but the localisation of K82 alone is not discussed, and no mention is made of a preference to the base of the cell (Fujikawa et al., 2013). Increased imaging sensitivity and resolution used during this study, through use of the Airyscan, may be the reason why the phenomenon is now visible. The reason for the novel localisation seen here could be due to possible differences in keratin bundle arrangement between the base and apex of the cell, altering binding affinity, or the presence of an additional protein to which hair-specific keratins may localise.

4.3.6. Hair-specific keratins alter the behaviour of specific KAPs when co-expressed in HaCaTs

Following characterisation of hair-specific keratins alone in HaCaTs, work aimed to observe the behaviour of cells expressing both hair-specific keratin and selected KAPs. HaCaTs expressing both eGFP-KAP7.1 and either K82-mCherry or K85-mCherry have indistinguishable behaviour. KAP7.1, when expressed with either hair keratin, showed complete colocalisation to either K82 or K85, colocalising to keratin filaments similarly to when expressed alone. Similarly, behaviour of the hair keratins appeared unaltered when expressed alongside KAP7.1. However, complete colocalisation of KAP7.1 and hair-specific keratin, when KAP7.1 previously colocalised completely to K14 suggests a degree of interaction between KAP7.1 and both K82 and K85. If KAP7.1 colocalised completely to epidermal K14 while co-expressed with hair-specific keratin, earlier data would suggest the presence of filaments at the apex of the cell decorated with eGFP-KAP7.1 without the presence of hair keratin. As this is not the case, results suggest that the presence of either K82-mCherry or K85-mCherry may cause KAP7.1 to localise preferentially to hair-specific keratin due to increased binding affinity to these proteins, and apical keratin filaments remains unlabelled by eGFP-KAP7.1 or K82/K85-mCherry.

Further work examining cells co-expressing KAP7.1 and K82 utilised FRAP. Recovery of KAP7.1 was shown to recover rapidly following photobleaching, as was observed in previous experiments with cells expressing KAP7.1 alone. Conversely, the recovery of K82-mCherry was insignificant over the time-course of the experiment, as expected from epidermal keratin. These data provide further evidence that hair-specific keratins integrate into epidermal keratin filaments while KAP7.1 interaction is much more dynamic in nature,

perhaps involving flux on and off the filaments. Interestingly, the recovery of KAP7.1, while rapid in relation to K82, is slower than previous recovery seen in cells expressing only KAP7.1. An explanation for this could be that KAP7.1 interaction with hair-specific keratin, while still dynamic in nature, could be of greater affinity than those with epidermal keratin. These data, gathered from cells co-expressing KAP7.1 and hair specific keratins, provide evidence of interaction between these proteins.

Striking results were also provided from co-expression of eGFP-KAP11.1 alongside K82-mCherry or K85mCherry. When transfected alongside K82, KAP11.1 not only changed in behaviour, by showing increased localisation to keratin filaments, but also appeared to recruit K82 into the granules formed. This suggests an interaction between KAP11.1 and K82, beyond that seen from KAP11.1 and its interaction with epidermal keratin. This behaviour may be important for the production and the structure of the hair fibre. Although the behaviour of K85 appeared unchanged when expressed alongside KAP11.1, its effect on KAP11.1 localisation was significant. KAP11.1 showed clear localisation, like that seen in HGT KAPs, to the keratin filaments. There was also a lack of granule formation, with more cytosolic background. This interaction between KAP11.1 and K85 suggests KAP11.1's ability to bind K85 without the formation of granules through self-aggregation and may be relevant for fibre production.

5. <u>Investigating the use of fluorescent dyes within hair</u>

5.1. <u>Introduction</u>

Hair is a complex fibre, consisting of multiple regions and many layers. These layers, predominantly the cuticle layers, provide protection against both physical and chemical insults. It is of interest, particularly for the development of cosmetics which are required to be taken up into the hair, to understand compound uptake and the pathways by which this occurs. Findings in this area are also important with regard to wool treatment and dyeing which is an important commercial step in the production of this material, work examining dye uptake into wool forms the basis of early work, of a similar nature, with human hair (Wortmann et al., 1997). The study of substance incorporation into the hair is also useful in the field of forensics, specifically with regard to hair analysis for drug testing (DeLauder and Kidwell, 2000; Pötsch and Moeller, 1996).

It is currently understood that compounds are likely to move through one of two routes, which depends upon their size and polarity. The transcellular route, also referred to as the intracellular route, describes passage through cuticle and cortical cells towards the centre of the fibre. This pathway is regarded as the most likely mechanism for the uptake of small hydrophilic molecules (Brady, 1992). Passage through the highly cross-linked layers within the hair, particularly the cuticle which includes the α-layer and exocuticle, results in prior hair damage having a significant impact on the uptake of compounds which use this pathway, where damage results in uptake occurring more rapidly (Robbins, 1988). An alternative pathway for diffusion is via the intercellular route, also referred to as the extracellular route. The intercellular route is preferred in the case of large hydrophobic or non-polar molecules, such as is the case for most fluorescent dyes. Initial uptake occurs between individual cuticle cells and via the intercellular CMC towards the centre of the fibre, which contains lipid and protein lowers of comparatively high mobility (Wortmann et al., 1997). The intercellular area, which possess less cross-linking than intracellular regions, are more prone to swelling in aqueous conditions, further increasing mobility (Formanek et al., 2006; Kelch et al., 2000; Robbins, 2012b). Over long periods of time molecules are thought to migrate into individual cortical cells, therefore using a combination of intercellular and intracellular routes (Brady, 1992).

Although these routes have been visualised to a certain extent previously (Brady, 1992; Hadjur et al., 2002; Pötsch and Moeller, 1996), there are still many unanswered questions

and knowledge is limited with regard to the initial uptake, rate of diffusion, and eventual partitioning of compounds. In general, there exists a lack of recent and high-resolution imaging of these phenomena. Moreover, dynamic uptake and movement of dye within the fibre has not been visualized in real time, which is likely to reveal in greater detail the path by which diffusion takes place, rather than the eventual partitioning seen using static means (Gummer, 2001). Further understanding in these areas will provide useful for the formulation and understanding of cosmetic products, in particular hair dyes. In addition, knowledge of how particular dyes typically are taken up, and partition into the hair, could be leveraged to allow for investigations into how the permeability of hair is altered following damage. Dyes which show partitioning into certain regions of the fibre, allowing specific labelling, may also be useful for the imaging of hair morphology and the understanding of structural changes in specific areas.

Hair dyes are commonly used cosmetics designed to change natural hair colour (Guerra-Tapia and Gonzalez-Guerra, 2014). There are a number of mechanisms by which this can be achieved, permanent dyes, also known as oxidative dyes, are the most widely used method. These involve the use of low molecular weight compounds which are able to penetrate deep into the hair cortex, before combining under oxidising conditions to produce larger formed dyes which are less able to diffuse out of the fibre. This method results in a stable final colour due to the formation of these immobile dye compounds (Harrison and Sinclair, 2003). Oxidative dyes use an oxidant, usually hydrogen peroxide, alongside either ammonium hydroxide or monoethanol amine to create a pH of 9 - 10.5. High pH results in greater oxidative capability of hydrogen peroxide while also causing the hair to swell, allowing uptake to occur more rapidly. Hydrogen peroxide is responsible for both oxidation of the hair's natural colourant, melanin, to allow lightening of the fibre, in addition to oxidation of the dye precursors to form the desired chromophores which are too large to easily diffuse out of the hair and therefore result in stable colouration (Brown et al., 1985; Corbett, 1998).

5.1.1. Chapter Aims

The aims of this work are to further understand and visualise the diffusion and formation of dyes using dye precursors, and to further apply these and other fluorescent compounds for the study of permeability and specific labelling of the fibre. We aimed to screen several compounds, first for their ability to fluoresce, and subsequently to assess their uptake within hair. Advanced light microscopy techniques were to be applied throughout to accomplish

this and to image dye movement with high spatio-temporal resolution not present in existing literature.

5.2. Results

5.2.1. Screening of potential fluorescent compounds for imaging in hair

To enable the investigation of the diffusive properties of compounds found within cosmetics, molecules were required that were able to both diffuse through hair within a reasonable timeframe, and create fluorescence emission either sufficiently detectable over hair's auto fluorescence or in a spectrally distinct zone. Chemical compounds regularly used in hair dyeing cosmetics would naturally be assumed to be taken up into the hair readily. Therefore, a variety of these compounds were screened for their fluorescence characteristics at a range of excitation wavelengths, to determine if their fluorescence would be sufficient to detect when within hair. These were screened while in solution using a range of excitation wavelengths to create emission curves using a Synergy H4 plate reader. Fluorescence could be reasonably expected in many cases due to the compounds in question being chromophores, responsible for the formation of hair-colouring dyes in the cosmetic products.

Compounds used belonged to two groups of chemicals used in oxidative hair dyes; primary dyes, and couplers. Couplers are, during oxidative dyeing, oxidised through the action of hydrogen peroxide into chromophores, which are typically p-diamines and p-aminophenols. Primary dyes are also oxidised to active imines which are able to form complexes with their unoxidized counterparts and coupler molecules in order to form large, complex colour molecules (Guerra-Tapia and Gonzalez-Guerra, 2014). The compounds screened at this stage, belonging to the groups of both couplers and primary dyes, are listed in table 5.1 (couplers) and table 5.2 (primary dyes), along with their corresponding reference numbers, used later in figure 5.1.

Coupler - Name	Number
2-methylresorcinol	1
2-amino-4-hydroxyethylamino-anisole sulfate	2
2,4-diaminophenoxy ethanol HCl	3
2-methyl-5-hydroxyethylaminophenol	4
4-Amino-2-hydroxytoluene	6
1-naphthol	7
3-aminophenol	10
Resorcinol	12

Table 5.1: Hair dye couplers used and their number assigned during this study.

Primary Dye - Name	Number
2-(methoxymethyl)-1,4-benzenediamine	5
4-aminophenol	8
1-hydroxyethyl-4,5-diamino pyrazole sulphate	9
N,N-bis(2-hydroxyethyl)-p-phenylenediamine sulphate	11

Table 5.2: Hair dye primary dyes used and their number assigned during this study.

A range of discreet excitation wavelengths, comprising 355 nm, 405 nm, 458 nm, 488 nm, 514 nm, and 543 nm were chosen due to the laser wavelengths which would be available for subsequent imaging using the Zeiss 880 with Airyscan. Fluorescence emission of the 12 compounds was seen to vary significantly across the range of these excitation wavelengths. Examples of emission curves generated using the plate reader are displayed in figure 5.1. Among the most notable was 1-napthol, which displayed a broad peak of emission from 450 – 500 nm following excitation at 355 nm excitation. Also showing substantial fluorescence at a range of excitation wavelengths were 2-methylresorcinol and resorcinol. Resorcinol exhibited considerable fluorescence at a peak emission of around 540 nm when excited at 458 nm, 488 nm, and 514 nm. 2-methylresorcinol, on the other hand, produced an emission of 550 nm when excited at higher wavelengths, including 514 nm and 543 nm. These results are summarised in table 5.3.

A

355 Excitation

● 1 ● 2 ● 3 ● 4 ● 5 ● 6 ● 7 ● 8 ● 9 ● 10 ● 11 ● 12

B

514 excitation

● 1 ● 2 ● 3 ● 4 ● 5 ● 6 ● 7 ● 8 ● 9 ● 10 ● 11 ● 12

C

543 excitation

● 1 ● 2 ● 3 ● 4 ● 5 ● 6 ● 7 ● 8 ● 9 ● 10 ● 11 ● 12
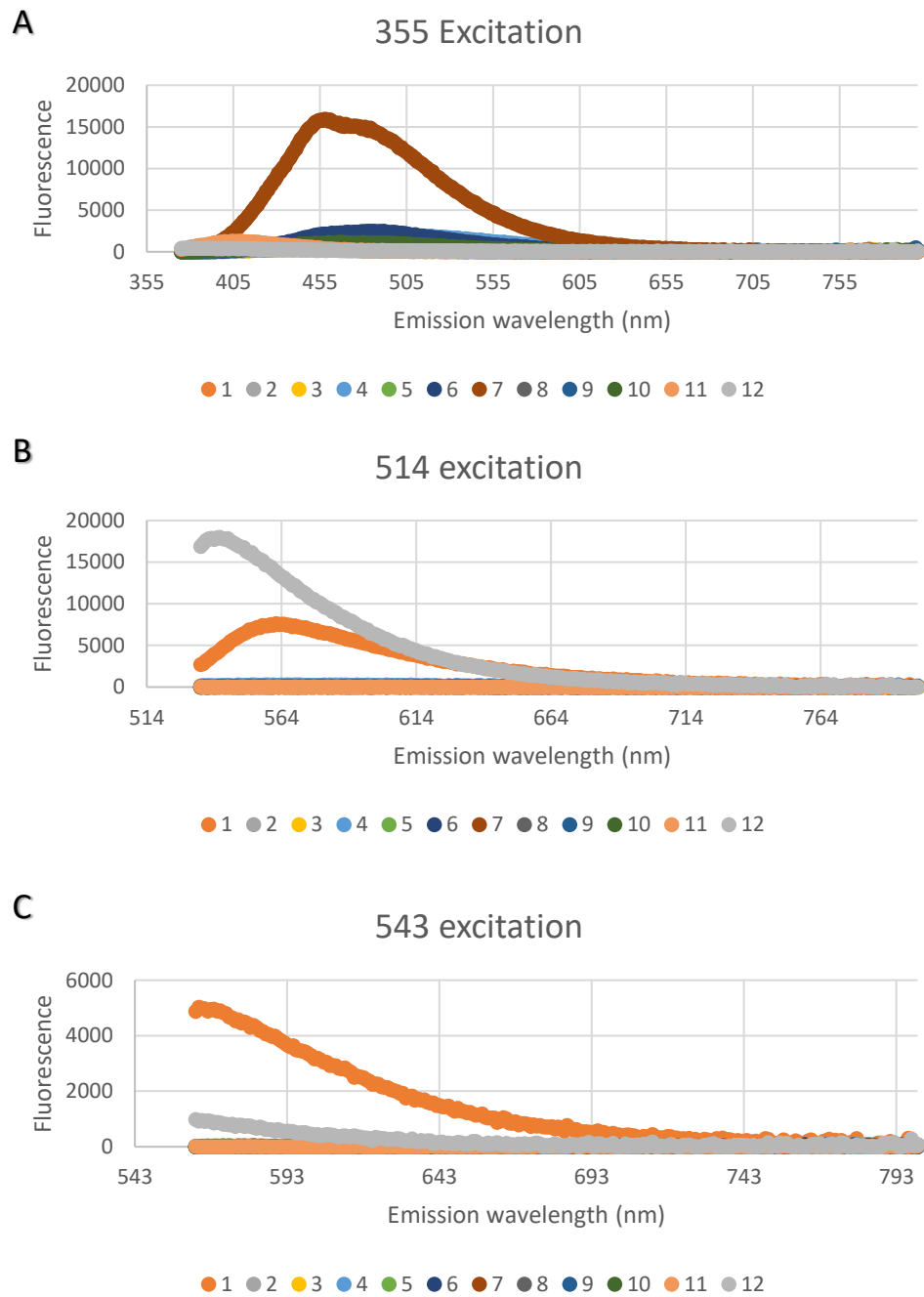
Figure 5.1: Some hair dye compounds express distinct fluorescence characteristics.
Emission curves of all hair dye components examined when excited at 355 nm (A), 514 nm (B), and 543 nm (C).

Laser line	Compound	Emission Peak	Reading
355	7	455	15800
458	12	540	4000
458	1	550	1100
488	12	540	15000
488	1	550	6000
514	12	540	18000
514	1	550	7500
543	1	555	5000

Table 5.3: Summary of the hair dye components which are most fluorescent.

Hair is able to fluoresce naturally, due in large part to fluorescent amino acids, such as tryptophan and its derivatives as discussed in chapter 1. In order to detect fluorescent compounds within hair, it is also necessary to consider the hair's auto-fluorescence at the wavelengths used. In order to characterise the fluorescence of the hair, fibres were screened for fluorescence at a range of excitation wavelengths. A number of emission spectra were created using excitation wavelengths in increments of 20 nm, from 260 nm to 540 nm in order to compile the 3D excitation / emission spectra shown in figure 5.2. Results showed that the hair fibre is most fluorescent when excited at wavelengths between 340 – 440 nm. This excitation resulted in fluorescence emission over a wide range of wavelengths, from approximately 400 nm to 540 nm.

When combined, results from the screening of both the selected compounds and of the fibre itself show that resorcinol and 2-methylresorcinol fluoresce markedly in a manner that is distinct from the hair's auto-fluorescence. These compounds may therefore be useful in visualising uptake of hair dye components within a hair fibre, as their fluorescence is likely to be discernible from hair auto-fluorescence. 1-napthol, despite showing fluorescence when excited at 355 nm, displayed substantial overlap with the auto-fluorescence of hair and so was not used for further in-hair investigation.
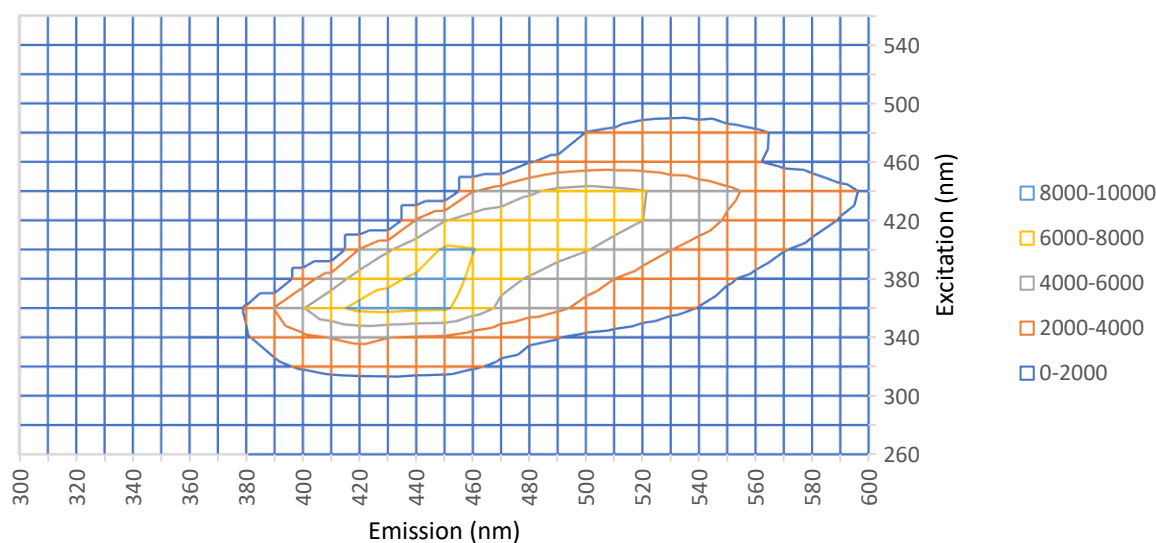
Figure 5.2: Autofluorescence of hair encompasses a wide range of wavelengths. 3D representation of hair autofluorescence carried out by completing a number of emission curves at 20 nm increments from 260 – 540 nm using the Synergy H4 plate reader.

5.2.2. Screening of dye formation and the effect on fluorescence characteristics

Dye compounds which are fluorescent would allow the uptake into hair to be imaged using light microscopy. To investigate if the dynamic formation of dyes could also be visualised using fluorescence, screening was carried out using the same excitation wavelengths as those used for the individual compound fluorescence screening. Dye formation requires the combination of coupler and primary dye constituents under oxidising conditions. During this experiment, formed dyes were created by the combination of each primary dye with each coupler, in the form of a crossover array as shown in figure 5.3A. Fluorescence properties of the formed dyes were then examined in relation to their constituent primary dyes and couplers.

Following this screening, results showed that compounds within the three groups: primary dyes, couplers, and formed dyes shared broadly similar properties. Primary dyes were often most fluorescent at lower excitation wavelengths, such as 355 nm. Couplers were regularly fluorescent at higher excitation wavelengths, such as 488 nm and greater. Formed dyes rarely showed substantial fluorescence, and in no circumstance were they more fluorescent than either their constituent primary dye or coupler at any wavelength. A typical example is shown in figure 5.4 where 4-amino phenol, a primary dye, is most fluorescent at 355 nm, 2-methylresorcinol is most fluorescent at higher wavelengths, and the dye formed by

combination of these two compounds shows little fluorescence at any excitation wavelength.
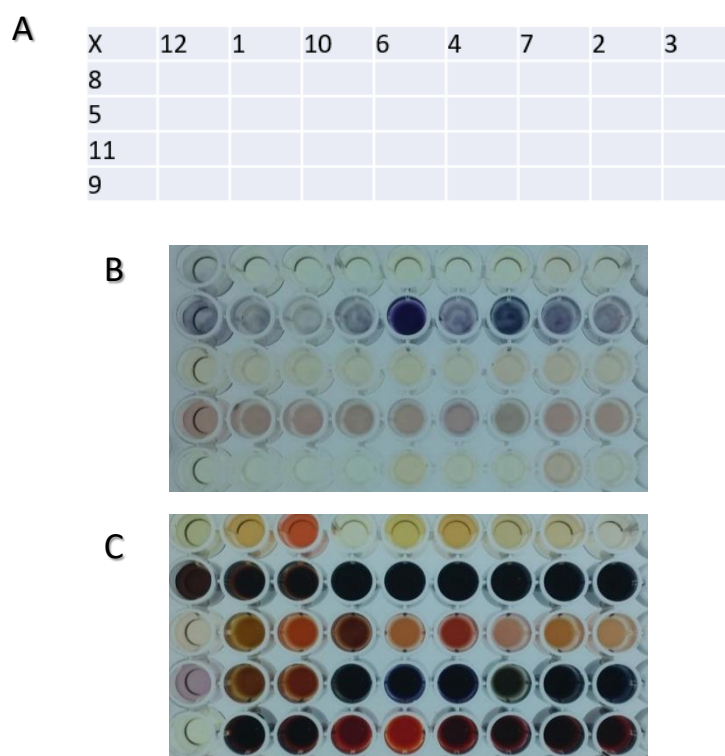
Figure 5.3: Formed dyes are visible in solution.
A – Diagram illustrating configuration in which hair dye compounds were added in order to investigate reaction of each coupler (columns) with each primary dye (rows). Example of colour formation before (B) and after (C) 24 hr incubation.

A

B
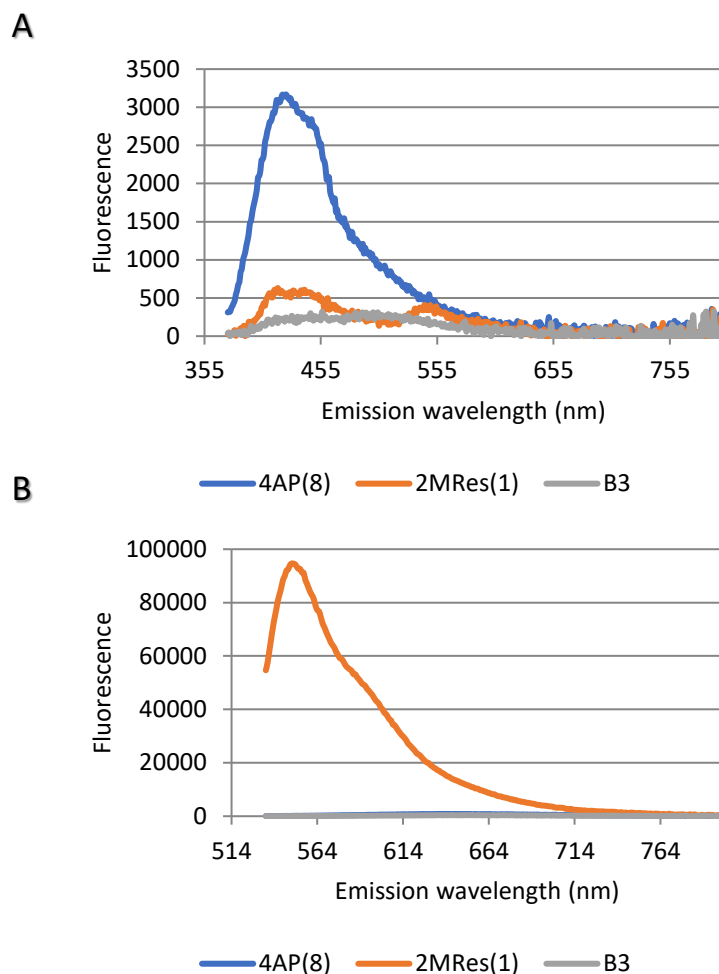
Figure 5.4: Formed dyes are less fluorescent than individual components.
Example of emission curves of primary dye 4-aminophenol and coupler 2-methylresorcinol in comparison with the dye formed following combination of these (B3) when excited at 355 nm (A) and 514 nm (B).

These results suggested that formed dyes would not be detectable within hair using their fluorescence and so work was continued using dye precursors individually, resorcinol and 2-methylresorcinol specifically, to reveal how these compounds are taken up into hair. Nevertheless, this work is relevant for determining where dyes eventually are formed. Hydrogen peroxide, also involved in dye formation, is able to be taken up into the hair readily. Therefore, the uptake of the precursors is likely to determine the extent of dye formation. Additionally, this work reveals that the conversion of fluorescent couplers, such as 2-methylresorcinol, into formed dyes would result in the disappearance of coupler fluorescence. However, this method for observing dye formation was not carried out during this study.

5.2.3. <u>Examining the fluorescence of selected compounds within hair</u>

Resorcinol and 2-methylresorcinol have been shown here shown to display fluorescence in spectral regions where hair's autofluorescence was less prominent. In order to confirm that fluorescence of these compounds would be distinguishable from hair autofluorescence, fibres were incubated in 1% aqueous dye solutions (w/v), also containing 4% (v/v) monoethanol amine in order to increase dye uptake through facilitating fibre swelling. Additionally, fluorescein was included as a positive control, which has previously been used for its fluorescence properties to aid in the light microscopy of hair (Ruetsch et al., 2003). The treated hairs were then lambda-scanned at each chosen excitation wavelength using LSCM, comprising 405 nm, 458 nm, 488 nm, 514 nm, and 543 nm, allowing the creation of emission spectra for each excitation wavelength, a selection of which are shown in figure 5.5. Additionally, the fluorescence of these compounds, in addition to the autofluorescence, is summarised in table 5.4.

Following 458 nm excitation, resorcinol, 2-methlyresorcinol, and fluorescein emission curves were detectable above that seen from hair autofluorescence alone. However, fluorescence from resorcinol was particularly weak. Fluorescein was most fluorescent of the compounds tested within hair when excited at 458 nm.

The fibre's auto-fluorescence was detected to a small degree following excitation at 458 nm. This was not the case at 488 nm excitation, where the now substantial fluorescence of each of the 3 compounds allowed a laser power to be selected which produced negligible autofluorescence. Unlike in the earlier hair-free screening, 2-methlyresorcinol displays greater fluorescence at 488 nm in comparison to resorcinol. One possible reason for this discrepancy is that 2-methlyresorcinol is present at greater quantities within the hair, suggesting that it is more readily taken up into the fibre. Fluorescein, as when excited at 458 nm, remains the most fluorescent when excited at 488 nm.

At 543 nm excitation, fluorescein and resorcinol show little fluorescence. However, 2-methlyresorcinol displays considerable fluorescence above the negligible background autofluorescence at this wavelength. Therefore, this excitation wavelength is preferable for the investigation of 2-methylresorcinol uptake as any fluorescence detected can be considered to originate from the compound itself rather than the fibre.

Two compounds which had previously shown to fluoresce when excited at 405 nm, 2-amino-4-hydroxyethylamino-anisole sulphate and 4-amino-2-hydroxytoluene, were investigated

using this wavelength while within hair. Both of these compounds exhibited detectable fluorescence, data not shown. However, due to the laser power required for this, and the prevalence of hair auto-fluorescence at this wavelength, auto-fluorescence was detectable and therefore these were deemed unsuitable for further study within hair.
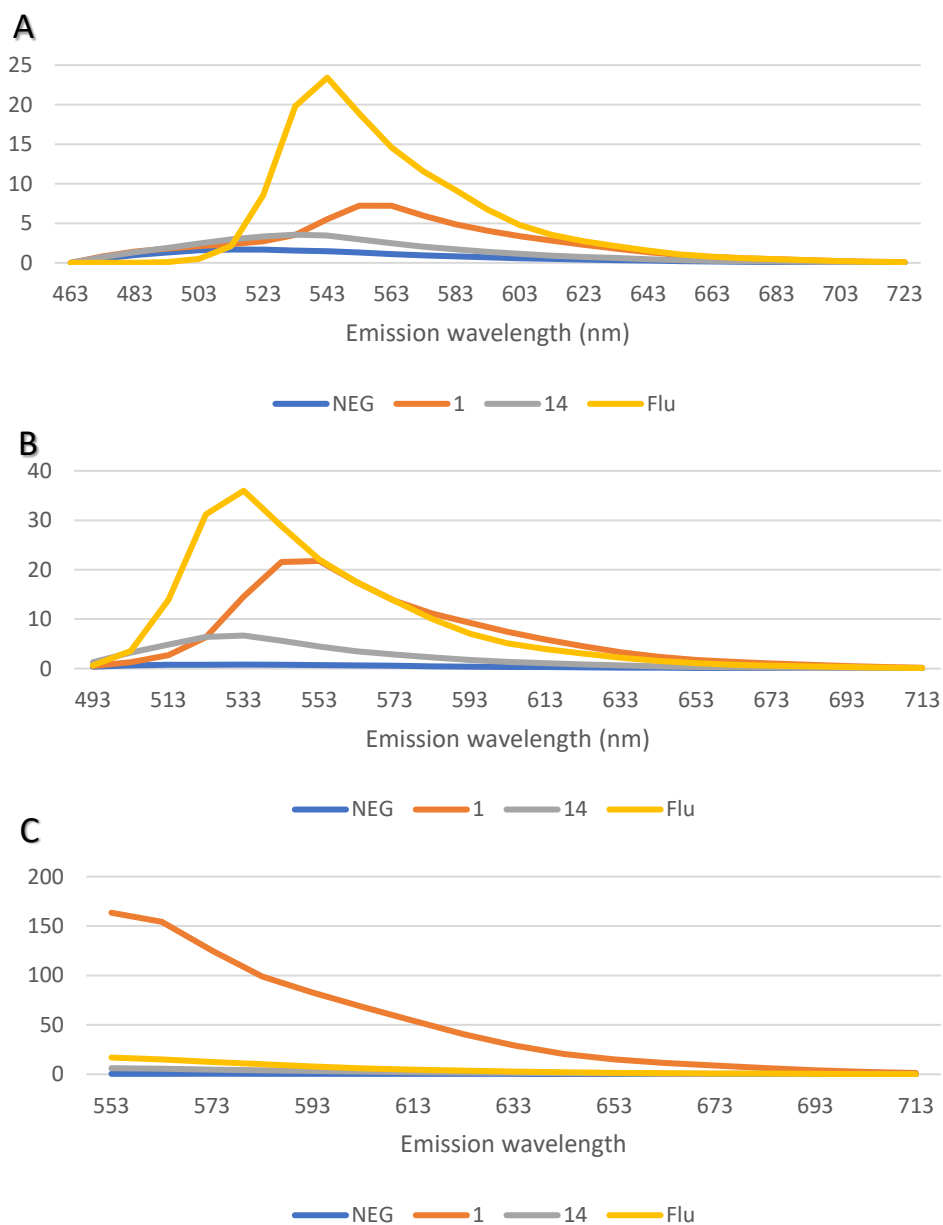
Figure 5.5: Selected dyes are detectable above hair autofluorescence while within hair. *Emission curves of hair containing 2-methyresorcinol (1), resorcinol (14), and fluorescein when excited at (A) 458 nm, (B) 488 nm, and (C) 543 nm alongside emission curves of hair autofluorescence (NEG).*

Excitation wavelength (nm)	Autofluorescence	Fluorescein	Resorcinol	2-methylresorcinol
458	+	+++	+	++
488	-	+++	+	++
543	-	-	-	+++

Table 3.4: Summary of hair autofluorescence and dye fluorescence within hair.

In summary, 2-methylresorcinol exhibits substantial fluorescence at 543 nm, and there is an absence of autofluorescence following excitation at 543 nm. Therefore, 2-methylresorcinol with excitation at 543 nm provides a good combination for the study of a hair dye component within hair.

5.2.4. Investigating the uptake of 2-methylresorcinol into hair

Of interest for the development of cosmetics, forensics, the analysis of hair for drug abuse, and with relevance to the treatment of wool fibres, is the understanding of the rate and means by which compounds move into the hair fibre (DeLauder and Kidwell, 2000; Guerra-Tapia and Gonzalez-Guerra, 2014; Wortmann et al., 1997). In order to observe this uptake over time, adjacent fibre sections were incubated in solutions containing 2-methylresorcinol and mono-ethanol amine for increasing periods of time from 0 – 5 hrs. These sections were then imaged using LSCM where they were excited at 543 nm and broad-spectrum emission captured from 560 nm to 760 nm. Equal laser power was used for each sample in order to allow direct comparison of 2-methylresocinol fluorescence. A number of optical sections were captured while hair was in a longitudinal orientation to allow for the composition of a partial transverse section through orthogonal sectioning.

Figure 5.6 shows images from this examination of dye uptake, from 0 to 5 hrs. During this time, fluorescence was seen to increase within the hair. As discussed earlier, this increase in fluorescence can be attributed entirely to the movement of 2-methylresorcinol into the fibre, as hair autofluorescence is negligible using these imaging parameters, displayed in the 0 hr timepoint (figure 5.6).
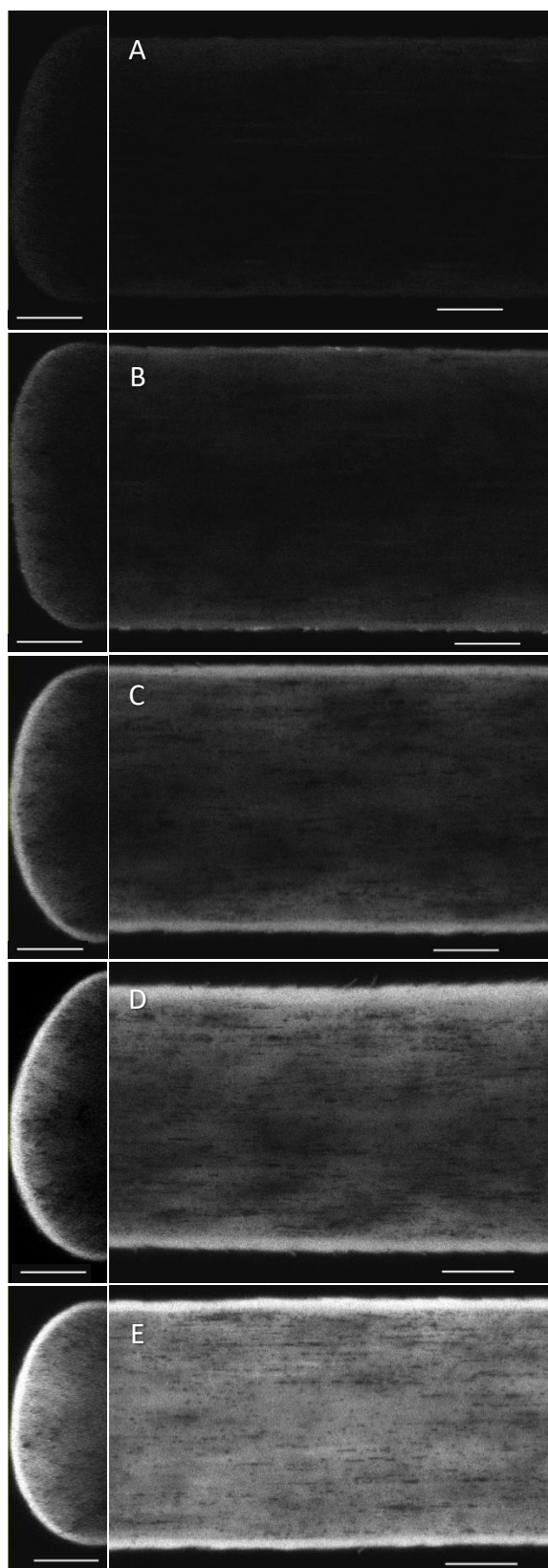
Figure 5.6: 2-methylresorcinol uptake into hair occurs over 5 hours. *Optical sections and a corresponding partial transverse section created through orthogonal projection of multiple optical sections. Untreated fibre (A) is compared to fibres incubated in solution containing 2-methylresorcinol for 1hr (B), 2hr (C), 3hr (D), and 5hr (E). Scale bars 20µm.*

2-methylresorcinol was observed to accumulate in the cuticle during the first stage of uptake, and this accumulation continued during incubation to result in a brightly fluorescent cuticle in relation to the cortex at each time point examined. Dye presence within the cuticle was not observed as layers, but rather as equal staining of the whole cuticle. This suggests that, rather than dye uptake occurring between cuticle cells, it instead takes place via the intracellular route, moving through both high and low sulphur regions.

Progression of 2-methylresorcinol occurred more slowly from the cuticle into the cortex, in comparison to its initial uptake into the cuticle. This uptake often was observed in discreet areas beneath the cuticle rather than as a complete wave, as can be seen particularly following 2 hr incubation in figure 5.6. This trend continued into the 3 hr sample, where dye movement increased to some areas and not others, resulting in uneven staining across the fibre, despite fluorescence in certain areas having reached the centre. Boundaries between these areas were not well defined, instead appearing diffuse. Rather than this uneven staining across the fibre being attributed to discrete uptake pathways, it could instead be credited to differences in permeability along the fibre, at the boundary between cuticle and cortex. The limiting factor for the dye uptake appeared to be its ability to move from cuticle to cortex, and this could be altered by damage, for example, to the cuticle-cortex CMC in certain areas.

At 5 hrs, staining appeared more homogenous, with a less steep gradient of fluorescence intensity across the longitudinal section than in earlier timepoints. An exception to the homogenous nature of the staining was the presence of unstained granules, often in linear arrangements, and most prevalent at the outer cortex. These granules are attributed to melanin particles, which the dye is unable to penetrate. The identification of these granules as melanin was supported by imaging of white hair, which lacks melanin, following uptake of 2-methyl resorcinol (figure 5.7A) where the melanin granules were no longer visible. Also shown in figure 5.7 is hair following uptake of resorcinol, which also displayed homogenous staining, similar in nature to the staining of hair by 2-methylresorcinol.

In summary, 2-methylresorcinol can be visualised within the hair fibre and its uptake observed over a range of time points. The staining process appears to take place over two stages where 2-methylresorcinol first accumulates in the cuticle, which occurs readily, Diffusion into the cortex below occurs over longer time periods and appears to be both variable and location dependent. This 2-stage uptake eventually results in fairly homogenous staining, with the exception of melanin granules which do not appear to allow entry of 2-

methylresorcinol. No discrete pathways of dye uptake were visualised, with the many layers of the cuticle appearing equally stained, suggesting uptake occurs through the intracellular route.
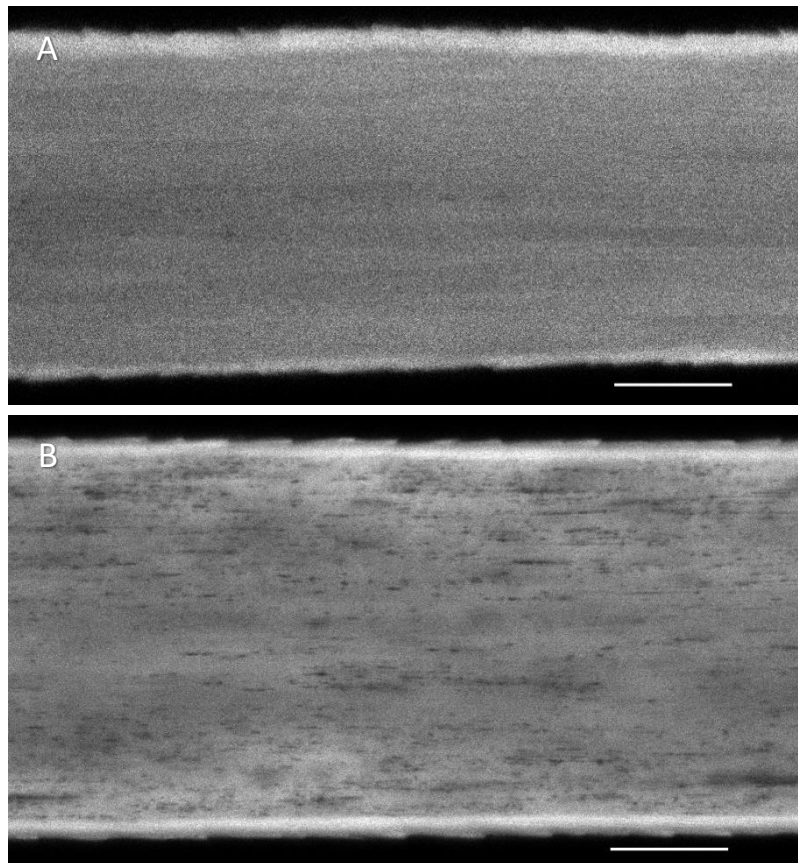
Figure 5.7: White hair does not contain melanin. Resorcinol resembles 2-methylresorcinol. A – White hair containing 2-methylresorcinol does not display granules in linear arrangement. B – Hair stained with resorcinol appears homogenous, similar to fibres stained with 2-methylresorcinol.

5.2.5. <u>Investigating the effect of monoethanol amine on hair permeability</u>

Monoethanol amine or ammonia are used in oxidative dye formulations to increase the pH. This basic pH results in greater efficacy of hydrogen peroxide radical generation (Torres et al., 2014) and also allows greater uptake into the fibre due to swelling of the hair (Bolduc and Shapiro, 2001; Robbins, 1988c). In order to visualise the extent of this effect on dye uptake, hair sections were incubated in solutions containing 2-methylresorcinol and increasing quantities of monoethanol amine. Hair sections were then imaged longitudinally as described previously.

Homogenous staining throughout the fibre, with the exception of dye exclusion from melanin granules and accumulation in the cuticle, was observed as previously (figure 5.8). The homogenous nature of this staining was unchanged regardless of the concentration of monoethanol amine. However, the degree of staining observed was altered through increasing monoethanol amine. Incubation of hair in a solution containing only 2-methyl resorcinol, and lacking monoethanol amine, resulted in very little staining in comparison to other formulations, appearing similar to negative control hair. With increasing monoethanol amine concentration, dye uptake was seen to increase, with this trend continuing up to the maximum concentration used, at 8% monoethanol amine.

Taken together these results suggest that the presence of monoethanol amine, and therefore basic pH, does increase uptake of hair dye compounds. Rather than allowing a novel route for uptake, this likely occurs through swelling of the fibre increasing uptake through existing routes.
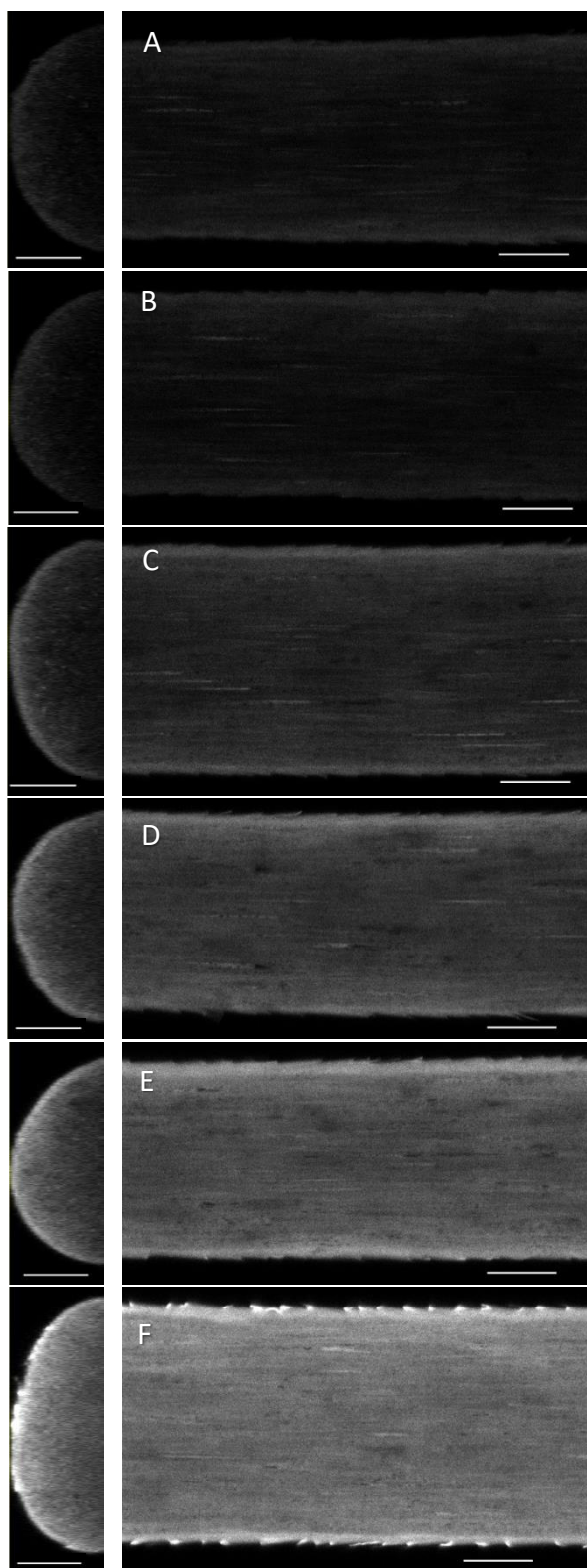
Figure 5.8: Increasing monoethanol amine concentration result in greater dye uptake. *Optical sections and a corresponding partial transverse section created through orthogonal projection of multiple optical sections. Untreated fibre (A) is compared to fragments incubated in 2-methylresorcinol solution containing (B) 0%, (C) 2%, (D) 4%, (E) 6%, and (F) 8% monoethanol amine. Scale bars 20 μm.*

5.2.6. <u>Direct imaging of the hair transverse section for improved resolution</u>

The transverse section of hair is often the more relevant when tracking dye movement from the cuticle to the centre of the fibre, in comparison to the longitudinal section. Using the method of obtaining a partial transverse section, through creation of a 3D representation of orthogonal sections, provides a sub-optimal resolution. This is because the resolution of confocal light microscopy in the z plane is approximately 500 nm, versus approximately 200 nm resolution in the x and y planes. In order to directly obtain images of the transverse section of hair, therefore increasing resolution, physical microtome sectioning is typically used.

To accomplish this, hair fragments were embedded into resin before microtome sectioning to 1 µm thickness. Sections were then imaged using LSCM and the Airyscan detector, and excited at 405 nm, to obtain transverse sections directly, without the need for reconstruction from multiple longitudinal sections.

Images obtained via this method, shown in figure 5.9A-B, allowed visualisation of hair structures not seen in longitudinal imaging, or through the use of orthogonal sectioning to obtain a transverse section. Arrangement of the medulla, where present, was clearly visible. Also, the CMC, a continuous network spanning the fibre, was visible within the cortex and appeared more fluorescent than the cortical cells it surrounded. Also exhibiting substantial fluorescence were structures at the centre of individual cortical cells, thought to be nuclear membrane remnants which are left behind following keratinisation. These structures were visible with optimal resolution allowing excellent definition of the fibre's morphology, not previously described in the literature with the use of light microscopy.

However, physical sectioning often resulted in damage to the hair, or artefacts. These ranged in severity from the partial or whole loss of the cuticle or its layers, as seen in figure 5.9A where only a single layer is visible for the cuticle. Alternatively, fractures could occur across the entire fibre section, particularly in fibres which had undergone bleaching treatment such as that seen in figure 5.9B.

An alternative method was developed, through the use of a 3D-printed device (figure 2.1) which allowed for hair to be held stationary in a vertical orientation to allow direct imaging of the transverse section, without the need for embedding and microtome sectioning. This device was termed the vertical imaging device (VID).
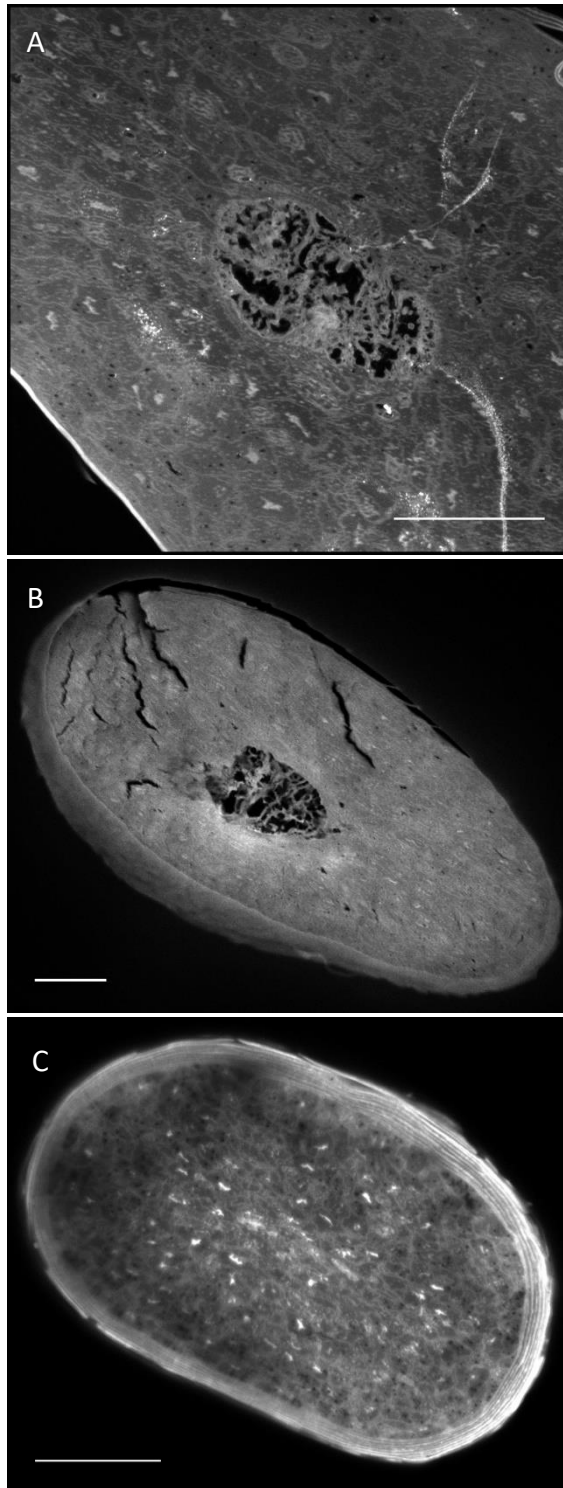
Figure 5.9: Directly imaging the transverse cross section provides greater structural information. *Images of (A) untreated hair following microtome sectioning, (B) bleached hair following microtome sectioning, and (C) untreated hair imaged using the VID. Scale bars 20 µm.*

Images taken using the VID, shown in figure 5.9C, provided excellent resolution, similar to that seen from microtome sections. Structures such as the CMC and nuclear remnants were clearly visible. Additionally, the cuticle is preserved intact, allowing imaging of several cuticle layers. This method of imaging hair provides high resolution images of the transverse section with minimal damage, and without the need for time-consuming embedding and sectioning processes. The elimination of the need for embedding and sectioning of the fibre, combined with the ability to insert and image several hair fibres simultaneously using the VID provides a high-throughput method for cross-sectional imaging of hair. Further, the use of the VID also allows the dynamic imaging of dye penetration in hair while observing at the cross section.

5.2.7. <u>Examining the effect of hydrogen peroxide bleaching on dye uptake into hair</u>

Chapter 3 investigated hydrogen peroxide bleaching and the effect of this treatment upon hair. Melanin destruction, the intended outcome of hydrogen peroxide bleaching, was visualised alongside measurement of undesired chemical change following damage. Oxidative damage, such that occurs during bleaching, is likely to impact dye uptake into the fibre, particularly in the case of movement which occurs via the intracellular pathway. Due to the homogenous nature of uptake by which 2-methylresorcinol migrates into hair, it is a good candidate for the study of hair permeability following bleaching damage. Further, the use of the VID allows high throughput imaging of the transverse sections of stained hair fragments directly, resulting in a means for rapid measurement of dye uptake at high resolution.

In order to test the ability of this method for quantifying damage to hair following bleaching, fragments of hair from the same individual, either bleached or untreated, were incubated in a solution of 2-methyl resorcinol for equal amounts of time. Melanin is destroyed during hydrogen peroxide bleaching, as was demonstrated in chapter 3. Therefore, white hair lacking melanin was used for this experiment to remove melanin's potential fluorescence quenching effects as a variable. These hairs were then imaged using LSCM and the VID, allowing transverse sections to be imaged directly without the need for physical sectioning.
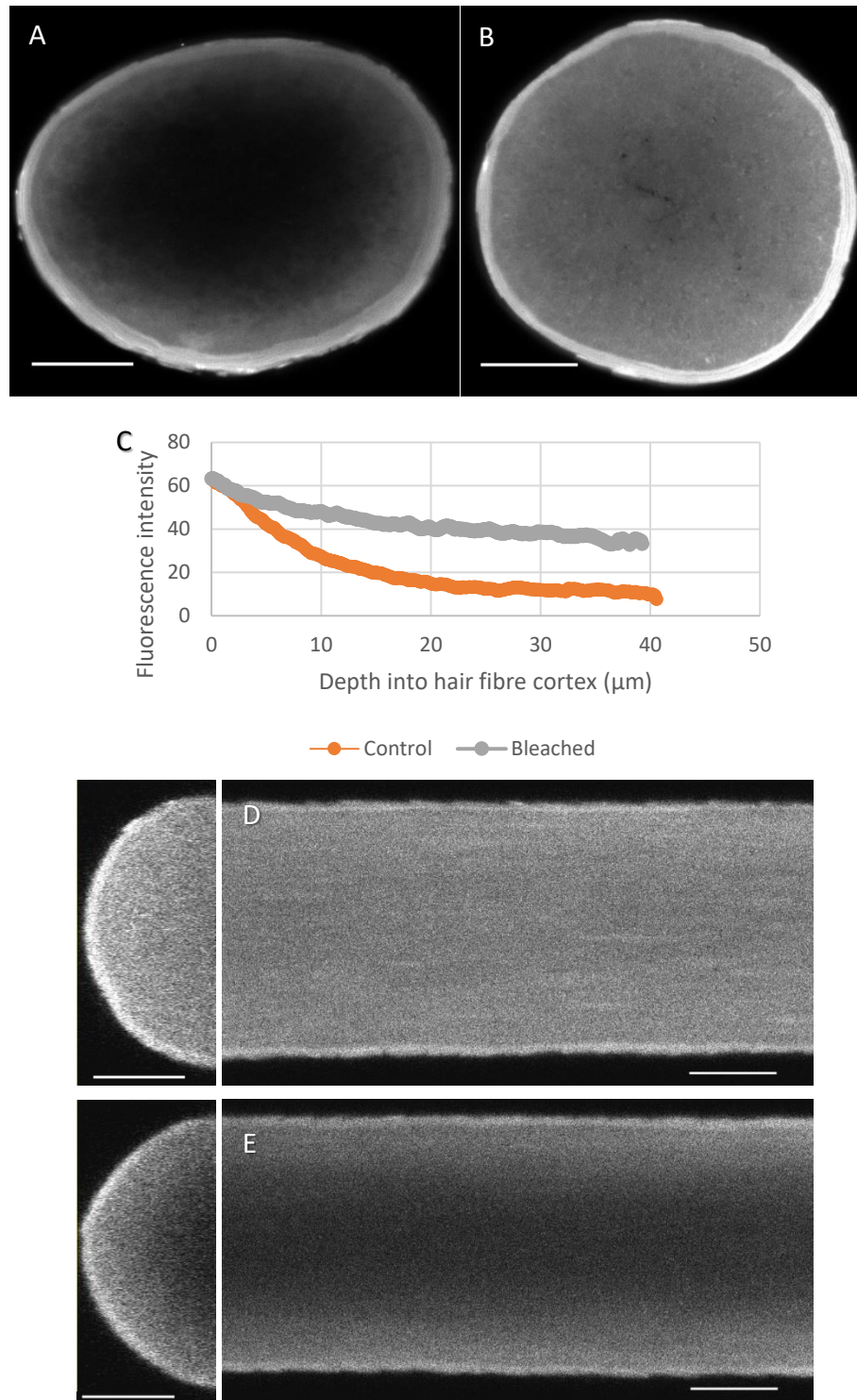
Figure 5.10: Peroxide bleaching results in increased hair permeability. *Example images taken using the VID of untreated (A) and bleached (B) fibres following incubation in 2-methylresorcinol. (B) Graph depicting fluorescence intensity decreasing with depth into hair fibre. (C) Similar experiment carried out without the VID, involving creation of an orthogonal section of the transverse cross section. Examples include bleached (D) and untreated (E) fibres.*

Following incubation in 2-methylresorcinol the untreated control hair sections, which are shown in figure 5.10A, displayed a clear gradient of fluorescence from outer to inner cortex. Within the incubation period dye had been unable to travel to the centre of the fibre in quantity large enough to produce significant fluorescence. Bleached hair (figure 5.10B), on the other hand, exhibited more even staining across the transverse section, with a much lower gradient of fluorescence between the inner and outer cortex. Data shown in figure 5.10C illustrates the difference in the gradient, within the cortex alone, between control and bleached samples. Notably, the fluorescence just below the cuticle, in the outer cortex, is similar in both bleached and control hairs. However, this rapidly changes with distance towards the centre of the hair. In both control and bleached hair sections, accumulation of dye within the cuticle was seen, as with previous experiments. Results therefore suggest that bleaching increases permeability of the fibre cortex. However, there did not seem to be an effect of bleaching on movement of dye across the cuticle-cortex boundary.

An identical experiment was performed with the hairs imaged in a longitudinal orientation, and transverse sections generated from the 3D projection of optical sections. Examples of images are shown in figure 5.10D-E. This experiment resulted in similar findings, albeit the transverse sections created were at a lower resolution than when imaged directly.

5.2.8. Investigating Nile red staining of the hair fibre

Previously tested dyes have displayed broadly homogenous staining within the fibre, particularly in the case of 2-methyl resorcinol and resorcinol. However, it would be of interest to selectively stain regions of hair, through the use of selectively fluorescent dyes, or dyes which move through the hair via a specific route. This may be accomplished using Nile red. Nile red is a lipophilic stain which will not fluoresce in polar solvents but is detectable when in lipid-rich environments (Greenspan et al., 1985). Nile red may therefore be useful for selectively staining regions of hair such as the CMC, which incorporates lipid membranes, in both the cuticle and cortex.

To investigate this, and test Nile red as a specific stain for lipid regions in hair, Nile red was applied to sections of hair prepared by cryo-sectioning. Cryo-sectioning was utilised to avoid the use of embedding resins which were brightly fluorescent following exposure to Nile red (data not shown).
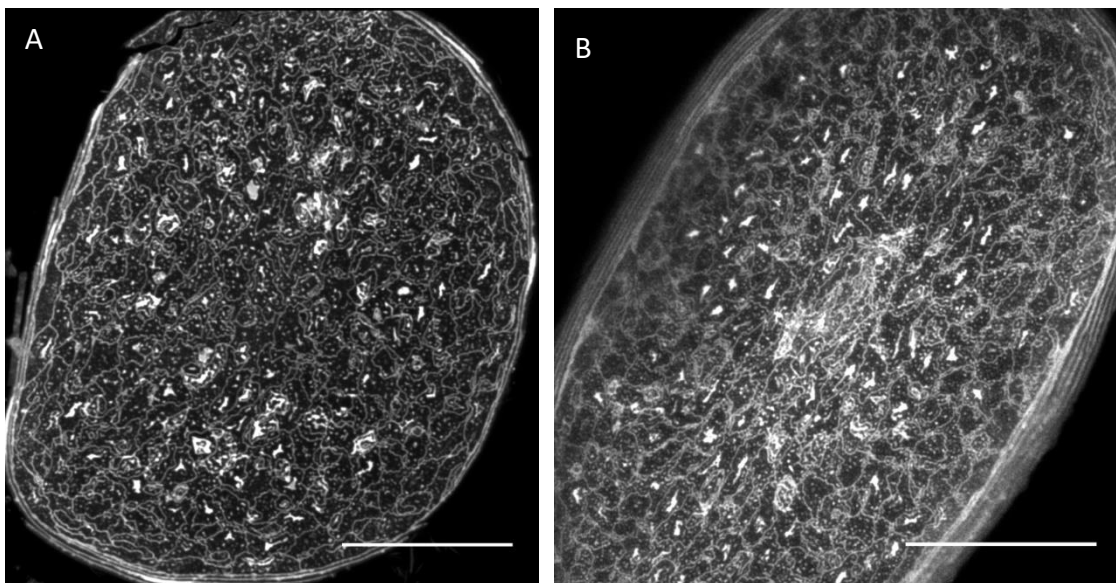
Figure 5.11: Nile red provides contrast for detection of lipid-rich regions. Images of Nile red stained hair obtained through cryo-sectioning (A) and the use of the VID (B). Scale bars 20 µm.

Nile red was applied directly to 1 µM sections of fibre following cryo-sectioning. These sections were then imaged using LSCM and the Airyscan detector. Within hair, Nile red was shown to clearly highlight the CMC throughout the cortex and also between layers of the cuticle. This is shown in figure 5.11A. Nile red also resulted in the staining of intracellular structures which are likely to be nuclear or organelle remnants (Szabo et al., 2012). As Nile red was applied directly to sections of hair, uptake through traditional pathways did not occur. The specific staining seen here was instead due to Nile red's selective fluorescence.

This method of selectively staining the lipid compartments of the fibre may be useful for observing changes to the morphology of hair, or alternatively used to detect changes in the chemical composition of these areas specifically. In order to assess this, sections of hair that had undergone a lipid-depletion treatment, and also sections which had undergone this before subsequent lipid restoration treatment using oleic acid, were prepared alongside untreated hairs. All samples were cryo-sectioned before directly staining with Nile red. Samples were subsequently imaged using LSCM and the Airyscan detector.
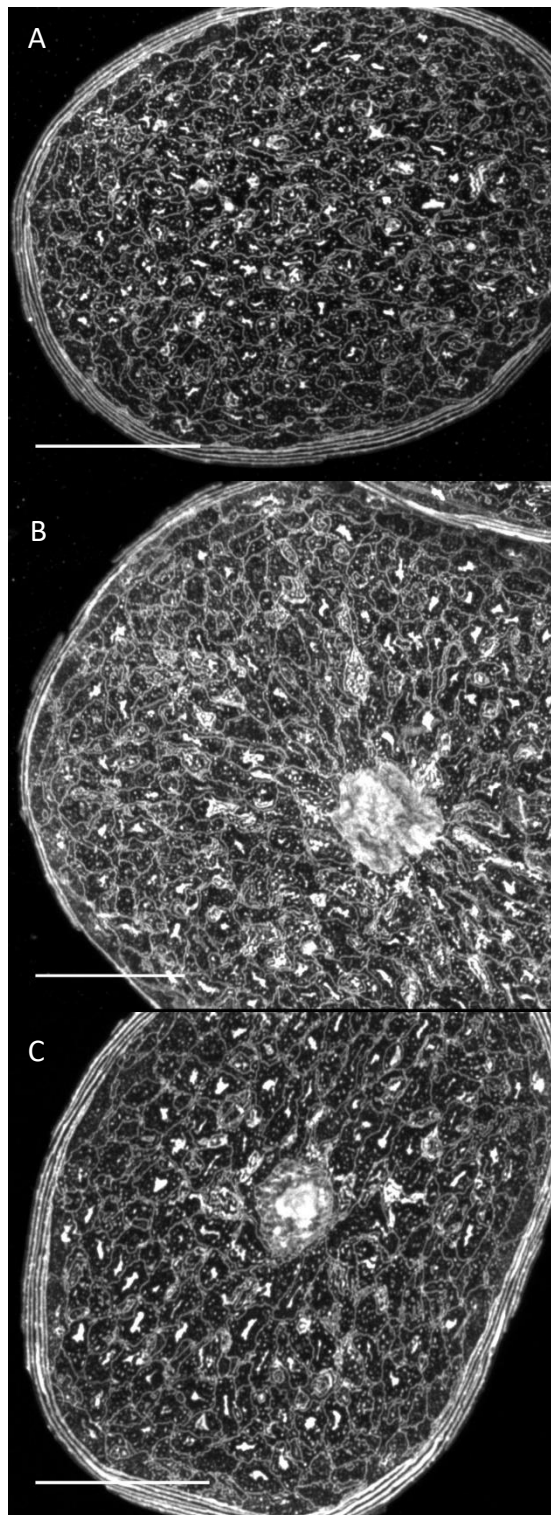
Figure 5.12: Lipid depletion and subsequent restoration do not affect Nile red staining.
Images depicting (A) untreated, (B) lipid depleted, and (C) lipid depleted and restored fibres which are stained with Nile red.

Following lipid depletion, there was little change in the staining of hair with Nile red, similar findings resulted from the staining of oleic acid-treated hairs sections, as seen in figure 5.12.

These results show that Nile red clearly is able to selectively stain for the lipid regions within hair. This method is useful for visualising the morphology of the whole hair and also for highlighting the location of lipid-rich regions. However, treatments which are thought to affect these regions had little effect on the Nile red staining. This may indicate that these treatments had little effect on the lipid regions themselves. However, it is also possible that, despite changes being made to the CMC lipid membranes by the lipid depletion and subsequent restoration, these regions remain sufficiently lipid-rich throughout and so do not result in altered Nile red fluorescence.

Nile red could also be combined with the use of the VID to allow dynamic staining of hair without the need for cryo-sectioning. Hairs were incubated in a Nile red solution before imaging using LSCM and the VID, therefore Nile red is taken up through the fibre cuticle rather than being applied directly to sections. Hairs imaged in this means appeared to be stained in a way that was identical to those stained directly, following cryo-sectioning (5.11B). The use of the VID, rather than imaging of cryo-sections did not result in a large drop in image quality. In summary, Nile red is effective for the direct staining of cryo-sections or for uptake into hair and subsequent imaging for the purpose of visualising hair morphology and location of lipid-rich regions. However, treatments examined here did not produce subsequent changes in the staining visualised within the CMC.

5.2.9. Visualising Rhodamine B and its uptake into hair

All dyes tested had so far appeared to move into hair via the intracellular pathway. This cannot be confirmed in the case of Nile red, which was seen only in the CMC, but is otherwise selectively fluorescent only in a lipid environment and so may have permeated the whole fibre. Therefore, CMC staining is not necessarily due to uptake specifically through this pathway. It was necessary to find an alternative stain which travelled via the intercellular pathway, through the CMC, rather than through the intracellular pathway and whose fluorescence was not dependent on its environment. Fluorescent dye which travelled in this manner would be useful for staining of the hair in order to visualise this intercellular pathway with high contrast. Importantly, this dye would also allow for insights to be made into the hypothesised 2-stage dye movement (Brady, 1992) using both intercellular and intra-cellular pathways and the dynamics of this movement.

Rhodamine B was examined as an alternative to the previously investigated compounds. This was chosen due to its regular use in biological imaging and additionally due to its lipophilic nature. Calculated logP values, which describe the partitioning of compounds between octanol and water, were used to estimate the degree to which the studied compounds were lipophilic (table 5.5). Higher values suggest greater partitioning into octanol and therefore a more lipophilic nature. LogP values suggested that Rhodamine B (logP: 2.37) was more lipophilic than 2-methylresorcinol (logP: 0.97) and resorcinol (LogP: 0.7) and so may be more likely to be taken up via the intercellular route. Uptake of Rhodamine B was explored through the use of hair fragments incubated over a range of timepoints in a solution containing Rhodamine B. Hair fragments were imaged through the use of LSCM and the Airyscan detector alongside the VID.

A number of examples are shown in figure 5.13. Uptake was shown to occur slowly in comparison to dyes imaged previously, such was the case with 2-methylresorcinol where dye could be seen to reach the centre of the fibre within 5 hrs. Following incubation for 30 hrs, fluorescence originating from Rhodamine B was still largely absent from the centre of the fibre. However, at 96 hrs the fibre appeared stained at the centre.

Dye	logP	MW (g/mol)
Resorcinol	0.7	110.1
2-methylresorcinol	0.97	124.1
Fluorescein	2.64	332.3
Nile red	4.39	318.4
Rhodamine B	2.37	479.0

Table 5.5: Molecular weight and calculated LogP values of studied dyes. *The partition coefficient (logP) of each dye was calculated by the ALOGPS 2.1 software tool provided by vcclab.org (Tetko, I. V. et al. 2005). The logP is the ratio of concentrations of a compound in a mixture of 1-octanol/water and provides a measure of lipophilicity for a given compound.*
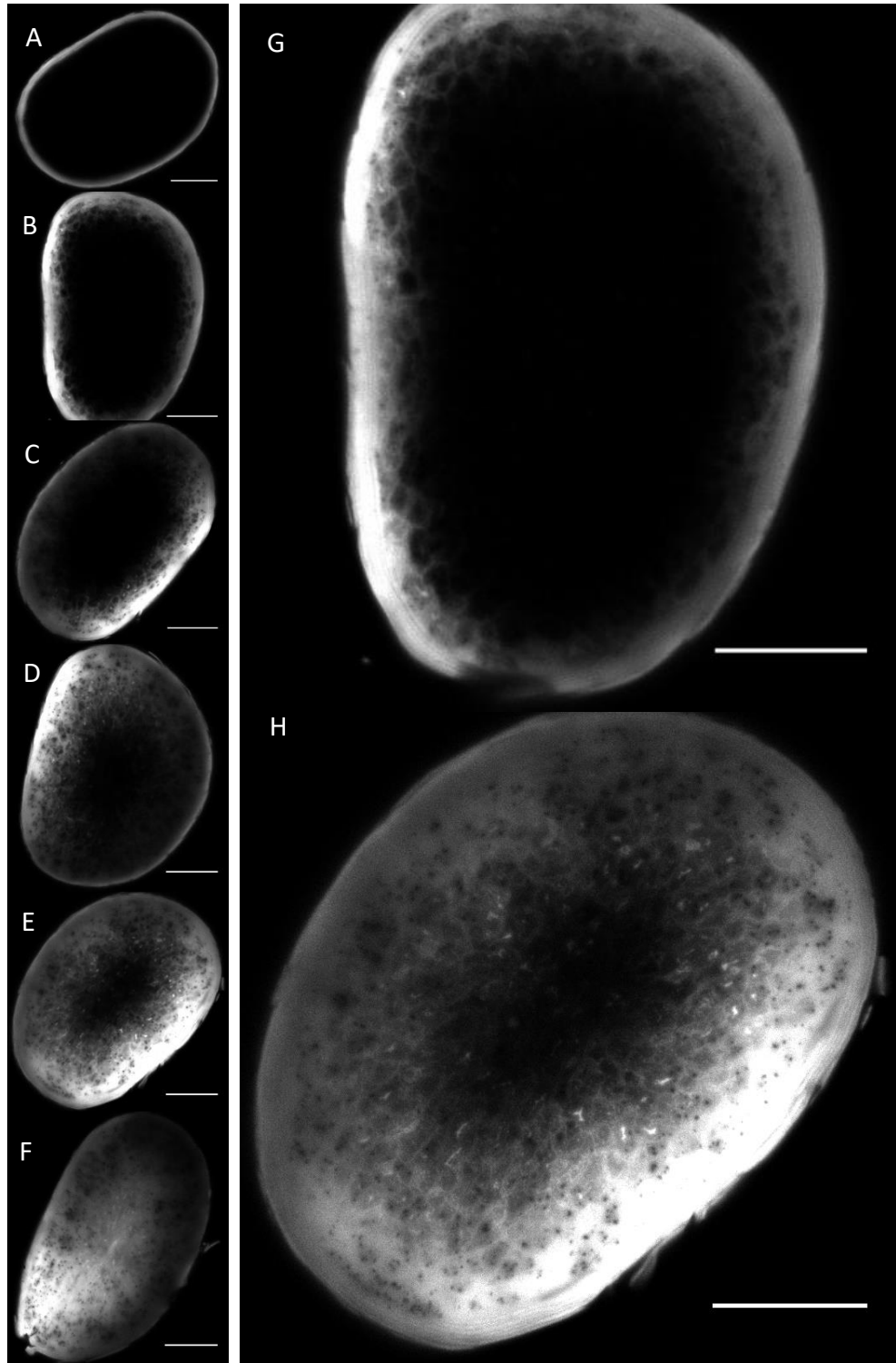
Figure 5.13: Rhodamine B uptake occurs in 2 stages. *Images depicting uptake timepoints of rhodamine B over (A) 2hr, (B) 8hr, (C) 16hr, (D) 24 hr, (E) 30 hr, (F) 96 hr with enlarged examples of 8 hr (G) and 30 hr (H). Images taken using the VID. Scale bars 20μm.*

Also notable, in addition to the slow dye movement, was the manner of dye uptake. Initially, fluorescence was seen to be largely confined to the cuticle, similar to the pattern of uptake seen from 2-methylresorcinol. However, unlike in the case of 2-methylresorcinol, dye within the cuticle was clearly seen to exist within discreet layers, rather than staining of the cuticle evenly. This suggests movement of Rhodamine B via the intercellular pathway, between cuticle cells, rather than the intracellular pathway that 2-methylresorcinol appeared to take through the cuticle. Also unlike in the case of 2-methyl resorcinol, uptake within the cortex occurred in 2 stages. First, dye was seen to migrate through the intercellular network of the cortex, the CMC. Subsequently, the dye appeared to diffuse at a slower rate into individual cortical cells from the surrounding CMC. Both of these stages can be observed within a single image, as in figure 5.14. Dye which had reached the inner cortex was seen to localise almost entirely to the CMC whereas at the outer cortex, dye was seen to be equally spread throughout CMC and cortical cells. This 2-stage dye movement suggests a propensity for Rhodamine B, a lipophilic compound, to move through the CMC, likely the lipid membranes, before undertaking movement into individual cells much more slowly.
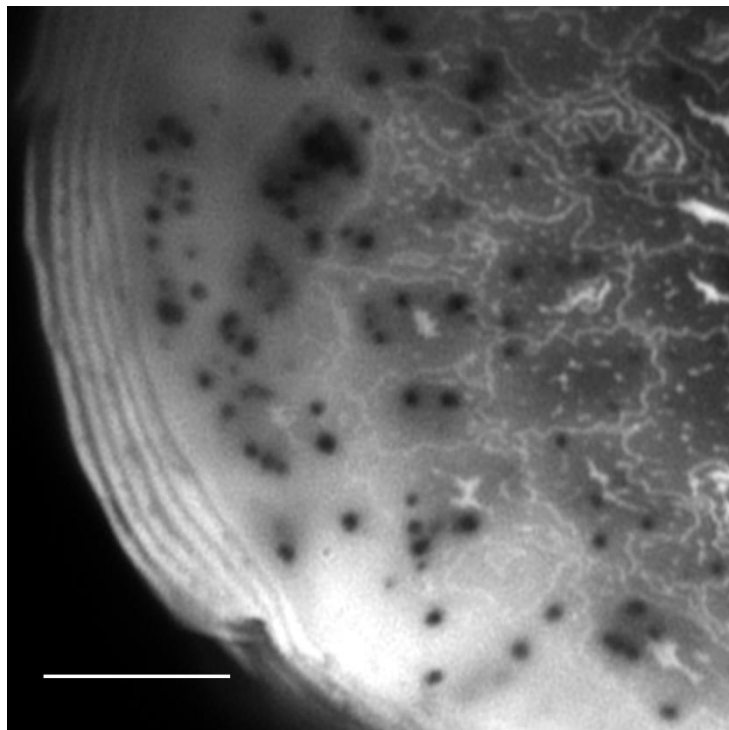
Figure 5.14: Rhodamine B moves from the CMC into cortical cells over time. *Image of Rhodamine B stained hair where outermost cortical cells are fully stained while inner cortex cells remain unstained.*

In order to visualise this movement occurring in real time, FRAP was applied during time series imaging of Rhodamine B-stained fibres. These fibres were no longer immersed in Rhodamine B, and so movement of dye would be entirely due to mobile dye already present within the fibre. FRAP utilises high intensity laser power to photobleach a designated region of a sample, in this case a hair containing Rhodamine B held vertically through use of the VID. Recovery of fluorescence is subsequently observed through time-series imaging. In this case, fluorescence recovery will occur due to movement of Rhodamine B into the previously photobleached region, and so will provide insights into dye movement. Hairs, following incubation in a solution containing Rhodamine B, were imaged using LSCM, the Airyscan detector, and the VID for time series over a number of minutes (supplementary figure 4). During this time series a section of the hair was photobleached, resulting in a drastic decrease in Rhodamine B fluorescence within that region. Recovery of fluorescence to the region was then observed, allowing insights into the dynamics of Rhodamine B migration in hair.
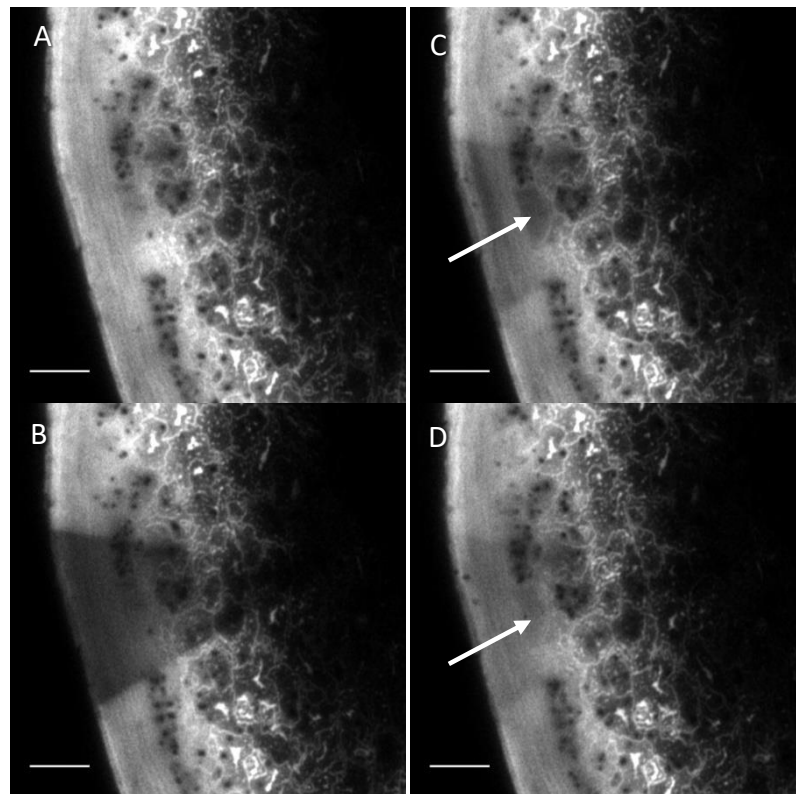
Figure 5.15: Dynamic imaging of Rhodamine B movement also demonstrates 2 stages. *Individual images depict selected timepoints during FRAP experiment carried out on Rhodamine B stained hair. Images are taken (A) pre-bleaching, (B) immediately post-bleaching, (C) 125 s post-bleaching with unstained cortical cell labelled, and (D) 600 s post-bleaching with stained cortical cell labelled. Scale bars 5 µm.*

Images from an example time-series acquisition are shown in figure 5.15. Before photobleaching, dye was seen to be present in both the CMC and cortical cells of the upper cortex, immediately beneath the cuticle. Deeper into the cortex, dye was largely confined to the CMC allowing visualisation of the 2 stages of dye movement within the cortex via static means. Photobleaching was subsequently shown to result in a large decrease in fluorescence across the designated region, as desired (5.15B).

Recovery was then observed with regular image acquisition. After 125 s of recovery, fluorescence was seen to have recovered substantially, with recovery largely taking place within the CMC. This is most clearly seen around the cortical cell labelled, where little recovery has occurred within the cell despite dye movement into the CMC surrounding it (figure 5.15C). Following 600 s of recovery, the second stage of dye movement was seen where Rhodamine B has moved from the CMC into nearby cells, resulting in near-complete recovery. These two stages of dye movement occur in a similar manner to that seen in uptake timepoints, where movement is primarily via the intercellular pathway before the dye is able to more slowly move into individual cortical cells. Notably, this recovery occurred in 5 minutes rather than the much longer timescales seen for initial dye uptake, suggesting that movement occurred much more quickly than during initial uptake. This could be explained by alteration of the CMC lipid component by the incorporation of Rhodamine B during initial uptake, subsequently allowing more rapid movement.

This experiment demonstrates the ability for Rhodamine B to move throughout the CMC, or intercellular route, of hair. This phenomenon can be visualised through static time points and also through the use of dynamic imaging and FRAP. Despite initial uptake of Rhodamine B occurring slowly, fluorescence recovery is comparatively rapid. This may suggest that the presence of Rhodamine B within the CMC is altering the organisation and permeability of these membranes and allowing for faster dye movement.

5.3. Discussion

Work In this chapter aimed to use fluorescent compounds in combination with hair for a number of objectives. Fluorescent compounds were used to visualise the uptake pathways hypothesised to allow movement throughout the fibre, both intracellular and intercellular, which have never previously been visualised dynamically. Fluorescence would also be used to examine permeability changes to the hair following insults such as hydrogen peroxide

bleaching. Finally, fluorescent dyes would be examined as a means for highlighting the morphology of hair.

5.3.1. Particular hair dye compounds are suited for in-hair characterisation

To begin, a range of compounds typically found within hair dye products were screened for their fluorescent properties. The goal of this was to eventually examine the behaviour of several different compounds within hair which had not yet been studied using the techniques available. Previous work of a similar nature has often used commercially available fluorescent stains such as uranine, closely related to fluorescein, in order to examine hair permeability for example (Ruetsch et al., 2003) rather than compounds which are likely to come into contact with hair. Work here aimed to characterise the movement and route by which these compounds are taken up into hair, using state of the art light microscopy techniques to allow high-throughput observation of the transverse section.

Several of the screened compounds were shown to be detectable in isolation but only a small number possessed characteristics that were deemed fluorescent enough and sufficiently distinct from the auto-fluorescence of hair, none more-so than 2-methylresorcinol. During screening, similarities in emission were shown within the groups of hair dye components; couplers and primary dyes, likely due to possessing chemical structures which are alike and therefore resulting in similar fluorescence characteristics. Following reaction of these components together however, formed dyes were observed to possess little ability to fluoresce when excited over the range of wavelengths tested. Reaction of coupler and primary dye therefore results in a compound with little ability to fluoresce following excitation at the wavelengths used here and so would not be detectable by their fluorescence alone while within hair. It was therefore decided to study the movement of individual dye components within hair.

5.3.2. 2-methylresorcinol is taken up into hair via intracellular means

2-methlyresorcinol was shown to be sufficiently detectable in hair to allow for imaging without the creation of background through auto-fluorescence. Within hair, the staining of 2-methylresorcinol exhibited several interesting properties. Initial uptake of the dye occurred only within the cuticle. This uptake occurred without the appearance of layered staining within the cuticle, suggesting that uptake was not occurring between cuticle cells. Instead, uptake was likely taking place via intracellular means, with dye moving across high and low sulphur layers of the cuticle. Taken together with later work, the logP value and

molecular weight of 2-methylresorcinol may provide an explanation for this. 2methyl-resorcinol has a logP value of 0.97, suggesting that it is substantially less lipophilic than Rhodamine B (logP: 2.37). Further, 2-methylresorcinol (124.1 g/mol) is also much smaller than rhodamine B (479.0 g/mol), which can be represented through molecular weight. Therefore, the small, hydrophilic 2-methylresorcinol molecule is more readily able to move intracellularly.

Strikingly, there was clear accumulation of dye in the cuticle resulting in a brightly fluorescent cuticle with little dye immediately progressing into the cortex. Data therefore suggests that a significant barrier to entry into the hair, particularly for 2-methylresorcinol, is the cuticle-cortex boundary. The structure most likely responsible for this is the cuticle-cortex CMC. The CMC is a continuous network which connects all cells of the hair, including both cuticle and cortex cells. The CMC within the cortex may be referred to as the cortex-cortex CMC, and likewise the CMC of the cuticle is the cuticle-cuticle CMC. These CMC regions are distinct between cuticle and cortex, particularly in the lipids present (Robbins, 2009). However, the CMC between the cuticle and the cortex, the cuticle-cortex CMC, is thought to be a hybrid between these, with the membrane on the cuticle side incorporating covalently bound fatty acids connected on their hydrophobic end to a hydrophobic protein in the delta-layer (figure 5.16). Conversely, the cortex side may comprise a lipid bilayer of fatty acids and a layer of hydrophilic protein within the delta-layer (Robbins, 2009). Work within this study suggests
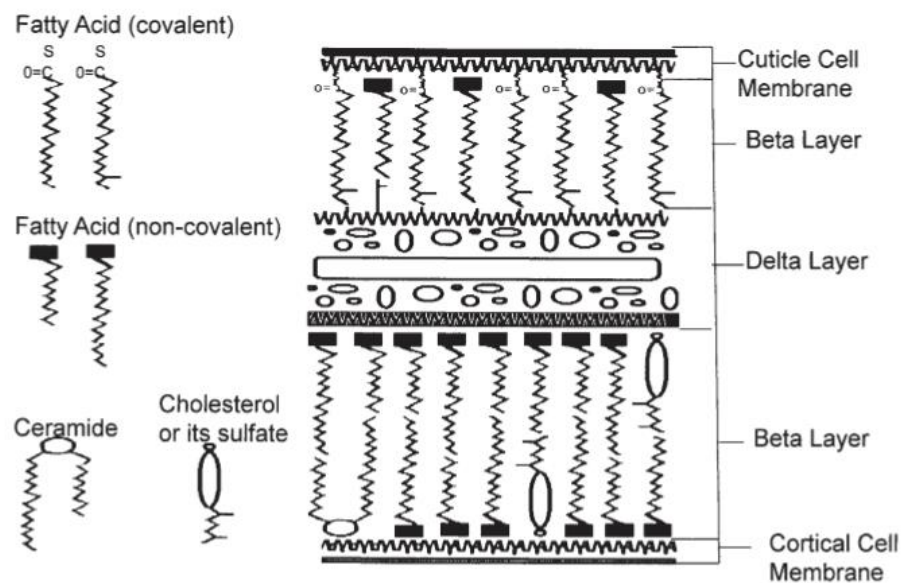
Figure 5.16: Figure demonstrating the proposed arrangement of the cuticle-cortex CMC. *Image taken from Robbins, 2009 to demonstrate the hypothesised arrangement of the cuticle-cortex CMC.*

that movement of dye across this membrane may be time or concentration dependent. This may be due to the necessity to move between regions with substantially different chemical composition. Of further interest was the movement of dye across this boundary at higher rates in distinct areas. This could be due to inherent abnormalities in these areas, such as a thinner or thicker CMC altering the time taken to cross the boundary. Alternatively, increased uptake could be due to physical or chemical damage in these discrete regions which has reduced the barrier function of the cuticle-cortex CMC. As the hairs used for this study are chemically untreated, physical damage is more likely the case in this instance.

Movement of the dye within the cortex also was observed to occur with a diffuse nature, despite initially occurring at discrete points from the cuticle-cortex boundary. This again suggests largely intracellular movement, likely due to the comparatively small, hydrophilic nature of 2-methylresorcinol. Staining resulted in fairly homogenous localisation of dye, with the exception of granules occurring in linear arrangements. Earlier work within this study, within chapter 3, has identified these as melanin granules which are destroyed during hydrogen peroxide bleaching. These granules exclude 2-methylresorcinol and they appear as dark voids possessing little fluorescence. Exclusion of dye may be due to the dense nature of melanin arrangement itself or alternatively due to the surrounding melanoprotein in which it is tightly embedded (Ghiani et al., 2008). Nevertheless, melanin granules make up a small proportion of the hair's mass and volume and therefore exclusion from these has little effect on the total amount of dye uptake (Robbins, 2012b). Further, dye components such as 2-methylresocrinol are often used for oxidative dyeing in the presence of hydrogen peroxide and ammonia which have been shown within chapter 3 to destroy these melanin granules.

In summary, 2-methylresocinol appears to move throughout hair largely through intracellular means, and the necessity to move through the lipid-containing cuticle-cortex CMC is a rate-determining step of this uptake. This suggests that the rate of dye movement could be affected by altering the protein cross-linking in hair, thereby increasing movement through the intracellular regions which are heavily cross-linked. Alternatively, targeting of hair lipids, particularly those in the cuticle-cortex CMC may result in rapid movement across the cuticle-cortex boundary and allow for uptake to occur at a higher rate.

5.3.3. Monoethanol amine increases dye uptake into hair

Further work examined the effect of monoethanol amine on dye uptake. This compound is used as an alternate means of increasing pH during oxidative dyeing, rather than ammonia (Bailey et al., 2014). Increasing concentrations of monoethanol amine were shown to be effective in increasing the amount of dye which was taken into the fibre. Monoethanol amine and ammonium hydroxide alike have been hypothesised to improve dye uptake through the facilitation of hair swelling (Ahn and Lee, 2002; Robbins, 1988). It is unknown if the swelling caused, and therefore increased dye uptake, is due entirely to the increased pH, or if monoethanol amine, or alternatively ammonia, has an additive effect in the process. However, swollen fibres are subsequently more permeable to both water and other reagents, this agrees with the results shown here.

Imaging of increased dye uptake with varying concentration of monoethanol or ammonia has not been published previously. Results here demonstrate that, particularly in the case of dyes which rely largely on intracellular movement, the incorporation of monoethanol amine is important for this dye uptake.

5.3.4. Direct imaging of the transverse cross-section of hair improves spatial resolution

Importantly, it was demonstrated how direct imaging of the hair cross-section while in a transverse orientation was beneficial for observing hair morphology and dye uptake. Imaging of the hair longitudinal section directly is not the optimum orientation for the visualisation of dye uptake, while creation of a transverse section through multiple longitudinal sections requires longer acquisition times and results in a sub-optimal resolution of this transverse section; approximately 500 nm rather than approximately 200 nm. Conversely, the most common method of obtaining a transverse section of hair, through the use of microtome sectioning, is time consuming for each sample and can often result in artefacts where physical damage is caused to the fibre.

Therefore, an improved method for the imaging of a hair transverse section was exhibited within this work. The use of the VID allowed imaging of the transverse section directly, without the need for embedding and sectioning. This significantly increased throughput of samples and decreased sample preparation time. Furthermore, this method was shown to produce images similar to those obtainable with microtome sectioning. Images of hair auto-fluorescence taken following this method allowed visualisation of structures within the hair

such as the individual cuticle layers, the CMC, and the structure of the medulla, which are not visible through imaging of the longitudinal optical sections.

Therefore, development of the VID technique allows for imaging of hair with reduced preparation time but importantly also has the potential to provide improved data and allow findings not possible through other means of imaging hair. Images are improved through the reduced manipulation required for this technique. Embedding and sectioning of hair may result in changes to the fluorescence of endogenous fluorophores and dyes within, in addition to physical damage to the hair during sectioning, owed to the rigid nature of the fibre. The use of the VID requires a single cut of the hair, which can be repeated immediately if unsatisfactory results are achieved. Further, thin hair sections are no longer representative of a portion of the fibre for observation of dye movement and dynamics. The use of the VID with stained hair sections allows dynamics to observed, using techniques such as FRAP, allows information to be gathered which is not possible with other methods.

5.3.5. Hydrogen peroxide bleaching of hair increases dye uptake within the cortex

The combination of fluorescent dyes, 2-methylresorcinol in particular, alongside the VID allowed for further study. Work was carried out to examine the degree of uptake, and therefore hair permeability, following hydrogen peroxide bleaching. Hydrogen peroxide bleaching was shown by this method to increase the permeability of the fibre cortex. Findings here agree with previous work which examined uptake of fluorescent dye following various forms of cosmetic damage (Ruetsch et al., 2003). Work within this study developed upon previous work through the use of a fluorescent dye which is likely to be used in combination with hair, rather than uranine which is not found within hair products. Further, the use of the VID allowed imaging of hair fragments following substantially less pre-processing, therefore reducing artefacts.

Interestingly, it was observed that the fluorescence of 2-methylresorcinol was equal when comparing the outer-most cortex of bleached and control hairs. This suggests that the bleaching treatment has not affected the rate at which 2-methylresorcinol crosses the cuticle-cortex boundary, thought to be due to the cuticle-cortex CMC. It is unknown what the rate-limiting step of this process is. However, due to the composition of the CMC it is likely due to the crossing of the lipid membranes. These data suggest that hydrogen peroxide bleaching is not adversely affecting the permeability of these lipid membranes. Conversely, the gradient of fluorescence within the cortex is much decreased following bleaching,

suggesting a large effect of bleaching upon the intracellular movement of dye across this region. This intracellular region is largely composed of protein, predominantly cross-linked keratin and keratin-associated proteins (Robbins, 2009). This suggests that hydrogen peroxide bleaching has a substantial effect upon this protein cross-linking and therefore the permeability of the cortex.

Results here show that hydrogen peroxide bleaching is able to adversely affect the uptake of dyes which utilise predominantly intracellular movement. It is therefore important to note previous hair care when estimating the degree of dye uptake into a fibre, which is relevant for the application of cosmetics. This may also be of interest for the study of drug detection in hair, as fibres which have been subjected to substantial damage may be more permeable to compounds of interest.

This work has utilised novel imaging methods and previously uncharacterised hair dye compounds. Results have provided insights into the movement of 2-methylresocrinol into hair. Further, understanding of the damage which occurs during hydrogen peroxide bleaching is progressed through this experimentation. The use of fluorescent dyes and the VID with hair can provide insights into cortical damage which are not possible through other methods of damage assessment such as cuticle assessment (Velasco et al., 2009).

5.3.6. Nile red provides high contrast for imaging of lipid-rich regions within hair

Further use of the VID was exhibited through combination with Nile red, a selectively fluorescent dye. This combination was successfully used to selectively label lipid-rich regions of the fibre. Nile red, being selectively fluorescent depending upon environment, was unlikely to stain homogenously as seen with 2-methylresorcinol (Greenspan et al., 1985). As expected, Nile red resulted in staining of the CMC, cuticle layers, and structures thought to be nuclear remnants (Szabo et al., 2012) in particular. Although the selective fluorescence of Nile red would result in little fluorescence while present in the proteinaceous regions of hair regardless, it is likely that due to Nile red's large size (318.4 g/mol) and lipohilic nature (logP: 4.39) uptake would occur via intercellular means. The use of the VID for this method was shown to be comparable to the use of physical hair cryo-sectioning, a time-consuming process which can produce physical artefacts.

Within this work, several treatments were examined, attempting to first deplete and then restore hair lipids. Neither of these treatments appeared to significantly change the staining of hair by Nile red. This suggests that although the lipid depletion treatment does affect hair

lipids (Marsh et al., 2018), the environment is still such that Nile red fluorescence is facilitated due to a non-polar environment remaining (Greenspan et al., 1985).

Nevertheless, this method of Nile red staining and imaging provides excellent contrast of lipid-rich regions in the hair not seen previously. This method could therefore be useful for imaging of both hair morphology, through observation of lipid localisation, and also investigation of changes to these lipid regions.

5.3.7. <u>Rhodamine B uptake into hair occurs in two stages</u>

The exocuticle on the outer surface of each scale cell, with its highly crosslinked A-layer, has been suggested as the most likely barrier to dye penetration also suggested by Brady 1992.

In order to visualise compound movement through the intercellular pathway, other dyes were tested which were likely to be taken up via this means. Rhodamine B was examined during this work due to its large size and lipophilic nature meaning that uptake through the lipid regions of hair was likely. Again, the VID was utilised allowing high throughput imaging of a dynamic nature, not possible through the use of thin hair sections.

Uptake was seen to occur slowly in comparison to 2-methylresorcinol, likely due to the size of Rhodamine B resulting in altered movement. However, similarly to 2-methyl resorcinol, uptake was also seen to be hindered by the cuticle-cortex boundary. In the case of rhodamine B, it is possible that crossing the proteinaceous delta-later of the cuticle-cortex CMC, which is necessary for progression towards the centre of the fibre, is the rate-limiting step at this point (Robbins, 2009b). Further, it was observed that localisation of the dye within the cuticle conformed to clear layers. As the most likely barrier to dye penetration within the cuticle is the highly cross-linked exocuticle, and the A-layer in particular, it is likely that the dye is localised primarily to the cuticle-cuticle CMC and possibly the endocuticle which possesses fewer cross-links in comparison (Brady, 1992; Robbins, 2012b).

Subsequent uptake of rhodamine B into the cortex also was seen to occur, in the first instance, via the intercellular pathway. This is likely due to rhodamine B's size and partition coefficient as discussed, allowing movement of dye through the lipid layers of the cortical CMC (Robbins, 2009b). Uptake through the cortical CMC was seen to precede intracellular diffusion, at a slower rate, to allow for complete uptake of the dye. This 2-stage dye uptake has previously been suggested (Brady, 1992). However, this has never been observed in such detail despite previous work using Rhodamine B which found partitioning only in the cortex

(Hadjur et al., 2002) or earlier work which did suggest that rhodamine B entered the proteinaceous regions given enough time, but images are of low resolution to see this phenomenon fully (Pötsch and Moeller, 1996).

Advanced light microscopy techniques were used to visualise this dye movement dynamically. FRAP was employed to confirm the same 2-stage movement seen using time-point study, and hypothesised within the literature (Brady, 1992). Uptake into the photobleached region was indeed seen to strikingly progress in this 2-stage mechanism as proposed. However, also of interest was the speed by which recovery took place, which occurred at a much-increased rate than that of initial dye uptake, possibly suggesting that incorporation of rhodamine B into the membranes of hair may alter permeability. This is important as, although there is little precedent for this in existing literature, it is possible that previous treatments incorporating a dye which moves via the intercellular route may in fact alter the dynamics during further treatments.
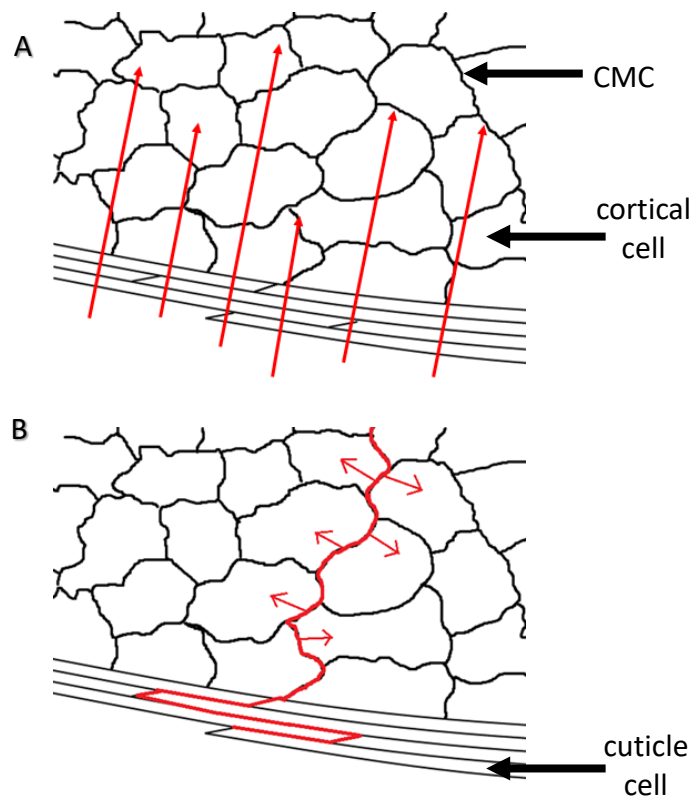
Figure 5.17: Figure demonstrating the observed dye uptake pathways. *Schematic representing the movement of dye via (A) – the intracellular route, across both low and high sulphur regions of hair and (B) – the intercellular route, involving movement between cuticle cells and throughout the CMC before slower movement into cortical cells.*

5.3.8. <u>Summary</u>

In summary, this work encompasses a number of findings which further understanding, in addition to outlining methods which will be of great use in further study. Both 2-methylresorcinol and rhodamine B have been highlighted as examples of fluorescently detectable compounds which move into hair via the intracellular and intercellular routes respectively (figure 5.17). This uptake has been observed in high spatial resolution and 2-stage dye movement has been observed dynamically. Findings suggest that, in particular, a compound's lipophilicity and size may have a great impact on its movement within hair. Additionally, knowledge of previous hair damage and treatments performed upon hair is of great importance when estimating the degree of uptake, both of dyes for the use of cosmetics and of drugs when examining drug abuse. Nile red, on the other hand has been shown to provide excellent contrast between the lipid-rich regions of hair and their surroundings, providing utility for the study of these regions and indeed the morphology of the fibre as a whole. Finally, the implementation of the VID has been shown to be useful for high-throughput imaging of the transverse cross section of the hair fibre without the need for microtome sectioning.

6. Discussion and future work

This study as a whole comprised several aims which are linked by the intention to further understand human hair and its keratin associated proteins through the use of advanced light microscopy modalities. FLIM was evaluated as an alternate quantitative measure for damage occurring to hair following various cosmetic and natural forms of damage. Alongside correlative techniques, FLIM was utilised to further understand the chemical changes occurring following damage. Work centred around the understanding of how keratin associated proteins may interact with keratins to produce a resilient hair fibre was accomplished through the characterisation of a number of KAPs. KAPs where characterised through transient transfection in HaCaT cells, both alone and in combination with selected hair-specific keratins. Finally, work involving the use of fluorescent compounds to supplement LSCM of hair allowed understanding, and direct imaging of, the routes by which compounds are taken up into hair. Additionally, these fluorescent compounds were used for assessing permeability and for specific labelling of the fibre.

6.1. Quantification and understanding of hair damage using FLIM

Previous work using FLIM for the study of hair is extremely limited, and is entirely comprised of the use of multiphoton FLIM for this purpose (Ehlers et al., 2007, 2006). Therefore, the use of single-photon FLIM, particularly at the wavelengths used here, is completely novel for the study of human hair.

6.1.1. Observations of untreated hair using FLIM

Work began with characterisation of untreated hair using this methodology. The average lifetime of hairs at this stage was shown to exhibit little variation between fibres and between individuals, a property which is useful for a measure of damage. This is unlike certain other methods of damage assessment, where there is a large degree of inherent variability between individuals and between hairs, such as is the case with cuticle peeling (Kaliyadan et al., 2016).

As discussed in chapter 3, an optional cuticle-cortex boundary is likely the effect of altered chemical composition between the cuticle and the cortex, although it is unknown if this is due to intrinsic differences such protein composition or even due to age, race, or sex (Giesen et al., 2011; Laatsch et al., 2014). This cuticle-cortex boundary is also likely different to the phenomenon observed during dye uptake in chapter 5, where the dye was seen to pause at

the cuticle-cortex boundary. In the case of dye uptake, this is likely due to a distinct, thin layer between these regions of hair. Conversely, the boundary seen within FLIM suggests a different chemical composition for the cuticle as a whole.

The difference in cuticle and cortex average lifetime would be of interest for further study, particularly to determine in the first instance if this was due to an intrinsic difference in the fibre or due to an external force. Similar techniques to those used in chapter 3 could be employed to determine which chemical components may be responsible for a lower average lifetime in the cuticle, or vice versa in the cortex. Manual removal of the cuticle could also be employed for studies of this region in isolation. It would be of interest to determine if there exists a chemical treatment which results in a lower average lifetime to exist in the cuticle, or in fact in the upper cortex as was seen as a gradient of average lifetime, as the mechanisms for damage hypothesised within chapter 3 serve only to increase the average lifetime. It would also be of great interest to determine that this phenomenon is due to an intrinsic difference, and could allow the use of FLIM for determining either macroscopic properties of hair from only a single fragment, such as colour, shine, or curl. Alternatively, it is possible that changes in FLIM such as this boundary may be due to differences in age, sex, race, or even diet (Giesen et al., 2011; Laatsch et al., 2014).

6.1.2. The imaging of hair melanin using LSCM

Within chapter 3, techniques which are previously unpublished were shown to allow visualisation of melanin granules and their destruction following bleaching. However, there is a great deal of future work possible using these light microscopy techniques which would serve to further the understanding of melanin destruction. In the first instance, this could include additional endpoint studies examining various hair colours, and therefore different composition of the two types of melanin found in hair; eumelanin and pheomelanin (Ito and Wakamatsu, 2011) to determine the effect of hydrogen peroxide on these. Importantly, it would also be possible to examine this destruction dynamically using these techniques in combination with the VID. Work is currently being undertaken in the lab in this area.

6.1.3. The impact of hydrogen peroxide bleaching on fluorescence lifetime

Work continued using FLIM to quantify the chemical change occurring following bleaching, which was seen to increase the average lifetime of hair. This phenomenon has never previously been described in the literature. Further work of interest in this area would be to determine if similar chemical change, and lightening of the hair, could be achieved through

the use of other alkalisers. Ammonia, along with other alkalisers found in hair products such as mono ethanol amine, is suspected to have an accelerating effect to processes such as oxidative dyeing due to swelling of the hair and therefore increased uptake (Robbins, 1988). However, in the case of hydrogen peroxide bleaching, the active ingredients are small and likely to move through the hair with ease. Therefore, pH may be the only determining factor for the degree of average lifetime change seen here. The plateau seen from increasing hydrogen peroxide is more difficult to explain. It would be expected that increased hydrogen peroxide has a linear relationship with the formation of radicals, therefore the reduced effect of hydrogen peroxide may be due to a lack of so-called precursor for chemical change, either due to complete depletion or due to a lack of access which will be discussed later.

Nevertheless, the average lifetime of hair was clearly shown to be affected by bleaching. Further work using this technique could focus on 2 key areas. FLIM is particularly useful in being able to observe changes in chemical composition within a sample. Although in the case of hydrogen peroxide bleaching there was a clear change to average lifetime across the fibre, it would be of interest to observe particularly how the lifetimes react spatially, following beaching and other photo-chemical forms of damage. This work would be supplemented through the use of the VID which would allow direct imaging of the transverse cross-section of hair for examination of lifetimes. The VID could also be used in the second area of interest, which is to observe these chemically changes occurring dynamically. Chemical damage applied to the hair whilst imaging is taking place, using the VID or with the hair orientated longitudinally, could provide further insights into the dynamics of these chemical changes. Work to this effect is currently ongoing within the lab.

6.1.4. <u>Investigating the source of fluorescence lifetime changes following oxidative damage to hair</u>

Results from within this study, alongside significant evidence in the literature, suggested that oxidation of tryptophan by hydrogen peroxide would result in a number of products, broadly termed kynurenines, which could account for the changes observed in fluorescence lifetime (Daly et al., 2009; Grosvenor et al., 2010). Although this mechanism of damage through oxidation has been previously described, in both wool and hair following photodamage (Daly et al., 2009; Dyer et al., 2014, 2010), this work is novel in detecting tryptophan oxidation in human hair following hydrogen peroxide bleaching, and in observing this tryptophan oxidation through the use of FLIM. Indeed, it was confirmed here that L-kynurenine concentration within hair increases following hydrogen peroxide bleaching, providing

further evidence for the hypothesis that FLIM is able to detect tryptophan oxidation. An experiment of interest for future work in this area wold be the quantification of several tryptophan oxidation products, this work would serve to inform on the changes in concentration of fluorescent tryptophan oxidation products as a whole. Existing work has characterised the likely mechanisms by which radicals may act upon tryptophan, resulting in a mechanism for oxidation as shown in figure 6.1.

6.1.5. The effects of hydrogen peroxide bleaching on in-tact proteins of hair

Study of the overall soluble protein composition of hair found that KAPs were adversely affected by oxidative treatment. These changes to protein composition, and KAPs in particular, may be a driving factor in the perceived changes to the macroscopic look and feel of hair following hydrogen peroxide bleaching. Due to the wide-ranging possible effects of radical damage upon proteins, which may act upon both the backbone and individual
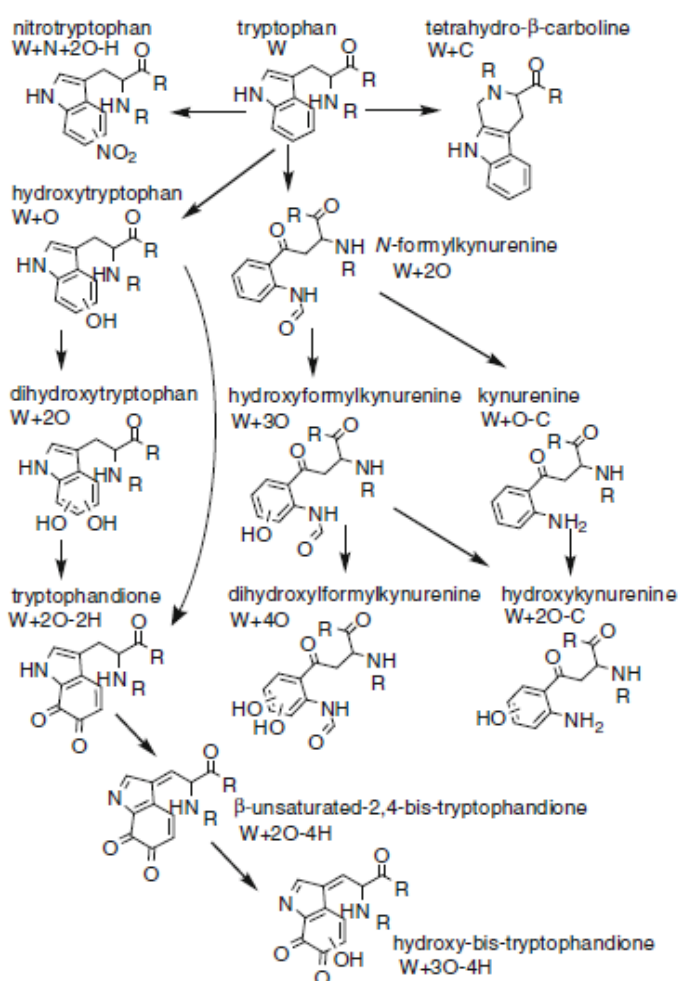
Figure 6.1: Tryptophan oxidation pathway. *The pathway for tryptophan oxidation proposed by Grosvenor et al. Figure taken from Grosvenor et al. 2010.*

residues to cause fragmentation, further cross-linking, and altered binding affinities (Davies, 2016; Hoting et al., 1995; Salvi et al., 2001; Tatsuda et al., 1987), it is not possible to determine the cause of KAP loss from the soluble fraction.

Further work here could aim to determine if KAPs or KAP fragments are detectable in the wash immediately following bleaching through the use of MALDI-TOF, this could provide evidence that the KAPs are washed out of the hair. This would be of particular interest in relation to the plateauing and also the dialysis experiments discussed. It is possible that oxidation of tryptophan is occurring only on select residues which are easily accessible, resulting in the plateau seen following increased hydrogen peroxide. It is logical that KAPs, which form the matrix surrounding keratins (Robbins, 2012) will be the most easily accessible proteins and so the majority of modification may happen to tryptophan residues of KAPs. This loss of KAPs could also correlate with the subsequent drop in average lifetime following dialysis, as KAPs incorporating these modified residues are lost from the fibre. An alternate method for further study would be LC-MS/MS of trypsin-digested hair samples. This experiment could be carried out to determine if KAPs were still present and perhaps cross-linked into the fibre, and so no longer soluble. LC-MS/MS could additionally provide further uses in this area of work. Specifically searching for tryptophan residues which are modified may reveal key peptides and proteins which are the primary targets of this oxidation and perhaps explain why KAPs in particular are adversely affected.

6.1.6. Hair damage from alternate sources and the effect upon fluoresce lifetime

Final work in this area observed the average lifetime of hairs treated with a range of photochemical insults. Of great interest here was the similarities between the effects of photooxidation and hydrogen peroxide bleaching upon average lifetime, which was not observed following non-oxidative forms of damage. Therefore, it may be summarised that FLIM has been shown to be a sensitive, quantitative, and spatially resolvable measure of oxidative damage to hair. FLIM is able to measure this damage through the production of tryptophan oxidation products which possess a distinct lifetime within hair.

6.2. Functional characterisation of keratin associated proteins

Despite the knowledge that KAPs are important for the structure of hair, previous literature aiming to characterise the behaviour of KAPs is limited, often taking a biochemical or basic light microscopy approach with just a single KAP from the repertoire of nearly 100 gene members (Wu et al., 2008).

In prior work, certain singular KAP members have been shown to self-interact via disulphide bonding (Fujikawa et al., 2013, 2012; Fujimoto et al., 2014). Additionally, using biochemical methods, KAP members have been shown to interact with hair-specific keratins, particularly at the head domain of these keratins, while no interaction was seen with epidermal keratins (Fujikawa et al., 2013, 2012; Fujimoto et al., 2014; Matsunaga et al., 2013).

Work outlined in this thesis aimed to characterise a wide array of KAPs beyond those studied to date, in order to more fully represent this large family of proteins.

6.2.1. HGT KAP localisation to epidermal keratin filaments

Among the observations made here, HGT KAPs in particular were seen to localise to epidermal keratin filaments throughout HaCaTs while HS and UHS KAPs did not, agreeing with previous literature (Fujikawa et al., 2013, 2012). This potential interaction is not described previously in the literature. However, it has been previously hypothesised by Matsunaga et al. that HGT KAPs may have a unique role in changing the alignment of KIFs through unique binding interactions (Matsunaga et al., 2013). Further evidence for this is provided by Bornschlögl et al. who observed the formation of an IF network just above the dermal papilla within the hair follicle, which is consistent with the location of hair-specific keratin and HGT KAP expression in particular (Bornschlögl et al., 2016; Langbein et al., 2001, 1999; Rogers et al., 2006). Experiments carried out by Bornschlögl et al. also suggested that cysteine cross-linking was not a significant driving force in the fibre's mechanical properties during this stage, and instead it was hypothesised that isopeptide bonds between these keratins and HGT KAPs may serve to stabilise the early hair fibre (Bornschlögl et al., 2016). Work carried out during the current study suggests that HGT KAPs may have a role in binding epidermal keratins present within the hair follicle (Langbein and Schweizer, 2005). Alternatively, colocalisation seen here could be due to sequence homology between epidermal keratin and the region of hair-specific keratin required for this unique role proposed in earlier work (Matsunaga et al., 2013). This interaction may involve the formation of isopeptide bonds which is made possible through the transglutaminase 3 activity present at the base of the hair follicle (Thibaut et al., 2009). The hypothesised role of HGT KAPs is summarised in figure 6.2.

Nevertheless, the colocalisation of HGT KAPs with epidermal keratin is an entirely novel finding and requires further work to complete understanding of this apparent interaction. In the first instance, it would be necessary to confirm this observed interaction between HGT

KAPs and epidermal keratin 14, or its binding partner K5. This could be performed using cells transiently transfected with eGFP-KAP using a GFP pull-down assay, for subsequent identification of binding partners. Specific antibody could also be used in order to carry out co-immuno precipitation (Co-IP). Reducing and non-reducing conditions could be employed at this stage in order to determine if the binding relies on di-sulphide bonds or alternate interactions. It would be of particular interest to use this method for determination of the region of epidermal keratin necessary for this interaction. Although previous studies have found the head region of hair-specific keratin is needed for interaction with KAP (Fujikawa et al., 2013; Fujimoto et al., 2014), this interaction between HGT KAP and epidermal keratin may take place in a different region. Additionally, identification of the binding region would allow a search to be made to determine if sequence homology is present with other keratins, specifically keratins which are found to a greater extent within hair. Separately, work could be carried out utilising immuno-staining of whole hair, including the follicle, targeting K14 and HGT KAP in order to determine if these are present in close proximity and may interact within the follicle. Finally, a cell line stably expressing labelled epidermal keratin 14 could be utilised in order to further study the dynamics of this interaction. This could serve to determine if binding by HGT KAP alters the dynamics of epidermal keratin filaments, in addition to confirming that HGT KAP is indeed in flux on and off the filament. This area of work would aim to better characterise the roles of HGT KAPs which appear to be distinct from those of HS and UHS KAPs.

6.2.2. <u>KAP localisation to actin structures in HaCaTs</u>

The localisation of KAP17.1 to actin structures was confirmed through staining with phalloidin in this study. There is no previously proposed role for KAPs to interact with actin, and in fact little work exists with relevance to actin's role in hair, due to the prevalence of keratin (Furumura and Ishikawa, 1996; Vermorken et al., 1981). However, it is logical that there may be a need for cross-linking of the KAP-keratin network of hair with the actin network, in order to produce a stable fibre. Further work in this area should begin initially by identifying the interacting protein to which KAP17.1 localises. This may be actin or an actin-binding protein and could be determined through the use of GFP pull-down on HaCaT cells transiently transfected with eGFP-KAP17.1. Furthermore, the effect of anti-actin drugs upon cells transiently transfected with eGFP-KAP17.1 could be observed, with regard to their effect on KAP17.1 localisation. Similar to future work with epidermal keratin, a cell line stably expressing fluorescently-labelled actin would allow study of the dynamics of actin with and

without KAP17.1 binding, to determine if KAP alters actin dynamics. Findings here are important to understand the role of KAP17.1 in binding actin structures, which may be important for the rigid structure of the hair cuticle.
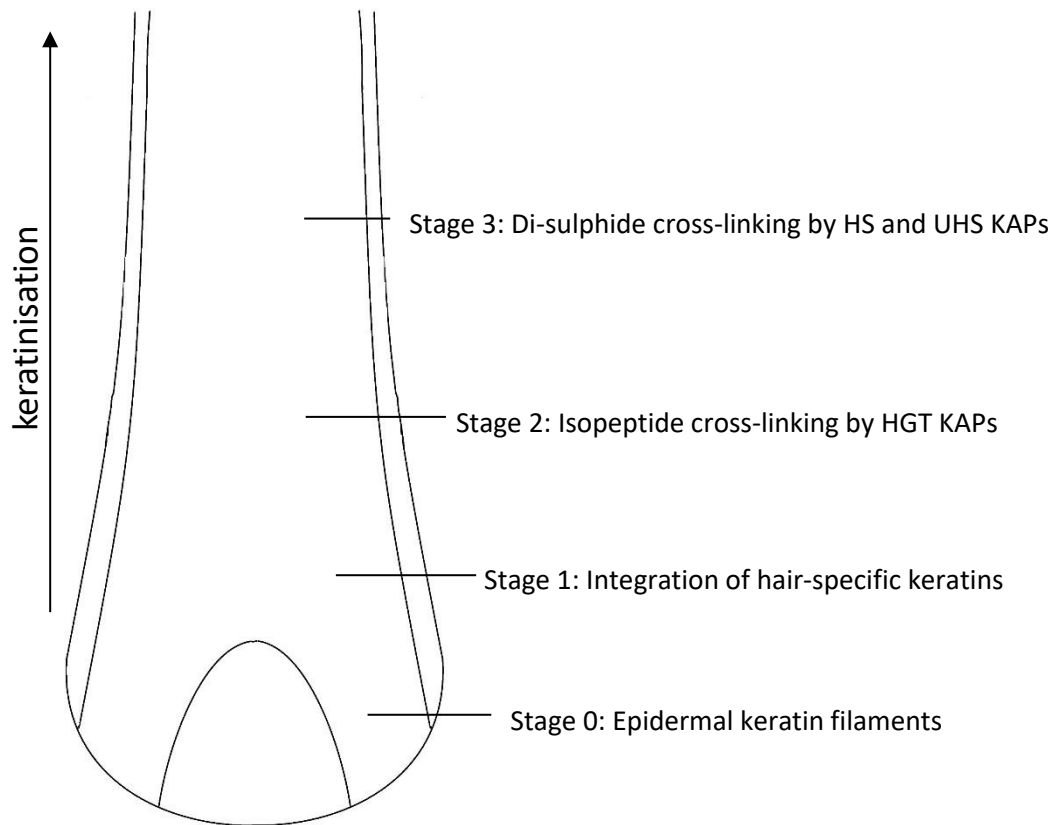
Figure 6.2: Hypothesised roles for KAPs during the stages of keratinisation. *Schematic detailing the hypothesised processes which occur during keratinisation. Stage 0: Cells contain epidermal keratin only. Stage 1: Expression of hair-specific keratins which are able to integrate into epidermal keratin filaments. Stage 2: Expression of primarily HGT KAPs which stabilize the fibre without the need for di-sulphide cross-linking. Stage 3: Expression of primarily HS and UHS KAPs which form di-sulphide cross-links with cytoskeletal components* (Bornschlögl et al., 2016; Matsunaga et al., 2013)*.*

6.2.3. Localisation of KAPs to cell-cell junctions

Significantly, the localisation of certain KAPs, particularly eGFP-KAP7.1, to punctae at the cell periphery was described during this study. This localisation of KAPs has not been described previously in the literature. However, earlier work by Matsunaga et al. may be of relevance to this finding, as HGT KAP8.1 binding to desmoplakin was demonstrated in a cell-free environment (Matsunaga et al., 2013). Therefore, work in this study serves to further the hypothesis that certain KAPs may possess a role for binding and stabilising the interaction of keratin with cell adhesion proteins. There logically exists a role for KAPs with this purpose, in order to ensure that connections between individual hair cells and the CMC, hypothesised to be a desmosomal remnant (Alibardi et al., 2013), are stable. In the first instance, continuation of this work would involve confirmation that KAP is indeed localising to a cell adhesion protein such as desmoplakin. This could be confirmed through antibody staining with an alternate antibody to that used during this study. Future work could confirm direct interaction through biochemical methods such as co-IP or GFP pull down in order to further understand KAP roles in binding of cell-adhesion proteins.

6.2.4. Granule formation by HS and UHS KAPs

Granules, seen in HaCaTs transfected with HS and may indicate self-interaction. Self-interaction of KAPs has been demonstrated in previous literature (Fujikawa et al., 2012; Fujimoto et al., 2014) and could be an intended function of these proteins, producing greater numbers of cross-links within the fibre and providing added stabilisation (figure 6.2). Further work here would aim to demonstrate self-interaction through co-IP of differentially tagged KAP monomers to determine if dimer formation was observed. Additionally, this work could be performed in reducing and non-reducing conditions in order to discover if this interaction requires the formation of disulphide bonds. As the granule-forming KAPs contain high proportions of cysteine, there is significant likelihood that di-sulphide bonds may stabilise this interaction. Work here may uncover if a number of KAPs, particularly those with high amounts of the amino acid cysteine, do indeed possess a means to self-interact as suggested in earlier literature.

6.2.5. The behaviour of hair-specific keratins in HaCaTs

Previously undescribed in the literature, hair-specific keratins were able to integrate into existing epidermal keratin filaments. This may suggest that during early fibre production, hair-specific keratins expressed may continue to build upon keratin networks established by

epidermal keratin (figure 6.2). Of interest during this work was the localisation of hair-specific keratins to the base of the cell preferentially. The epidermal keratins K5 and K14 are thought to be the primary keratins expressed within HaCaTs (Bragulla and Homberger, 2009), therefore these are likely to be distributed equally from cell base to apex. Antibody labelling revealed a gradient in K14 which was likely due to disruption of antibody binding by hair-specific keratin. A cell line stably-transfected with fluorescently-labelled K14, as discussed earlier, could be used in the future to determine if K14 is indeed distributed equally throughout the cell while hair-specific keratin localises towards the base. Nevertheless, localisation of hair-specific keratin could suggest that these populations of keratin fibres within the cell are functionally distinct or differ in their properties. In the first instance, a pull-down assay targeting hair-specific keratin or the conjugated fluorophore mCherry could be utilised to determine the possibly interactions responsible for this localisation. This localisation of hair-specific keratins K82 and K85 could indicate specific binding sites and therefore roles in the hair fibre.

6.2.6. The co-transfection of KAPs and hair-specific keratin

Work in chapter 4 subsequently characterised the behaviours of select KAPs when expressed alongside hair-specific keratin. The behaviour of KAP7.1, when expressed alongside hair-specific keratin suggested preferential colocalisation of this KAP to hair-specific keratin over that previously seen epidermal keratin. Further work here could include a similar experiment with the inclusion of epidermal keratin labelling with a distinct fluorophore. Observation of epidermal keratin filaments at the apex of these cells which are undecorated by eGFP-KAP7.1 would further develop the hypothesis that KAP7.1 is preferentially localising to hair-specific keratin. Indeed, biochemical methods could also be applied here to, in the first instance, confirm that interactions are taking place between KAP7.1 and both epidermal and hair-specific keratins. This could be completed through the use of co-IP. Affinities of KAP could also be elucidated through the use of alternate methods such as isothermal titration calorimetry, in order to determine if the nature of interaction is distinct between epidermal and hair-specific keratins. This work could further inform on the specific role in hair of KAP7.1 and possibly the entire repertoire of HGT KAPs studied.

Striking results were also obtained through the co-expression of KAP11.1 with hair-specific keratins suggesting that HS KAP11.1, which formed granules when expressed in the presence of epidermal keratin only, may interact directly with hair specific keratins within the hair. Co-IP, to confirm interactions between KAP11.1 and these hair-specific keratins would be of

interest in future work. Immuno-staining of intact hair could also be employed to determine if KAP11.1 is expressed in close proximity to these keratins, or keratins with substantial sequence homology.

6.2.7. <u>Experimental approach</u>

As discussed during the introduction to chapter 4, the approach used of transiently transfecting HaCaT cells with individual KAPs was used in order to view their behaviour in isolation, rather than in the complex environment of the hair fibre. However, transient transfection under the CMV promoter, as performed here, may cause over-expression artefacts (Goldman et al., 2010). During this study, care was taken to minimise the probability of misattributing these artefacts to genuine localisations of the observed proteins. This was accomplished by observing many cells within transfected populations, expressing transgenic protein to varying degrees which was indicated by their fluorescence intensity. The localisations described within this study were observed in cells exhibiting a wide range of fluorescence intensities. Alternative or additional approaches to further minimise the impact of over-expression in future work could be to use a weak promoter for expression of the transfected gene, or indeed an inducible promoter.

Another possible change could be made to the method of imaging the live cells, whereby the live cell buffer used, described in methods section 2.3, could instead be replaced by phenol red-free media. The live cell buffer was used to remove the background fluorescence of phenol red. However, phenol red-free media may improve the survivability of the cells while also minimising background fluorescence.

Transiently transfected live cells were imaged during this study using the Zeiss 880 with Airyscan. This instrument provides super-resolution imaging with high signal to noise due to an array of hexagonal detectors as discussed in chapter 1. Due to the filamentous nature of the structures being observed during this work, the super-resolution of the Airyscan was necessary to fully resolve these and draw the conclusions here. However, an alternate future approach could involve the use of modalities such as spinning disk microscopy, which minimises the photodamage caused to the live-cells (Goldman et al., 2010).

FRAP was applied here to allow visualisation of fluorescent protein movement within live cells. Observations made were largely qualitative in nature, with images used to describe the flux of protein on and off of localised structures. However, FRAP may also be used more quantitatively to calculate a diffusion coefficient of the fluorescent molecule, as described

by Ellenberg et al. In future work, FRAP measurements could be made in a more controlled manner to allow calculation of this diffusion coefficient (Ellenberg et al., 1997).

Although certain biochemical methods, such as pull-down assays and co-immuno precipitation, have been suggested here as useful methods for further work. There are alternate methods which may also provide useful information on the relationship between KAPs and keratins. For example, previous work by Honda et al. observed the formation of intermediate filaments in vitro through the combination of human hair keratins using electron microscopy (Honda et al., 2014). Cell-free study of this IF formation and subsequent alterations through combination with recombinant or hair-extracted KAPs could provide a wealth of information regarding the interaction of these two protein families. Furthermore the in vitro assembly of hair keratin into hydrogels may be of wider interest due to the increased use of these biomaterials for medical and research applications (Lee et al., 2014; Wang et al., 2015). Therefore, not only could the use of KAPs during this assembly process inform on KAP-keratin interactions, but selective use of KAPs during production could provide hydrogels with desired physical characteristics such as increased stiffness. This is an area of research which the lab aims to explore imminently.

6.2.8. Roles of KAP outside of the hair follicle

KAPs have been shown during this study to display a range of localisations never previously described, these highlight potential interactions with KIFs and other cytoskeletal components likely to be of great importance for the formation of a rigid hair fibre. These results expand significantly on the limited KAP literature published and determination of KAP functions here may be applied translationally for the establishment of future hair treatments and cosmetics. However, although the expression of KAPs is usually low outside of the hair follicle (Wu et al., 2008), recently published work suggests that KAPs may also be important in the biological mechanism of diseases or effects outside of the hair follicle, as will be discussed.

Work by Luckett-Chastain et al. has suggested a role for KAPs in the mechanism of irritant contact dermatitis (ICD) in interleukin-6 (IL-6) deficient mice. Within this work, KAPs were seen to be differentially modulated in IL-6 mice, in comparison to control mice. This suggests a role for KAPs in the mechanism for increased ICD severity in IL-6 deficient mice (Luckett-Chastain et al., 2018). In work also examining mouse skin, Le Vu et al. demonstrated the mechanism of oral ingestion of collagen, or application of collagen derived peptides to

mouse skin keratinocyte and fibroblast co-culture, which is thought to have a beneficial effect on skin. Analysis found upregulation of both KRTAP and KRT genes in both the skin and co-culture, which may provide the mechanism for the beneficial effect of oral ingestion of collagen on skin (Le Vu et al., 2015).

KAPs have also recently been suggested as undertaking a role in the mechanism of cancer proliferation and tissue invasion. Work by Sack et al. found that a number of KAP genes (KRTAPs) were among the top growth-promoting and oncogenes (GO) found in hTERT-immortalized human mammary epithelial cells and able to stimulate proliferation at rates similar to oncogenes like MYC. KRTAP subfamilies found contain GO genes were also shown to be expressed at significantly higher levels in breast carcinoma with in-depth study revealing that upregulation of KRTAP genes in cancer may promote proliferation through upregulation of E2F-mediated DNA replication (Sack et al., 2018). Additionally, Berens et al. found correlation between the mRNA expression of UHS KRTAP5.5 and the degree of endothelial invasion of a murine mammary cancer cell line in vitro. It was suggested that KAP5.5 may be necessary for the stability of keratin filaments in these cells, governing cytoskeletal function and invasion. A positive correlation in human cancers was found between KRTAP5.5 and KRT18 expression, and furthermore, increased KRT18 expression was shown to correlate to lower relapse-free survival. Direct correlation of relapse-free survival and KRTAP5.5 was not possible due to the expression of KRTAP often being below the threshold for detection. It was suggested that KAPs may be regulators of IFs which are kept in low abundance in all epithelial cells outside of the hair follicle. This could be relevant for the binding of keratin by KAPs seen within this study. Alternatively, these cancer cells may rely on a pathway for cytoskeleton maintenance not regularly utilised outside of the hair follicle (Berens et al., 2017).

As discussed, findings within this chapter will be useful for the further study of KAPs in order to fully understand the interactions required to form a stable hair fibre. This understanding may be applied for the development of cosmetics and hair therapeutics. However, importantly, KAPs may also have a much wider reaching role than that of hair fibre formation, and this work greatly increases current understanding of how this large family of proteins may behave outside of the hair follicle. In particular, their ability to interact with proteins other than hair-specific keratin.

6.3. The use of fluorescent compounds during LSCM of human hair

Existing work concerned with the uptake of dyes into natural fibres is largely in relation to wool, rather than human hair (Wortmann et al., 2012). Furthermore, work often utilises commercially available fluorescent dyes rather than compounds likely to come into contact with hair, such as those found in oxidative hair dyes (Hadjur et al., 2002; Pötsch and Moeller, 1996; Ruetsch et al., 2003). This study aimed to use advanced light microscopy techniques to image hair in combination with a range of fluorescent molecules, including compounds found in common hair treatments, and assess their dynamics and route of uptake.

6.3.1. <u>Hair-dyeing compounds for LSCM of hair</u>

Of particular interest when observing the uptake of 2-methylresorcinol was the cuticle-cortex boundary, which appeared to present a substantial barrier for uptake similar to that seen later with Rhodamine B, a dye which moved primarily by intercellular pathways. The requirement for a dye to progress from the cuticle to an outer lipid β-layer, followed by the proteinaceous đ-layer, and subsequently the inner lipid β-layer (Robbins, 2009), before continuing on its path, either inter- or intra- cellularly towards the hair centre does logically present an obstacle. Where dye uptake throughout the hair is desired, such as is the case with oxidative dyeing (Guerra-Tapia and Gonzalez-Guerra, 2014), it is likely that the cuticle-cortex boundary provides the rate limiting step for this process. Therefore, it would be of particular interest in the field of cosmetics to further understand how this barrier function may be reduced or subverted. In order to achieve this, it is likely necessary that further understanding is achieved with regard to the exact step in this process which is rate-limiting. This may be distinct depending on the preferred route of movement for individual dyes. For example, it is likely that lipohilic dyes will move from the cuticle CMC to the outer β-layer of the cuticle-cortex CMC with ease. However, movement into the đ-layer of the cuticle-cortex CMC may be slow. The resolution achievable with conventional light microscopy is unlikely to allow differentiation between CMC layers. Instead, the use of super-resolution techniques such as stimulated emission depletion (STED) microscopy or alternatively transmission electron microscopy with both hydrophilic and lipohilic stains may be employed for this purpose. Furthermore, once the rate-limiting step is identified, treatments which target lipids of the CMC, either covalently or ionically linked, or proteins of the đ-layer, for removal or alteration may be tested for their efficacy in increasing the rate of dye movement across this barrier. It would be desirable to allow greater dye movement across this barrier reversibly, or without altering the macroscopic properties of hair, allowing treatments to be

conducted rapidly without permanent hair damage. Translation of these findings into cosmetic products could be of great interest.

6.3.2. The impact of hydrogen peroxide bleaching on hair permeability

It was shown that bleaching, through treatment with hydrogen peroxide, resulted in increased hair permeability throughout the cortex, but did not appear to increase dye uptake across the cuticle-cortex boundary. This is of relevance to the point previously discussed as it appears bleaching had a large impact on intracellular dye movement, likely due to affecting hair's proteins. This may suggest that, in the case of 2-methylresorcinol, damage to the d-layer of the cuticle-cortex CMC does not increase dye uptake across this boundary. It would be of interest in future work to determine if this was the case for the uptake of Rhodamine B across the cuticle-cortex boundary, where the d-layer may present an obstacle to uptake. Nevertheless, the use of dye uptake to measure damage was highlighted as a useful tool for assessing cortex permeability. Future work here could use this method in combination with an additional, lipophilic dye, such as rhodamine B. Together, findings from the use of typically intracellular and intercellular could advise on changes occurring to each of these regions following various forms of damage. It would also be of interest to see the effect of hydrogen peroxide bleaching on the uptake of Rhodamine B. Intracellular movement of this dye was seen to proceed slowly in untreated hair. However, in hair which possesses a more permeable intracellular region, such as that following bleaching, it is possible that intracellular movement in particular will proceed more rapidly or even become predominant over intercellular movement. Information such as this would be of great interest as it would highlight that knowledge of previous hair treatment is important in estimating the uptake of both dyes during cosmetic treatments and also other compounds such as drugs for the purpose of hair analysis for drug abuse (Kimura et al., 1999).

6.3.3. The use of alkalisers for the uptake of compounds

The use of monoethanol amine was shown to be important in determining the rate of dye uptake, particularly of the intracellular dye 2-methylresorcinol. It is thought that various compounds such as ammonia and monoethanol amine act upon the hair to cause swelling, thereby increasing the uptake of water and other compounds (Robbins, 1988). It is unknown in the case of this study whether the effect of monoethanol amine is due entirely to the increased pH, or if monoethanol amine has an additive effect alongside pH, resulting in further increased swelling and dye uptake. This is unlike the case of ammonia's role in the chemical change detected by FLIM, discussed earlier. In the case of bleaching, small

molecules are likely to easily move into the hair, so swelling has a reduced effect. The effect of ammonia in that case was likely due largely to the increased efficacy of hydrogen peroxide radical generation (Torres et al., 2014). However, in the case of dye uptake swelling, facilitated by monoethanol amine is the primary cause of increased permeability. Work of interest in the future would be to compare the efficacy of two commonly used alkalisers in hair products, monoethanol and ammonia for increased dye uptake into hair. This could be undertaken using methods similar to those used here and would provide insights into the preferred agent for increasing uptake of compounds during treatment. It may indeed be the case that all compounds do not react similarly to increased alkaliser. Therefore, experimentation comparing the effect of alkaline conditions upon rhodamine B uptake would also be of use, in order to determine if swelling has the largest impact in the intra- or inter- cellular regions. Understanding here could be applied to hair chemistries to improve their efficacy.

6.3.4. <u>Rhodamine B uptake into the hair fibre</u>

Rhodamine B was shown as discussed to move primarily via the intercellular route, finally moving into cortical cells in a second stage. This was observed in high resolution and imaged dynamically, which has not been observed in previous literature, confirming the hypothesis of 2-stage dye movement (Brady, 1992). This study has used dyes which move primarily by both intercellular and intracellular pathways, which as discussed is likely correlated to both their size, suggested by their molecular weight, and also their lipophilicity, indicated by the partition coefficient or LogP. It would be of interest to apply techniques used here to a wide range of fluorescent compounds to determine the degree to which movement is predictable based upon size and lipophilicity. Completion of this could allow modelling of compound movement which is not typically observable through the use of fluorescence, and aid in developing the composition of products to be used with hair.

A particularly interesting observation from FRAP of rhodamine B was that movement into the photobleached region occurred at a rate much more rapid than that of original dye uptake. Although FRAP prevents fluorescence of molecules bleached, they are still present within the photobleached region. It is therefore possible that rhodamine B presence within the hair alters the dynamics for further uptake. One way to confirm if subsequent uptake would be affected by rhodamine B presence would be to undertake staining with another dye immediately following rhodamine B staining, this dye would require fluorescence characteristics distinct from rhodamine B. Uptake quantified with and without the presence

of rhodamine would suggest whether dynamics of uptake are indeed altered. This could also be repeated with both intercellular and intracellular secondary dyes, to determine if rhodamine B alters movements exclusively in one region of the hair.

6.3.5. <u>The use of the VID for imaging hair fibres</u>

Finally, throughout work in chapter 5 the VID was demonstrated as a means of achieving high throughput imaging of the transverse cross section of hair with minimal sample preparation. Furthermore, images were achievable using this that were not possible with sections prepared normally, through the use of a microtome. For example, FRAP is certainly less representative of true dye movement when observing this in a 1 μm section, while the VID allows FRAP to be performed at an optical section several microns into a fibre which is substantially more intact. Additionally, the use of the VID avoids the presence of both physical artefacts, such as damage to the cuticle, in addition to chemical changes, such as fluorescent dye loss during the embedding and sectioning process. Therefore, the VID substantially broadens the options of hair imaging, particularly in combination with fluorescent dyes and the observation of dynamic dye movement. Much of the further work discussed here would utilise the VID and specifically the VID could also be used for FRAP of hair containing a wide range of compounds following uptake to further characterise the movement that takes place in real time.
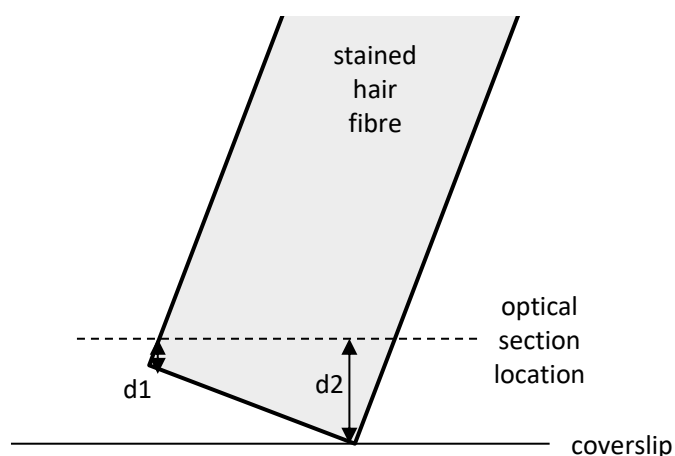

Figure 6.3: Fluorescence intensity and image depth using the VID. An exaggerated example of how imaging depth across the fibre may vary due to the hair approaching the coverslip at an angle when using the VID. Depths d1 and d2 result in varying fluorescence intensity across the image.

However, an issue with imaging using the VID became apparent during this work. The cut performed on hair to be imaged, carried out with a razor blade, may result in damage to the fibre end. This damage is often only visible directly at the cover slip and so optically sectioning several microns into the sample eliminates artefacts. This is similarly the case where the fibre transverse section does not sit flat against the cover glass, and optical sectioning is required to image the entire cross-section as illustrated in figure 6.3. In the case of Rhodamine B, the fluorescence intensity decreases dramatically with depth into the fibre from the cut end. Therefore, discrepancies in fluorescence intensity across the image are clearly visible when using this technique (figure 5.13). The conclusions drawn within this work are not dependent on the fluorescence intensity, and are valid despite this phenomenon. However, for the calculation of diffusion quantitatively it would be necessary to overcome this. This could be accomplished through the use of alternative cutting techniques which produce fewer artefacts, or indeed by traditional embedding and sectioning in order to normalise the imaging depth between samples.

Work within this area has significantly furthered the understanding of how dyes with different chemical properties may be taken up into hair. Additionally, findings have identified specific regions of hair which may be of interest for intervention with regard to improving dye uptake. This work has been completed using state of the art light microscopy techniques which are novel to the field of hair.

6.4. Conclusion

This work has focused upon the study of hair and its keratin-associated proteins through the use of advanced light microscopy not previously applied to these areas.

The use of single-photon FLIM, never previously utilised for the imaging of hair, was shown to detect regions of differing chemical composition within untreated hair fibres, with a potential use in the future for correlation with macroscopic hair characteristics. Of perhaps greater interest was the ability of FLIM to detect the degree of chemical change following hydrogen peroxide bleaching with increasing severity. Due to the constant average lifetime of untreated hair, FLIM therefore may serve as a useful means of determining the degree of hair damage, without the need for untreated fibre controls. Furthermore, this metric can be obtained rapidly, without destruction of the sample, and can provide spatial information with regard to chemical change.

FLIM was found to be sensitive to chemical change following oxidative damage specifically, resulting from either hydrogen peroxide bleaching or from photooxidation. The cause of increased average lifetime following oxidative damage was identified, through the use of full-FLIM, as an increase in fluorescence from a distinct high-lifetime component of hair which was correlated to the increase of L-kynurenine concentration. It is therefore hypothesised that FLIM is sensitive to changes in the concentrations of a number of fluorescent tryptophan oxidation products which are produced by hydrogen peroxide bleaching and by photooxidation (Daly et al., 2009; Grosvenor et al., 2010).

Advanced light microscopy techniques were also applied to a depth not previously explored for the observation of hair in combination with fluorescent dyes. Compounds with relevance to hair were shown to vary in their fibre uptake characteristics due to their size and lipophilicity. Uptake of these compounds was observed through both intracellular and intercellular pathways with high spatial resolution.

Of particular interest was the observation of a rate-limiting barrier in the hair at the cuticle-cortex boundary, which appeared to slow uptake of dyes which move by either the intracellular or intercellular pathways. This barrier is a likely candidate for further study and alteration of the barrier function here could have significant impact on the efficacy of hair treatments.

The utility of fluorescent dyes for study of the permeability of hair following damage was demonstrated. Hydrogen peroxide bleaching was shown to result in decreased hair barrier function with relation to dye which moves intracellularly, allowing insights to be made with regard to the nature of damage.

Furthermore, a novel device, termed the VID, was demonstrated which allows high-throughput imaging of hair's transverse cross-section. This method eliminates artefacts associated with typical sample preparation and allows dynamic imaging of dye movement through the transverse cross section. This device was used to dynamically image the 2-stage uptake of rhodamine B into the hair fibre cortex for the first time.

Two-dimensional SDS-PAGE was carried out to supplement advanced light microscopy findings and revealed that keratin-associated proteins were also seen to be adversely affected by hydrogen peroxide bleaching. The specific roles of these proteins in creating a rigid hair fibre are poorly understood. Functional characterisation of a wide selection of

KAPs, never studied before in such depth, revealed a variety of potential interactions possible between KAPs and cytoskeletal components.

Distinct KAPs were shown in particular to localise to both epidermal keratin and actin structures within HaCaTs to differing degrees, localisations which have not been described previously in the literature. These localisations suggest distinct roles for KAPs within the hair follicle during fibre production and potentially elsewhere, outside the hair follicle.

Hair-specific keratins were also characterised, and were shown to integrate with existing epidermal keratin filaments while showing a preference for the base of the cell. Integration suggests that hair-specific keratin may continue to build upon epidermal keratin filaments during hair fibre keratinisation. KAPs were also observed in combination with these hair-specific keratins and were shown to behave differentially in their presence, furthering the understanding of individual interactions which may take place with the hair fibre.

The further study of KAPs may be translated for application into the fields of cosmetics, for alteration of specific KAP-keratin or KAP-KAP interactions for desired effects. Additionally, it was discussed how the study of KAPs may be important in diseases unrelated to hair such as skin conditions (Luckett-Chastain et al., 2018) and cancer (Berens et al., 2017; Sack et al., 2018). Finally, understanding of how KAPs influence KIF formation in vitro may also be of importance in the production of keratin-based biomaterials, for the use of medical and research applications (Lee et al., 2014).

7. Bibliography

Ahn, H.J., Lee, W.-S., 2002. An ultrastuctural study of hair fiber damage and restoration following treatment with permanent hair dye. Int. J. Dermatol. 41, 88–92.

Albani, J.R., 2014. Origin of tryptophan fluorescence lifetimes. Part 2: fluorescence lifetimes origin of tryptophan in proteins. J. Fluoresc. 24, 105–117.

Alibardi, L., 2017. Ultrastructural localization of hair keratins, high sulfur keratin-associated proteins and sulfhydryl oxidase in the human hair. Anat. Sci. Int. 92, 248–261.

Alibardi, L., 2009. Embryonic keratinization in vertebrates in relation to land colonization. Acta Zool. 90, 1–17.

Alibardi, L., Dalla Valle, L., Nardi, A., Toni, M., 2009. Evolution of hard proteins in the sauropsid integument in relation to the cornification of skin derivatives in amniotes. J. Anat. 214, 560–586.

Alibardi, L., Tsuchiya, M., Watanabe, S., Nöcker, B., 2013. Ultrastructural localization of desmoglein and plakophilin in the human hair suggests that the cell membrane complex is a long desmosomal remnant. Acta Histochem. 115, 879–886.

Almeida, F.V., Walko, G., McMillan, J.R., McGrath, J.A., Wiche, G., Barber, A.H., Connelly, J.T., 2015. The cytolinker plectin regulates nuclear mechanotransduction in keratinocytes. J. Cell Sci. 128, 4475–4486.

Axelrod, D., Koppel, D.E., Schlessinger, J., Elson, E., Webb, W.W., 1976. Mobility measurement by analysis of fluorescence photobleaching recovery kinetics. Biophys. J. 16, 1055–1069.

Bailey, A.D., Zhang, G., Murphy, B.P., 2014. Comparison of damage to human hair fibers caused by monoethanolamine- and ammonia-based hair colorants. J. Cosmet. Sci. 65, 1–9.

Bazzi, H., Christiano, A.M., 2007. Broken hearts, woolly hair, and tattered skin: when desmosomal adhesion goes awry. Curr. Opin. Cell Biol. 19, 515–520.

Becker, W., 2012. Fluorescence lifetime imaging--techniques and applications. J. Microsc. 247, 119–136.

Berens, E.B., Sharif, G.M., Schmidt, M.O., Yan, G., Shuptrine, C.W., Weiner, L.M., Glasgow, E., Riegel, A.T., Wellstein, A., 2017. Keratin-associated protein 5-5 controls cytoskeletal function and cancer cell vascular invasion. Oncogene 36, 593–605.

Bhushan, B., 2010. Biophysics of Human Hair: Structural, Nanomechanical, and Nanotribological Studies, Biological and Medical Physics, Biomedical Engineering. Springer-Verlag, Berlin Heidelberg.

Bhushan, B., Chen, N., 2006. AFM studies of environmental effects on nanomechanical properties and cellular structure of human hair. Ultramicroscopy 106, 755–764.

Birbeck, M.S.C., Mercer, E.H., 1957. THE ELECTRON MICROSCOPY OF THE HUMAN HAIR FOLLICLE. J. Biophys. Biochem. Cytol. 3, 203–214.

Bolduc, C., Shapiro, J., 2001. Hair care products: waving, straightening, conditioning, and coloring. Clin. Dermatol. 19, 431–436.

Bornschlögl, T., Bildstein, L., Thibaut, S., Santoprete, R., Fiat, F., Luengo, G.S., Doucet, J., Bernard, B.A., Baghdadli, N., 2016. Keratin network modifications lead to the mechanical stiffening of the hair follicle fiber. Proc. Natl. Acad. Sci. U. S. A. 113, 5940–5945.

Bowden, P.E., Quinlan, R.A., Breitkreutz, D., Fusenig, N.E., 1984. Proteolytic modification of acidic and basic keratins during terminal differentiation of mouse and human epidermis. Eur. J. Biochem. 142, 29–36.

Bradbury, J.H., O'shea, J.M., 1969. Keratin Fibres II. Separation and Analysis of Medullary Cells. Aust. J. Biol. Sci. 22, 1205–1216.

Brady, P.R., 1992. Diffusion of dyes in natural fibres. Rev. Prog. Color. Relat. Top. 22, 58–78.

Bragulla, H.H., Homberger, D.G., 2009. Structure and functions of keratin proteins in simple, stratified, keratinized and cornified epithelia. J. Anat. 214, 516–559.

Bringans, S.D., Plowman, J.E., Dyer, J.M., Clerens, S., Vernon, J.A., Bryson, W.G., 2007. Characterization of the exocuticle a-layer proteins of wool. Exp. Dermatol. 16, 951–960.

Brown, K.C., Pohl, S., Kezer, A.E., Cohen, D., 1985. Oxidative dyeing of keratin fibers. J. Soc. Cosmet. Chem. 36, 31–37.

Cabanillas, B., Novak, N., 2016. Atopic dermatitis and filaggrin. Curr. Opin. Immunol., Allergy and hypersensitivity * Host pathogens 42, 1–8.

Carragher, N.O., Frame, M.C., 2004. Focal adhesion and actin dynamics: a place where kinases and proteases meet to promote invasion. Trends Cell Biol. 14, 241–249.

Castañón, M.J., Walko, G., Winter, L., Wiche, G., 2013. Plectin–intermediate filament partnership in skin, skeletal muscle, and peripheral nerve. Histochem. Cell Biol. 140, 33–53.

Choi, H.-J., Park-Snyder, S., Pascoe, L.T., Green, K.J., Weis, W.I., 2002. Structures of two intermediate filament-binding fragments of desmoplakin reveal a unique repeat motif structure. Nat. Struct. Biol. 9, 612–620.

Choi, W.J., Pi, L.-Q., Min, G., Lee, W.-S., Lee, B.H., 2012. Qualitative investigation of fresh human scalp hair with full-field optical coherence tomography. J. Biomed. Opt. 17, 036010.

Chou, C.-C., Buehler, M.J., 2012. Structure and Mechanical Properties of Human Trichocyte Keratin Intermediate Filament Protein. Biomacromolecules 13, 3522–3532.

Clement, J.L., Hagege, R., Le Pareux, A., Connet, J., Gastaldi, G., 1981. New concepts about hair identification revealed by electron microscope studies. J. Forensic Sci. 26, 447–458.

Cooper, G.M., 2000. The Cell, 2nd ed. Sinauer Associates.

Corbett, J.F., 1998. Hair Colorants: Chemistry and Toxicology. Micelle Press.

Crewther, W.G., Dowling, L.M., Steinert, P.M., Parry, D.A.D., 1983. Structure of intermediate filaments. Int. J. Biol. Macromol. 5, 267–274.

Daly, S., Bianchini, R., Polefka, T., Jumbelic, L., Jachowicz, J., 2009. Fluorescence and coloration of grey hair. Int. J. Cosmet. Sci. 31, 347–359.

Dario, M.F., Freire, T.B., Pinto, C.A.S. de O., Prado, M.S.A., Baby, A.R., Velasco, M.V.R., 2017. Tryptophan and kynurenine determination in human hair by liquid chromatography. J. Chromatogr. B Analyt. Technol. Biomed. Life. Sci. 1065–1066, 59–62.

Davies, M.J., 2016. Protein oxidation and peroxidation. Biochem. J. 473, 805–825.

Dawber, R., 1996. Hair: Its structure and response to cosmetic preparations. Clin. Dermatol. 14, 105–112.

de Cássia Comis Wagner, R., Kiyohara, P.K., Silveira, M., Joekes, I., 2007. Electron microscopic observations of human hair medulla. J. Microsc. 226, 54–63.

DeLauder, S.F., Kidwell, D.A., 2000. The incorporation of dyes into hair as a model for drug binding. Forensic Sci. Int. 107, 93–104.

Delva, E., Tucker, D.K., Kowalczyk, A.P., 2009. The desmosome. Cold Spring Harb. Perspect. Biol. 1, a002543.

Dimitrow, E., Riemann, I., Ehlers, A., Koehler, M.J., Norgauer, J., Elsner, P., König, K., Kaatz, M., 2009. Spectral fluorescence lifetime detection and selective melanin imaging by multiphoton laser tomography for melanoma diagnosis. Exp. Dermatol. 18, 509–515.

Dominguez, R., Holmes, K.C., 2011. Actin structure and function. Annu. Rev. Biophys. 40, 169–186.

Dyer, J.M., Cornellison, C.D., Grosvenor, A.J., Clerens, S., Deb-Choudhury, S., 2014. Molecular marker approaches for tracking redox damage and protection in keratins. J. Cosmet. Sci. 65, 25–36.

Dyer, J.M., Plowman, J.E., Krsinic, G.L., Deb-Choudhury, S., Koehn, H., Millington, K.R., Clerens, S., 2010. Proteomic evaluation and location of UVB-induced photo-oxidation in wool. J. Photochem. Photobiol. B 98, 118–127.

Ehlers, A., Riemann, I., Anhut, T., Kaatz, M., Elsner, P., König, K., 2006. Fluorescence lifetime imaging of human skin and hair. Multiphoton Microsc. Biomed. Sci. VI 60890N-60890N–10.

Ehlers, A., Riemann, I., Stark, M., König, K., 2007. Multiphoton fluorescence lifetime imaging of human hair. Microsc. Res. Tech. 70, 154–161.

Ellenberg, J., Siggia, E.D., Moreira, J.E., Smith, C.L., Presley, J.F., Worman, H.J., Lippincott-Schwartz, J., 1997. Nuclear Membrane Dynamics and Reassembly in Living Cells:

Targeting of an Inner Nuclear Membrane Protein in Interphase and Mitosis. J. Cell Biol. 138, 1193–1206.

Er Rafik, M., Doucet, J., Briki, F., 2004. The intermediate filament architecture as determined by X-ray diffraction modeling of hard alpha-keratin. Biophys. J. 86, 3893–3904.

Fedorkova, M.V., Smolina, N.V., Mikhalchik, E.V., Balabushevich, N.G., Ibragimova, G.A., Gadzhigoroeva, A.G., Dmitrieva, E.I., Dobretsov, G.E., 2014. Effects of ultra violet radiation on the soluble proteins of human hair. J. Photochem. Photobiol. B 140, 390–395.

Fischer, H., Szabo, S., Scherz, J., Jaeger, K., Rossiter, H., Buchberger, M., Ghannadan, M., Hermann, M., Theussl, H.-C., Tobin, D.J., Wagner, E.F., Tschachler, E., Eckhart, L., 2011. Essential role of the keratinocyte-specific endonuclease DNase1L2 in the removal of nuclear DNA from hair and nails. J. Invest. Dermatol. 131, 1208–1215.

Formanek, F., DE Wilde, Y., Luengo, G.S., Querleux, B., 2006. Investigation of dyed human hair fibres using apertureless near-field scanning optical microscopy. J. Microsc. 224, 197–202.

Fraser, R.D.B., Parry, D.A.D., 2007. Structural changes in the trichocyte intermediate filaments accompanying the transition from the reduced to the oxidized form. J. Struct. Biol. 159, 36–45.

Fuchs, E., Yang, Y., 1999. Crossroads on cytoskeletal highways. Cell 98, 547–550.

Fujii, T., Takayama, S., Ito, Y., 2013. A novel purification procedure for keratin-associated proteins and keratin from human hair.

Fujikawa, H., Fujimoto, A., Farooq, M., Ito, M., Shimomura, Y., 2013. Characterization of the human hair shaft cuticle-specific keratin-associated protein 10 family. J. Invest. Dermatol. 133, 2780–2782.

Fujikawa, H., Fujimoto, A., Farooq, M., Ito, M., Shimomura, Y., 2012. Characterization of the Human Hair Keratin–Associated Protein 2 (KRTAP2) Gene Family. J. Invest. Dermatol. 132, 1806–1813.

Fujimoto, S., Takase, T., Kadono, N., Maekubo, K., Hirai, Y., 2014. Krtap11-1, a hair keratin-associated protein, as a possible crucial element for the physical properties of hair shafts. J. Dermatol. Sci. 74, 39–47.

Furumura, M., Ishikawa, H., 1996. Actin bundles in human hair follicles as revealed by confocal laser microscopy. Cell Tissue Res. 283, 425–434.

Ghiani, S., Baroni, S., Burgio, D., Digilio, G., Fukuhara, M., Martino, P., Monda, K., Nervi, C., Kiyomine, A., Aime, S., 2008. Characterization of human hair melanin and its degradation products by means of magnetic resonance techniques. Magn. Reson. Chem. MRC 46, 471–479.

Giesen, M., Gruedl, S., Holtkoetter, O., Fuhrmann, G., Koerner, A., Petersohn, D., 2011. Ageing processes influence keratin and KAP expression in human hair follicles. Exp. Dermatol. 20, 759–761.

Goldman, R.D., Swedlow, J., Spector, D.L., 2010. Live Cell Imaging: A Laboratory Manual. Cold Spring Harbor Laboratory Press.

Gong, H., Zhou, H., McKenzie, G.W., Yu, Z., Clerens, S., Dyer, J.M., Plowman, J.E., Wright, M.W., Arora, R., Bawden, C.S., Chen, Y., Li, J., Hickford, J.G.H., 2012. An Updated Nomenclature for Keratin-Associated Proteins (KAPs). Int. J. Biol. Sci. 8, 258–264.

Greenspan, P., Mayer, E.P., Fowler, S.D., 1985. Nile red: a selective fluorescent stain for intracellular lipid droplets. J. Cell Biol. 100, 965–973.

Grosvenor, A.J., Morton, J.D., Dyer, J.M., 2010. Profiling of residue-level photo-oxidative damage in peptides. Amino Acids 39, 285–296.

Guerra-Tapia, A., Gonzalez-Guerra, E., 2014. Hair Cosmetics: Dyes. Actas Dermo-Sifiliográficas Engl. Ed. 105, 833–839.

Gummer, C.L., 2001. Elucidating penetration pathways into the hair fiber using novel microscopic techniques. J. Cosmet. Sci. 52, 265–280.

Gurden, S.P., Monteiro, V.F., Longo, E., Ferreira, M.M.C., 2004. Quantitative analysis and classification of AFM images of human hair. J. Microsc. 215, 13–23.

Hadjur, C., Daty, G., Madry, G., Corcuff, P., 2002. Cosmetic assessment of the human hair by confocal microscopy. Scanning 24, 59–64.

Haines, R.L., Lane, E.B., 2012. Keratins and disease at a glance. J. Cell Sci. 125, 3923–3928.

Harland, D.P., Plowman, J.E., 2018. Development of Hair Fibres, in: Plowman, J.E., Harland, D.P., Deb-Choudhury, S. (Eds.), The Hair Fibre: Proteins, Structure and Development, Advances in Experimental Medicine and Biology. Springer Singapore, Singapore, pp. 109–154.

Harland, D.P., Walls, R.J., Vernon, J.A., Dyer, J.M., Woods, J.L., Bell, F., 2014. Three-dimensional architecture of macrofibrils in the human scalp hair cortex. J. Struct. Biol. 185, 397–404.

Harrison, S., Sinclair, R., 2003. Hair colouring, permanent styling and hair structure. J. Cosmet. Dermatol. 2, 180–185.

Hartsock, A., Nelson, W.J., 2008. Adherens and Tight Junctions: Structure, Function and Connections to the Actin Cytoskeleton. Biochim. Biophys. Acta 1778, 660–669.

Higgins, C.A., Westgate, G.E., Jahoda, C.A.B., 2009. From telogen to exogen: mechanisms underlying formation and subsequent loss of the hair club fiber. J. Invest. Dermatol. 129, 2100–2108.

Holzinger, A., 2009. Jasplakinolide: an actin-specific reagent that promotes actin polymerization. Methods Mol. Biol. Clifton NJ 586, 71–87.

Honda, Y., Koike, K., Kubo, Y., Masuko, S., Arakawa, Y., Ando, S., 2014. In vitro assembly properties of human type I and II hair keratins. Cell Struct. Funct. 39, 31–43.

Hoting, E., Zimmermann, M., Hilterhaus-bong, S., 1995. Photochemical alterations in human hair. I. Artificial irradiation and investigations of hair proteins. J Soc Cosmet Chem 46, 85–99.

Huang, B., Bates, M., Zhuang, X., 2009. Super resolution fluorescence microscopy. Annu. Rev. Biochem. 78, 993–1016.

Huff, J., 2015. The Airyscan detector from ZEISS: confocal imaging with improved signal-to-noise ratio and super-resolution [WWW Document]. Nat. Methods.

Hughes, A.L., 1999. Adaptive Evolution of Genes and Genomes. Oxford University Press.

Imai, T., 2011. The influence of hair bleach on the ultrastructure of human hair with special reference to hair damage. Okajimas Folia Anat. Jpn. 88, 1–9.

Inoue, T., Iwamoto, Y., Ohta, N., Inoue, K., Yagi, N., 2007. Structural analysis of the cell membrane complex in the human hair cuticle using microbeam X-ray diffraction: relationship with the effects of hair dyeing. J. Cosmet. Sci. 58, 11–17.

Ito, S., Wakamatsu, K., 2011. Diversity of human hair pigmentation as studied by chemical analysis of eumelanin and pheomelanin: Human hair pigmentation. J. Eur. Acad. Dermatol. Venereol. 25, 1369–1380.

Jachowicz, J., McMullen, R.L., 2011. Tryptophan fluorescence in hair—Examination of contributing factors. J. Cosmet. Sci. 62, 291.

Jenkins, B.J., Powell, B.C., 1994. Differential expression of genes encoding a cysteine-rich keratin family in the hair cuticle. J. Invest. Dermatol. 103, 310–317.

Jones, L.N., 2001. Hair structure anatomy and comparative anatomy. Clin. Dermatol. 19, 95–103.

Jones, L.N., Rivett, D.E., 1997. The role of 18-methyleicosanoic acid in the structure and formation of mammalian hair fibres. Micron 28, 469–485.

Joo, K.-M., Kim, A.-R., Kim, S.-N., Kim, B.-M., Lee, H.K., Bae, S., Lee, J.-H., Lim, K.-M., 2016. Metabolomic analysis of amino acids and lipids in human hair altered by dyeing, perming and bleaching. Exp. Dermatol. 25, 729–731.

Kadir, M., Wang, X., Zhu, B., Liu, J., Harland, D., Popescu, C., 2017. The structure of the "amorphous" matrix of keratins. J. Struct. Biol. 198, 116–123.

Kaliyadan, F., Gosai, B.B., Al Melhim, W.N., Feroze, K., Qureshi, H.A., Ibrahim, S., Kuruvilla, J., 2016. Scanning Electron Microscopy Study of Hair Shaft Damage Secondary to Cosmetic Treatments of the Hair. Int. J. Trichology 8, 94–98.

Kariya, N., Shimomura, Y., Ito, M., 2005. Size polymorphisms in the human ultrahigh sulfur hair keratin-associated protein 4, KAP4, gene family. J. Invest. Dermatol. 124, 1111–1118. https://doi.org/10.1111/j.0022-202X.2005.23662.x

Kelch, A., Wessel, S., Will, T., Hintze, U., Wepf, R., Wiesendanger, R., 2000. Penetration pathways of fluorescent dyes in human hair fibres investigated by scanning near-field optical microscopy. J. Microsc. 200, 179–186.

Kerwin, B.A., Remmele, R.L., 2007. Protect from Light: Photodegradation and Protein Biologics. J. Pharm. Sci. 96, 1468–1479.

Khan, I., Maldonado, E., Vasconcelos, V., O'Brien, S.J., Johnson, W.E., Antunes, A., 2014. Mammalian keratin associated proteins (KRTAPs) subgenomes: disentangling hair diversity and adaptation to terrestrial and aquatic environments. BMC Genomics 15, 779.

Kimura, H., Mukaida, M., Mori, A., 1999. Detection of stimulants in hair by laser microscopy. J. Anal. Toxicol. 23, 577–580.

Kolsch, A., Windoffer, R., Wurflinger, T., Aach, T., Leube, R.E., 2010. The keratin-filament cycle of assembly and disassembly. J. Cell Sci. 123, 2266–2272.

Laatsch, C.N., Durbin-Johnson, B.P., Rocke, D.M., Mukwana, S., Newland, A.B., Flagler, M.J., Davis, M.G., Eigenheer, R.A., Phinney, B.S., Rice, R.H., 2014. Human hair shaft proteomic profiling: individual differences, site specificity and cuticle analysis. PeerJ 2.

Lagarde, J.M., Peyre, P., Redoules, D., Black, D., Briot, M., Gall, Y., 1994. Confocal microscopy of hair. Cell Biol. Toxicol. 10, 301–304.

Langbein, L., Rogers, M.A., Winter, H., Praetzel, S., Beckhaus, U., Rackwitz, H.-R., Schweizer, J., 1999. The Catalog of Human Hair Keratins I. EXPRESSION OF THE NINE TYPE I MEMBERS IN THE HAIR FOLLICLE. J. Biol. Chem. 274, 19874–19884.

Langbein, L., Rogers, M.A., Winter, H., Praetzel, S., Schweizer, J., 2001. The Catalog of Human Hair Keratins II. EXPRESSION OF THE SIX TYPE II MEMBERS IN THE HAIR FOLLICLE AND THE COMBINED CATALOG OF HUMAN TYPE I AND II KERATINS. J. Biol. Chem. 276, 35123–35132.

Langbein, L., Schweizer, J., 2005. Keratins of the human hair follicle. Int. Rev. Cytol. 243, 1–78.

Le Vu, P., Takatori, R., Iwamoto, T., Akagi, Y., Satsu, H., Totsuka, M., Chida, K., Sato, K., Shimizu, M., 2015. Effects of Food-Derived Collagen Peptides on the Expression of Keratin and Keratin-Associated Protein Genes in the Mouse Skin. Skin Pharmacol. Physiol. 28, 227–235.

Lee, H., Noh, K., Lee, S.C., Kwon, I.-K., Han, D.-W., Lee, I.-S., Hwang, Y.-S., 2014. Human hair keratin and its-based biomaterials for biomedical applications. Tissue Eng. Regen. Med. 11, 255–265.

Lee, Y.J., Rice, R.H., Lee, Y.M., 2006. Proteome analysis of human hair shaft from protein identification to posttranslational modification. Mol. Cell. Proteomics 5, 789–800.

Leeder, J.D., Marshall, R.C., 1982. Readily-Extracted Proteins from Merino Wool. Text. Res. J. 52, 245–249.

Leeder, J.D., Rippon, J.A., 1985. Changes Induced in the Properties of Wool by Specific Epicuticle Modification. J. Soc. Dye. Colour. 101, 11–16.

Li, S.W., Ouyang, H.S., Rogers, G.E., Bawden, C.S., 2009. Characterization of the structural and molecular defects in fibres and follicles of the Merino felting lustre mutant. Exp. Dermatol. 18, 134–142.

Liu, F., Chen, Y., Zhu, G., Hysi, P.G., Wu, S., Adhikari, K., Breslin, K., Pospiech, E., Hamer, M.A., Peng, F., Muralidharan, C., Acuna-Alonzo, V., Canizales-Quinteros, S., Bedoya, G., Gallo, C., Poletti, G., Rothhammer, F., Bortolini, M.C., Gonzalez-Jose, R., Zeng, C., Xu, S., Jin, L., Uitterlinden, A.G., Ikram, M.A., van Duijn, C.M., Nijsten, T., Walsh, S., Branicki, W., Wang, S., Ruiz-Linares, A., Spector, T.D., Martin, N.G., Medland, S.E., Kayser, M., 2018. Meta-analysis of genome-wide association studies identifies 8 novel loci involved in shape variation of human head hair. Hum. Mol. Genet. 27, 559–575.

Longo, V.M., Pinheiro, A. da S., Sambrano, J.R., Agnelli, J. a. M., Longo, E., Varela, J.A., 2013. Towards an insight on photodamage in hair fibre by UV-light: An experimental and theoretical study. Int. J. Cosmet. Sci. 35, 539–545.

Luckett-Chastain, L.R., Gipson, J.R., Gillaspy, A.F., Gallucci, R.M., 2018. Transcriptional profiling of irritant contact dermatitis (ICD) in a mouse model identifies specific patterns of gene expression and immune-regulation. Toxicology 410, 1–9.

Lukinavičius, G., Reymond, L., D'Este, E., Masharina, A., Göttfert, F., Ta, H., Güther, A., Fournier, M., Rizzo, S., Waldmann, H., Blaukopf, C., Sommer, C., Gerlich, D.W., Arndt, H.-D., Hell, S.W., Johnsson, K., 2014. Fluorogenic probes for live-cell imaging of the cytoskeleton. Nat. Methods 11, 731–733.

Marsh, J.M., Whitaker, S., Felts, T., Shearouse, W., Vatter, M., Määttä, A., Thompson, M., Hawkins, T.J., 2018. Role of internal lipids in hair health. J. Cosmet. Sci.

Marshall, R.C., 1983. Characterization of the proteins of human hair and nail by electrophoresis. J. Invest. Dermatol. 80, 519–524.

Matsunaga, R., Abe, R., Ishii, D., Watanabe, S., Kiyoshi, M., Nöcker, B., Tsuchiya, M., Tsumoto, K., 2013. Bidirectional binding property of high glycine–tyrosine keratin-associated protein contributes to the mechanical strength and shape of hair. J. Struct. Biol. 183, 484–494.

Melhuish, W.H., Smith, G.J., 1993. Photobleachable fluorescent species in wool keratin. J. Soc. Dye. Colour. 109, 163–165.

Millington, K.R., 2006. Photoyellowing of wool. Part 1: Factors affecting photoyellowing and experimental techniques. Color. Technol. 122, 169–186.

Moll, R., Divo, M., Langbein, L., 2008. The human keratins: biology and pathology. Histochem. Cell Biol. 129, 705–733.

Nagase, S., Tsuchiya, M., Matsui, T., Shibuichi, S., Tsujimura, H., Masukawa, Y., Satoh, N., Itou, T., Koike, K., Tsujii, K., 2008. Characterization of curved hair of Japanese women with reference to internal structures and amino acid composition. J. Cosmet. Sci. 59, 317–332.

Naito, S., Takahashi, T., Hattori, M., Arai, K., 1992. Histochemical Observation of the Cell Membrane Complex of Hair. Seni Gakkaishi 48, 420–426.

Negri, A.P., Cornell, H.J., Rivett, D.E., 1993. A Model for the Surface of Keratin Fibers. Text. Res. J. 63, 109–115.

Niessen, C.M., 2007. Tight Junctions/Adherens Junctions: Basic Structure and Function. J. Invest. Dermatol. 127, 2525–2532.

Nogueira, A.C.S., Dicelio, L.E., Joekes, I., 2006. About photo-damage of human hair. Photochem. Photobiol. Sci. 5, 165–169.

Oh, J.W., Kloepper, J., Langan, E.A., Kim, Y., Yeo, J., Kim, M.J., Hsi, T.-C., Rose, C., Yoon, G.S., Lee, S.-J., Seykora, J., Kim, J.C., Sung, Y.K., Kim, M., Paus, R., Plikus, M.V., 2016. A Guide to Studying Human Hair Follicle Cycling In Vivo. J. Invest. Dermatol. 136, 34–44.

Orwin, D.F.G., 1979. The Cytology and Cytochemistry of the Wool Follicle, in: Bourne, G.H., Danlelli, J.F., Jeon, K.W. (Eds.), International Review of Cytology. Academic Press, pp. 331–374.

Orwin, D.F.G., Thomson, R.W., Flower, N.E., 1973. Plasma membrane differentiations of keratinizing cells of the wool follicle: II. Desmosomes. J. Ultrastruct. Res. 45, 15–29.

Panteleyev, A.A., Jahoda, C.A., Christiano, A.M., 2001. Hair follicle predetermination. J. Cell Sci. 114, 3419–3431.

Pawley, J. (Ed.), 2006. Handbook of Biological Confocal Microscopy, 3rd ed. Springer US.

Plowman, J.E., Paton, L.N., Bryson, W.G., 2007. The differential expression of proteins in the cortical cells of wool and hair fibres. Exp. Dermatol. 16, 707–714.

Pollard, T.D., Borisy, G.G., 2003. Cellular motility driven by assembly and disassembly of actin filaments. Cell 112, 453–465.

Pötsch, L., Moeller, M.R., 1996. On pathways for small molecules into and out of human hair fibers. J. Forensic Sci. 41, 121–125.

Powell, B.C., Nesci, A., Rogers, G.E., 1991. Regulation of keratin gene expression in hair follicle differentiation. Ann. N. Y. Acad. Sci. 642, 1–20.

Rice, R.H., Wong, V.J., Pinkerton, K.E., 1994. Ultrastructural visualization of cross-linked protein features in epidermal appendages. J. Cell Sci. 107, 1985–1992.

Riley, P.A., 1997. Melanin. Int. J. Biochem. Cell Biol. 29, 1235–1239.

Robbins, C., 2009. The cell membrane complex: three related but different cellular cohesion components of mammalian hair fibers. J. Cosmet. Sci. 60, 437–465.

Robbins, C.R., 2012. Chemical Composition of Different Hair Types, in: Chemical and Physical Behavior of Human Hair. Springer Berlin Heidelberg, Berlin, Heidelberg, pp. 105–176.

Robbins, C.R., 1988. Chemical and Physical Behavior of Human Hair. Springer New York, New York, NY, pp. 102–121.

Rogers, G., 2004. Hair follicle differentiation and regulation. Int. J. Dev. Biol. 48, 163–170.

Rogers, G., Koike, K., 2009. Laser capture microscopy in a study of expression of structural proteins in the cuticle cells of human hair. Exp. Dermatol. 18, 541–547.

Rogers, G.E., 1959. Electron Microscope Studies of Hair and Wool. Ann. N. Y. Acad. Sci. 83, 378–399. https://doi.org/10.1111/j.1749-6632.1960.tb40914.x

Rogers, G.E., Reis, P.J., Ward, K.A., Marshall, R.C., 1989. The Biology of Wool and Hair. Springer Netherlands.

Rogers, M.A., Langbein, L., Praetzel-Wunder, S., Giehl, K., 2008. Characterization and expression analysis of the hair keratin associated protein KAP26.1. Br. J. Dermatol. 159, 725–729.

Rogers, M.A., Langbein, L., Praetzel-Wunder, S., Winter, H., Schweizer, J., 2006. Human hair keratin-associated proteins (KAPs). Int. Rev. Cytol. 251, 209–263.

Rogers, M.A., Schweizer, J., 2005. Human KAP genes, only the half of it? Extensive size polymorphisms in hair keratin-associated protein genes. J. Invest. Dermatol. 124, vii–ix.

Rogers, M.A., Winter, H., Langbein, L., Wollschläger, A., Praetzel-Wunder, S., Jave-Suarez, L.F., Schweizer, J., 2007. Characterization of human KAP24.1, a cuticular hair keratin-associated protein with unusual amino-acid composition and repeat structure. J. Invest. Dermatol. 127, 1197–1204.

Ruetsch, S.B., Yang, B., Kamath, Y.K., 2003. Chemical and photo-oxidative hair damage studied by dye diffusion and electrophoresis. J. Cosmet. Sci. 54, 379–394.

Ruhrberg, C., Watt, F.M., 1997. The plakin family: versatile organizers of cytoskeletal architecture. Curr. Opin. Genet. Dev. 7, 392–397.

Sack, L.M., Davoli, T., Li, M.Z., Li, Y., Xu, Q., Naxerova, K., Wooten, E.C., Bernardi, R.J., Martin, T.D., Chen, T., Leng, Y., Liang, A.C., Scorsone, K.A., Westbrook, T.F., Wong, K.-K., Elledge, S.J., 2018. Profound Tissue Specificity in Proliferation Control Underlies Cancer Drivers and Aneuploidy Patterns. Cell 173, 499-514.e23.

Salbreux, G., Charras, G., Paluch, E., 2012. Actin cortex mechanics and cellular morphogenesis. Trends Cell Biol. 22, 536–545.

Salvi, A., Carrupt, P.-A., Tillement, J.-P., Testa, B., 2001. Structural damage to proteins caused by free radicals: asessment, protection by antioxidants, and influence of protein binding11Abbreviations: AAPH, 2,2'-azobis(2-amidinopropane) 2 HCl; and HSA, human serum albumin. Biochem. Pharmacol. 61, 1237–1242.

Schafer, K., Goddinger, D., Hocker, H., 1997. Photodegradation of tryptophan in wool. J. Soc. Dye. Colour. 113, 350–355.

Schmidt-Ullrich, R., Paus, R., 2005. Molecular principles of hair follicle induction and morphogenesis. BioEssays News Rev. Mol. Cell. Dev. Biol. 27, 247–261.

Schneider, M.R., Schmidt-Ullrich, R., Paus, R., 2009. The Hair Follicle as a Dynamic Miniorgan. Curr. Biol. 19, R132–R142.

Shimomura, Y., Aoki, N., Rogers, M.A., Langbein, L., Schweizer, J., Ito, M., 2002. hKAP1.6 and hKAP1.7, two novel human high sulfur keratin-associated proteins are expressed in the hair follicle cortex. J. Invest. Dermatol. 118, 226–231.

Shimomura, Y., Ito, M., 2005. Human Hair Keratin-Associated Proteins. J. Investig. Dermatol. Symp. Proc. 10, 230–233.

Simpson, W.S., Crawshaw, G.H., Textile Institute (Manchester, E., 2002. Wool: science and technology. Cambridge, UK : Woodhead Publishing ; Boca Raton, FL : CRC Press.

Smith, G.J., Thorpe, M.R., Melhuish, W.H., Beddard, G.S., 1980. Fluorescence of tryptophan in keratin. Photochem. Photobiol. 32, 715–718.

Strnad, P., Usachov, V., Debes, C., Gräter, F., Parry, D.A.D., Omary, M.B., 2011. Unique amino acid signatures that are evolutionarily conserved distinguish simple-type, epidermal and hair keratins. J. Cell Sci. 124, 4221–4232.

Sun, T.T., Eichner, R., Nelson, W.G., Tseng, S.C., Weiss, R.A., Jarvinen, M., Woodcock-Mitchell, J., 1983. Keratin classes: molecular markers for different types of epithelial differentiation. J. Invest. Dermatol. 81, 109s–15s.

Suzuta, K., Ogawa, S., Takeda, Y., Kaneyama, K., Arai, K., 2012. Intermolecular disulfide cross-linked structural change induced by permanent wave treatment of human hair with thioglycolic acid. J. Cosmet. Sci. 63, 177–196.

Swift, J., 1999. Human Hair Cuticle: Biologically conspired to the owner's advantage. J. Cosmet. Sci. 50, 23–47.

Szabo, S., Jaeger, K., Fischer, H., Tschachler, E., Parson, W., Eckhart, L., 2012. In situ labeling of DNA reveals interindividual variation in nuclear DNA breakdown in hair and may be useful to predict success of forensic genotyping of hair. Int. J. Legal Med. 126, 63–70.

Tatsuda, M., Uemura, M., Torii, K., Matsuoka, M., 1987. Studies on hair damage and demelanization by ultraviolet light. J. Soc. Cosmet. Chem. Jpn. 21, 43–49.

Thibaut, S., Cavusoglu, N., de Becker, E., Zerbib, F., Bednarczyk, A., Schaeffer, C., van Dorsselaer, A., Bernard, B.A., 2009. Transglutaminase-3 enzyme: a putative actor in human hair shaft scaffolding? J. Invest. Dermatol. 129, 449–459.

Tojkander, S., Gateva, G., Lappalainen, P., 2012. Actin stress fibers – assembly, dynamics and biological roles. J Cell Sci 125, 1855–1864.

Torres, C., Crastechini, E., Feitosa, F., Pucci, C., Borges, A., 2014. Influence of pH on the Effectiveness of Hydrogen Peroxide Whitening. Oper. Dent. 39, E261–E268.

Ulrich, V., Fischer, P., Riemann, I., Königt, K., 2004. Compact multiphoton/single photon laser scanning microscope for spectral imaging and fluorescence lifetime imaging. Scanning 26, 217–225.

Vasioukhin, V., Bauer, C., Degenstein, L., Wise, B., Fuchs, E., 2001. Hyperproliferation and Defects in Epithelial Polarity upon Conditional Ablation of α-Catenin in Skin. Cell 104, 605–617.

Velasco, M.V.R., Dias, T.C. de S., Freitas, A.Z. de, Júnior, N.D.V., Pinto, C.A.S. de O., Kaneko, T.M., Baby, A.R., 2009. Hair fiber characteristics and methods to evaluate hair physical and mechanical properties. Braz. J. Pharm. Sci. 45, 153–162.

Vermorken, A.J., Weterings, P.J., Kibbelaar, M.A., Lenstra, J.A., Bloemendal, H., 1981. Isolation and characterization of actin from human hair follicles. FEBS Lett. 127, 105–108.

Wang, H., Parry, D.A., Jones, L.N., Idler, W.W., Marekov, L.N., Steinert, P.M., 2000. In vitro assembly and structure of trichocyte keratin intermediate filaments: a novel role for stabilization by disulfide bonding. J. Cell Biol. 151, 1459–1468.

Wang, S., Wang, Z., Foo, S.E.M., Tan, N.S., Yuan, Y., Lin, W., Zhang, Z., Ng, K.W., 2015. Culturing Fibroblasts in 3D Human Hair Keratin Hydrogels. ACS Appl. Mater. Interfaces 7, 5187–5198.

Wardman, P., 1994. Excited States and Free Radicals in Biology and Medicine. Contributions from Flash Photolysis and Pulse Radiolysis. Br. J. Cancer 69, 796.

Wertz, P.W., Downing, D.T., 1989. Integral lipids of mammalian hair. Comp. Biochem. Physiol. B 92, 759–761.

Wilson, T., 2011. Resolution and optical sectioning in the confocal microscope. J. Microsc. 244, 113–121.

Windoffer, R., Beil, M., Magin, T.M., Leube, R.E., 2011. Cytoskeleton in motion: the dynamics of keratin intermediate filaments in epithelia. J. Cell Biol. 194, 669–678.

Windoffer, R., Leube, R.E., 2001. De novo formation of cytokeratin filament networks originates from the cell cortex in A-431 cells. Cell Motil. Cytoskeleton 50, 33–44.

Windoffer, R., Wöll, S., Strnad, P., Leube, R.E., 2004. Identification of Novel Principles of Keratin Filament Network Turnover in Living Cells. Mol. Biol. Cell 15, 2436–2448.

Wortmann, F.J., Wortmann, G., Marsh, J., Meinert, K., 2012. Thermal denaturation and structural changes of α-helical proteins in keratins. J. Struct. Biol. 177, 553–560.

Wortmann, F.-J., Wortmann, G., Zahn, H., 1997. Pathways for dye diffusion in wool fibers. Text. Res. J. 67, 720–724.

Wu, D.-D., Irwin, D.M., Zhang, Y.-P., 2008. Molecular evolution of the keratin associated protein gene family in mammals, role in the evolution of mammalian hair. BMC Evol. Biol. 8, 241.